MAGNETIC AND MÖSSBAUER STUDIES OF SOME POLYNUCLEAR TRANSITION METAL COMPLEXES

A Thesis submitted for the

Degree of Doctor of Philosophy

of the

University of London

by

SANDRA VERONICA WAGGETT

Department of Chemistry
Imperial College of Science and Technology
London SW7 2AY

September 1972

ABSTRACT

Polymeric six-coordinate complexes of high-spin Fe^{II} have been prepared with some substituted pyridine ligands, and also with the diazines, pyrazine, pyrimidine and pyridazine, and some of their derivatives. Techniques such as electronic, I.R. and Mössbauer spectroscopy and magnetic susceptibility measurement have been used to gain information on the nature of the structural distortions and of the metal-ligand bonding.

Limitations in the theoretical treatment of the electronic and magnetic properties of the metal ion in such a low symmetry environment as is present in these complexes, and the relative insensitivity of some of the techniques to small variations in the bonding and distortion parameters, prevents detailed interpretation of the data. However, the identity and position of substituents on the heterocyclic rings appears to have a significant influence on the local symmetry, and thus the electronic properties, of the metal ion.

A proposed mid-I.R. criterion for distinguishing between terminal and bridging modes of coordination of pyrazine has been shown to be inapplicable in the complexes of this ligand studied here, and the validity of previous structural assignments based on this criterion is questioned.

In several of the linear polymeric complexes containing chloride bridges, the presence of extended intrachain ferromagnetic interactions between the metal ions has been found, the mechanism involving a superchange pathway via $\sim 90^{\circ}$ Fe-Cl-Fe linkages. It has also been found that the delocalised π-system of the pyrimidine ring provides a superexchange pathway for antiferromagnetic coupling of the spins of the metal ions between which it bridges. A similar capability for transmitting exchange interactions between metal ions has not, however, been detected here for bridging pyrazine or pyridazine rings.

The usefulness of Mössbauer spectroscopy for detection of relatively weak magnetic ordering of the intermolecular type in coordination compounds has been demonstrated.

Complexes of Cu^{II} have been prepared with the nucleoside analogues, 6-hydroxypurine and 6-mercaptopurine, and with the related heterocyclic base, 4-azabenzimidazole. It has been shown, by e.p.r. spectroscopy, that 6-hydroxypurine and 4-azabenzimidazole are capable of bridging discrete pairs of Cu^{II} ions and of promoting antiferromagnetic coupling between them. This behaviour parallels that found in the analogous dimeric adenine complexes, and is similar to that in the well-known binuclear compound, cupric acetate monohydrate.

In the Appendix, the construction of a Faraday Balance for magnetic susceptibility measurement in the range 1.6 to 300 K, and the problems which were encountered in its operation, are described.

ACKNOWLEDGEMENTS

I should like to express my grateful thanks to my supervisor, Dr D.M.L. Goodgame, for his guidance, interest and encouragement throughout the course of this work. My thanks are also due to Dr J.F. Gibson for his help as temporary supervisor during Dr Goodgame's absence.

I am indebted to Mr D.J. Lowe for the initial construction of the Faraday Balance, and for all his help during the trying time of solving the operational difficulties.

I wish also to thank Dr N.J. Hill, Dr A.A.S.C. Machado and Miss C.P.J. Vuik for many helpful discussions during this work.

My grateful thanks are due to Mrs U.O. Fowler for typing this manuscript, and to my husband, I.P. Evans, for his patience and help during the preparation of this thesis.

Finally, I am sincerely grateful to the University of London for the award of a Postgraduate Studentship (1968-71) and to Professor G. Wilkinson F.R.S. for a Demonstratorship in this Department (1971-72).

To my Parents

To my Husband

CONTENTS

Ligand Abbreviations

The following abbreviations have been used in the text:

py	pyridine
α-pic	2-methylpyridine
β-pic	3-methylpyridine
γ-pic	4-methylpyridine
quin	quinoline
iso-quin	iso-quinoline
4-CN-py	4-cyanopyridine
3-CN-py	3-cyanopyridine
4-Cl-py	4-chloropyridine
3-Cl-py	3-chloropyridine
$3,5\text{-}Cl_2\text{-py}$	3,5-dichloropyridine
3-Br-py	3-bromopyridine
3-I-py	3-iodopyridine
pz	pyrazine
Mepz	methylpyrazine
pd	pyridazine
pm	pyrimidine
5-Mepm	5-methylpyrimidine
4-Mepm	4-methylpyrimidine
$2\text{-}NH_2$ pm	2-aminopyrimidine
ad	adenine anion
adH	adenine (6-aminopurine)
hxH	6-hydroxypurine (hypoxanthine)
azbH	4-azabenzimidazole
mpH	6-mercaptopurine

CHAPTER 1 THE MAGNETIC PROPERTIES OF SOLIDS

The magnetic properties of solids have long been of interest to physicists, mathematicians and chemists owing both to the technical importance of magnetic materials,[1-3] and to the relationships between magnetic properties and the nature of chemical bonding.[4-9]

A division may be made in the treatment of magnetic phenomena, depending upon whether the paramagnetic species are effectively isolated from one another (magnetically dilute systems), or whether interactions can occur between them (magnetically concentrated systems). In the former case, the magnetic properties of the isolated systems may be related to the electron configuration and to the nature of the ligand environment. In the latter case, magnetic exchange interactions, which can be represented as an effective coupling of the spins of the individual paramagnetic species, give rise to ferro- and antiferromagnetic ordering effects, which depend on the structural relationships between the species. These interactions may arise simply because the distance between the species is small (historically termed 'direct exchange'), or because intervening anions or ligand molecules are capable of transmitting the magnetic coupling effects (termed 'super exchange').

A long established experimental technique for investigation of the magnetic properties in both dilute and concentrated systems is the measurement of magnetic susceptibility and effective moment, and their temperature dependence, and various instrumental methods have been designed for this purpose (see Appendix). In dilute systems, the susceptibility and moment may provide information on the effects on the electronic states of the paramagnetic ion, of the symmetry of the ligand field, spin-orbit coupling and the degree of covalency between metal and ligands. Such information may complement or supplement that obtained from other techniques such as electronic, e.p.r. and Mössbauer spectroscopy. In concentrated systems, the major interest is in the nature and mechanism of the exchange processes, and susceptibility measurements provide a means of detecting, and determining the sign and magnitude of, the spin-spin coupling. Other

powerful techniques such as neutron diffraction,[10] ferro- and antiferromagnetic resonance[11] and measurement of specific heat anomalies[12] have been developed by physicists for detailed investigation of magnetic structure, and e.p.r. and Mössbauer spectroscopy have also proved increasingly important for detection and investigation of magnetic exchange effects.

In this work, magnetic susceptibility measurements have been used, in conjunction with electronic, e.p.r. and Mössbauer spectroscopy to investigate the structural properties of a series of distorted octahedral polymeric complexes of Fe^{II}, and to obtain information on the magnetic exchange interactions present in these compounds, and in some polynuclear complexes of Cu^{II}. The construction and operation of a Faraday balance, for susceptibility measurement in the temperature range 300 - 1.6 K, is described in the Appendix. Unfortunately, owing to operational difficulties with this apparatus, the amount of magnetic data obtained is rather limited, but some interesting features of these systems have been determined.

A brief, general account of the theoretical treatment of the magnetic properties of transition metal ions in both dilute and concentrated systems is given below, to indicate the nature of the information afforded, with reference to that obtained from other techniques, and the interpretation of experimental results. Relevant theory for the Fe^{II} and Cu^{II} systems is presented in Chapters 3 and 6.

Magnetically Dilute Systems

The general theory of paramagnetism has been developed on a quantum mechanical basis by Van Vleck.[13] The application of a magnetic field to a set of electronic states, ψ_i, lifts the spin degeneracy of each state (first order Zeeman effect) and can mix some of the character of excited states into the ground state (second order Zeeman effect). For each state, the first and second order Zeeman coefficients can be obtained by application of the magnetic moment operator.[13,5,6]

$$\bar{\mu} = (\bar{L} + 2\bar{S})\beta H \qquad 1.1$$

($\bar{L}$, $\bar{S}$ are the total orbital and spin angular momentum operators, β is the Bohr magneton and H is the applied field) to the wavefunctions, ψ_i. The total suceptibility, χ_A, for one gram-ion of the system is

then obtained by performing a Boltzmann summation over the Zeeman levels of all the thermally populated states.

For a transition metal ion in a complex, the appropriate states, ψ_i, are those resulting from the perturbation of the free ion ground term by the combined effects of the ligand field potential and spin-orbit coupling,[14-17] which may be obtained by operation with the Hamiltonian:

$$\mathcal{H} = V_C + V_{NC} + \lambda \bar{L}.\bar{S} \qquad 1.2$$

(V_C, V_{NC} are the cubic and non-cubic crystal field potential operators, λ is the spin-orbit coupling constant) on the basis set of wavefunctions, $|M_L, M_S\rangle$, appropriate to the ground term, (specified by L, S).

For a ligand field of cubic symmetry, the magnetic properties are isotropic (i.e. $\chi_x = \chi_y = \chi_z$), but for non-cubic symmetry the properties are anisotropic, and the principal molecular susceptibilities must be calculated separately by application of the magnetic moment operator in the appropriate directions. The average susceptibility is then given by

$$\chi_A = (\chi_z + \chi_y + \chi_x)/3.$$

For a randomly oriented powdered solid, the average susceptibility and moment are obtained from experimental measurement, whereas if single crystals are available, the three orthogonal principal crystal susceptibilities may be measured, and, with a knowledge of the crystal structure, may be related to the principal molecular susceptibilities.

Comparison between experimental data and theoretical expressions derived as above should provide some information on the nature and relative energies of the metal orbital states containing the magnetic electrons, and therefore give some indication of the strength and symmetry of the ligand environment. The magnitude of the orbital splitting of the free-ion ground term by V_C is usually sufficiently large to ensure that ligand field excited terms will be effectively unpopulated at normal temperatures, and the magnetic properties should be determined by the ligand field ground term only. Extensive discussion of the magnetic behaviour associated with the various ground terms for d^n transition metal ions in complexes has been presented.[4-8,13-32] (and refs. therein)

Particular interest has been shown in the magnetic properties of metal ions with cubic ligand field T ground terms.[5,6,17,18,21-32] The retention of orbital angular momentum for these terms can cause departure of the experimental magnetic moment from the widely applicable spin-only formula, $\mu_{so} = (4S(S+1))^{\frac{1}{2}}$, and the susceptibility from the Curie Law, $\chi_A = \frac{C}{T}$.[5,6,18] The value and temperature dependence of the observed susceptibility and moment depend on the relative magnitudes of the removal of the ground term degeneracy by non-cubic ligand fields and/or spin-orbit coupling, compared with the thermal energy, kT. If the splittings and thermal energy are comparable, the susceptibility will follow the Curie-Weiss Law, $\chi_A = \frac{C}{T+\theta}$, although no physical significance can be attributed to the value of the Weiss constant, θ.

Much work has been carried out to develop theoretical models which will reproduce the magnitude and temperature dependence of the magnetic properties of T terms. Calculations based on the use of the operators 1.1 and 1.2, which enable the properties to be expressed in terms of the crystal field splitting parameters[15,16,33] and the spin-orbit coupling constant, have generally been found to be inadequate. Refinements have been introduced to allow for additional effects such as interaction with excited terms under the non-cubic field operator and/or spin orbit coupling,[14-16,23] and the effects of covalency.[8,34,35] These refinements allow the magnetic properties to be expressed in terms of a number of variable parameters, related to specific properties of the metal-ligand interaction. However, such approaches are, of necessity, limited, since constraints must be placed on the number of parameters which are to be evaluated from the experimental data. The parameterisation adopted to account for the consequences of covalency is outlined below, since aspects of the approach are also important in the interpretation of the results of other techniques.

If there is a significant covalent contribution to the metal-ligand bonding, the appropriate wavefunctions, ψ_i, are no longer combinations of the pure free-ion one electron wavefunctions, but in fact correspond to molecular orbitals, produced by mixing of metal orbitals with ligand orbital combinations of the correct symmetry.[8,13-17,36] A rigorous description of the molecular orbital functions amenable to theoretical treatment of magnetic and electronic properties is a matter of some

difficulty, but the main consequences of covalent overlap are quite well established.[8,34-38]

Covalent bonding effectively expands the radial portion of the free-ion d-wavefunctions (the nephelauxetic effect[38]), both through reduction of the effective nuclear charge, Z, by the presence of ligand electron density (central field covalency), and by delocalisation onto the ligands by molecular orbital formation (symmetry restricted covalency).

The orbital splittings by the ligand field now comprise the ionic contribution due to the crystal field electrostatic potential (expressed in terms of the crystal field splitting parameters[15,16,33]) and the covalent contribution due to the differences in antibonding energy shifts for the various σ- and π-molecular orbitals formed between the ligand and metal d-orbitals.[8] This latter contribution has been shown to be of the same order of magnitude or greater than the former, even in transition metal salts which are considered to be predominantly ionic in character.[39] Calculation of the nature of the orbital splittings may still be carried out within the framework of the crystal field model, using the relevant operators V_C, V_{NC}, but the ligand field splittings are treated as variable parameters of the system.

The reduction of the contribution of the d electrons to the total orbital angular momentum, by delocalisation onto the ligands, is incorporated by introduction of the orbital reduction factor, K, into expressions containing $\bar{L}$. K = 1 for no delocalisation, and decreases as the degree of covalency increases. The significance of this parameter has been reviewed.[8,34,35]

The spin-orbit coupling constant, λ, is a function of Z/r^3, where r is the effective distance of the d electron from the nucleus, and is therefore expected to be reduced from the free-ion value, λ_0, as the degree of covalency increases. The Racah parameters of interelectronic repulsion are also roughly dependent on $1/r$, and are generally smaller for transition metal ions in complexes than in the free-ion.

In the treatment of magnetic properties,[8,35] the spin orbit coupling operator in 1.2 thus becomes $K\lambda\bar{L}.\bar{S}$, and the magnetic moment operator (1.1) becomes $(K\bar{L} + 2\bar{S})\beta H$. K and λ may both be treated as variable parameters, and the values of K and $\frac{\lambda}{\lambda_0}$ are not necessarily expected to be numerically related. This method of allowing for the effects of covalency is

limited, since both K and λ may be anisotropic.[8,35]

Theoretical expressions for the temperature dependence of the magnetic properties of T ground terms, calculated by use of the modified forms of 1.1 and 1.2, will therefore contain the ligand field splitting parameters, K and λ. For axial distortions, one ligand field parameter, Δ, is required and the calculation is relatively straightforward. For rhombic distortions, the calculation becomes computationally far more difficult, and two parameters, Δ,ϵ, are required. The effect of mixing with excited ligand field terms on the orbital angular momentum of the ground term may be treated by introduction of an additional parameter,[28] but it has been shown that, where such interactions are expected to be significant, calculation of the magnetic properties within the full free-ion ground term is a more valid approach.[31,32]

The amount and significance of information obtained from evaluation of these parameters, by fitting the experimental data to the theoretical model, depends obviously on the limitations of the theory, and also on the accuracy and temperature range of the experimental measurement. Calculations of this type, with varying degrees of refinement, have shown that the variation of the average susceptibility and moment with these parameters is often not large compared with the experimental error, and, with the multiplicity of parameters available, unambiguous evaluation of a single set for a given system is not always possible. This is especially the case for measurements carried out in the 300 - 80 K range, most commonly used by chemists. The sensitivity of the average magnetic properties to the variation of the parameters is generally much greater below the latter temperature, and measurements down to liquid helium temperature are desirable.[40] The principal values of susceptibility and moment are also far more sensitive to the parameters than the average values,[29,41,42] and magnetic anisotropy measurements on single crystals can provide more information on distorted systems.

Some success has been achieved in fitting average data to the three parameter model, ν, K, λ (where $\nu = \frac{\Delta}{\lambda}$) for axially distorted systems,[28] but, in the absence of reasonable constraints on the values of the parameters, the goodness of fit does not necessarily justify the correctness or adequacy of the model. In many cases, the values of K and λ obtained

cannot easily be rationalised[35] on the basis of chemical knowledge of the nature of the ligands. Also, inclusion of an additional rhombic distortion parameter may simply increase the ambiguity of the fitting, without providing any meaningful information concerning the structural geometry.

It is worthwhile to consider briefly how the ligand field splittings and covalency effects manifest themselves in the electronic spectra, e.p.r. and Mössbauer properties of the system, and to what extent the results of the various techniques may be related.

The electronic spectrum[37,43,44] may provide information on the separation between ground and excited states in cubic fields, and also on the orbital splittings of excited terms in non-cubic fields. In the latter case, the excited state splittings may be related to those of the ground state by the crystal field splitting parameters and the Racah parameters of interelectronic repulsion. However, in the presence of covalency, attempts to correlate the observed ligand field splittings in terms of the crystal field parameters may be invalidated, since the nature and magnitude of the covalent contribution in ground and excited states may not be comparable.

E.p.r. spectroscopy[45-48] allows direct determination of the spectroscopic g-values for the ground electronic level, which may provide information on the effects of ligand field distortions and spin-orbit coupling on the orbital angular momentum of this level. For systems with spin greater than $\frac{1}{2}$, the ligand field distortions may also be manifested in the zero-field splitting parameters, D and E. The g-values and nuclear hyperfine interaction parameter, A, are also sensitive to the effects of covalency.

The Mössbauer quadrupole splitting[49-52] also depends on the thermal population of the states produced under the combined effects of the ligand field and spin-orbit coupling, and is sensitive to covalency (see Chapter 3). Some attempts have been made[17,53,54] to correlate magnetic properties and quadrupole splittings for high spin iron(II) complexes with axial symmetry, but the treatment requires many approximations. The Mössbauer isomer shift is also sensitive to electron configuration and covalency, but generally in a more qualitative sense.

In general, quantitative agreement between ligand field distortion and covalency parameters, evaluated from magnetic and these other techniques, is not good. This reflects both the limitations of the theoretical approaches to the various properties, and also that the properties of the different electronic states investigated by these techniques, may vary widely in their relative sensitivity to specific effects of the ligand environment. However, qualitative or semi-quantitative information derived from a combination of these techniques may still provide considerable insight into the structural and bonding properties of transition metal complexes.

Magnetically Concentrated Systems

The phenomenon of magnetic exchange has been extensively studied by physicists and mathematicians, who have been primarily concerned with intermolecular effects which involve the entire lattice in cooperative interactions. Such effects are found in many metals, alloys and transition metal oxide, sulphide and halide systems.[1-4] More recently, interest has been shown by chemists[55-65] in the intramolecular exchange interactions which frequently occur in small discrete polynuclear clusters of paramagnetic transition metal ions. These clusters are generally isolated from other clusters in the lattice by the presence of relatively large diamagnetic ligands.

Two broad areas of work on magnetically-ordered systems may be distinguished: firstly, the development of a quantitative theory to describe the properties of the systems, and, secondly, the investigation of the origin and mechanism of the exchange processes.

Theoretical Approach to Exchange Interactions

The concept of exchange has been discussed at great length,[4,9,13,61,66-72] and the theoretical approach which has generally been successful for representation of the interaction is the Heisenberg-Dirac-Van Vleck model.

Under the full Hamiltonian for electrostatic interaction between two electrons (spins s_1, s_2) on atoms (1,2), two non-degenerate states are produced, corresponding to two-electron orbital wavefunctions which are symmetric, ψ_{sym}, and antisymmetric, ψ_{anti}, with respect to electron interchange. The total two-electron wavefunctions are required, by the

Pauli principle, to be antisymmetric with respect to electron exchange, and ψ_{sym} must therefore be combined with an antisymmetric spin function (s_1, s_2 antiparallel), and ψ_{anti} with a symmetric spin function (s_1, s_2 parallel). Therefore, as a result of the quantum mechanical exchange effect, the energies of the singlet and triplet total spin states are differentiated, and it can be shown that this is equivalent to an apparent spin coupling between the two atoms, represented by the Heisenberg Hamiltonian:[66,67]

$$\mathcal{H}_{ex} = -2J_{12}\ \bar{s}_1 . \bar{s}_2 \qquad 1.3$$

where J_{12} is called the exchange coupling constant and $\bar{s}_1$, $\bar{s}_2$ are the spin operators for the electrons. If $J_{12} > 0$, the ground state is that with spins parallel (i.e. ferromagnetic exchange), while for $J_{12} < 0$, the ground state is that with spins antiparallel (i.e. antiferromagnetic exchange).

An alternative formulation of the exchange Hamiltonian which is frequently used,[64] defines J_{12} as twice the magnitude and opposite in sign to that given in 1.3.

The exchange Hamiltonian may be generalised for interactions between n paramagnetic ions:

$$\mathcal{H}_{ex} = -2 \sum_{j>i=1}^{n} J_{ij}\ \bar{S}_i . \bar{S}_j \qquad 1.4$$

where J_{ij} is the exchange coupling constant between the i^{th} and j^{th} atoms of total spin S_i, S_j, respectively. The exchange coupling constants are very sensitive to orbital overlap, and interactions are generally considered only between nearest neighbours or next nearest neighbours.

Although the interaction may be represented as a spin-spin coupling, it is not equivalent to a simple dipolar coupling. This latter may be present in addition to the exchange effect, but is generally several orders of magnitude smaller.

The form of the exchange Hamiltonian assumes that the magnetic properties of the interacting ions are due only to their spin angular momentum, and that the orbital angular momentum is zero. Therefore, effects such as ligand field splittings and spin-orbit coupling for the individual ions are excluded from this approach, which severely limits its quantitative application.

In transition metal cluster compounds, where n is generally 2, 3 or 4, and the number of discrete J_{ij} values is small, the eigenvalues of the exchange Hamiltonian (1.4) may be obtained by use of the vector model, originally used by Kambe[73] for a trinuclear cluster, and subsequently adapted and extended for many other cases.[61,63] and refs. therein For a binuclear system with only one exchange interaction, the energy levels are:

$$E(S') = -J_{12}\ [S'(S'+1) - S_1(S_1+1) - S_2(S_2+1)]$$

where $\bar{S}' = \bar{S}_1 + \bar{S}_2$.

S' can take values $(S_1 + S_2), (S_1 + S_2 - 1) \ldots\ldots |S_1 - S_2|$, giving $(S_1 + S_2 + 1)$ levels, each level having $(2S' + 1)$-fold degeneracy and being separated from the ground level by $J_{12}\ (S'(S' + 1))$. The sign of J_{12} indicates that the level with largest S' lies lowest for ferromagnetic interaction, whereas that with smallest S' is lowest for antiferromagnetic interaction.

Application of a magnetic field lifts the degeneracy of each level to give levels, $g\beta HM_{S'}$, ($M_{S'} = S' \rightarrow 0 \rightarrow -S'$, and g is the spectroscopic splitting factor), by the first order Zeeman effect. The susceptibility of the cluster can be obtained by performing a Boltzmann summation among the spin levels, and if the interacting atoms have the same spin, the susceptibility per metal ion, χ_A, can be determined. The second order Zeeman effect is normally incorporated as an $N\alpha$ term.

A more generalised theoretical treatment has been given[63] for calculation of the magnetic properties of systems with several discrete J_{ij} interactions. If the interacting ions have identical spin, the susceptibility, χ_A, and effective moment per metal ion can be expressed in terms of the temperature, the various J_{ij} parameters, the g-value and the $N\alpha$ term. It should therefore be possible to determine the magnitude and sign of the exchange interactions from fitting of the experimental data to the appropriate model. However, with the multiplicity of parameters, especially when more than one J_{ij} value can occur, unambiguous fittings are not always possible. A knowledge of the crystal structure is generally desirable, since a reasonable limit on the number and relative importance of discrete J_{ij} parameters to be considered can often be made on the basis of the geometrical disposition

of the ions in the cluster. Nevertheless, in many cases, especially for binuclear clusters, the structure of the complex may be predicted from the goodness of fit to the theoretical model.[63]

Methods have been given[74] for determination of the sign and magnitude of J_{ij} from particular features of the experimental χ_A or χ_A^{-1} v. temperature plots. For example, relationships have been given between J_{ij} and (i) the Weiss constant θ (obtained from the extrapolation of the χ_A^{-1} v. T plots in the 'high temperature' paramagnetic region), and (ii) the Néel or Curie temperatures. Experimental determination of these features depends on the magnitude of the exchange interactions compared with the temperature range available for measurement, and the relationships are generally only suitable for clusters containing one exchange interaction. Attempts to determine J_{ij} from the θ-value must be treated with caution, since a contribution to θ may arise from degenerate ground states of the individual paramagnetic ions.

Some attempts have been made[63,73] to include the effects of orbital angular momentum and spin-orbit coupling for the interacting ions, but detailed consideration of the mechanism of exchange coupling is required.[9]

In addition to magnetic susceptibility measurements, exchange interactions in discrete clusters may also be detected and investigated by e.p.r. and Mössbauer spectroscopy. In the e.p.r. spectrum, transitions may be observed which arise from spin states (S') of the cluster, rather than from those of the isolated ion.[55,65,66] The best known example of this is the observation of the spectrum of an $S' = 1$ triplet excited state in binuclear antiferromagnetic complexes of $S = \frac{1}{2}$ ions, especially Cu^{II}. The interpretation of such spectra has been discussed in many articles and reviews, with reference to the information which may be afforded on the magnitude of the exchange interaction.[55,65,66] and refs. therein.

Evidence for antiferromagnetic exchange in some binuclear complexes of high-spin Fe^{III} has also been obtained from the Mössbauer effect.[152] The observation of small internal fields at the Fe nucleus, using the applied magnetic field technique at low temperatures, has been interpreted[75] as consistent with an $S' = 0$ ground state, rather than an $S = 5/2$ state in the absence of exchange. Also, the observation of peak asymmetry of the quadrupole doublet in these[75] and other binuclear Fe^{III} complexes[76,77] has been considered to be due to relaxation effects

between the S' spin states of the exchange-coupled system.

Although the theoretical approach represented by the Heisenberg exchange Hamiltonian is quite easily applicable to small clusters, the problem becomes computationally far more difficult in the treatment of intermolecular systems, where pair-wise spin coupling must be considered over the entire three-dimensional lattice.

In lattice ferromagnets, the interactions between the magnetic ions favour a parallel alignment of all the individual spins, giving rise to a spontaneous magnetisation. Owing to domain formation, it is necessary to align the moments of the various domains by an external field to determine the magnitude of the magnetisation, and the magnetic properties may show field dependence. The simplest concept of a lattice antiferromagnet consists of two equivalent interpenetrating ferromagnetic sublattices, with the spins on each sublattice aligned antiparallel. The relevant coupling interactions are therefore intrasublattice and intersublattice. The sublattice structure may be more complex than this simple model, giving rise to a multiplicity of exchange interactions. In addition, the sublattice arrangements may not be simply related to the geometry of nearest neighbours, and therefore the signs and relative magnitudes of the exchange interactions may not be easily predictable. Very complex interactions may occur, with the possibility of non-colinear alignment of the spins on the various sublattices.[4]

The general problem of exchange interactions in lattice systems has been approached by 'effective field' theories,[78] which have been to some degree successful in representing the main features of the magnetic behaviour. Since exchange interactions affect the alignment of the spins, they have been considered to be equivalent to an effective magnetic field. The exchange interactions within a small section of the lattice are then treated as exactly as possible by use of the exchange Hamiltonian, and this section is then assumed to be coupled to the rest of the lattice by an effective field.

Some insight into the nature of cooperative phenomena has been obtained by investigation of 'artificial clusters', produced by dilution of the system into an isomorphous diamagnetic lattice.[74]

Magnetic susceptibility measurements are still of great use in investigation of lattice systems, but, as mentioned earlier, techniques such as neutron diffraction are required for detailed examination of the magnetic substructure and magnetisation direction.

Mössbauer spectroscopy has also been of use in the study of magnetic exchange in lattice systems.[49,50] The presence of an 'internal magnetic field' within the atom will lift the degeneracy of the ground and excited nuclear spin levels, and the allowed transitions between the resulting levels give rise to magnetic hyperfine structure in the spectrum. There are several contributions to the internal field, the most important generally being the Fermi contact interaction, arising from the nuclear interaction with an imbalance of s-electron spin density, caused by polarisation effects with unpaired spins in the d-valence shell. The observation of magnetic hyperfine splitting requires that the frequency of transitions between orientations of the net spin, caused by electronic spin relaxation processes, should be slow relative to the Larmor frequency of the nuclear spin in the magnetic field. This may be effectively fulfilled when cooperative exchange interactions are present. Below the magnetic ordering temperature, the internal field is generally proportional to the average spin, i.e. the magnetisation, and information may be obtained from its sign, magnitude and temperature dependence.

The long range cooperative behaviour in lattice systems is generally prevented in small clusters by the effective isolation from other clusters by the diamagnetic ligands. However, many transition metal complexes are known, in which the paramagnetic ions are arranged in long linear chains (or sheets), through bridging by, particularly, halide ions or multidentate organic ligands. Such systems may behave as extended lattices in one (or two) dimensions, exhibiting intrachain and possibly also interchain interactions. The magnetic properties of one-dimensional infinite linear chains have been described by the Ising and Heisenberg models, in the limit of completely anisotropic and isotropic interactions, respectively, and intermediate cases have also been considered.[79,80]

Mechanism of Exchange Interactions

A distinction was made at the beginning of this chapter between the terms 'direct exchange' and 'superexchange'. Historically, 'direct

exchange' was considered to occur when the interacting ions were sufficiently close for direct non-orthogonal overlap of orbitals containing unpaired electrons. This is equivalent to covalent bond formation between the metal ions, and gives rise to antiferromagnetism. Examples of strong direct metal-metal bonding are known.[57-59]

'Superexchange', involving the ligands bridging the metal ions, has been proposed to account for exchange interactions in systems where the metal-metal separation is too large for direct overlap. Binuclear cupric acetate monohydrate is a well-known example in which both direct (the δ-bond) and superexchange processes have been invoked to account for the antiferromagnetism present. (Ref. 73 contains a brief review).

Since the original concept of Kramers,[69] many mechanisms for the superexchange process have been proposed,[4,70,81-83] and refs. therein to explain qualitatively how the magnetic effect is transmitted, and these have shown the importance of covalent overlap between metal and ligand orbitals. Most mechanisms invoke some degree of electron transfer between the metal d-orbitals and the intervening ligand σ- or π-orbitals with which they overlap. In some cases, transfer involving one metal ion at a time is proposed, while in others, simultaneous involvement of both metal ions is required. In all cases, the spin direction of the electron transferred (relative to the net spin on the metal ion) depends on the electron occupancy of the overlapping metal and ligand orbitals, and the orthogonality relationships between the ligand orbitals and the metal d-orbitals containing the unpaired electrons. The resulting alignment (parallel or antiparallel) of the net spins on the two metal ions in a particular M-L-M bridge can be determined by consideration of these factors for each side of the bridge. Mechanisms involving ligand-electron polarisation have also been proposed.[84]

A set of semi-empirical rules (the Goodenough-Kanamori rules)[4,83] have been formulated on the basis of these mechanisms, to enable qualitative prediction of the sign and relative magnitude of contributions to the exchange in a given M-L-M system. They emphasise the importance of the ligand field in determining both the metal d-orbitals which contain the magnetic electrons, and also the nature and degree of covalent overlap between the metal and ligand orbitals. In general, exchange interactions

involving overlap of metal e_g orbitals with σ-type ligand orbitals will be much greater than that involving t_{2g} orbital overlap with π-type ligand orbitals. The geometry of the bridge is also important, and a distinction is usually made between the two common cases in which the M-L-M angle is close to 180° and to 90°, respectively.

These rules have proved extremely useful for the qualitative understanding of superexchange processes. However, more recently, Anderson has proposed[71] that there is no real conceptual difference between the so-called 'direct' and 'superexchange' processes. The intervening ligand is considered to effectively expand the metal d-orbital wavefunctions, through covalent mixing, so that they may interact directly through the delocalised pathway. The exchange processes then arise from interactions between the fractions of unpaired spin density from each metal ion residing in the ligand orbitals. On this basis, Anderson distinguishes two significant contributions to the exchange process, which encompass many of the predictions of the semi-empirical rules, and are termed:

(i) Superexchange or Kinetic Exchange, which promotes 'incipient' covalent bond formation, through the intervening ligand, between unpaired electrons in orbitals which are non-orthogonal by symmetry. This predicts antiferromagnetism by the Pauli principle.

(ii) Direct or Potential Exchange, arising from the repulsive electrostatic potential energy between unpaired electrons in orbitals which are orthogonal by symmetry. This interaction is ferromagnetic by the same considerations which give rise to Hund's rule, and is generally very much weaker than the superexchange process.

This approach has enabled the relationship between exchange interaction and covalent bonding to be treated on a more quantitative basis.[8,9]

CHAPTER 2 COMPLEXES OF IRON(II) HALIDES WITH SUBSTITUTED PYRIDINE AND DIAZINE LIGANDS

The first part of this work is concerned with investigation of the structural, electronic and magnetic properties of series of polymeric complexes of Fe^{II} chloride (and in some cases bromide) with some substituted pyridines, and with the three isomeric diazines, pyrazine, pyrimidine and pyridazine, and a selection of their derivatives.

In this chapter the background and underlying interest in these studies is given. The relevant theory required for interpretation of the experimental measurements on these compounds is given in Chapter 3, and the experimental results and information obtained are discussed in Chapter 4, for the pyridine complexes, and in Chapter 5, for the diazine complexes.

I. Complexes with substituted pyridines

There have been numerous studies of the complexes[28,40,44,53,54,85-102] formed between Fe^{II} halides or pseudohalides and unidentate heterocyclic amines of the pyridine and quinoline type, and compounds have been isolated and characterised in each of a number of different stoichiometries and coordination geometries.

Most attention has been given to complexes of the formula FeL_4X_2 (L = py, β-pic, γ-pic, iso-quin; X = Cl, Br, I and pseudohalides NCS, NCSe, NCO) and the literature contains many reports on the preparation[85-89,91] and investigation of the structural and electronic properties of these compounds,[28] using techniques such as electronic,[44,54,89,91,92] I.R.[89,91] and Mössbauer spectroscopy[53,54,89,93] and magnetic measurements.[40,53,54,89] The experimental data has been correlated and interpreted in terms of a monomeric, tetragonally-distorted octahedral structure, with the halogens occupying trans positions. Conclusions have been drawn on the nature of the bonding, the magnitude of distortions present and the ordering and separation of the energy levels of the ferrous ion in these compounds. In a recent Mössbauer study,[93] the temperature dependence of the quadrupole splitting was interpreted as consistent with a cis-configuration for $Fepy_4Cl_2$, but an X-ray crystallographic study[95] has confirmed the earlier evidence from powder diffraction patterns[90] that the chlorides are in fact in trans positions.

Compounds of the type FeL_6X_2 (L = py, β-pic, γ-pic; X = Cl, Br, I) have also been reported.[89,91,96] Although it was originally suggested[91] that all six amine ligands are coordinated to the metal, it has since been shown[89,96] that only four are present in the primary coordination sphere, corresponding to a formulation $FeL_4X_2 \cdot 2L$. Complexes of the formula FeL_2X_2 (L = quin, 3Me-iso-quin; X = Cl, Br) have been prepared, and have been shown to be monomeric with distorted tetrahedral geometry.[89,97-99]

A range of compounds remains which has so far received very little detailed attention. Thermogravimetric studies of the decomposition of some FeL_4X_2 compounds has shown[94,100] that intermediates may be formed as follows:

$$FeL_4X_2 \rightarrow FeL_2X_2 \rightarrow FeLX_2 \rightarrow FeL_{2/3}X_2 \rightarrow FeX_2 .$$

(L = py, β-pic, γ-pic; X = Cl, (Br)).

The compounds $Fepy_2Cl_2$, $FepyCl_2$, $Fe(\gamma\text{-pic})_2Cl_2$ and $Fepy_2Br_2$ have been isolated by controlled thermal decomposition of the corresponding 4:1 compounds,[88,101,102] and $Fepy_2Cl_2$[102,103] and FeL_2X_2 (L = 3,5-Cl_2-py, 4-CN-py; X = Cl,Br)[88] have been prepared by direct reaction. Very little investigation has been carried out on these compounds and, of this, $Fepy_2Cl_2$ has received most attention.

On the basis of the similarity of the X-ray powder pattern of $Fepy_2Cl_2$ to that of α-$Copy_2Cl_2$, it has been concluded[101,102,104] that the compound possesses the same polymeric 6-coordinate structure.[105] In the cobalt complex,[105] the metal ions are arranged in parallel linear chains, with each adjacent pair in a chain linked by two symmetric chloride bridges, to give an approximate plane of four chloride ions (internal chain Cl-Co-Cl angle = 85.5°) around each metal ion. The amine molecules occupy trans axial positions (Co-Co-N angle ≈ 90°) to complete the tetragonally-distorted octahedron. The planes of the rings lie approximately normal to the chain direction, although the solution to the structure retains the possibility of an ≈ 10° tilt about the Co-N-C_4 axis.

The room temperature magnetic moment of $Fepy_2Cl_2$ has been reported[101] as 5.75 BM. The I.R. and far I.R. spectra have also been measured,[106,107] although in the latter case the metal ligand vibrations remained unassigned until a recent study,[108,109] which also includes Raman data.

The electronic spectra have been measured[44,88,92] for FeL_2X_2 (L = py, 3,5-Cl_2-py, 4-CN-py; X = Cl,Br) and for $FepyCl_2$, and have been interpreted in terms of a tetragonally-distorted octahedral configuration for all the compounds.

A Mössbauer study[100] of the thermal decomposition shown above for $Fepy_4Cl_2$ indicates that the compounds $FepyCl_2$ and $Fepy_{2/3}Cl_2$ probably also possess six-coordinate structures, involving more extensive halogen-bridging, since their quadrupole splitting and nuclear isomer shift values are similar to those for $Fepy_2Cl_2$.

Analogous polymeric octahedral complexes are known for many other halides of bivalent first row transition metal ions, notably cobalt, nickel, manganese, copper and chromium, with a wider range of substituted pyridine ligands.[110] The basic molecular structure of the 2:1 adducts is considered to be similar to that of α-$Copy_2Cl_2$, although additional distortions may be introduced by the presence of ring substituents, either by intrachain interactions or interchain packing considerations. In the copper and chromium cases, the halide bridges are known to be asymmetric,[105,111] due presumably to the operation of the Jahn-Teller effect.

A very large amount of experimental investigation has been carried out on these systems,[110] using spectroscopic and magnetic techniques, to determine the nature of the metal-ligand bonding, the magnitude and type of distortion present, and the variation of these with the identity of the substituted pyridine ligand. However, interpretation of the experimental data is complicated by the very low site symmetry (C_i) of the ligand environment of the metal ion in the chain. Interpretations based on the approximate microsymmetry of the central metal ion of each repeat unit of the chain (considered to be O_h or D_{4h} for an α-$Copy_2Cl_2$-type structure, or D_{2h} for a $Cupy_2Cl_2$-type structure) have provided little conclusive information on the detailed effect of the ligand environment on the electronic properties of the metal ion.

It was therefore considered worthwhile to investigate the properties of a series of polymeric bis(substituted pyridine) adducts of Fe^{II} halides, for which Mössbauer spectroscopy is readily of use, in addition to electronic spectroscopy and magnetic measurements, for obtaining information on the environment of the metal ion. These polymeric

compounds may be especially interesting since the presence of extended halogen-bridging may provide a mechanism for magnetic superexchange interactions, such as is found in many anhydrous halides and halide dihydrates of bivalent first row transition metal ions, which contain halogen bridges.[3,110,112]

For the purpose of magnetic studies, it was essential to ensure that the compounds could be prepared in a pure state. Preparation by thermal decomposition of FeL_4X_2 compounds is not desirable for formation of pure FeL_2X_2 species, since further decomposition can occur, and the method can produce samples with a high proportion of crystal defects. The preferred product of a direct synthesis from a particular metal halide and amine ligand depends on many factors, which have been extensively discussed in the preparative studies of Co^{II} and Ni^{II} pyridine complexes.[110] In the case of the Fe^{II} compounds, the σ-donor ability of the ring nitrogen atom, which may be roughly equated with the basicity of the ligand, appears to be of great importance. Thus, with relatively strongly basic ligands, such as pyridine itself and derivatives substituted with electron-donating groups, e.g. alkyl groups (Table 2.1), the FeL_4X_2 compounds are the preferred products. In attempts to prepare pure FeL_2X_2 compounds from such ligands, there is a high risk of contamination with the 4:1 species.[102]

However, introduction of electron-withdrawing substituents, e.g. halogens, CN, into the ring decreases the basicity of the ligand and hence the σ-donor ability of the nitrogen atom, favouring preferential formation of the polymeric FeL_2X_2 compounds. Introduction of substituents in the 2-position of the ring is undesirable, since the steric effect of the group adjacent to the coordinating atom tends to hinder complex formation, or may favour production of a tetrahedral species. The ligands used for this study were therefore limited to pyridines substituted in the 3- or 4-positions with electron-withdrawing groups.

II. Complexes with Diazines and their derivatives

There has been considerable interest in the metal complexes formed with the three isomeric diazines, pyrazine, pyrimidine and pyridazine (Fig.2.1).

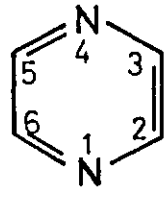

pyrazine
(1,4-diazine)

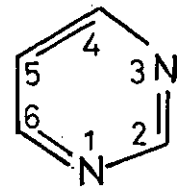

pyrimidine
(1,3-diazine)

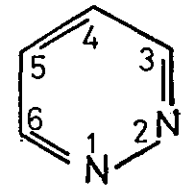

pyridazine
(1,2-diazine)

Fig. 2.1.

Compared with pyridine, these molecules have a second potential donor nitrogen atom, and two modes of bonding may therefore be envisaged, i.e. terminal coordination through one nitrogen atom only, or formation of a bridge between two metal atoms, through bonding by both nitrogen atoms. A third possibility for pyrimidine and pyridazine, involving chelation to one metal atom, is considered unlikely owing to the orientation of the lone pairs or the nitrogen atoms.

The diazines are much weaker bases than pyridine (Table 2.1) and are reported[113] to protonate or quarternise at one nitrogen atom only, the other being deactivated. However, it has been shown that both nitrogen atoms are capable of simultaneous σ-donation, e.g. with BCl_3, pyrazine forms the compound

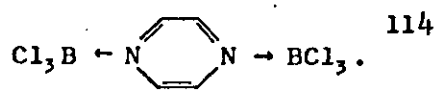

[114]

Many metal complexes of the diazines and their derivatives are known, displaying both terminal and bridging coordination.

Co^{II}, Ni^{II} and Cu^{I} halide complexes with pyrazine and its methyl derivatives have been studied in some detail,[114-119] and pyrazine

complexes have also been prepared with Cr^{o} and Mo^{o},[120] Ti^{IV} and Zr^{IV},[121] In^{III} and Tl^{III},[123] Ag^{I}[124] and Ag^{II},[125] Mo^{IV},[126] Ru^{II} and Ru^{III},[127] and Sn^{IV}.[128]

Some systematic studies of the complexes formed with the three parent diazines have also been carried out for the halides of Co^{II}, Ni^{II}, Mn^{II}, Fe^{II}[129] and for Cu^{II},[129-131] and also for Zn^{II}, Cd^{II} and Hg^{II}.[132-134] Complexes of substituted pyrimidines with Co^{II}, Ni^{II} and Cu^{II} have been prepared and studied,[135-137] and pyridazine complexes with several bivalent transition metal salts have been reported.[138]

Very little work has been carried out on the Fe^{II} complexes with these ligands. The compounds $Fepz_2X_2$ (X = Cl, Br) and $Fepz_2Cl_2 \cdot 2H_2O$ and the series $FeLCl_2$ (L = pz, pm, pd), have been prepared, and on the basis of the electronic spectra, I.R. spectra and room temperature magnetic moments, have all been considered to contain high-spin Fe^{II} in a six-coordinate environment.[129,138]

In the $FeLCl_2$ compounds, six-coordination may be achieved by chloride bridging, to give again an approximate plane of four chloride ions around each metal ion, with the diazine molecules in axial positions forming interchain bridges (for pyrazine and pyrimidine Fig.2.2(a)) or intrachain bridges (for pyridazine Fig.2.2(b)). This would produce a trans-FeN_2Cl_4 environment. It is not necessary to invoke the more extensively chloride-bridged structure proposed for complexes such as $FepyCl_2$, owing to the presence of two potential donor sites in the diazine ligands.

Two different coordination environments could be envisaged for the $Fepz_2X_2$ complexes, depending on the relative bridging tendencies of the halogen and the diazine. The first would involve bridging halide and terminal pyrazine, to produce a trans FeN_2X_4 environment, (Fig.2.2(c)), and the second would involve bridging pyrazine and terminal halide to give an FeN_4X_2 species. The simplest geometrical arrangement which could be suggested for this latter case is the regular sheet structure in Fig.2.2(d)).

If both $FeLCl_2$ and FeL_2X_2 complexes possess the FeN_2X_4-type halogen-bridged structures then they would closely resemble the polymeric substituted-pyridine compounds, and may provide a useful comparison

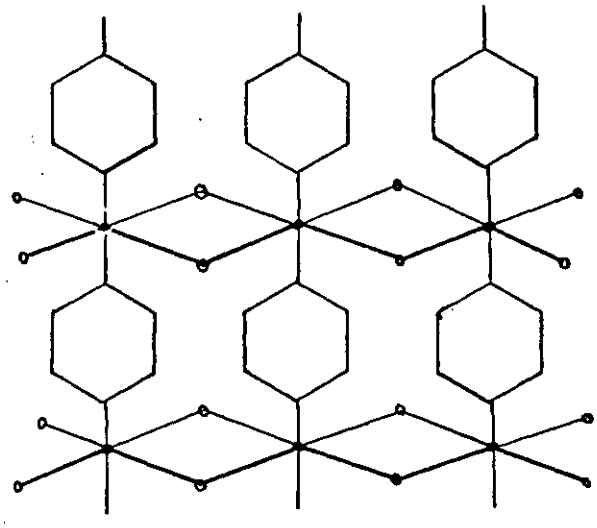

$FepzX_2$ 2.2(a)

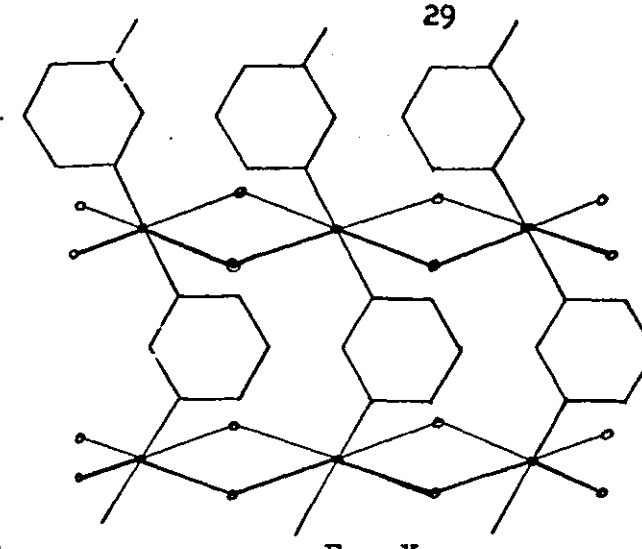

$FepmX_2$

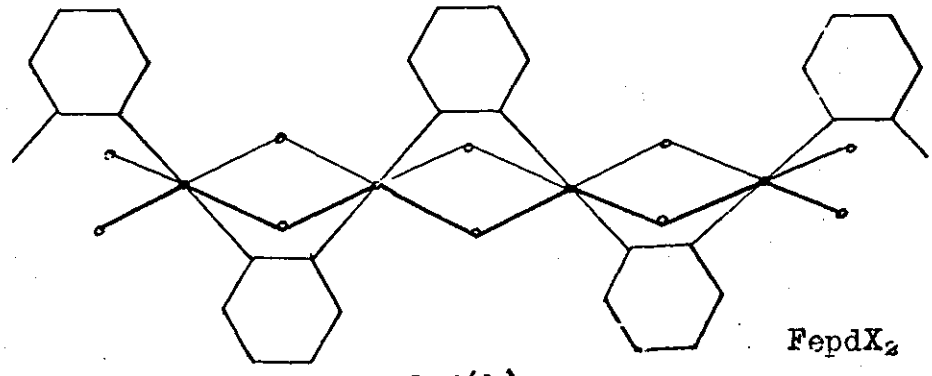

$FepdX_2$

2.2(b)

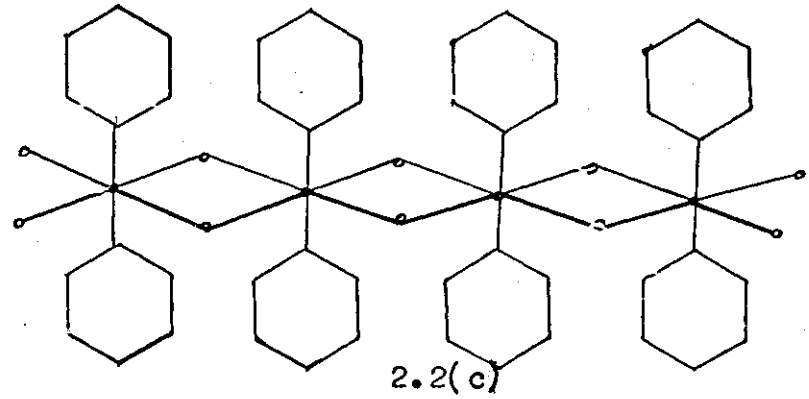

$Fepz_2X_2$

2.2(c)

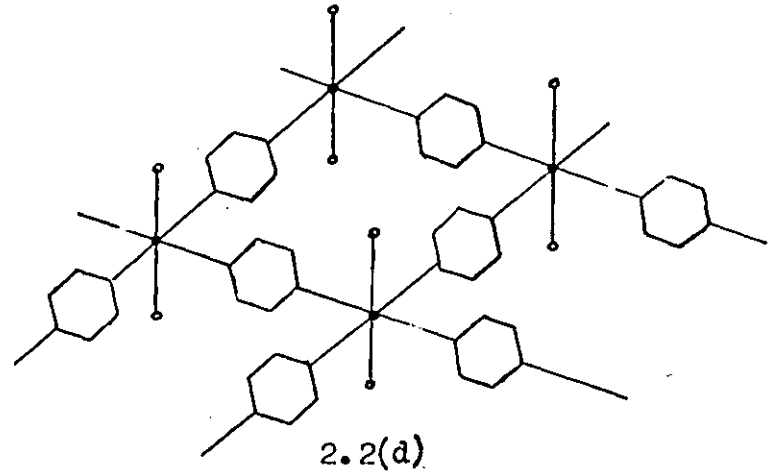

$Fepz_2X_2$

2.2(d)

Fig. 2.2 Possible structural arrangements for the diazine complexes

• Fe ○ X

of electronic properties. The presence of the halogen bridges may again provide a pathway for magnetic superexchange interactions. However, for the $FeLCl_2$ complexes, the nature of the diazine ligands introduces a new factor into the consideration of possible exchange pathways. The bridging heterocyclic ligand would provide a delocalised π-system linking adjacent metal ions, either within the same chain (pyridazine) or between two chains (pyrazine and pyrimidine). Exchange interactions involving the π-system of a bridging heterocyclic amine have been suggested previously.[131,139-142]

If the $Fepz_2X_2$ complexes are in fact diazine bridged (Fig.2.2(d)) then the π-system of the pyrazine ligand would constitute the only superexchange pathway between metal ions. Determination of the structure of these 2:1 compounds and comparison of their magnetic properties with those of the 1:1 compounds and also those of the substituted pyridine complexes could then provide some interesting information on the relative efficiency of halogen and heterocyclic amine bridges in transmitting magnetic exchange effects between metal ions. A series comprising both 1:1 and 2:1 complexes with the diazines and some of their derivatives has therefore been prepared, and investigated by magnetic and spectral techniques.

In addition to the intrinsic interest in the magnetic behaviour of these compounds, it was hoped that structural information might be obtained to test the validity of criteria proposed by earlier workers for distinguishing between the modes of bonding of pyrazine in metal complexes.

From the original studies[117-119] of the Co^{II} and Ni^{II} complexes with pyrazine and its methyl-derivatives, it was proposed that terminally-bound and bridging pyrazine can be distinguished on the basis of a mid-I.R. criterion. An electron diffraction study[143] of pyrazine has demonstrated the D_{2h} symmetry of the free molecule, and full vibrational assignments have been made on this basis.[144-146] In complexes in which pyrazine coordinates to two metal atoms, the centre of symmetry of the molecule is retained, but if the molecule is terminally bound through one nitrogen atom only, the symmetry will be lowered to C_{2v}. At least one additional I.R. active mode of the pyrazine molecule is predicted to occur in the

latter case, and observation of a band at ~ 980 cm^{-1} has been considered to provide conclusive evidence of terminally-bound pyrazine.[117-119] A band at ~ 1250 cm^{-1} has been considered to fulfil a similar purpose for complexes of methylpyrazine.

On this basis, six-coordinate complexes of the type $M^{II}MepzX_2$ (M = Ni, X = Cl,Br; M = Co, X = Cl) were considered to contain bridging halide and pyrazine, while those of the type $M^{II}pz_2X_2$ (M = Ni, X = Cl,Br, I,NCS; M = Co, X = Cl,Br,I) were considered to contain bridging halide, but terminally-bound pyrazine. Similar considerations were applied for the structural assignment of other six-coordinate complexes with methylpyrazine and dimethylpyrazines.[117-119]

Following these structural assignments, the electronic spectra of the Co^{II} [117] and particularly the Ni^{II} [118,119] complexes were interpreted, and conclusions were drawn on the effect on the ligand field splittings of the mode of coordination of the ligand and the position of ring substituents. Firstly, by comparison of the electronic spectra of the $Nipz_2X_2$ complexes with those of the presumably structurally-similar $Nipy_2X_2$ complexes, it would appear that the ligand field strength of terminally-bound pyrazine is comparable to or greater than that of pyridine, even though the basicity of the former ligand is much lower. A greater degree of metal to ligand π-back bonding for pyrazine was invoked to explain this. A later thermogravimetric study[147] also compared the dissociation heats of the Mpz_2X_2 complexes with those of Mpy_2X_2, and concluded that the larger values in the former compounds are indicative of more extensive π-back bonding.

Secondly, by comparison of the electronic spectra of $Copz_2Cl_2$ and $CopzCl_2$,[119] it was concluded that the ligand field strength of terminally-bound pyrazine is significantly greater than that of bridging pyrazine. This was considered to be due to the fact that in the formation of covalent bonds between the metal atoms and the ligand, two metal atoms are competing for the same set of ligand molecular orbitals in the latter case.

Thirdly, it was concluded[118,119] that, in the Ni^{II} complexes in which the metal environment is 'N_2X_4' through bridging X, the ligand field strength is decreased by ~ 2000 cm^{-1} when the bonded nitrogen atoms are sterically hindered by an α-methyl substituent.

It must be noted that all of these conclusions depend on the assignment of a halogen-bridged structure to the Mpz_2X_2 complexes, and that this in turn depends on the mid-I.R. criterion. This criterion was not checked by crystal structure determination for the complexes concerned, and in view of some of the consequences it entails in interpretation of the stuctural and electronic properties of these systems, it may be open to doubt. For example, in the compounds Mpz_2I_2 ($M = Ni^{II}$, Co^{II}) it requires the iodide ion to bridge in preference to the pyrazine molecule, which appears somewhat unlikely in view of the proven bridging ability of the diazines[124,148,149] compared with the noted reluctance of iodide to bridge first row transition metal ions. Also, from consideration of the relative positions of the halogens and heterocyclic amines in the spectrochemical series, it seems plausible that the high ligand field strength in the Mpz_2X_2 complexes, upon which all of the above conclusions are based, could be more reasonably interpreted as consistent with an MN_4X_2 environment, corresponding to a diazine-bridged structure. Indeed, the values of the ligand field splitting, 10 Dq, obtained for the $Nipz_2X_2$ complexes are remarkably similar to those found for complexes of the type $Ni(Mepz)_5X_2$ ($X = Cl, Br, I, NCS$),[118,119] which are considered to contain monomeric six-coordinate $Ni(Mepz)_4X_2$ units, with each diazine molecule bonded to the metal atom through the unhindered nitrogen atom, and one ligand molecule of solvation.

The mid-I.R. criterion has been used for structural characterisation in many other pyrazine complexes,[121-123,125,126,132] and in discussions of the properties of other transition metal complexes with heterocyclic amine ligands reference has been made to the supposed halogen-bridged structures of the Mpz_2X_2 complexes.[150,151] It therefore becomes important to investigate the general validity of this criterion. Of particular interest to the present work, the criterion has been applied to $Fepz_2Cl_2$,[147] and a halogen-bridged structure has been assigned from observation of a band at 987 cm^{-1}. The far I.R. spectra of this compound and several other Mpz_2Cl_2 complexes have also been interpreted as consistent with a halogen-bridged structure.[129]

Table 2.1.

Ligand	Base Strength pK_a
py	5.2
β-pic	5.7
γ-pic	6.0
4-CN-py	1.90
3-CN-py	1.45
4-Cl-py	3.80
3-Cl-py	2.84
3,5-Cl_2-py	0.70
3-Br-py	2.84
3-I-py	3.25
pz	0.60
Mepz	1.40
pd	2.30
pm	1.30
5-Mepm	1.80
4-Mepm	2.00
2-NH_2-pm	3.50

CHAPTER 3 ELECTRONIC SPECTRA, MAGNETIC AND MÖSSBAUER PROPERTIES OF 'OCTAHEDRAL' HIGH-SPIN Fe^{II}

The experimental measurements carried out in this present work indicate that the compounds in both the pyridine and diazine series contain high-spin Fe^{II} in a six-coordinate environment, with varying degrees of distortion from regular octahedral symmetry. The theory required for interpretation of the electronic spectra, magnetic measurements and Mössbauer spectra of Fe^{II} in 'weak' ligand fields of regular, axially-distorted and rhombically-distorted octahedral symmetry is therefore outlined below.

The ^5D term in 'octahedral' ligand fields

In Fig.3.1, the lifting of the orbital degeneracy of the ^5D ($3d^6$) ground term of Fe^{II} in 'weak' crystal fields is shown for:

(a) regular octahedral (O_h) symmetry,

(b) a tetragonal distortion from O_h, lowering the symmetry to D_{4h}, and corresponding to a compression along the z-axis (i.e. the principal fourfold axis (001) of the octahedron, defined as in Fig.3.1(e)),

(c) an additional rhombic distortion, lowering the symmetry to D_{2h}, and corresponding to a compression along the x-axis (Fig.3.1(e))

(d) a trigonal distortion from O_h, lowering the symmetry to D_{3d}, and corresponding to a compression along the z-axis (i.e. the principal threefold rotation axis (111) of the octahedron, defined as in Fig.3.1(f)),

assuming that the ligands occupy the vertices of the octahedron.

The electron configuration of the ground state is $t_{2g}^4 e_g^2$.

The ordering of the orbital states shown is that predicted from consideration of electrostatic repulsion between the ligands and the metal d-orbitals. Thus, for a compression along z in either tetragonal or trigonal symmetry, the singlet component of the $^5T_{2g}$ term is expected to lie lowest, with the $^5A_{1g}$ component highest in the tetragonal case.

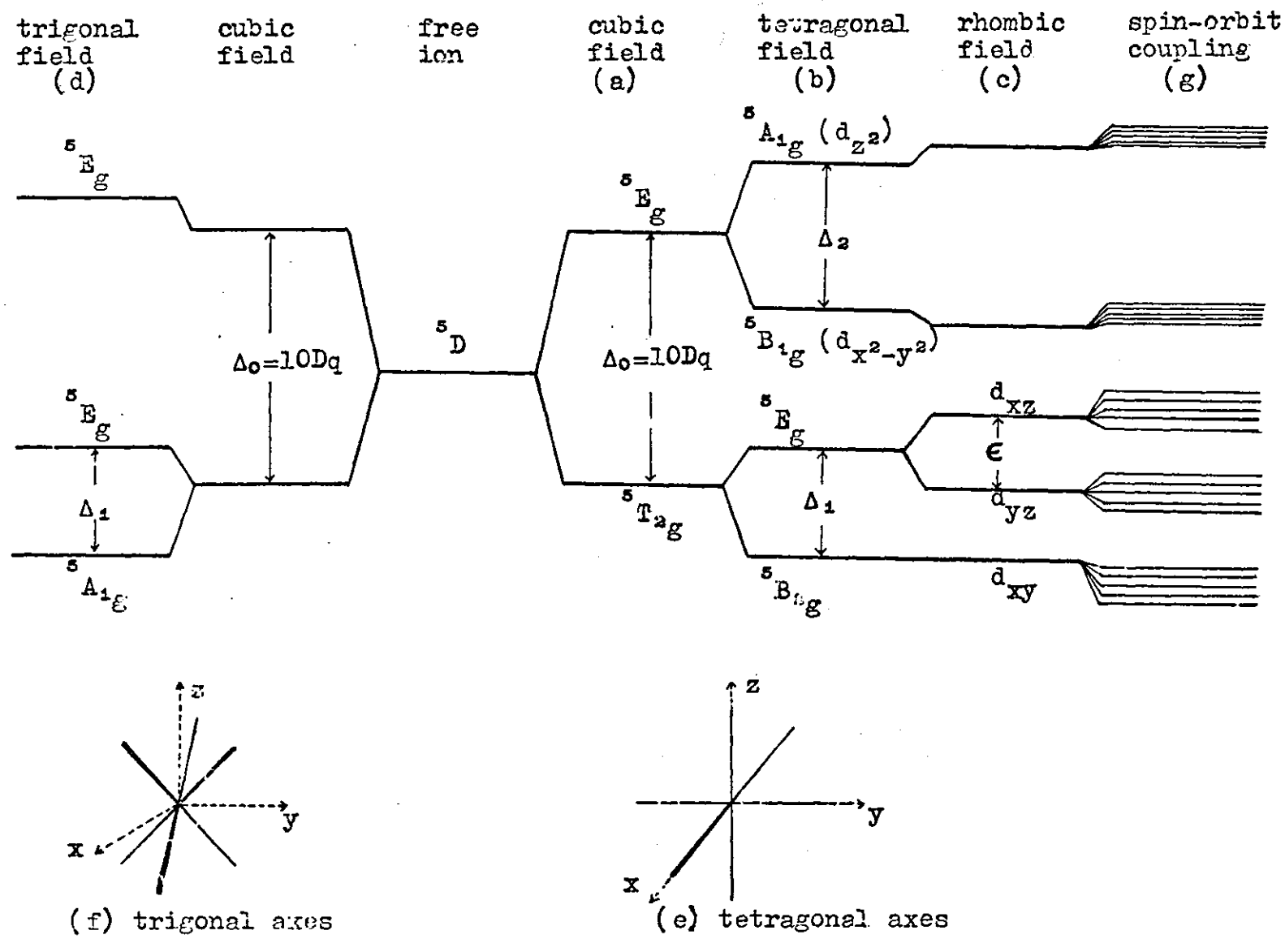

Fig. 3.1 Splitting of the ^5D term by the ligand field and spin-orbit coupling.

The distortion and the splittings, Δ_1 and Δ_2, are defined as positive in this case. However, it has been shown[32,54] that either the singlet or the doublet component of $^5T_{2g}$ may lie lowest for an axial compression, depending on the relative magnitudes of the second and fourth order radial parameters, Ds and Dt (D_{4h}) or Dσ and Dτ (D_{3d}) in Ballhausen's notation.[15]

On this crystal field model, the cubic field splitting $\Delta_o = 10\ D_q$, and the axial splittings are given by:[15]

$$\Delta_2 = 4\ Ds + 5\ Dt \qquad D_{4h}$$
$$\Delta_1 = 3\ Ds - 5\ Dt \qquad D_{4h}$$
$$\text{and}\quad \Delta_1 = 3\ D\sigma - 5\ D\tau \qquad D_{3d}$$

A single parameter axial field model,[33] which has been used in the calculation of magnetic[26,33] and Mössbauer properties,[51,52] assumes the fourth order parameter Dt or Dτ to be zero, so that for D_{4h} symmetry, $\Delta_2 = 4/3\ \Delta_1$. The additional rhombic splitting of the ^5E_g term (D_{4h}) is also given by $\epsilon = 12\ Dr$ (the smaller fourth order term being neglected).

The components of the cubic field $^5T_{2g}$ and ^5E_g terms can become intermixed under the trigonal and rhombic potential operators.

The effect of spin-orbit coupling is shown in Fig. 3.1(g), for the case $V_{NC} \gg \lambda.\bar{L}.\bar{S}$. The fivefold spin degeneracy of each orbital state is lifted, and considerable mixing of the orbital character can occur. The free ion value, λ_o, for Fe^{II} is $-103\ cm^{-1}$.

As mentioned in Chapter 1, the effects of covalent overlap with ligand orbitals can alter the relative separation of the antibonding molecular orbitals of predominantly metal d-orbital character from that predicted by the crystal field model. On the molecular orbital model of McClure,[153] account is taken of covalent interaction by replacing the crystal field splitting parameters with the differences in σ- and π-antibonding and π-bonding energies of the ligands. For high spin Fe^{II} in a tetragonal field, Δ_2 depends only on the differences in σ-antibonding energies of the axial and in-plane ligands, i.e. $\Delta_2 = \frac{8}{3}(\sigma_z - \sigma_{xy})$. The splitting of the $^5T_{2g}$ term may depend on both π-antibonding and π-bonding energies of the ligand, depending on the occupancy of the ligand orbitals which can overlap with the t_{2g} orbitals of the metal.

The Angular Overlap model has been developed to attempt to place this empirical method on a quantitative theoretical basis. An assessment of the relationships between the crystal field and molecular orbital model parameters has been given,[44] but the limitations of this correlation (mentioned also in Chapter 1) have been emphasised.

Electronic Spectra

In weak ligand fields of 'octahedral' symmetry, spin-allowed transitions are predicted between the lowest-lying component of the $^5T_{2g}$ term to the two components of the ^5E_g term. The transitions are symmetry forbidden for a centrosymmetric system, but achieve weak intensity through vibronic coupling.

In regular octahedral or trigonal symmetry, the ^5E_g level remains degenerate, and only one spin-allowed transition is predicted. However, in systems which are assumed to possess these symmetries, the observed band is often broad and asymmetric or split into two components.[92] This may be due to a dynamic Jahn-Teller effect or to additional distortions due to lattice packing effects, although the two causes are often inseparable. The magnitude of the splitting caused by the Jahn-Teller effect has been estimated theoretically[154] to be of the order of $\sim 2000\ cm^{-1}$, but the validity of the calculation is questionable.

In tetragonal or rhombic symmetry, two transitions are predicted to the components of the ^5E_g term. In the tetragonal case, the measured band separation may be expressed in terms of the axial field splitting parameters, i.e. $\Delta_2 = 4\ Ds + 5\ Dt$, but evaluation of the two parameters from the single experimental value of Δ_2 is not possible. The electronic spectrum does not allow evaluation of the $^5T_{2g}$ splitting, since the transition between the components of this term is not observed.

For systems in which considerable covalency is expected to be present, the excited term band separation may be expressed, by the method of McClure, as $\Delta_2 = \frac{8}{3} d\sigma$.

If the rhombic distortion destroys the centre of symmetry of the molecule, the intensity of the observed bands is expected to increase.

In all cases, if the splitting of the $^5T_{2g}$ level may be assumed to be small, an estimate of the cubic ligand field strength, $\Delta_o = 10\ Dq$, may be obtained from the mean of the band positions.

The spin-orbit coupling splitting of the levels is usually manifested in the broadening of the observed bands, but is rarely large enough to be resolved as fine structure.

Magnetic Properties

The magnetic properties of the ferrous ion in weak octahedral ligand fields, in the presence of an axial distortion and spin-orbit coupling, have been calculated[26,29,30,53] by the procedures outlined in Chapter 1 for magnetically dilute systems.

The calculations of Figgis et al.,[26] König et al.[29,30] and Golding et al.,[53] have been carried out within the $^5T_{2g}$ term only, and interaction with the ^5E_g term has been neglected. Under these conditions, the behaviour is identical for tetragonal and trigonal distortions. In the first two cases, the value of μ_{eff} has been tabulated in terms of the parameters $\frac{kT}{\lambda}$, K and ν ($= \frac{\Delta}{\lambda}$). The orbital reduction factor has been included in the magnetic moment operator but not in the spin-orbit coupling operator, so that the total reduction in the spin-orbit coupling interaction is manifested in the reduction of λ from λ_o. In the last case, the orbital reduction factor has not been included and the effects of covalency are allowed for only by the parameterisation of λ.

In all three calculations, only the second order terms in the axial field potential has been used, so that $\Delta_1 = 3$ Ds.

Figgis et al. have presented values for the average moment only, whereas König et al. have calculated both principal and average moments. The main features of the behaviour of the average moment are outlined below.

In regular cubic symmetry, i.e. $\nu = 0$, the isotropic moment at room temperature ($kT = 200$ cm^{-1}) is 5.64 BM ($K = 1$, $\lambda = \lambda_o$). The spin-only value for the $S = 2$ term is 4.90 BM, and therefore considerable orbital contribution is present in O_h symmetry. As the temperature is decreased, μ_{eff} increases slightly to a maximum of $\sim$ 5.70 BM ($kT = 100$ cm^{-1}) and then decreases quite rapidly towards the spin-only value. The moment is predicted to approach zero as the temperature approaches zero. Reduction in K and λ decreases both the magnitude and the temperature dependence of μ_{eff}.

In axial symmetry, the distortion has very little effect on μ_{eff} unless it raises the orbital degeneracy by an amount greater than the spin-orbit coupling. Thus for $\nu \approx \pm$ 1-2, the value of μ_{eff} at room temperature remains high i.e. $\sim$ 5.63 BM (kT = 200 cm^{-1}, κ = 1, $\lambda = \lambda_o$). For increasing positive values of Δ_1, the room temperature value of μ_{eff} drops more rapidly towards the spin-only value, than for corresponding negative values of Δ_1. However, the temperature dependence of μ_{eff} in the former case tends to be reduced as the distortion increases, whereas in the latter case the temperature dependence is still quite pronounced, and increases with increasing distortion. In both cases, reduction in κ and λ decreases μ_{eff} towards the spin only value. The retention of some orbital contribution even for large, positive values of Δ_1 indicates the efficiency of spin-orbit coupling in mixing orbital angular momentum into the ground state.

Although the symmetry of the axial distortion does not affect the magnetic properties calculated within the $^5T_{2g}$ ground term, a significant difference is found[32] when the calculation is performed within the full ^5D term. For the tetragonal case, it has been shown[32] that the mixing in of the cubic ^5E_g term by spin-orbit coupling alters the value of μ_{eff} by the order of 0.05 BM, which is often not significant since it is of the order of the experimental error of measurement. However, for the trigonal case, mixing in of the excited ^5E_g term can occur under both spin-orbit coupling and the axial field potential. It has been shown[32] that, in trigonal symmetry, the value of μ_{eff} can be extremely sensitive to small departures of the angle between any bond and the principal rotation axis from the octahedral angle, for certain values of the crystal field splitting parameters. This sensitivity is greatly enhanced by the interaction with the excited ^5E_g term.

The effect of a rhombic distortion on the magnetic behaviour has generally not been treated in detail. The removal of the remaining orbital degeneracy of the $^5T_{2g}$ term should decrease the value of μ_{eff} more rapidly towards the spin-only value, but again the actual behaviour depends on the relative magnitudes of the rhombic splitting and spin-orbit coupling effects. The excited state mixing under the rhombic potential

and spin-orbit coupling are also expected to be important. The magnetic properties should become completely anisotropic, but if, for example, the magnitudes of a positive tetragonal and an additional rhombic distortion are such that one of the components of the ^5E_g level (D_{4h}) drops close to the ground singlet i.e. ($\Delta_1 - \frac{\epsilon}{2}$) is small, then spin-orbit coupling between the two lowest levels should reintroduce orbital contribution to the moment, and the magnetic properties may have approximate symmetry about the x- or y-axis.

Exchange Interactions between Ferrous Ions:

An expression for the susceptibility and effective moment for an S = 2 ion in an exchange-coupled pair has been given,[155] in terms of g, J_{12} and T. A tabulation of the variation of the moment with T and J has also been given[156] for antiferromagnetic exchange between nearest neighbours in a linear chain of up to 10 metal ions of S = 2. These calculations are of quantitative use only in systems for which the orbital angular momentum of the ground term is completely 'quenched'.

The mechanism for exchange coupling between ferrous ions through intervening ligands will be discussed as appropriate in Chapters 4 and 5.

Mössbauer Spectra and Hyperfine Interactions

The nuclear transition most commonly studied for iron is the ^{57}Fe ($I = \frac{1}{2}$) $\leftrightarrow$ ^{57}Fe ($I = \frac{3}{2}$) transition, involving a γ-ray of energy 14.4 KeV. The Mössbauer hyperfine effects, which arise from interactions between the nuclear ground and excited spin states and the surrounding electronic change and spin density distributions, can provide information on the nature and symmetry of the ligand environment of the metal atom. Some aspects of the theory of these interactions for high-spin Fe^{II} in an 'octahedral' environment are reviewed.

(i) Nuclear Isomer Shift

This arises from the electrostatic interaction between the nuclear charge distribution and the charge density of the s electrons, which have a finite probability of existence at the nucleus. The theory of the interaction has been extensively discussed.[49,50]

The factors which affect the total s-electron density at the nucleus, and hence the isomer shift, have been investigated both theoretically and experimentally.[157-160] In high-spin compounds, the isomer shift decreases with increasing oxidation state, i.e. as the removal of 3d electrons decreases the shielding of the core 3s electrons. The characteristic range for Fe^{II} is ~ + 1.1 to + 1.6 min/sec. relative to sodium nitroprusside.

The effect of covalency on the isomer shift has been investigated, especially in low-spin compounds,[159] where the high degree of covalent overlap with ligand orbitals appears to be more important than the formal oxidation state. For high-spin Fe^{II}, the isomer shifts in series of related compounds of predominantly ionic character have been observed[160-162] to decrease fairly consistently with decreasing electronegativity of the ligand. This has been interpreted as indicative of a higher degree of metal 3d radial expansion with decreasing electronegativity, reducing the shielding on the core 3s electrons. Correlations between the isomer shifts and both quadrupole splittings and the 'internal' fields, which are also sensitive to 3d delocalisation, have been proposed[160-162] in support of this interpretation. However, an alternative explanation has been given,[163] which considers the effect to be due to overlap distortion of the core s-electrons and direct augmentation of the metal 4s-orbital occupancy, through σ-donation from filled ligand orbitals. An additional mechanism, involving reduction in the 3d-electron density, and thus the shielding of the 3s orbitals, through π-back bonding into empty ligand orbitals, may also contribute where such orbitals are available on the ligands.

There is also some evidence[164] that the isomer shift is sensitive to coordination number, when comparison is made between compounds with related ligands.

It must be noted that the measured 'centre shift' in the Mössbauer spectrum is not due solely to the nuclear isomer shift, since there is also a contribution from the second order Doppler effect.[165,166] This latter effect depends on the mean square velocity of the ^{57}Fe nucleus,

and is therefore a function of the lattice dynamics of the particular solid under investigation. It will generally introduce a temperature dependence into the measured 'centre shift' (of the order of ~ 0.05 mm/sec. per 100 K).[167] The variation of the s.o.d.e. in a series of related compounds may not be negligible compared with the variation in the measured 'centre shifts',[165,166] and it is difficult to eliminate this effect by calculation. Therefore, interpretation of small differences in measured shifts in terms of variation of the nuclear isomer shift with bonding effects may only be of limited significance.

(ii) Nuclear Quadrupole Interaction and Quadrupole Splitting

The interaction between the nuclear quadrupole moment of the ^{57}Fe $I = \frac{3}{2}$ state and a non-zero electric field gradient (e.f.g.) at the nucleus partially lifts the spin degeneracy of this state to give two sublevels, $m_I = \pm \frac{3}{2}$ and $m_I = \pm \frac{1}{2}$. The separation between these two levels and the resulting separation of the two observed peaks in the Mössbauer spectrum corresponding to transitions to these levels from the $I = \frac{1}{2}$ ground state, is termed the quadrupole splitting, ΔE_Q, and is given by:

$$\Delta E_Q = \pm \tfrac{1}{2} e^2 q Q (1 + \tfrac{1}{3}\eta^2)^{\frac{1}{2}}$$

Q is the quadrupole moment of the $I = \frac{3}{2}$ state and is positive, eq is the major component, V_{zz}, of the e.f.g. tensor † and η is the asymmetry parameter,

$$\frac{V_{xx} - V_{yy}}{V_{zz}}$$

The principal axes of the e.f.g. are defined such that $V_{zz} > V_{xx} \geq V_{yy}$. The quadrupole splitting is defined as positive if the $m_I = \pm \frac{3}{2}$ state lies highest.

The sign and magnitude of the e.f.g. in iron compounds depends on the electron configuration of the metal ion and the nature and symmetry of the ligand environment. In high-spin Fe^{II} compounds[51,52,168] the major contribution to the e.f.g. is q_{val}, which arises from the

---

† The e.f.g. and V are equated by convention

aspherical distribution of the one electron with spin antiparallel to the other five. The expectation values of q_{val} and η_{val} are not identical for each of the 3d orbitals,[51] and since the thermal transition times between these orbital levels (10^{-9} - 10^{-11} secs.) is generally greater than the quadrupole precession times ($\sim 10^{-8}$ sec.), the effective field gradient will be an average of the contributions from the various levels, each weighted by the appropriate Boltzmann factor. The sign, magnitude and temperature-dependence of the e.f.g., and hence of the quadrupole splitting, will therefore depend on the nature and magnitude of the splittings of the ^5D ground term by the ligand field and spin-orbit coupling.

The valence quadrupole splitting for high-spin Fe^{II} in distorted octahedral fields has been conveniently expressed in the form:[51,52,161]

$$\Delta E_Q = {}^2/_7\, e^2Q(1 - R) \langle r^{-3} \rangle_{3d}\, \alpha^2\, F(\Delta_t, \zeta, \lambda, T) \qquad 3.1$$

where (1 - R) is the Sternheimer antishielding factor, and $\langle r^{-3} \rangle$ is the expectation value of r^{-3} for the 3d electrons. The term ${}^2/_7\, e^2Q(1 - R)\langle r^{-3} \rangle_{3d}$ represents the maximum value of ΔE_Q, for the case of the 'odd' electron stabilised in any one of the free-ion d-orbitals. The function F( ) is a reduction factor which incorporates the decrease in ΔE_Q from the free-ion value, and the temperature dependence, due to the effects of a non-cubic ligand field and spin-orbit coupling. The effects of covalency are included by the introduction of the parameter α^2 (generally $0.6 \leq \alpha^2 \leq 0.9$)[51] to allow for the variation in $\langle r^{-3} \rangle_{3d}$ and possibly also (1 - R) by expansion of the d-orbital radial functions on compound formation. λ is also allowed to vary from λ_o, but although some treatments have used the simplifying assumption that $\frac{\lambda}{\lambda_o} = \alpha^2$,[51] it appears that the two effects of covalency must be treated separately.[161]

The absolute value of the free-ion ΔE_Q cannot be determined independently, since Q cannot be directly measured. Estimates varying from 3.7 - 4.0 mm/sec. have been obtained[169] by experimental measurement of the low-temperature limit of the quadrupole splitting in predominantly ionic compounds, for which the values of the ligand field and spin-orbit coupling parameters are available from other techniques. However, these

values include the α^2 parameter relevant to the particular compound. A value of 4.8 mm/sec. has been obtained[162] by extrapolation of an empirical 'covalency' calibration to the ionic limit, $\alpha^2 = 1$.

The sign, magnitude and temperature variation of F( ) has been given.[51,52] For regular cubic fields, F( ) = 0, and no valence quadrupole splitting should arise. In fields of tetragonal symmetry, (i.e. $\eta = 0$, $\epsilon = 0$) F( ), and hence ΔE_Q, is positive if the singlet state lies lowest, i.e. $\Delta_1 > 0$. As the ratio $\frac{\Delta_1}{kT}$ increases, F( ) increases towards a maximum value of 1 ($\Delta_1 \gg \lambda$). Also for $\Delta_1 \gg \lambda$, the temperature dependence of F( ) decreases as Δ_1 increases. As the ratio $\frac{\Delta_1}{\lambda}$ decreases, the spin-orbit coupling reduces the value of F( ), and this effect is especially important at low temperature and small values of Δ_1. For the doublet state lowest, i.e. $\Delta_1 < 0$, F( ) is negative and has a maximum value of $\frac{1}{2}$. The sign and low-temperature limit of ΔE_Q are thus extremely useful for determination of the nature of the ground state. For randomly oriented powdered samples, the sign of ΔE_Q cannot generally be obtained from the observed spectrum, but methods are available for its determination (p.48).

For trigonal distortions, the choice of a different set of basis wavefunctions for calculation of the ligand field and spin-orbit coupling effects, reverses the sign of F( ) for the two possible orbital ground states,[170] which can provide a means of distinguishing the two axial symmetries in a compound of unknown structure.

The effect of a rhombic field component (i.e. $\eta \neq 0$, $\epsilon \neq 0$) on the value of F( ) has also been calculated.[51,52] The rhombic distortion has only a small effect on F( ) when ϵ is relatively small, decreasing F( ) when $\Delta_1 > 0$, and increasing it when $\Delta_1 < 0$. However it is not generally possible to relate the effects to the nature of the rhombic distortion. Intermixing of the states under the rhombic operator may also alter the e.f.g. contribution of the ground levels.

Comparison of measured quadrupole splittings over a temperature range to the predicted behaviour of equation 3.1, may allow evaluation of the ligand field splitting, spin-orbit coupling and covalency parameters. However, as in the case of magnetic measurements, the multiplicity of parameters make unambiguous evaluation difficult. In

addition, there are several other contributions to the e.f.g. which may require consideration in particular cases. A lattice e.f.g. arises from an asymmetrical distribution of ionic charges in the lattice, and may not be negligible, especially in highly distorted systems. Attempts have been made to relate this e.f.g. to the ligand field splitting parameters,[51] but point-charge calculations have shown[171] that this approach may be seriously misleading. An additional effect of covalency, which is well known in low-spin Fe^{II} compounds, is the production of a 'bonding' e.f.g., caused by an aspherical distribution of ligand electron density approaching closer to the nucleus, through covalent overlap, than would otherwise be possible. These two effects would be expected to produce a temperature-independent contribution to the e.f.g. The effects on the valence and lattice e.f.g.'s of thermal variation of the lattice structure has also been considered.[172] Finally, asymmetric occupation of the 4p orbitals through covalency could also give rise to a contribution to the e.f.g.

Although in many cases, quadrupole splitting data on high-spin Fe^{II} compounds has been interpreted only in terms of the 3d valence e.f.g. one estimate[172] indicates that contributions from other sources could amount to as much as 1 mm/sec. Owing to these considerations and to the unknown structural factors in the compounds studied in this work, interpretation of quadrupole splitting data has been generally limited to qualitative comparison of the trends within the series of related complexes.

(iii) Nuclear Zeeman Interaction and Magnetic Hyperfine Splitting

The complete lifting of the nuclear spin degeneracy by a magnetic field at the nucleus has been mentioned in Chapter 1. The field, H, may be externally applied or may originate within the atom through the Fermi contact and other interactions. The nuclear Zeeman splitting can be represented by the Hamiltonian:

$$\mathcal{H}_M = -g_N \mu_N \bar{I} \cdot \bar{H}$$

for which the eigenvalues are

$$E_M = -g_N \mu_N m_I H$$

where m_I can take values, I, I-1, ... -I,

g_N is the nuclear g-factor

and μ_N is the nuclear magneton.

The ground, $I = \frac{1}{2}$ level for ^{56}Fe is split into two substates, and the $I = \frac{3}{2}$ level into four substates. The selection rule for transitions of magnetic dipole character between these substates is $m_I^e - m_I^g = 0, \pm 1$, so that six of the possible eight transitions should be observed. Assignment of the observed peaks to the appropriate transitions (using the relative intensity ratios) and measurement of the peak separations, enables the field at the nucleus to be determined by solution of simple simultaneous equations in terms of the g_N factors for the ground and excited states.[167]

In high-spin Fe^{II} compounds, contributions to the 'internal' field, H_n, arise from both the spin and orbital magnetism of the ground state of the metal ion.[173,174] The former gives rise to both the Fermi contact interaction (Chapter 1) and also to an anisotropic dipolar interaction in a non-cubic environment. There is also a nuclear interaction with the orbital current produced by unquenched 3d orbital angular momentum. The Fermi contact term has been calculated[174] to be -550 kG for the free ferrous ion, while the dipolar and orbital fields are of the order of +10 to 100 kG each. All three contributions are affected by covalency, through their various dependences on the 3d radial functions, and a large spread in the magnitude of the total 'internal' fields is observed with variation of the ligand environment.

The requirement of relatively long spin-relaxation times for production of a static 'internal' field, and thus observation of magnetic splitting, has been mentioned in Chapter 1. In spontaneously magnetised materials, the 'internal' field corresponds to the average values of the atomic momenta as determined by the nature and magnitude of the exchange interactions. Since the average magnetisation becomes zero at the Curie or Néel point, observation of the collapse of the magnetic hyperfine splitting pattern provides a means of determining the ordering temperature.

In paramagnetic high-spin Fe^{II} compounds, where spin-relaxation is generally fast, magnetic hyperfine splitting may be observed if an external field, H_o, is applied to produce an appreciable magnetisation.[173]

Fields of at least 30 kG are usually required. The effective field 'seen' by the nucleus is then

$$H_{eff} = H_o + \frac{\langle S \rangle}{S} H_n$$

where $\frac{\langle S \rangle}{S}$ is the fractional magnetisation produced. The magnetic hyperfine interaction due to the 'internal' field, H_n, may be represented phenomenologically in an analogous manner to that used in e.p.r. spectroscopy by:[175]

$$\mathcal{H}_M = A\, \bar{I}.\bar{S}'$$

where S' is the effective spin of the ground state of the metal ion, and A is the effective hyperfine interaction tensor, which incorporates the effects of orbital momentum. The symmetry of the A tensor may then provide some information on the symmetry of the magnetic properties.

If a quadrupole interaction is present in addition to the magnetic interaction, the number, separation and relative intensities of the observed peaks in the spectrum may become quite complex. The nature and energies of the nuclear spin substates will depend on the relative magnitudes of the quadrupole and magnetic interactions, the symmetry of the e.f.g., and the orientation of the magnetic field axes to the principal axes of the e.f.g.

The eigenvalues of the combined magnetic and quadrupole interaction Hamiltonians may be obtained quite readily for certain cases, in which there is a simple relationship between the magnetic field direction and the e.f.g. axes.[167] The m_I values still serve as good quantum numbers in these cases, and the intensity ratios of the six peaks can be computed and used to assist in peak assignment.

However, in the general case of a non-axially symmetric e.f.g., with the magnetic field direction at some arbitrary angle to one of the principal e.f.g. axes, interpretation of the spectrum becomes extremely difficult. In such systems, as the value of η increases, the eigenstates of the combined interaction may no longer correspond to pure m_I states, but to linear combinations of the basis set. The transition probabilities between ground and excited states for which $m_I^e - m_I^g = \pm 2$, can become

non-zero, and more than six peaks may be observed in the spectrum. The relative intensities will then depend on the extent of mixing of the states, and their usefulness in assignment of the observed peaks is decreased. Methods for computer simulation of the observed spectra of such systems have been developed,[176] but require prior estimation of reasonable values for the magnetic and e.f.g. parameters and the angle transformations between their respective axes. An analytical method has also been given[177] for derivation of the nuclear energy level scheme and hyperfine parameters from the observed spectrum, but is quite complicated for the general case.

An important application of combined magnetic and quadrupole interactions is the determination of the sign of the quadrupole splitting in randomly-oriented powdered solids. It has been shown[178] that an externally applied field will cause the transition to the $m_I = \pm \frac{3}{2}$ state to split into a doublet, while that to the $m_I = \pm \frac{1}{2}$ state will split into a triplet (unresolved quartet). If the doublet lies at more positive velocity in the observed spectrum, the quadrupole splitting is positive (as defined for the $m_I = \pm \frac{3}{2}$ state lying highest in energy).

CHAPTER 4 EXPERIMENTAL RESULTS AND DISCUSSION ON THE Fe^{II} COMPLEXES WITH SUBSTITUTED PYRIDINES

Polymeric FeL_2Cl_2 complexes have been prepared with the ligands, L = 4-CN-py, 3-CN-py, 4-Cl-py, 3-Cl-py, 3,5-Cl_2-py, 3-Br-py and 3-I-py, by reaction of the metal salt with the stoichiometric quantity of the ligand, in anhydrous ethanol solution and in a nitrogen atmosphere. The corresponding bromide complexes with 4-CN-py and 3,5-Cl_2-py have also been prepared by a similar method. No pure complexes of the FeL_4X_2 type could be obtained with these ligands for the chloride and bromide, but reaction of ferrous iodide with both 2:1 and 4:1 ligand to metal ratios resulted in the isolation of relatively unstable FeL_4I_2 complexes (L = 4-CN-py, 3,5-Cl_2-py) in each case. The preparative details are given at the end of this chapter.

The extreme insolubility of the polymeric complexes in all common solvents which do not decompose them made recrystallisation impossible, but the elemental analyses (Table 4.1) and the Mössbauer spectra indicate their purity. The polymers are relatively stable, the bromides less so than the chlorides, and if stored under dry nitrogen, remain undecomposed for several weeks. The complexes with the more volatile ligands (i.e. 3-Cl-py, 4-Cl-py) tend to lose ligand after a few days' storage, and it was generally desirable to prepare new samples immediately prior to each physical measurement. The iodide complexes darken considerably and lose ligand after a few days. All the compounds are completely decomposed by water, and deteriorate fairly rapidly on exposure to moist air.

The compound $Fe(3\text{-Cl-py})_2Cl_2$ was prepared many times by the same procedure. In almost every case, the complex precipitated after ~ 10 secs. stirring as a microcrystalline solid, and on the basis of physical evidence is denoted form A. In one preparation, the only observed difference was that the solid precipitated immediately on mixing the chloride and ligand solutions, as a very fine powder. This sample was found to differ in its electronic properties from form A, and is denoted form B. It appeared to be slightly less stable than the A form towards loss of ligand.

Structural and Bonding Considerations

As stated in Chapter 2, the basic molecular structure of the polymeric complexes is assumed to be similar to that of α-$Copy_2Cl_2$. Assuming that the N-Fe-N bond coincides closely with the z-axis of the d-orbital coordinate system, then from consideration of the relative positions of heterocyclic amines and the halides in the spectrochemical series, the axial ligand field would be expected to be stronger than the in-plane field, so that the orbital ordering scheme should be that for a tetragonal compression along z, (Fig.3.1(b)). Additional distortions may be expected, lowering the microsymmetry of each metal ion from D_{4h}. The halide bridges may be non-planar, the metal-halide bond angles may depart from 90°, and the bond lengths in the x,y plane may not all be equivalent. In the somewhat related compound $FeCl_2 \cdot 2H_2O$, which has a similar halogen-bridged structure,[179] two discrete Fe-Cl bond lengths, in diagonal pairs, are present, and the Cl-Fe-Cl bond angle is ~ 88°.

In the amine complexes, the extent of such distortions may depend on the steric requirements of the ring-substituents. It may be expected that with substituents in the 3- and 3,5-positions, orientation of the rings so that their planes are normal to the chain direction would be favoured, to minimise interaction between the rings on adjacent Fe^{II} atoms. However the effects of the substituents in packing together of the chains may impose other orientations of the rings. Molecular model construction (using the structural parameters for α$Copy_2Cl_2$)[105] indicates that considerable steric interference would occur between the 2-hydrogen atom of the ring and the bridging halide for angles between the plane of the ring and an M-Cl bond of less than ~ 10-15°. Owing to the possibility of these distortions, the orbital ordering scheme in these compounds may be better represented by Fig. 3.1(c).

It is of course possible that the halide ions do not lie close to the x and y axes of the metal d-orbital coordinate system. Small departures of the halides from these axes would affect the relative separations but not the order of the levels in Fig. 3.1(c). An extreme situation could be envisaged in which the halides are positioned at ~ 45° to the x and y axes. In this case, the energy level scheme in Figs. 3.1 (a) - (c) would be altered by interchanging the dxy and the dx^2-y^2 orbitals, which

does not greatly affect the electronic properties. This situation is proposed for the rhombically-distorted FeF_2,[51] but there is also a significant contribution to the ground state from admixture of the d_{z^2} orbital with the dx^2-y^2 under the rhombic potential.

The isolation of two distinct forms of $Fe(3\text{-Cl-py})_2Cl_2$, both of which appear to have six-coordinate chloride-bridged structures, indicates that considerable structural variation may occur within this series of complexes. The X-ray powder patterns of the two forms were obtained, together with those of $Fe(3\text{-CN-py})_2Cl_2$ and $Fe(3,5\text{-Cl}_2\text{-py})_2Cl_2$ for comparison. The two forms gave significantly different patterns, and although none of the compounds gave identical patterns, the most marked similarities were between the A form and $Fe(3,5\text{-Cl}_2\text{-py})_2Cl_2$, and the B form and $Fe(3\text{-CN-py})_2Cl_2$.

The degree of covalency in these complexes may be quite considerable. In addition to σ-bonding to the metal through the ring N-atom, the amine ligands have filled π- and empty π*-orbitals available which may overlap with the metal dxz and dyz orbitals. Since the CN- and halogen-substituents have electron-withdrawing inductive effects, the reduction of ring electron density should favour π-back donation from the metal to the amine π*-orbitals. The general importance of back-donation in the bonding of pyridine-type ligands to metal ions have been established,[180] and some evidence has been given that 3- and 4-CN-py have quite a high tendency to back-accept.[181] Both σ- and π-covalent interactions between the metal orbitals and those of the bridging halides are also possible.

Electronic Spectra

The diffuse reflectance spectra of the complexes have been measured in the 4000 - 26,000 cm^{-1} region at room temperature and the results are collected in Table 4.2. All the complexes show a relatively weak resolved doublet in the 5000 - 10,000 cm^{-1} region, due to the metal $^5T_{2g} \leftrightarrow {}^5E_g$ transition, but the position of the lower component is difficult to measure accurately, since it is somewhat obscured by a ligand vibration. There is also an intense band in the 20,000 - 26,000 cm^{-1} region due to metal-ligand charge transfer mechanisms or ligand $\pi \leftrightarrow \pi^*$ transitions.

In the polymeric complexes the relatively large separation of the bands (3,000 - 3,800 cm^{-1}) is consistent with a tetragonally- or rhombically-distorted octahedral structure. Since considerable covalency may be expected in these compounds, the excited state splittings, Δ_2, are best discussed in terms of the McClure model. σ_z, due to the axial amine ligands, is expected to be larger than σ_{xy}, due to the halide ions in the plane, and $d\sigma$ is therefore positive. The calculated values are listed in Table 4.2.

For the chloride complexes, the $d\sigma$ values are significantly lower than that for $Fepy_2Cl_2$ (Δ_2 = 4100 cm^{-1}, $d\sigma$ = 1540 cm^{-1}),[88,92] which reflects the decrease in the σ-donor ability of the amine by introduction of the electron-withdrawing groups. There does not appear to be a definite correlation between the $d\sigma$ values and the base strength of the amine (Table 2.1), particularly when comparing the values for the CN-substituted amines with those for the halogen-substituted amines. This may indicate a significant variation in σ_{xy} within the series. Comparing the $d\sigma$ and pKa values for the complexes with halogen-substituted pyridines, the $d\sigma$ value of the B form of $Fe(3\text{-Cl-py})_2Cl_2$ appears to be anomalously low relative to that of the A form. Any weakening in the amine to metal σ donation would not only decrease σ_z but may also increase σ_{xy}, since the resulting larger effective charge on the metal ion may enhance the halide to metal σ donation. A possible cause of this effect may be that in the B form packing considerations cause the rings to take up an orientation which produces steric interference between the substituents or between the 2-hydrogens and the chloride bridges. A lengthening of the Fe-N bonds may then occur to minimise the interaction, with possibly, simultaneous alterations of the arrangement in the plane. The possibility of the two forms corresponding to cis and trans isomers of the compound seems unlikely, owing to the low-temperature transition from the A to the B form, which has been detected by Mössbauer spectroscopy and is discussed below.

The $d\sigma$ values are larger by ~400 - 800 cm^{-1} and opposite in sign to those found[88,89] for the monomeric octahedral FeL_4Cl_2 complexes (L = py, β-pic, γ-pic, iso-quin). σ_{Cl} may be expected to decrease when the halide is bridging rather than terminal, as suggested by the longer bond lengths in the former case (e.g. in α-$Copy_2Cl_2$[105] and $Copy_4Cl_2$,[182]

the Co-Cl distances are 2.49Å and 2.32Å, respectively). The larger values of $|d\sigma|$ in the polymers suggest that the decrease in σ_{Cl} outweighs that in σ_L (due to the presence of the electron withdrawing substituents). It is also possible that a rhombic distortion in the polymers may increase the excited state splitting, relative to that in the monomers.

The estimated values of 10 Dq, obtained from the mean of the band positions, are included in Table 4.2. The magnetic and Mössbauer data, presented later, suggest that the $^5T_{2g}$ splitting is relatively small, and therefore these values may be quite meaningful. The values are fairly constant (~7600 - 8000 cm^{-1}) for the chloride complexes, although that for the B form of $Fe(3\text{-Cl-py})_2Cl_2$ is again anomalously low. The values are ~ 1000 cm^{-1} lower than in the FeL_4Cl_2 monomers,[88,89] reflecting the decreased bonding strength of both the substituted amines and the bridging chloride, and also the expected reduction in the total field strength in passing from an 'N_4Cl_2' to an 'N_2Cl_4' environment.

For the bromide complexes measured, the values of Δ_2 (and thus $d\sigma$) are slightly higher, and the values of 10 Dq slightly lower, than those for the corresponding chloride complexes, which is consistent with the relative ligand field strength of the two halides. The differences are much less marked than those found in the monomeric FeL_4X_2 complexes,[88,89] e.g. the difference in $d\sigma$ for the $Fe(3,5\text{-Cl}_2\text{-py})_2X_2$ complexes is virtually negligible.

The band positions in the spectra of the 4:1 iodide complexes are similar to those found for the complexes FeL_4I_2 (L = py, γ-pic, iso-quin),[89] and they are therefore assumed to possess the same monomeric trans octahedral structure. The $d\sigma$ value for $Fe(4\text{-CN-py})_2I_2$ is only slightly lower than those in the other FeL_4I_2 complexes, but the value for $Fe(3,5\text{-Cl}_2\text{py})_2I_2$ is comparatively very small. The values of 10 Dq are however somewhat higher than those in the py, γ-pic and iso-quin complexes. This may suggest a greater degree of metal to amine π-back bonding with the cyano- and halogen-sibstituted pyridines. Decrease of the metal electron density by back donation should enhance the transfer of charge along the Fe-I bond, thus increasing σ_I and contributing to the total ligand field strength. Such an effect may also explain the small differences in $d\sigma$ for the polymeric chloride and bromide complexes.

I.R. Spectra

I.R. spectroscopy has not proved particularly useful in the investigation of these compounds. The spectra of the complexes compared with those of the free ligands generally show the frequency shifts and splittings which are expected when the amine is coordinated through the N-atom.[180]

The spectra of the two forms of $Fe(3\text{-}Cl\text{-}py)_2Cl_2$ show significant differences in the relative intensity and splitting of the ring breathing modes in the 1200 - 1000 cm^{-1} region. The C-C and ring C-N stretching modes in the 1600 - 1400 cm^{-1} region also appear to shift to slightly higher frequencies in the A than in the B form.

The stretching frequency of the cyano-group in the complexes with 3- and 4-CN-py showed only very small shifts (< 6 cm^{-1}) from the positions in the free ligands. This is consistent with bonding through the ring N-atom, and does not suggest any direct involvement of the cyano-group in bonding to the metal, contrary to a previous proposal[181] based on intensity measurements in solution.

For polymeric halide-bridged complexes of this type, one metal-nitrogen and two metal-halogen vibrations are predicted[106-109] to be active in the far I.R. The free ligands are generally transparent below ~ 300 cm^{-1}, and in the chloride complexes a broad adsorption envelope in the 270 - 200 cm^{-1} region appears to contain all the metal-ligand vibrations. Assignment of individual bands has not however been possible.

Mössbauer Measurements

The Mössbauer spectra of the first six polymeric chloride complexes in Tables 4.1 and 2 have been obtained at 300 K, 77 K, 4.2 K and 1.4 K. The remaining complexes all contain a 'heavy' atom (Br or I) and were found to give poorly resolved spectra, and the results on these compounds are given only where they are considered to be of sufficient accuracy.

Selected spectra for the six compounds, showing the best fit to the data obtained by a least-squares program, are presented in Figs. 4.1 to 4.6. The parameters obtained from the fitting are collected in Table 4.3, which also contains the room temperature parameters for a few of the other complexes.

All the complexes, except for the A form of $Fe(3\text{-}Cly\text{-}py)_2Cl_2$ showed one quadrupole doublet at 300 and 77 K for several preparations of each compound. The spectra at 300 and 77 K were obtained for five different preparations of $Fe(3\text{-}Cl\text{-}py)_2Cl_2$. In the first four cases, only one quadrupole doublet with small splitting (Fig. 4.4 (a)) was found at both temperatures, provided that the samples had not previously been cooled below 77 K. One of these samples was cooled to 4.2 and rewarmed to 77 K, and at the latter temperature the spectrum contained four peaks, (Fig. 4.4 (b)) corresponding to the original doublet and, in addition, a weaker doublet with larger quadrupole splitting. It was initially assumed that the extra peaks were due to a decomposition product. However, the fifth sample (from the odd preparation mentioned above) showed one doublet at 300 and 77 K with a significantly larger quadrupole splitting at both temperatures (Figs. 4.5 (a) and (b)), the value at 77 K being virtually identical to that of the new species in the previous sample (Table 4.3). The Mössbauer spectrum in fact provided the first indication that two different forms of the compound exist. This difference was then confirmed by X-ray powder patterns and the electronic spectra, as mentioned above, and the form with larger quadrupole splitting has been denoted form B. Several attempts were made to reproduce the preparation of pure form B at room temperature, but the Mössbauer spectra above 77 K indicated that only in one subsequent preparation was any B form obtained, as the minor product in a predominantly A form sample.

It therefore appears that although form B can be prepared directly at room temperature, form A is usually the preferred product. A structural transition appears to occur at some temperature between 77 and 4.2 K, in which the A form is to some degree converted to form B. The transition does not appear to be completely reversible, since some form B persists when the sample is rewarmed. Furthermore, the pure B form, when cooled to 4.2 K and rewarmed to 77 K, does not show any new Mössbauer peaks attributable to the A form, although the peaks are considerably broadened, as seen by comparison of the half-widths in Table 4.3.

The spectra of the other four compounds were remeasured at 77 K after cooling to 4.2 K, to investigate the possibility of structural changes at low temperature. No new peaks were observed, although there was generally

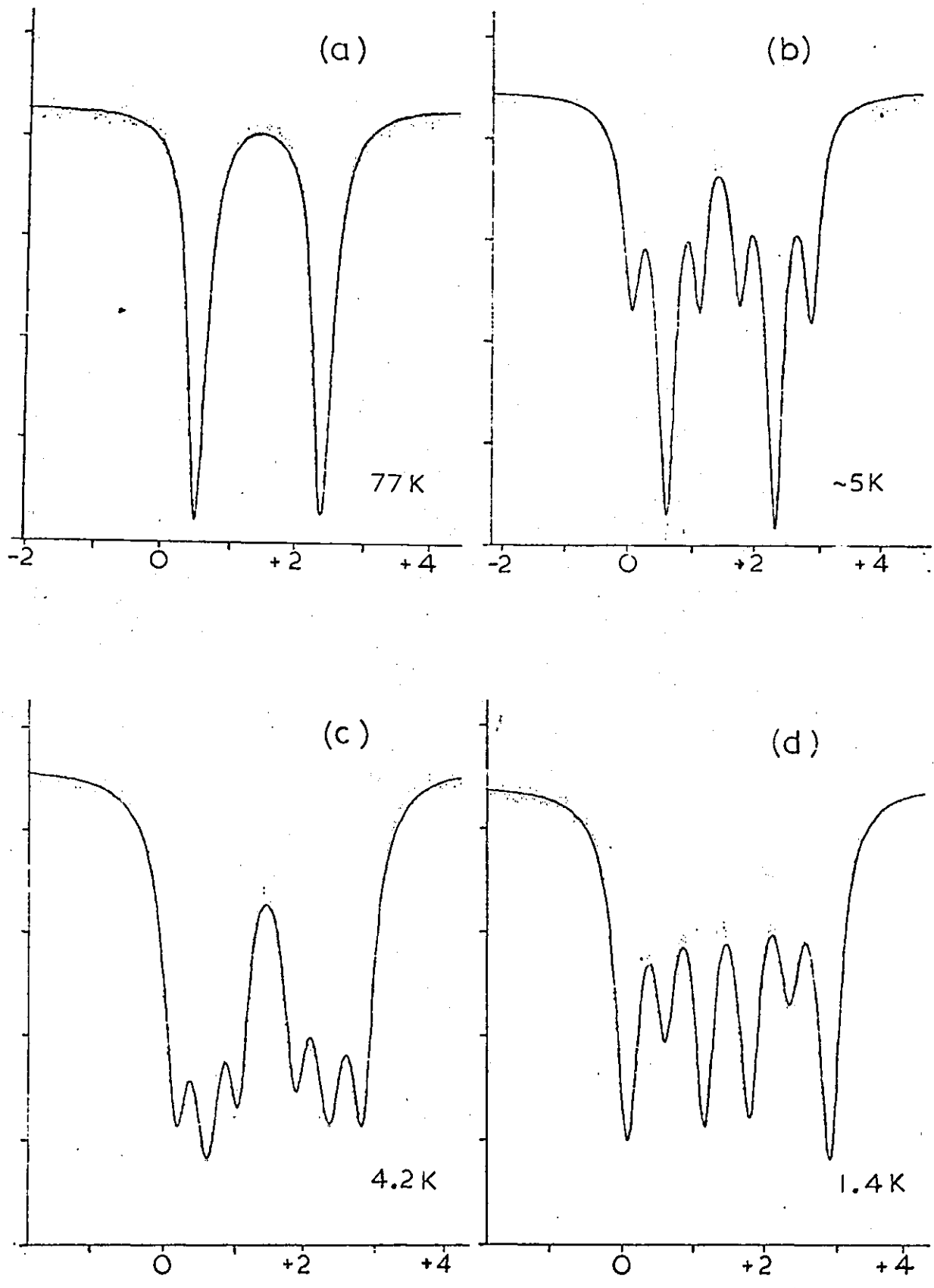

Fig. 4.1. Mössbauer Spectra of $Fe(4\text{-}CN\text{-}py)_2Cl_2$

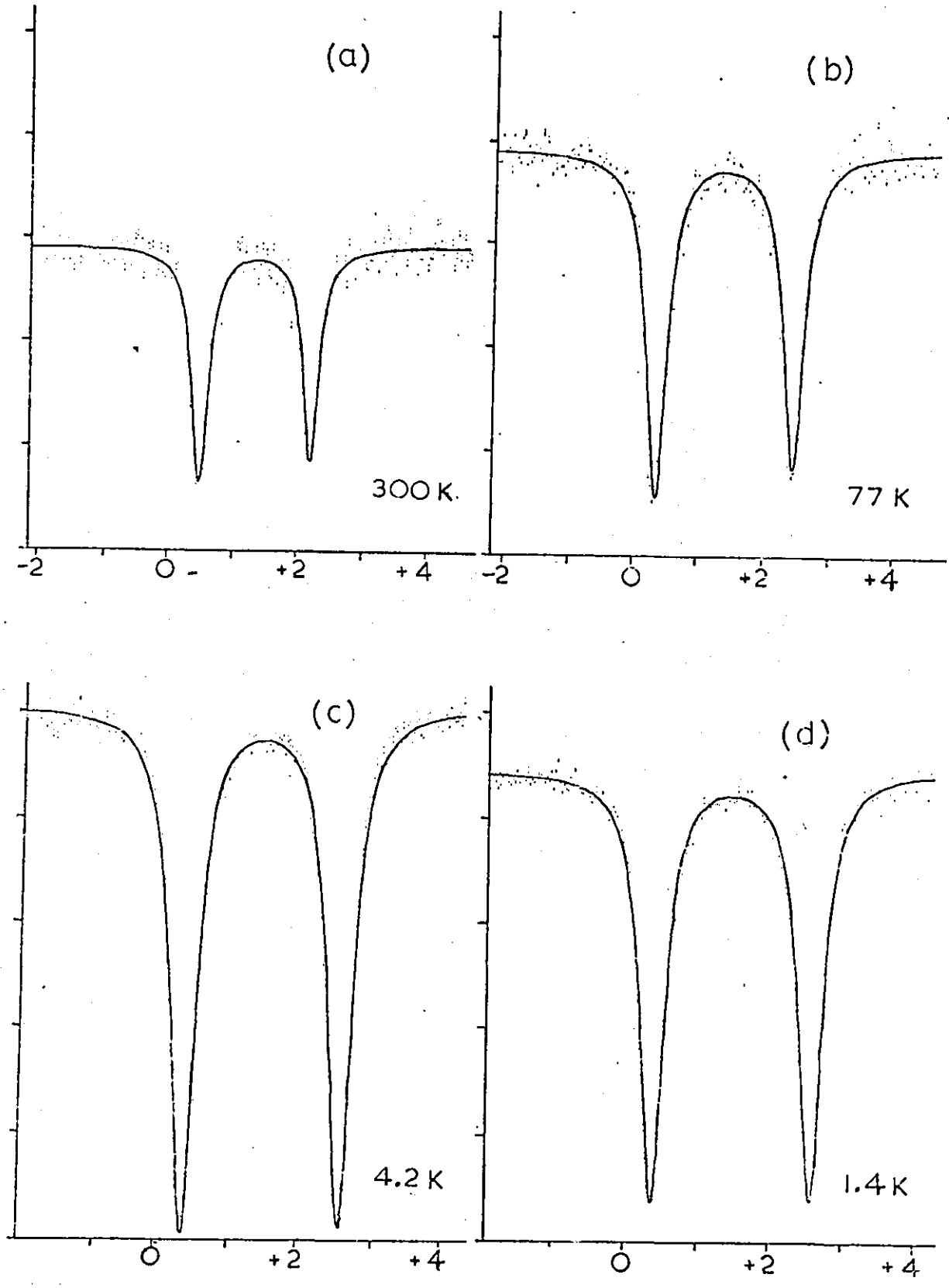

Fig. 4.2. Mössbauer Spectra of $Fe(3\text{-}CN\text{-}py)_2Cl_2$

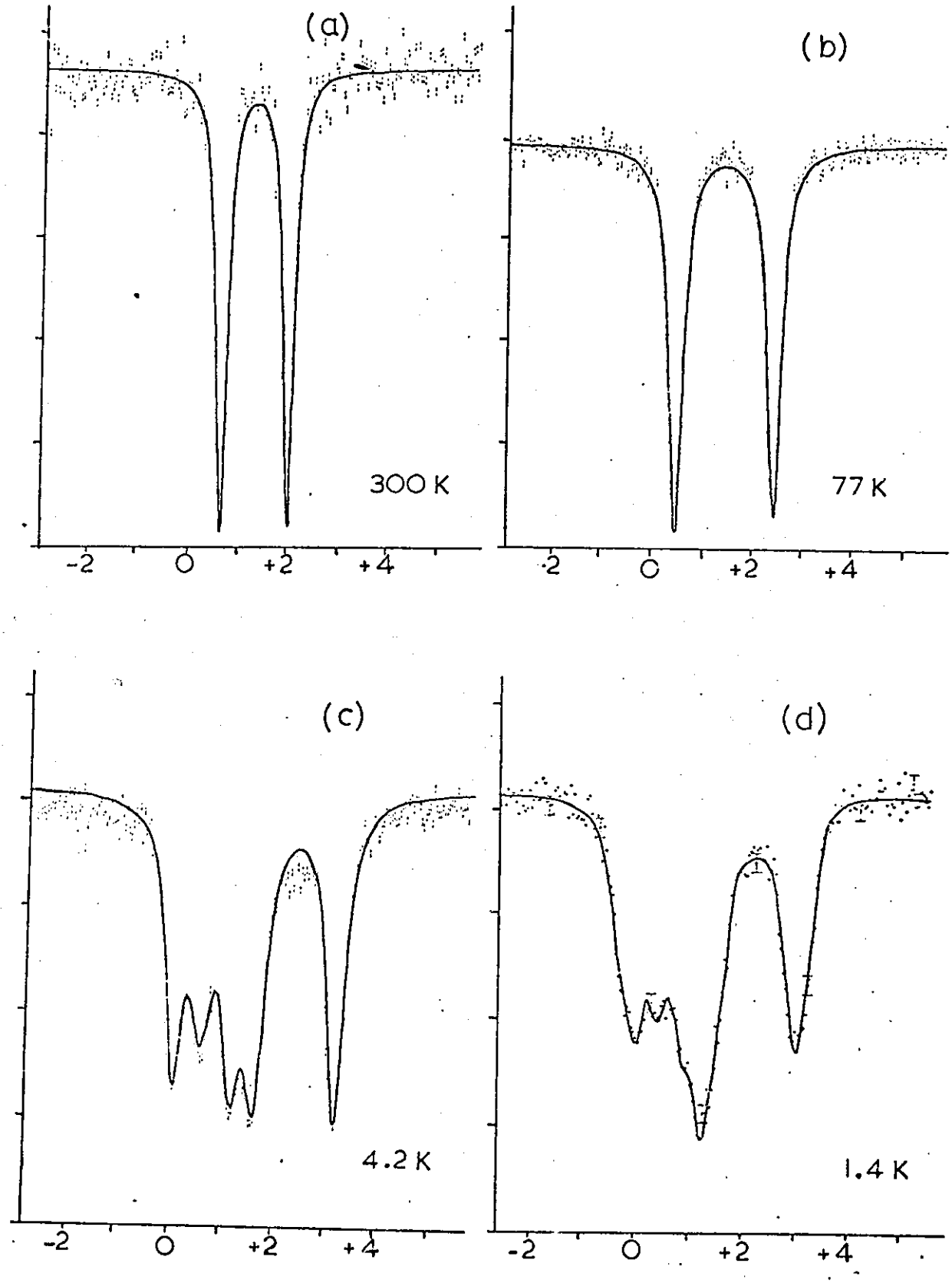

Fig. 4.3. Mössbauer Spectra of $Fe(4\text{-}Cl\text{-}py)_2Cl_2$

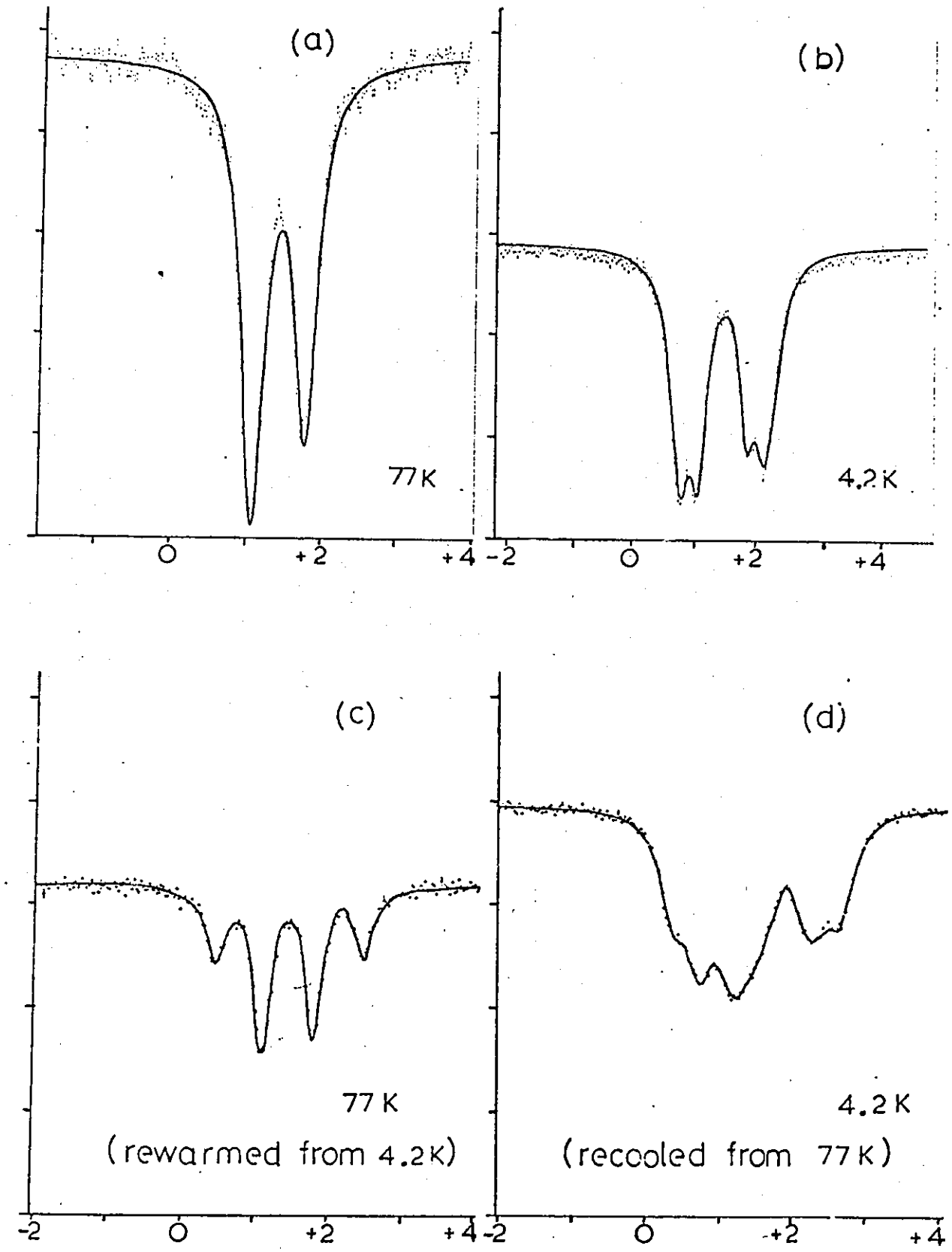

Fig. 4.4. Mössbauer Spectra of $Fe(3\text{-}Cl\text{-}py)_2Cl_2$ (A)

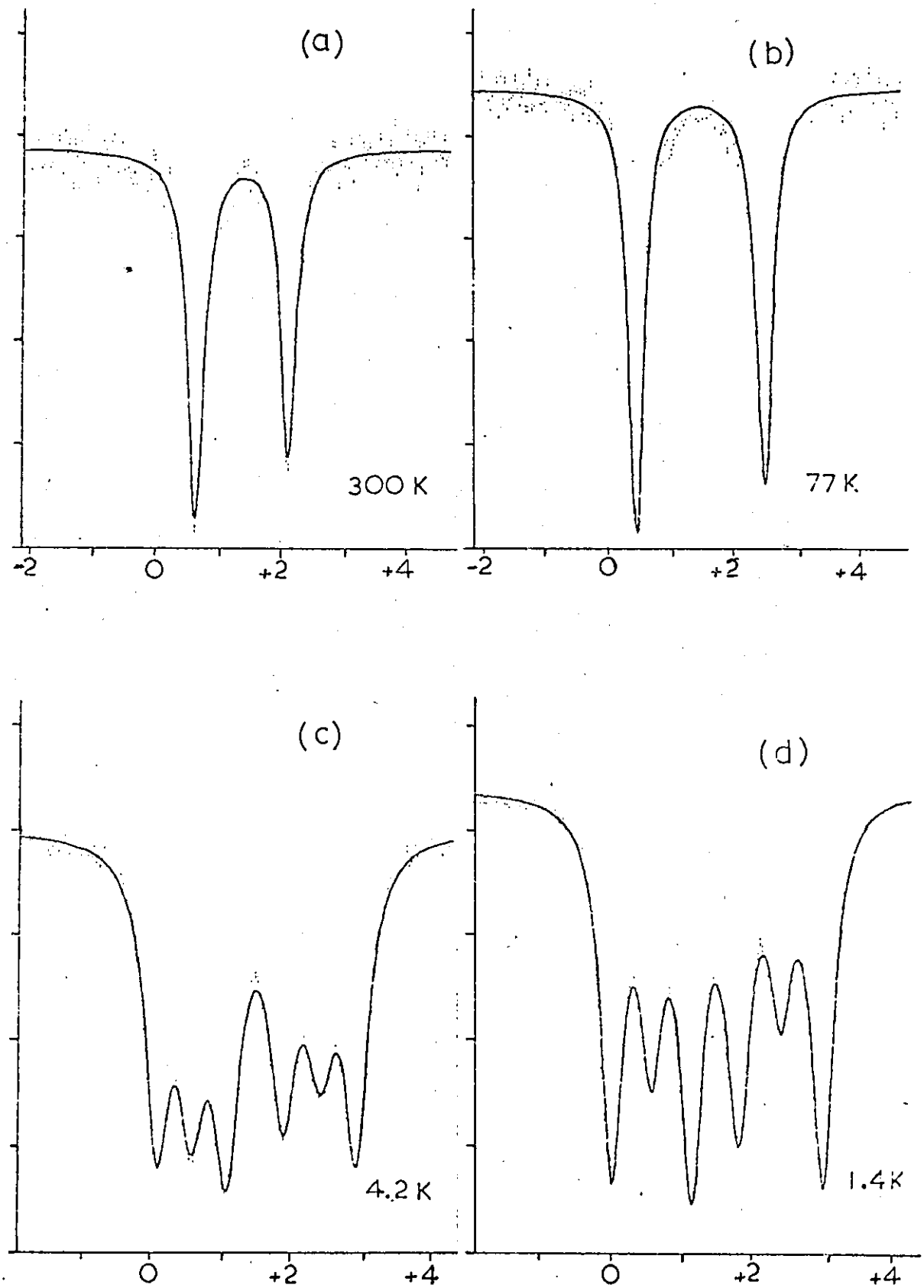

Fig. 4.5. Mössbauer Spectra of $Fe(3\text{-}Cl\text{-}py)_2Cl_2$ (B)

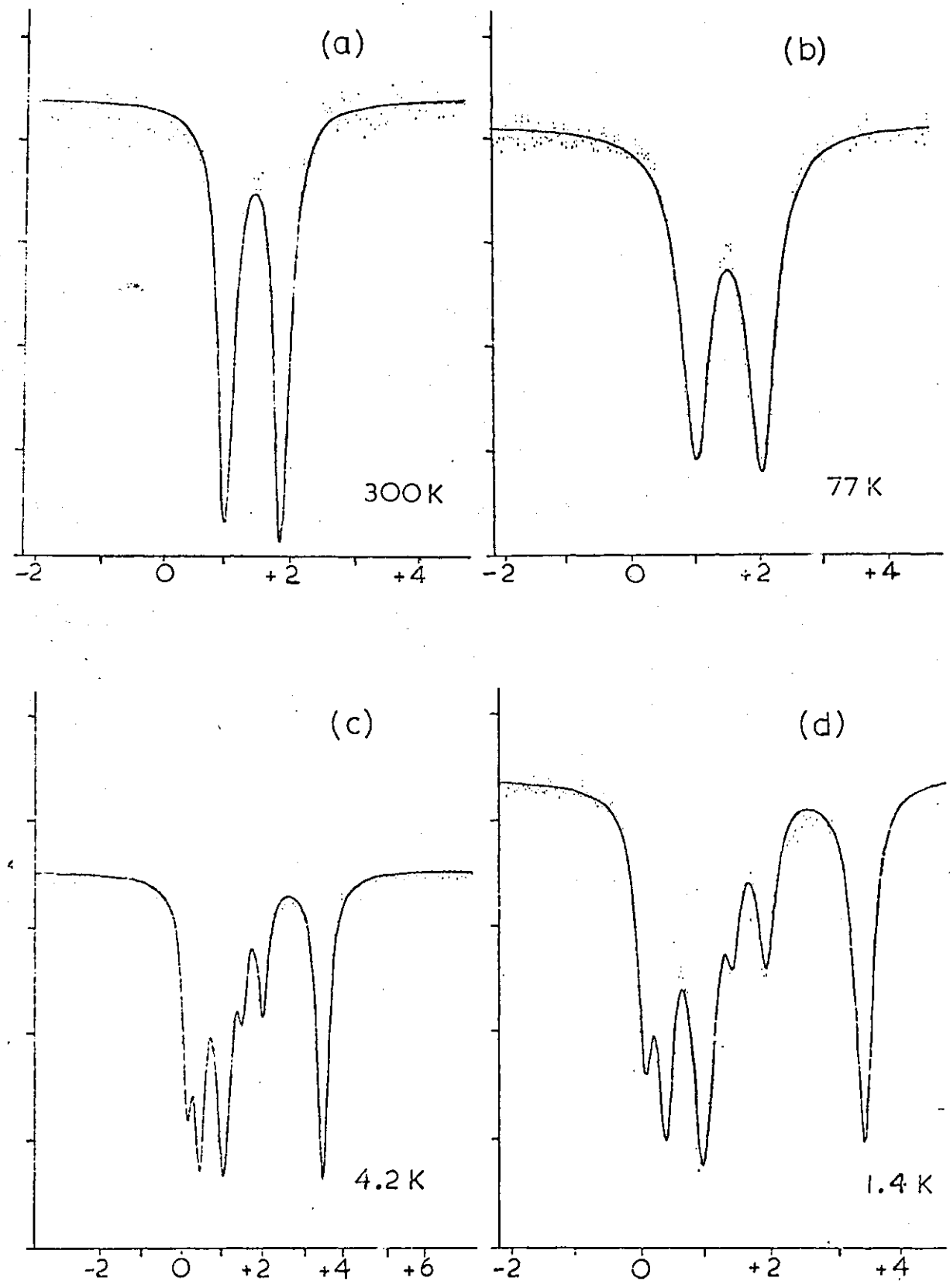

Fig. 4.6. Mössbauer Spectra of $Fe(3,5\text{-}Cl_2\text{-}py)_2Cl_2$

a slight increase in the half-widths of the lines, except in the case of $Fe(3,5\text{-}Cl_2\text{-}py)_2Cl_2$, which showed a slight decrease (Table 4.3). These observations cannot discount the possibility of a completely reversible structural change, but the spectra at 4.2 and 1.4 K appear to be consistent with the presence of only one species at these temperatures.

As can be seen from Figs. 4.1 to 4.6, all the complexes, except for $Fe(3\text{-}CN\text{-}py)_2Cl_2$ and possibly also $Fe(3\text{-}Cl\text{-}py)_2Cl_2$ (A) (discussed later), exhibit magnetic hyperfine splitting at 4.2 and 1.4 K. Since the spin-relaxation rates in paramagnetic high-spin Fe^{II} complexes are generally very fast, this observation, and evidence from the magnetic susceptibility data presented later, confirm that magnetic ordering is present at least in the complexes $Fe(4\text{-}CN\text{-}py)_2Cl_2$, $Fe(4\text{-}Cl\text{-}py)_2Cl_2$, $Fe(3\text{-}Cl\text{-}py)_2Cl_2$ (B) and $Fe(3,5\text{-}Cl_2\text{-}py)_2Cl_2$.

Nuclear Isomer Shifts*

The centre shift values at 300 K of all the complexes in Table 4.3 are in the characteristic region for high-spin Fe^{II} complexes, and increase by ~ 0.1 mm/sec. at 77 K, due presumably to the second order Doppler effect. The values are very similar to that reported[100] for $Fepy_2Cl_2$ (1.33 mm/sec. at 300 K, 1.46 mm/sec. at 78 K), and are only slightly higher than that for $Fepy_4Cl_2$[89] (1.31 mm/sec. at 300 K). The values are ~ 0.2 mm/sec. higher than those observed[89] for FeL_2X_2 compounds (L = quin, 3Me-iso-quin) with tetrahedral symmetry, which is consistent with the previously reported sensitivity of the isomer shift to coordination number and geometry in compounds with related ligands.

The variation of the values within the series is very small, and any correlation with bonding may be invalidated by variation of the second order Doppler effect. However, it is noted that the values for the bromide complexes are slightly lower than those for corresponding chlorides which is consistent with a greater degree of metal 3d delocalisation with the less electronegative halide. It is also

---

* Values are quoted relative to sodium nitroprusside.

observed that the values and temperature dependence of the centre shifts for the two forms of $Fe(3\text{-}Cl\text{-}py)_2Cl_2$ are significantly different. If this difference is due mainly to variation in the second order Doppler effect, it provides additional evidence for substantially different lattice structures for the two forms.

The centre shift values in the chloride series may be compared with those reported[164] for some 2:1 polymeric amide complexes, which are believed to possess the same chloride-bridged structure. The higher values in the amide series ($\sim$ 1.39 to 1.48 mm/sec. at 295 K) may reflect both weaker σ-donation and π-back acceptance by these O-donor ligands compared with the aromatic amines.

Quadrupole Splittings

The values of ΔE_Q for these complexes lie in the region $\sim$ 0.3 - 1.8 mm/sec. at 300 K and are very much lower than those found in most of the monomeric octahedral FeL_4X_2 complexes, and in the polymeric amide complexes.

For the complexes measured at lower temperatures, there is an increase in ΔE_Q of $\sim$ 0.6 mm/sec. at 77 K, except for the compounds $Fe(3,5\text{-}Cl_2\text{-}py)_2Cl_2$ and $Fe(3\text{-}Cl\text{-}py)_2Cl_2$ (A) which show very little temperature dependence of ΔE_Q, the value actually decreasing for the latter compound at 77 K. In the compound $Fe(3\text{-}CN\text{-}py)_2Cl_2$, which shows only a quadrupole doublet at 4.2 and 1.4 K, the value of ΔE_Q decreases by $\sim$ 0.2 mm/sec. at these temperatures compared with the value at 77 K.

Several of the compounds show a peak asymmetry of the quadrupole doublet, affecting half-widths, peak heights and areas (Table 4.3), which was reproducible for different samples and generally decreased with decreasing temperature. Asymmetry in the quadrupole peaks in powdered solids may arise from three causes. Firstly, partial orientation of crystallites in absorber preparation may confer on the spectrum some of the features of the peak asymmetry obtained in single crystal measurements. This is considered unlikely in these compounds, due to their extremely finely divided form and the reproducibility and temperature dependence of the asymmetry. Secondly, the Goldanskii-Karyagin effect,[183] due to anisotropy in the recoil-free fraction arising from differences in the "rigidity" of the structure in different directions, can cause a peak asymmetry which should decrease

as the temperature decreases. This cause does not seem unreasonable for these complexes, owing to their linear chain structure. A third possible cause is spin-relaxation effects creating a fluctuating 'internal' field at the nucleus.[184] The fact that magnetic ordering appears to be present in some of these compounds at low temperature suggests that there may be a contribution to the asymmetry at higher temperature from spin-spin interactions, and it is noted that the line widths at 77 K are considerably broadened.

Since the ΔE_Q values in these compounds lie in the region which could arise from either the orbital singlet or doublet ground states lowest in axial symmetry, it was necessary to determine the sign of ΔE_Q to enable the two to be distinguished. Two compounds were investigated by the applied magnetic field technique: $Fe(3\text{-}CN\text{-}py)_2Cl_2$ as representative of the compounds with larger and more temperature dependent values of ΔE_Q, and $Fe(3,5\text{-}Cl_2\text{-}py)_2Cl_2$ as representative of the remaining compounds with smaller ΔE_Q values.

The spectra obtained using an applied field of 60 kG, at 4.2 K for the former compound, and 31.5 K for the latter (since it is split by the internal field at 4.2 K) are shown in Figs. 4.7(a) and (b) respectively. The spectrum of $Fe(3\text{-}CN\text{-}py)_2Cl_2$ is clearly resolved into a doublet at higher velocity than a triplet, indicating a positive quadrupole splitting. The spectrum of $Fe(3,5\text{-}Cl_2\text{-}py)_2Cl_2$ corresponds to a situation in which the magnetic interaction is greater than the quadrupole interaction, and consists of an outer doublet and an inner triplet. The centroid of the doublet lies at more positive velocity than that of the triplet, indicating again a positive quadrupole splitting.

A theoretical fitting of the applied field spectra to extract the quadrupole and magnetic hyperfine interaction parameters was kindly undertaken by Dr B.W. Dale, P.C.M.U., Harwell. Difficulty was encountered in obtaining good fits, since relaxation effects appear to be present and to interfere with the line intensity ratios and line-shapes. A good fit could not be obtained for $Fe(3,5\text{-}Cl_2\text{-}py)_2Cl_2$, and the only information afforded was the confirmation of a small, positive value of ΔE_Q. The best fit to the data on $Fe(3\text{-}CN\text{-}py)_2Cl_2$ is the solid curve shown in Fig. 4.7(a). The peaks are extremely broad (0.38 mm/sec. half-width for

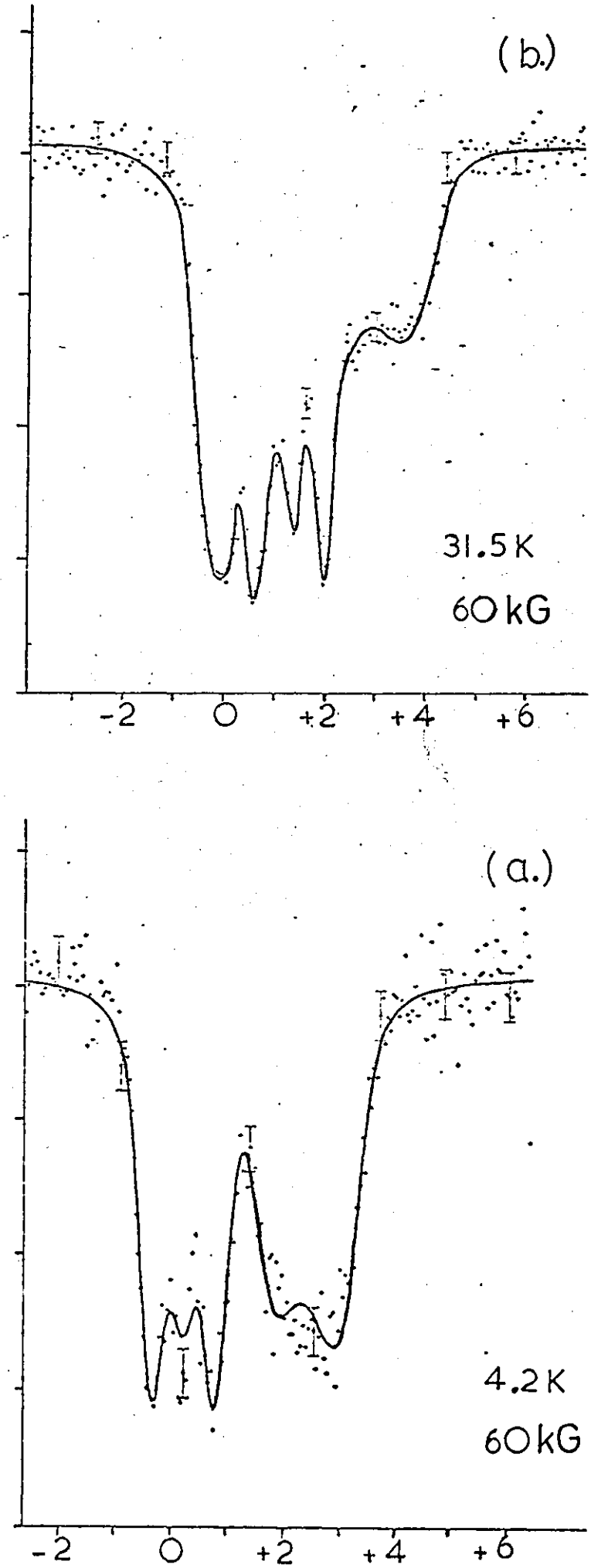

Fig. 4.7. Applied Magnetic Field Mössbauer Spectra of (a) $Fe(3\text{-}CN\text{-}py)_2Cl_2$
(b) $Fe(3,5\text{-}Cl_2\text{-}py)_2Cl_2$

a Lorentzian line-shape, with an assumed Gaussian broadening of half-width 0.28 mm/sec.), due to relaxation effects. The value of ΔE_Q from the fitting is +2.18 mm/sec., and assuming that the major e.f.g. axis, z, corresponds to the N-Fe-N direction, this indicates a singlet dxy ground state. The value of the asymmetry parameter, η, was found to be very small. The components of the magnetic hyperfine tensor, A, were found to have the relationship $A_x > A_y \approx A_z$, indicating that there may be approximate symmetry of the magnetic susceptibility tensor about an axis, x, in the plane perpendicular to the major e.f.g. axis, z, i.e. the single-ion ground state is that in which the spins are oriented parallel to an axis in the xy plane.

From the applied field results on these two compounds, it seems probable that all these polymeric compounds have positive quadrupole splittings and thus singlet dxy ground states.

Magnetic Hyperfine Splitting

As mentioned above, $Fe(3\text{-}CN\text{-}py)_2Cl_2$ shows only a slightly broadened quadrupole doublet at 4.2 and 1.4 K. The remaining compounds measured all show additional peaks at both temperatures, and the peak positions, half-widths and relative intensity data from the least-squares fittings are collected in Table 4.3.

The magnetic ordering temperatures of the compounds were determined by observation of the temperature at which the magnetic hyperfine splitting collapses to give a quadrupole doublet, and are listed in Table 4.4.

Compound	Magnetic Ordering Temperature (K)	
$Fe(3\text{-}CN\text{-}py)_2Cl_2$	< 1.4	
$Fe(4\text{-}CN\text{-}py)_2Cl_2$	5	+ 2, -1
$Fe(3\text{-}Cl\text{-}py)_2Cl_2$ (A)†	≤ 6	± 2
$Fe(3\text{-}Cl\text{-}py)_2Cl_2$ (B)	6	± 2
$Fe(4\text{-}Cl\text{-}py_2Cl_2$	6.2	± 0.5
$Fe(3,5\text{-}Cl_2\text{-}py)_2Cl_2$	10	± 2

† see text.

The splitting patterns and intensity ratios of these spectra are quite complicated and, in most cases, temperature dependent. This is not surprising since the temperatures of the measurements are not very much lower than the ordering temperatures, so that the 'internal' fields will vary with the local magnetisation. Analysis of the spectra in terms of the relative magnitudes and directions of the 'internal' field and the quadrupole interaction is therefore very difficult.

Attempts have been made to obtain realistic values of the 'internal' field, H_n, and the quadrupole and asymmetry parameters, ΔE_Q and η, in the field direction, from the observed band separations at the lowest temperature, using the theoretical equations for axial and non-axial systems with H_n parallel to one of the principal e.f.g. axes.[168] Various assignments of the peaks have been considered, corresponding to the possible orderings of the excited nuclear substates under the combined interactions. However, agreement with these models is not very good, which may indicate that the simplifying assumption of near coincident 'internal' fields and e.f.g. axes may not be generally valid for these compounds. Comparison of the observed splitting patterns with the computed spectra, presented by Collins and Travis,[185] for a quadrupole doublet in an applied magnetic field, has been used to assist in the interpretation.

For the compounds $Fe(4\text{-CN-py})_2Cl_2$ (Fig.4.1) and $Fe(3\text{-Cl-py})_2Cl_2$ (B) (Fig.4.5), the six-peak splitting pattern and the variation with temperature of the peak intensity ratios are quite similar. The latter is seen clearly in Figs. 4.1 (b) - (d), where the intensity of the outer peaks of each 'triplet' increases and that of the inner peaks decreases as the temperature is reduced from just below the ordering temperature to 1.4 K. The spectra at the latter temperature are extremely similar to that computed[185] for a species with positive quadrupole splitting in a small applied magnetic field, when the value of the asymmetry parameter approaches 1. The triplet-doublet pattern progresses to a symmetrical triplet-triplet pattern as η goes from zero to 1. The values of ΔE_Q at 1.4 K, which, on this basis, can be estimated from the separation of the inner peaks of each triplet, are 1.76 mm/sec. for $Fe(4\text{-CN-py})_2Cl_2$ and 1.85 mm/sec. for $Fe(3\text{-Cl-py})_2Cl_2$. These values are only slightly smaller than those found for the compounds at 77 K, and are consistent

with the slight reduction in ΔE_Q found for $Fe(3\text{-}CN\text{-}py)_2Cl_2$ at 1.4 K. This would appear to confirm an interpretation in terms of an 'internal' field of $\leq \sim 50$ kG, approximately parallel to the major e.f.g. axis, with an η value approaching 1.

An alternative interpretation, in terms of an almost zero quadrupole interaction along the 'internal' field direction, could be suggested in view of the almost equal spacing of the components of the triplets. Such an analysis gives $H_n \approx 100$ kG at 1.4 K for both compounds, with ΔE_Q in the field direction $< \sim 0.1$ mm/sec. and a large asymmetry parameter. The values of H_n calculated from the excited and ground nuclear state splittings vary by $\sim 10\%$. This interpretation suggests that the 'internal' field does not coincide with the major e.f.g. axis. On the whole, it appears that the previous interpretation may be more realistic.

The spectrum of $Fe(4\text{-}Cl\text{-}py)_2Cl_2$ at 4.2 K (Fig. 4.3(c)) appears to contain only five peaks, and that at 1.4 K (Fig. 4.3(d)) is considerably broadened, and a good least-squares fit to a Lorentzian or modified-Lorentzian line-shape could not be obtained. The spectra are similar to that expected for a system with positive quadrupole splitting in an externally applied field with the quadrupole interaction predominating i.e. a doublet at more positive velocity than a triplet. The asymmetry parameter may be quite small. The near superposition of the lower energy peak of the doublet and the highest energy peak of the triplet at 1.4 K is consistent with an increase in the magnitude of the magnetic interaction on cooling the compound further below its ordering temperature. Analysis of the 4.2 K spectrum on this basis gives $H_n \approx 50$ kG and $\Delta E_Q \approx +1.8$ mm/sec. This latter value is again only slightly lower than that found at 77 K and appears to indicate a near coincidence of the 'internal' field direction and the major e.f.g. axis.

The splitting pattern in $Fe(3,5\text{-}Cl_2\text{-}py)_2Cl_2$, (Fig. 4.6) is more complicated than those in the other compounds. The relative peak intensities and separations alter only slightly between 4.2 and 1.4 K which indicates that the magnetic ordering is nearing completion at the latter temperature. The magnetic and quadrupole interactions appear to be

of similar magnitude. The best fitting that could be achieved to a coincident axis model gave $H_n \approx 100$ kG and $\Delta E_Q \approx 1.2$ mm/sec. in the field direction. The error in the values is however quite large ($\sim 15 - 20\%$), and the complicated intensity ratios suggest that the nuclear states are considerably mixed, and thus the value of η may be considerable.

The A form of $Fe(3\text{-}Cl\text{-}py)_2Cl_2$, when initially cooled to 4.2 K gave a four peak spectrum (Fig. 4.4(c)). After warming to 77 K (at which the extra peaks due to the B form are evident) and recooling to 4.2 K, a more complex splitting pattern is found (Fig. 4.4(d)).

Three possible interpretations of this behaviour may be considered. Firstly, the splitting pattern in Fig. 4.4(c) may be due to magnetic ordering in the A form. The small separation of the peaks would indicate $H_n \approx 10 - 15$ kG, with $\Delta E_Q \approx 1.1$ mm/sec. This latter value is somewhat larger than that found at 77 K. If this interpretation is valid, it would mean that the transition to the B form has not occurred while cooling to 4.2 K, although the B peaks are present on rewarming to 77 K. The larger values of ΔE_Q for the B form indicate that it is probably less symmetric than the A, and the large asymmetry parameter deduced from the magnetic splitting of the pure B form suggests that the transition from A to B may involve a rhombic distortion in the chloride plane, in addition to any alteration in the axial bonding. The distortion could be caused by chain packing effects as the lattice structure alters with temperature. The transition may be time-dependent and may not therefore be able to occur on rapid cooling to 4.2 K, so that the compound is 'frozen' into the A structure. However, during the slower warming from 4.2 to 77 K the conversion may begin to take place. It is also possible that the transition may be brought about by the magnetic ordering in the A form. Structural distortions accompanying magnetic ordering processes have been considered[162] to contribute to an anomalous increase in ΔE_Q for several high-spin Fe^{II} compounds at their ordering temperatures. It is therefore conceivable that ordering in the A form may produce a small structural distortion below the ordering temperature (this could occur, for example, if the direction of spin alignment relative to the molecular axes for each ion in the ordered state is not the same as the spin direction of the individual paramagnetic ions). This would not be

inconsistent with the increase in ΔE_Q at 4.2 K compared with the values at 300 and 77 K. As the sample is rewarmed through the ordering temperature, some of the units may revert to the 'undistorted' A form, but a portion may be converted to a more distorted B form, if the energy difference between the A and B forms is very small. This proposal of almost equal energy forms would be supported by the fact that both A and B forms can be prepared at room temperature, and the pure B form once obtained does not appear to convert to the A form.

At 77 K (Fig. 4.4(b)) the structure may consist of a mixture of A and B modifications within the same chain. The quadrupole splittings of the two doublets at this temperature then distinguish the two Fe^{II} environments. It might then be expected that Fig. 4.4(d), on recooling to 4.2 K, should correspond to a superimposition of peaks from a mixture of the two magnetically split forms (i.e. Figs. 4.4(c) and 4.5(c)). It does not appear that Fig. 4.4(d) can be easily resolved into such a mixture of constituent A and B peaks and it is therefore possible that the 'internal' field seen by each metal ion in a chain becomes an average, depending upon the actual arrangement of A and B sites in the chain. There may thus be contributions from A-A, B-B and A-B exchange and the broad spectrum observed may comprise magnetic splitting patterns for the A and B sites in averaged values of the 'internal' field.

The second possible explanation is that a partial transition to the B form occurs on initial cooling to 4.2 K and that the four peaks in Fig. 4.4(c) do not arise from magnetic ordering in the A form, but correspond to quadrupole doublets from the A and B forms. The separation of the inner peaks is 0.74 mm/sec. which is very similar to the values of ΔE_Q at 300 and 77 K for the A form. However, the separation of the outer peaks is only 1.36 mm/sec., which is considerably lower than the value of ΔE_Q found for form B at 77 K, and also that determined from the magnetically-split spectrum of the B form at 1.4 K. It is possible that a decrease, followed by an increase, in ΔE_Q at very low temperature could occur through spin-orbit coupling effects,[51,52] or even that the higher value at 4.2 K in the magnetically-split spectrum could be caused by a distortion accompanying ordering as mentioned above. However, this interpretation requires the assumption that the temperature at which Fig. 4.4(c) was obtained must be slightly above 4.2 K, since no

magnetic splitting is observed for the 'B' peaks, although apparently below the ordering temperature of the B form. Fig. 4.4(d) may then again represent the true situation at 4.2 K, in which splitting due to an averaged 'internal' field is observed. In view of the numerous assumptions which are required for this interpretation, it seems far less convincing that the first.

A third explanation could be proposed, which avoids some of the difficulties in the second interpretation, that the outer peaks in Fig. 4.4(c) may arise from an intermediate species in the A to B transition. If the transition in a portion of the sample does begin to occur on initial cooling from 77 to 4.2 K, then the rapid rate of cooling may freeze this portion into an intermediate state of distortion between the A and B forms, which may be more consistent with the value of ΔE_Q calculated from the separation of the outer peaks. On rewarming to 77 K the conversion of the intermediate form to the B form may then take place. This interpretation would suggest that neither the A nor the intermediate form show magnetic ordering at 4.2 K.

On the whole, it seems that the first interpretation is the most acceptable, but it is considered that, although no definite evidence for the existence of an intermediate form can be cited, this possibility cannot be completely discounted. It must be mentioned that a further sample of what was believed to be the pure A form was measured at 4.2 K, and the splitting pattern was found to be substantially similar but not identical to that in Fig. 4.4(d). It would therefore appear that in this case some B form may have been produced on cooling, although it is also possible that a small amount of B could have been present initially from the preparation. The ordering temperature of this sample was found to be the same as that for the B form, within the error of the determination, and this would indicate that if the A form is also magnetically ordered, its ordering temperature must be less than or approximately equal to that of the B.

Magnetic Measurements

The results of the magnetic measurements on the compounds are presented in Table 4.5. Unfortunately, no magnetic data could be obtained for the B form of $Fe(3\text{-}Cl\text{-}py)_2Cl_2$, since the only known pure

sample prepared began to decompose before magnetic measurements could be made.

The room temperature values of μ_{eff} are all considerably greater than the spin-only value. The compounds measured in the 300 - 100 K region follow the Curie-Weiss Law ($\chi = \frac{C}{T+\theta}$) in this range. For the complexes with chloro-substituted pyridines, the values of μ_{eff} generally increase gradually as the temperature decreases, yielding small negative Weiss constants, θ. For the complexes with cyano-substituted pyridines, a slight decrease in the moment occurs below ~ 180 K, giving very small positive θ values.

In view of the magnetic ordering in some of these compounds, indicated by the Mössbauer data, it was intended to investigate the magnetic behaviour of all these complexes down to 1.4 K. Unfortunately, owing to operational difficulties with the Faraday Balance, it was only possible to measure one of the compounds over the full temperature range. The compound chosen was $Fe(3,5\text{-}Cl_2\text{-}py)_2Cl_2$, which has the highest ordering temperature from the Mössbauer results.

Between 300 and 50 K the susceptibility and moment increase gradually with decreasing temperature. The susceptibility and μ_{eff} v. temperature plots in the 70 to 1.4 K region are shown in Fig. 4.8, for the highest value of field used in the measurement. Below ~ 40 K the susceptibility and moment begin to increase quite rapidly and the values become markedly field-dependent. The maximum gradient of both curves, which is assigned as the ordering temperature, occurs at ~ 12.5 K. The increase in susceptibility begins to tail off at ~ 10 K and μ_{eff} is a maximum at this temperature, indicating that the sample is approaching magnetic saturation.

The ordering in this compound is therefore ferromagnetic. (The possibility of a ferromagnetic impurity in the compound can be discounted since no impurity peaks are observed in the Mössbauer spectra). The Curie temperature of ~ 12.5 K agrees quite well with that found from the Mössbauer determination. Although some degree of ordering is present above this temperature, as indicated by the magnetic results, the 'internal' fields are too small to cause splitting.

The negative Weiss constants found for several of the other compounds from the higher temperature data suggest that ferromagnetic ordering

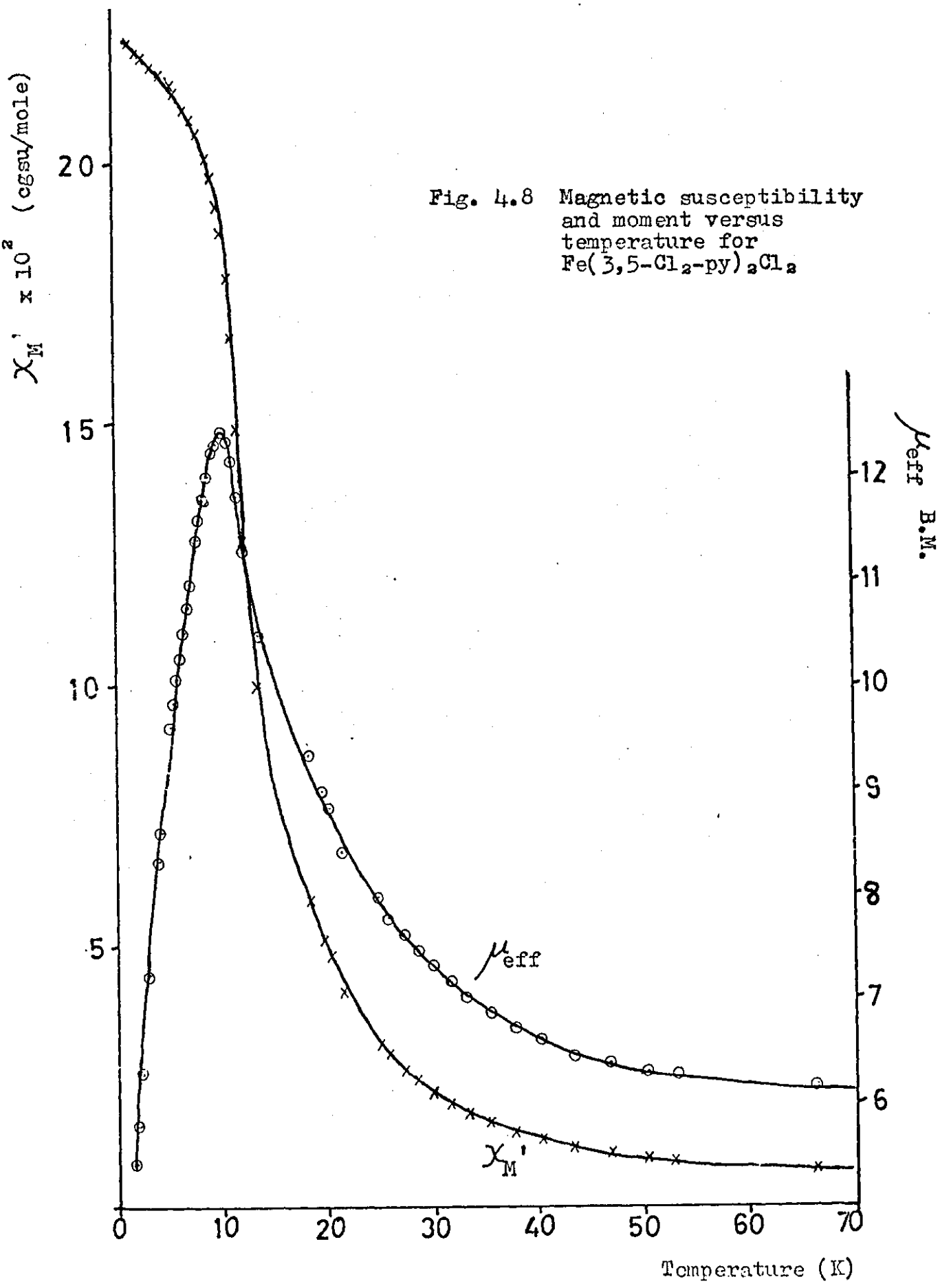

Fig. 4.8 Magnetic susceptibility and moment versus temperature for $Fe(3,5\text{-}Cl_2\text{-}py)_2Cl_2$

occurs in these compounds as well. The small positive θ value for $Fe(4\text{-}CN\text{-}py)_2Cl_2$ is not inconsistent with a ferromagnetic interaction, since there may well be a contribution to θ of positive sign from the nature of the ground state of the individual paramagnetic ions.

It is interesting to note that the A form shows quite a marked increase in the moment between 300 and 100 K which suggests that this form does itself exhibit magnetic ordering.

Discussion of the Results

The relatively large band separations in the electronic spectra of the polymeric complexes indicate considerable splitting of the excited ^5Eg level by the ligand field, consistent with a tetragonal or rhombic distortion.

The small values and positive sign of the quadrupole splittings, however, suggest relatively small separation of the components of the $^5T_{2g}$ level, with the singlet dxy state lying lowest in tetragonal or rhombic symmetry. If the quadrupole splittings are assumed to be due to q_{val} only, then for an axial system, the values of ΔE_Q at 300 K would imply values of $\frac{\Delta_1}{\lambda}$ in the range ~ -1 to -3.5 (Δ_1 positive, λ negative) i.e. the separation between singlet and doublet levels is $\sim 100 - 450\ cm^{-1}$, increasing in the order of increasing ΔE_Q (Table 4.3). If there is a considerable lattice contribution to the e.f.g. then the estimated values of Δ_1 will increase or decrease depending on the sign of q_{latt} relative to that of q_{val}. The treatment of Ingalls[51] and electrostatic considerations[186] for a trans MA_2B_4 system suggest that q_{latt} should be opposite in sign to q_{val} for these compounds, and therefore the values of Δ_1 may be underestimated. Similarly, if there are rhombic field components present, the low values of ΔE_Q could arise from larger values of $\frac{\Delta_1}{\lambda}$, as $\frac{\epsilon}{\lambda}$ increases. This possibility will be discussed further below.

The high values of μ_{eff} at room temperature also suggest small ground state splittings, so that considerable orbital contribution to the moment is retained. However, the presence of ferromagnetic interactions in some of the compounds at low temperature could give rise to contributions to the large moments at higher temperature.

From the very low values of the Curie temperatures and the temperature variation of the moments in the 300 to 100 K region, it does not appear that the degree of magnetic ordering could contribute greatly to the increase in the moment above the spin-only value at room temperature. For example, the fact that in $Fe(4\text{-}CN\text{-}py)_2Cl_2$ a slight decrease in the value of μ_{eff} is found below ~ 180 K may suggest that the high value at room temperature is due almost entirely to orbital contribution to the moment. It is also noted that $Fe(3\text{-}CN\text{-}py)_2Cl_2$, for which there is no definite evidence for ordering above 1.4 K from the Mössbauer data, has a comparably high moment.

However, in view of the fact that some contribution from magnetic ordering may be present, no attempt has been made to fit the higher temperature magnetic data to the variable parameter model described in Chapters 1 and 3. Similarly, fitting of the low temperature data for $Fe(3,5\text{-}Cl_2\text{-}py)_2Cl_2$ to a model for exchange interactions between S = 2 ions is invalidated by the presence of orbital contribution to the magnetism.

The temperature dependence of ΔE_Q for these compounds is quite small, and the low temperature limits, where measured directly or estimated from the magnetically-split Mössbauer spectra, are surprisingly low. This may be due to spin-orbit coupling effects, and would again indicate close-lying orbital states of the $^5T_{2g}$ level. A relatively high degree of covalency and a considerable lattice contribution could also partially account for the small ΔE_Q values at low temperatures.

The large excited state splittings and small ground state splittings could be rationalised in terms of the nature of the covalent interaction between metal and ligand orbitals. The difference in the relative σ-antibonding strengths of the amine and halides has been proposed to account largely for the excited state splitting. A considerable degree of π-back bonding with the amine π^*-orbitals could however reduce the separation between the bonding orbitals of predominantly metal dxz and dyz character and the lowest-lying dxy orbital, which is essentially non-bonding, thus decreasing the ground-state splitting.

The electronic spectra of analogous polymeric complexes of Ni^{II} halides with pyridine ligands have been interpreted[187-190] on the

basis of almost regular O_h microsymmetry. Subsequently, reassignment of the observed bands indicated[191-193] that the compounds are tetragonally distorted. The axial field splitting parameters, Ds and Dt, for $Nipy_2Cl_2$ have been calculated[193] to be 598 cm^{-1} and 330 cm^{-1}, respectively, although fitting to the theoretical model is not particularly good, indicating that the microsymmetry is lower than D_{4h}. Using the values of Δ_2 for the Fe^{II} compounds from the electronic spectra, and the rough estimates of Δ_1, from the ΔE_Q values, assuming axial symmetry, values of Ds and Dt for these compounds of $\sim 530 - 560$ cm^{-1} and $\sim 340 - 360$ cm^{-1}, respectively, can be obtained. The significance of these values for both Ni^{II} and Fe^{II} compounds is limited by the fact that the symmetries are almost certainly lower than axial, but the similarity in the values suggests that the estimates of the overall splitting of the $^5T_{2g}$ level in the Fe^{II} compounds from the Mössbauer data are of the correct order of magnitude. The relatively high values of Dt support the proposal of a considerable degree of covalency.

There is, however, a considerable amount of evidence for additional rhombic distortions in some of these compounds. The fact that the analysis of the paramagnetic hyperfine interaction in $Fe(3\text{-}CN\text{-}py)_2Cl_2$ indicates approximate magnetic symmetry around an axis perpendicular to the major e.f.g. axis may indicate a rhombic distortion in the xy plane, which lowers the energy of, say, the dxz orbital so that it lies close the ground dxy orbital, as mentioned in Chapter 3. The large orbital contribution to the moment may then arise mainly from spin-orbit coupling between these lowest two states. Such an effect would be consistent with the positive sign, low values and relatively small temperature dependence of ΔE_Q, since it would result in a very small separation between the dxy and dxz orbitals (for which the expectation values of q_{val} are $+\frac{4}{7}\langle r^{-3}\rangle_{3d}$ and $-\frac{2}{7}\langle r^{-3}\rangle_{3d}$, respectively), provided that the two orbitals do not actually become degenerate. The only observation unexplained by this proposal is the very low value of the asymmetry parameter, but η may not be well determined by the fitting procedure used.† The interpretation of the 'internal' field-split spectra of $Fe(4\text{-}CN\text{-}py)_2Cl_2$ and $Fe(3\text{-}Cl\text{-}py)_2Cl_2$ (B) at low temperature suggests

† Dr B.W. Dale personal communication.

a large asymmetry parameter, and similarly the splitting pattern of $Fe(3,5\text{-}Cl_2\text{-}py)_2Cl_2$ could indicate a significant rhombic component.

The most obvious origin of asymmetry in the xy plane that could be suggested is inequality in the Fe-Cl bond lengths. It is noted that in the compound $FeCl_2.2H_2O$, which has a small rhombic distortion in the xy plane due to the unequal Fe-Cl bond lengths, the spin-direction in the paramagnetic state is also believed[194] to be along the x axis, perpendicular to the major e.f.g. axis (z), and to coincide closely with the shorter Fe-Cl bond. Asymmetry in the Fe-Cl bond lengths in these amine complexes would probably not occur independently of other variations in the overall structure, since, for example, the preferred orientation of the rings and the Fe-N bond lengths will be to some extent dependent on the arrangement of the chlorides in the plane, owing to the possibility of steric interaction with the ring α-hydrogens. Orientation of the rings so that the degree of overlap of the metal dxz and dyz orbitals with the amine π^* orbitals is not equivalent could also contribute to an energy separation between the two bonding orbitals of predominantly metal t_{2g} character. Inequality in metal dxz,dyz -chloride p_z π-bonding would have a similar effect.

It must be noted that the evidence for a rhombic distortion in the compounds mentioned above has only been obtained at very low temperature, and, for three of the compounds, in the magnetically-ordered state. It cannot therefore be definitely inferred that such a distortion is also present at higher temperatures. In view of the fact that the transition from the A to the B form of $Fe(3\text{-}Cl\text{-}py)_2Cl_2$ at low temperature may involve a rhombic distortion, the possibility of a gradual structural variation, involving the entire lattice, in the other complexes on cooling cannot be discounted. It is also conceivable that, if such a temperature-dependent structural variation is possible, a rhombic distortion in the plane of chlorides could become the major distortion at low temperatures. In this case the major e.f.g. axis at low temperature may no longer correspond to the N-Fe-N direction, as proposed at higher temperature, and the low temperature Mössbauer data would assume a new significance. However, in the absence of any conclusive evidence for such an effect, a reinterpretation of the data is not considered worthwhile.

The ferromagnetic interaction found in $Fe(3,5\text{-}Cl_2\text{-}py)_2Cl_2$, and assumed for the other complexes exhibiting order, is consistent with the predictions of the Anderson theory and the Goodenough-Kanamori rules for exchange coupling between high-spin Fe^{II} ions, through an intermediate anion X, where M-X-M angle is close to 90°. Assuming that each chloride ion uses filled p_x and p_y orbitals for σ-overlap with the half-filled $d_{x^2-y^2}$ (e_g) orbitals on the Fe^{II} ions, the orbital arrangement for each side of the bridge is shown in Fig. 4.9(a). The Fe-Fe separation is probably too large (c.f. 3.66 Å in $\alpha\text{-}Copy_2Cl_2$) for direct overlap of metal valence orbitals. On the Anderson theory, a fraction of unpaired spin density from the $d_{x^2-y^2}$ orbitals on Fe(1) and Fe(2) will reside in the chloride p_x and p_y orbitals, respectively. Since the latter orbitals are orthogonal, the unpaired spins must align parallel (Hund's rule), and thus the net spins on Fe(1) and Fe(2) will be coupled ferromagnetically. The interaction is expected to be relatively weak, since it depends not only on the spin delocalisation from metal to anion, but also on the exchange effect between orthogonal anion orbitals.

There are additional mechanisms which could give rise to antiferromagnetic coupling between adjacent metal ions. π-overlap between the half-filled dxz (Fe(1)) and dyz (Fe(2)) orbitals with the same filled p_z orbital on the bridging chloride could occur (Fig. 4.9(b)). On the Anderson theory, a fraction of unpaired spin density from each t_{2g} orbital will reside in the same anion p orbital, and the net spins will therefore be coupled antiferromagnetically by the Pauli principle. The π-overlap should be significantly smaller than the σ-overlap mentioned above, and so the ferromagnetic interaction should predominate. Since the coupling mechanism holds identically for each side of the bridge, and for each pair of Fe^{II} neighbours, there should be an extended intrachain ferromagnetic interaction.

Such an interaction is also present in $FeCl_2.2H_2O$, but this compound exhibits overall antiferromagnetism due to additional interchain mechanisms.[194] The spin-alignment direction in the ferromagnetic chains has been shown by magnetic[194] and Mössbauer 'internal' field measurements[195] to lie in the plane perpendicular to the major e.f.g. axis (the O-Fe-O direction), and in fact is close to the short Fe-Cl

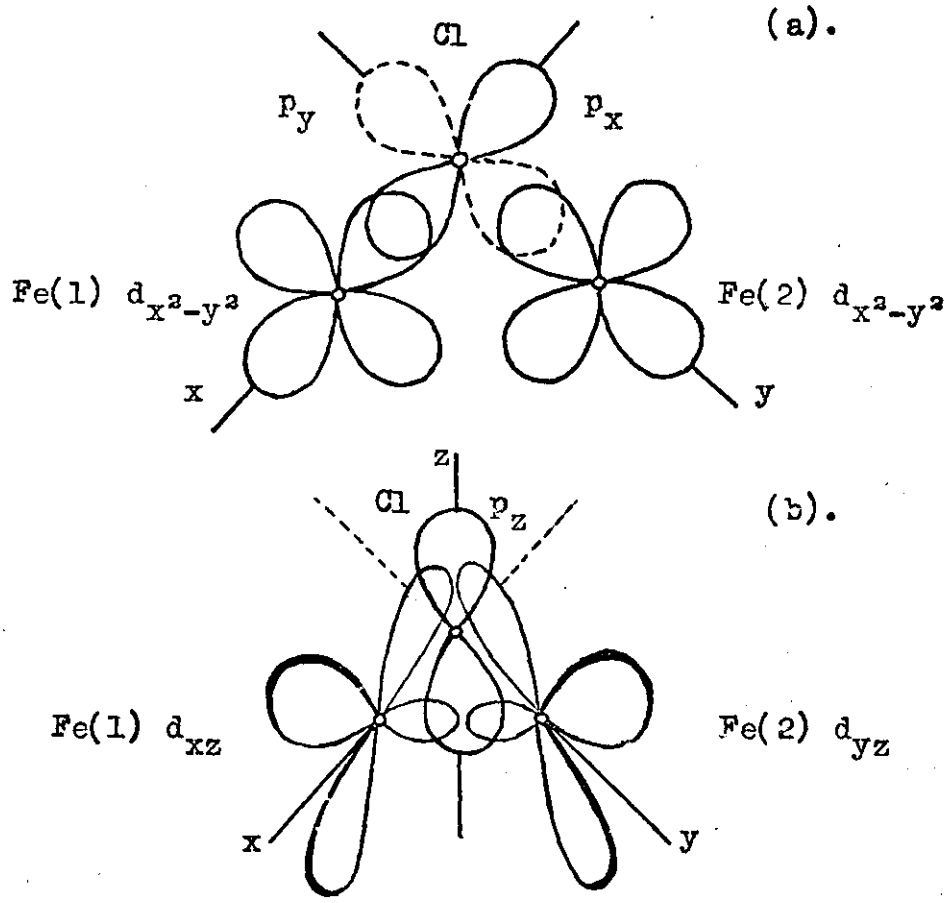

Fig. 4.9

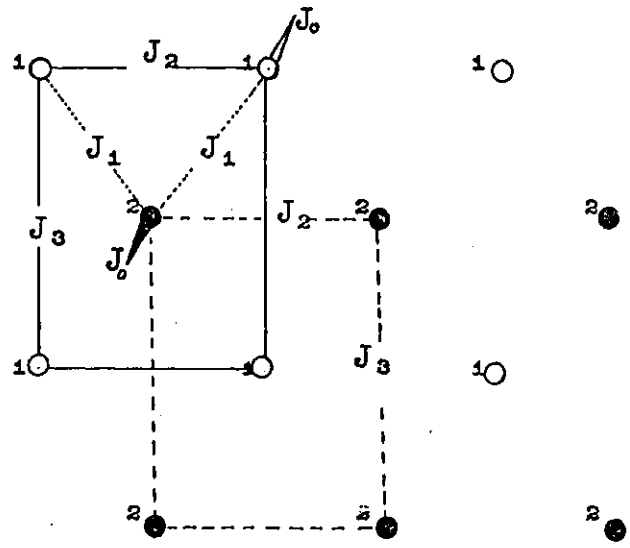

Fig. 4.10 Two-sublattice structure of $FeCl_2.2H_2O$ showing exchange interactions.

bond and thus to the spin direction in the paramagnetic state. The two-sublattice structure in zero field is shown in Fig. 4.10, in the plane normal to the chain direction. In addition to the ferromagnetic intrachain interaction, J_0, (approximately normal to the plane in Fig. 4.10), there is an antiferromagnetic interaction, J_1, involving an Fe-Cl-Cl-Fe pathway, which couples the spins on adjacent chains antiparallel, producing two sublattices. There are also two intra-sublattice interactions; J_2, (involving an Fe-Cl-Cl-Fe pathway and antiferromagnetic) which is responsible for the metamagnetic behaviour in this compound, and J_3, (coupling Fe^{II} ions which are separated by two water molecules) which is very weak and ferromagnetic.

The overall ferromagnetism observed in at least some of the substituted pyridine complexes suggests that any mechanism analogous to J_1 must be either ferromagnetic in these compounds, or so weakly antiferromagnetic that the relatively small magnetic fields used in the susceptibility measurements are capable of disturbing this coupling. The latter explanation seems plausible since the bulk of the amine groups compared with the small water molecule, and the absence of the efficient hydrogen-bonding mechanism (O-H --- Cl)[179] which holds the chains together in the dihydrate, may produce a larger chain separation in these compounds.

On the proposed mechanism for the ferromagnetic coupling, the magnitude of the interaction should depend on the extent of the Fe-Cl σ-overlap, which in turn will depend on the proximity of the anions to the x and y axes of the metal d-orbital system, on the closeness of approach of the Cl-Fe-Cl angle to 90°, and on the effective charge on the metal ion (and thus on the degree of metal-amine covalent interaction). It appears, from the limited amount of structural data available on polymeric halogen bridged complexes of this type, that the Cl-M-Cl angle approaches closer to 90° when the halide bridges are asymmetric, and therefore the rhombic distortion postulated above could enhance the exchange process. This suggestion may be supported by the smaller value of H_n deduced for the A form of $Fe(3\text{-}Cl\text{-}py)_2Cl_2$ relative to that for the B. It was also suggested, from comparison of the electronic spectra of the two forms, that σ_{Cl} in the B form

may be increased by a weakening in the N to Fe σ-donation. Such a weakening may also imply a decrease in the extent of metal to amine π-back-donation in the B form, resulting in a larger overall separation of the $^5T_{2g}$ levels and a decrease in the total covalency. These effects would be consistent with the larger ΔE_Q values found for the B form.

The relatively small values of the 'internal' fields estimated from the Mössbauer spectra are not altogether unexpected since the measurements were made just below their ordering temperatures. However, the persisting low value for $Fe(3,5\text{-}Cl_2\text{-}py)_2Cl_2$ at 1.4 K, at which the ordering must be nearing completion from the susceptibility data, suggests both a considerable contribution from the dipolar and orbital fields and a relatively high degree of covalency. The absence of magnetic splitting in $Fe(3\text{-}CN\text{-}py)_2Cl_2$ at 1.4 K could be due to a chance cancellation of the contributions to the 'internal' field.

It is apparent from the discussion that there are still many aspects of the problem of the structure and bonding in these polymers about which we can do little more than speculate. This difficulty arises partially from the general lack of a well-developed theoretical basis for interpretation of the experimental measurements on such low symmetry systems, and also from the relative insensitivity of spectral and magnetic properties to the effects of a symmetry lower than axial. Mössbauer spectroscopy has proved a very useful exception to the latter difficulty, and has enabled detection of quite subtle variations in the structural environment within this series of compounds.

In concluding this discussion, mention may be made of some other studies on polymeric systems of this type, which have been published during the course of this work and lend support to some of the results obtained here.

A paper has recently appeared[102] on the investigation of the electronic and structural properties of $Fepy_2Cl_2$, which may be considered as the parent compound of the chloride series presented here. The compound has been prepared both directly (sample A), and indirectly (sample B) by thermal decomposition of $Fepy_4Cl_2$. The powder patterns, I.R. and electronic spectra of the two samples at

room temperature have been reported to be identical, and the electronic spectra have been interpreted in terms of a tetragonal structure. Sample A shows only one quadrupole doublet in the range 300 to 78 K, ΔE_Q increasing from 0.56 mm/sec. at 300 to 1.28 mm/sec. at 78 K. Sample B shows only one doublet at 300 K (ΔE_Q = 0.57 mm/sec.), but below 195 K two doublets are observed, the ΔE_Q values being 1.27 mm/sec. and 0.63 mm/sec., respectively, at 78 K, with identical centre shifts. The former doublet is identified with that in sample A, and the appearance of the inner doublet is reported to be completely reversible and reproducible for various preparations of B.

The magnetic moments of the A and B samples are 5.33 BM (291 K) and 5.41 BM (288.5 K), respectively, and are thus significantly lower than the previous report of 5.75 BM at 300 K. For both samples, μ_{eff} begins to increase quite rapidly below ~ 50 K, becoming field dependent, and the values for the B sample are somewhat lower than those for the A. No Mössbauer data below 78 K has yet been obtained, and in the absence of supporting evidence for magnetic ordering from the Mössbauer, the authors have not been able to state definitely whether a ferromagnetic interaction is present, or whether the increase in μ_{eff} is due to a ferromagnetic impurity. Assuming the former case, the authors have rationalised the magnetic and Mössbauer behaviour in terms of a temperature-dependent structural change. Both A and B forms are assumed to possess symmetric bridging chlorides at room temperature, and the low value of ΔE_Q at 300 K is considered to be consistent with a very small reduction from O_h symmetry. The increase in ΔE_Q with decreasing temperature for the A form and the outer doublet in the B form is explained by assuming a transformation to a structure with asymmetric bridges, over a temperature range between 273 and 195 K. The decrease in symmetry is considered to produce a larger e.f.g. at the nucleus. The inner peaks in the B sample are considered to arise from a portion of the sample which is prevented from undergoing the structural distortion by the presence of crystal defects in the lattice, produced by the method of preparation.

The ferromagnetic ordering is explained by the same mechanism as given above, and it is proposed that the transition to the asymmetric structure is accompanied by an increase in the Cl-Fe-Cl bond angle towards 90° (as mentioned above), thus increasing the possibility of ferromagnetic exchange in the distorted form.

This observation of ferromagnetic ordering supports the results found in this work. The occurrence of a structural transition to a less symmetric form on cooling is also somewhat similar to the behaviour observed for $Fe(3\text{-}Cl\text{-}py)_2Cl_2$, although for $Fepy_2Cl_2$ it appears that only one structural modification exists at room temperature. It also seems that the transition is virtually complete and reversible, in the absence of crystal defects, at a higher temperature than found for $Fe(3\text{-}Cl\text{-}py)_2Cl_2$. We do not entirely agree with the proposal that a transition involving only a change from symmetric to asymmetric bridges accounts for the increase in ΔE_Q on cooling, since, as mentioned in Chapter 3, for a given positive value of Δ_1, a small rhombic component should in fact decrease the quadrupole splitting. However, as discussed above, a structural distortion in the plane is likely to be accompanied by alteration in the metal-amine bonding, and therefore the proposal can be justified.

A paper has recently appeared[196] which contains an investigation of the magnetic behaviour of $Nipy_2Cl_2$ and $Nipy_2Br_2$. The susceptibility data between 300 and 90 K have been shown to be consistent with a weak ferromagnetic intrachain interaction, confirming an earlier conclusion.[191] It is also interesting to note that a preliminary report[197] of the magnetic behaviour of $\alpha\text{-}Copy_2Cl_2$ indicates a rapid rise in the susceptibility at very low temperature, consistent with a ferromagnetic interaction. The Anderson theory predicts ferromagnetic coupling between Ni^{II} and Co^{II} ions through an $\sim 90^\circ$ halide bridge by the same mechanism as in the Fe^{II} case, although for Ni^{II} no competing antiferromagnetic mechanism is possible since the t_{2g} orbitals are completely filled. However, weak antiferromagnetic coupling has been tentatively proposed[198] for several analogous Cu^{II} compounds, from observation of small positive Weiss constants in the 300 to 100 K range. The coupling mechanism may differ in the Cu^{II} compounds from that in the Fe^{II}, Co^{II} and Ni^{II} compounds, owing to the different e_g configuration. The antiferromagnetism has been rationalised on the basis of an empirical theory which suggests ferromagnetic coupling along symmetrically-bridged Cu^{II} chains and antiferromagnetic coupling along asymmetrically-bridged chain, the latter being present in these compounds. No mechanism

has been proposed in support of this theory, and it is possible that the antiferromagnetism, if truly present, arises from interchain rather than intrachain interaction.

Ferromagnetic interactions in magnetically non-dilute inorganic complexes are probably more common than has often been considered. However the existence of ferromagnetism is often difficult to verify experimentally since additional antiferromagnetic interactions may be present. The series of compounds investigated here provide a good example of ferromagnetic behaviour which can be justified mechanistically from structural and bonding considerations.

Preparation of the Complexes

The general method of preparation of the chloride polymers was as follows:

Analak $FeCl_2.4H_2O$ (1 gm, 5 mM) was dissolved in a mixture of absolute ethanol (~ 15 ml) and dimethoxypropane (~ 5 ml), for dehydration. The solvent was previously deoxygenated by bubbling dry nitrogen gas for ~ 15 minutes, and contained coils of iron wire (previously activated by immersion in conc. HCl, and then washed well with distilled water and ethanol), for reduction of any ferric impurity. The solution was stoppered and left for at least 24 hrs, when it became very pale green. The solution was then filtered under nitrogen into a rapidly-stirred solution of the ligand (10 mM) in cold deoxygenated ethanol (10 ml)/dimethoxypropane (5 ml) mixture. Precipitation of the complex usually occurred immediately or within ~ 10 seconds of stirring. In all cases, stirring was continued for 5 - 10 minutes and then, if the precipitate was sufficiently granular, it was filtered under a stream of nitrogen, washed with cold ethanol/dimethoxypropane mixture and vacuum-dried. In most cases, the precipitate was microcrystalline and easily filterable, but in some cases, especially with 3,5-Cl_2-py, the extremely fine precipitate required stirring overnight before it became granular enough to filter.

The bromide complexes were prepared in a similar manner, using ferrous bromide solutions prepared by direct reaction of bromine and activated iron filings in ethanol/dimethoxypropane solution.

The 4:1 ferrous iodide complexes were obtained by an analogous method, using ferrous iodide solutions prepared as for the bromide, and either a 2:1 or 4:1 ligand to metal ratio.

Table 4.1 Elemental analyses for the substituted-pyridine complexes

Compound	Colour	C% required	N% required	H% required	C% found	N% found	H% found
$Fe(4\text{-}CN\text{-}py)_2Cl_2$	Orange	43.03	16.73	2.41	43.24	16.76	2.60
$Fe(3\text{-}CN\text{-}py)_2Cl_2$	Orange-yellow	43.03	16.73	2.41	42.80	16.97	2.87
$Fe(4\text{-}Cl\text{-}py)_2Cl_2$	Yellow	33.93	7.92	2.26	34.20	7.79	2.43
$Fe(3\text{-}Cl\text{-}py)_2Cl_2$ (A)	Yellow	33.93	7.92	2.26	34.13	7.93	2.40
$Fe(3\text{-}Clpy)_2Cl_2$ (B)	Yellow	33.93	7.92	2.26	34.03	8.21	2.40
$Fe(3,5\text{-}Cl_2\ py)_2Cl_2$	Yellow	28.41	6.63	1.43	28.77	6.79	1.82
$Fe(3\text{-}Br\text{-}py)_2Cl_2$	Yellow	27.11	6.33	1.81	27.65	6.05	1.94
$Fe(3\text{-}I\text{-}py)_2Cl_2$	Deep Yellow	22.38	5.21	1.49	21.73	5.64	1.80
$Fe(4\text{-}CN\text{-}py)_2Br_2$	Orange	33.96	13.20	1.89	34.20	13.60	2.03
$Fe(3,5\text{-}Cl_2\text{-}py)_2Br_2$	Yellow	23.44	5.47	1.17	23.19	5.69	1.60
$Fe(4\text{-}CN\text{-}py)_4I_2$	Orange-Red	39.62	15.42	2.21	38.53	14.41	2.64
$Fe(3,5\text{-}Cl_2\text{-}py)_4I_2$	Yellow	26.65	6.24	1.32	26.50	6.01	1.67

Table 4.2 Reflectance Spectra

Compound	Band Positions (d-d) transitions cm^{-1}	Δ_2 cm^{-1}	$d\sigma$ cm^{-1}	10 Dq cm^{-1}
$Fe(4\text{-}CN\text{-}py)_2Cl_2$	9,710, 6,070	+3640	+1370	7890
$Fe(3\text{-}CN\text{-}py)_2Cl_2$	9,710, 6,190	+3520	+1320	7950
$Fe(4\text{-}Cl\text{-}py)_2Cl_2$	9,580, 5,950	+3630	+1360	7770
$Fe(3\text{-}Cl\text{-}py)_2Cl_2$ (A)	9,660, 6,070	+3590	+1350	7870
$Fe(3\text{-}Cl\text{-}py)_2Cl_2$ (B)	9,240, 5,900	+3340	+1250	7570
$Fe(3,5\text{-}Cl_2\text{-}py)_2Cl_2$	9,080, 6,160	+2920	+1100	7620
$Fe(3\text{-}Br\text{-}py)_2Cl_2$	9,710, 6,140	+3570	+1340	7930
$Fe(3\text{-}I\text{-}py)_2Cl_2$	9,620, 6,160	+3460	+1300	7890
$Fe(4\text{-}CN\text{-}py)_2Br_2$	9,630, 5,770	+3860	+1450	7700
$Fe(3,5\text{-}Cl_2\text{-}py)_2Br_2$	8,790, 5,850	+2940	+1100	7320
$Fe(4\text{-}CN\text{-}py)_4I_2$	11,480, 6,380	-5100	-1910	8930
$Fe(3,5\text{-}Cl_2\text{-}py)_4I_2$	10,560, 7,730	-2830	-1060	9140

Table 4.3 Mössbauer Data

Compound	Temperature (K) (Figure)	Centre Shift (mm/sec)	ΔEQ (mm/sec)	Half Widths (mm/sec)	Intensity Ratios †	Area Ratio †
$Fe(4\text{-}CN\text{-}py)_2Cl_2$	300	1.34	1.25	0.26,0.25	1.07	1.28
	77 (4.1(a))	1.46	1.90	0.33,0.32	1.03	1.04
$Fe(3\text{-}CN\text{-}py)_2Cl_2$	300 (4.2(a))	1.33	1.73	0.32,0.30	1.05	1.16
	77 (4.2(b))	1.44	2.37	0.38,0.38	1.09	1.10
	4.2 (4.2(c))	1.48	2.19	0.41,0.41	1.02	1.02
	1.4 (4.2(d))	1.48	2.20	0.40,0.39	1.01	1.02
$Fe(4\text{-}Cl\text{-}py)_2Cl_2$	300 (4.3(a))	1.34	1.34	0.28,0.26	1.02	1.10
	77 (4.3(b))	1.46	1.97	0.35,0.34	1.05	1.07
$Fe(3\text{-}Cl\text{-}py)_2Cl_2$ (A)	300	1.36	0.74	0.29,0.27	1.25	1.54
	77 (4.4(a))	1.42	0.71	0.38,0.36	1.24	1.30
	‡ 77 (4.4(b))	A1.42	0.71	0.31,0.30	1.19	
		B1.46	2.08	0.31,0.36	1.04	
$Fe(3\text{-}Cl\text{-}py)_2Cl_2$ (B)	300 (4.5(a))	1.37	1.48	0.33,0.30	1.20	1.33
	77 (4.5(b))	1.47	2.04	0.30,0.31	1.11	1.08
	‡ 77(after re-warming from 4.2)	1.47	2.02	0.60,0.56	1.02	1.08
$Fe(3,5\text{-}Cl_2\text{-}py)_2Cl_2$	300 (4.6(a))	1.38	0.88	0.31,0.31	0.97	0.97
	77 (4.6(b))	1.44	1.03	0.29,0.27	0.95	1.00
$Fe(3\text{-}Br\text{-}py)_2Cl_2$	295	1.36	0.90			
$Fe(4\text{-}CN\text{-}py)_2Br_2$	295	1.32	<0.3			
$Fe(3,5\text{-}Cl_2\text{-}py)_2Br_2$	295	1.35	0.49			

† Lower velocity peak/higher velocity peak

‡ See text

continued

Table 4.3 continued

Compound	Temperature (K) (Figure)	Peak Positions (mm/sec)	Half Width (mm/sec)	Fractional Dips	Relative Peak Areas
$Fe(4\text{-}CN\text{-}py)_2Cl_2$	4.2	0.17	0.40	0.059	122.1
	(4.1(c))	0.62	0.53	0.068	189.9
		1.07	0.35	0.050	91.9
		1.87	0.39	0.050	102.6
		2.36	0.54	0.061	171.2
		2.84	0.40	0.062	127.7
	1.4	0.06	0.40	0.080	169.1
	(4.1(d))	0.61	0.34	0.045	81.5
		1.16	0.34	0.070	125.2
		1.79	0.37	0.070	134.1
		2.37	0.36	0.038	71.6
		2.93	0.37	0.086	166.3
$Fe(4\text{-}Cl\text{-}py)_2Cl_2$	4.2	0.16	0.40	0.035	52.48
	(4.3(c))	0.54	0.53	0.027	53.8
		1.14	0.45	0.031	52.8
		1.59	0.49	0.037	68.8
		3.16	0.42	0.046	74.1
$Fe(3\text{-}Cl\text{-}py)_2Cl_2$ (A)	4.2	0.76	0.40	0.110	209.7
	(4.4(c))	1.06	0.30	0.089	125.4
		1.82	0.27	0.065	83.4
		2.12	0.46	0.100	216.5
$Fe(3\text{-}Cl\text{-}py)_2Cl_2$ (B)	4.2	0.08	0.42	0.053	115.5
	(4.5(c))	0.57	0.49	0.044	113.6
		1.08	0.46	0.055	132.3
		1.88	0.45	0.045	107.3
		2.43	0.51	0.035	92.9
		2.94	0.41	0.055	117.2
$Fe(3\text{-}Cl\text{-}py)_2Cl_2$ (B)	1.4	0.01	0.38	0.073	144.0
	(4.5(d))	0.57	0.38	0.045	89.0
		1.15	0.40	0.072	150.3
		1.81	0.40	0.061	129.2
		2.42	0.37	0.035	67.1
		3.01	0.38	0.076	149.5

Continued

Table 4.3 continued

Compound	Temperature (K) (Figure)	Peak Positions (mm/sec)	Half Width (mm/sec)	Fractional Dips	Relative Peak Areas
$Fe(3,5\text{-}Cl_2\text{-}py)_2Cl_2$	4.2	0.09	0.35	0.035	63.6
	(4.6(c))	0.39	0.38	0.046	92.4
		0.99	0.48	0.057	143.4
		1.43	0.39	0.014	28.7
		1.98	0.33	0.022	38.7
		3.49	0.39	0.065	130.2
	1.4	0.05	0.34	0.037	48.6
	(4.6(d))	0.37	0.35	0.042	57.1
		0.97	0.48	0.051	95.4
		1.42	0.31	0.015	18.1
		1.99	0.32	0.022	26.6
		3.50	0.37	0.059	82.7

Table 4.5 Magnetic data

χ'_m = susceptibility per mole, corrected for the diamagnetism of the ligands. (cgsu/mole)

$\mu_{eff} = 2.828\ (\chi'_m \times T)^{\frac{1}{2}}$ B.M. *

$Fe(4\text{-}CN\text{-}py)_2Cl_2$ (θ = +2K)

Temperature (K)	296	277	256	211.5	179	140.5	111.5	91
$\chi'_m \times 10^3$	13.29	14.18	15.22	18.78	22.22	27.78	35.02	42.67
μ_{eff}	5.61	5.60	5.58	5.64	5.63	5.59	5.59	5.57

$Fe(3\text{-}CN\text{-}py)_2Cl_2$ (θ = +2K)

Temperature (K)	299	278.5	260.5	220	180.5	142	106	93
$\chi'_m \times 10^3$	13.39	14.38	15.39	18.16	22.10	28.04	37.79	42.62
μ_{eff}	5.66	5.66	5.66	5.65	5.65	5.64	5.66	5.63

$Fe(4\text{-}Cl\text{-}py)_2Cl_2$ (θ = -8K)

Temperature (K)	295	258	226.5	181.0	162	141.5	123	100
$\chi'_m \times 10^3$	13.15	15.25	17.65	22.01	24.81	28.71	33.03	41.48
μ_{eff}	5.57	5.61	5.66	5.64	5.67	5.70	5.70	5.76

$Fe(3\text{-}Cl\text{-}py)_2Cl_2$ (A) (θ = -20K)

Temperature (K)	295	260.5	220	181	162	143	114	95
$\chi'_m \times 10^3$	13.70	15.57	18.76	23.50	26.67	30.88	39.57	50.12
μ_{eff}	5.69	5.70	5.75	5.83	5.88	5.94	6.00	6.17

$Fe(3,5\text{-}Cl_2\text{-}py)_2Cl_2$ (θ = -19K in the 300 to 90K region)

Temperature (K)	301	281	258.5	242	225.3	201	181	167
$\chi'_m \times 10^3$	13.29	14.48	15.78	16.98	18.45	20.93	23.62	25.80
μ_{eff}	5.66	5.70	5.71	5.73	5.77	5.80	5.85	5.87

* error $\pm$ 0.05 B.M.

Table 4.5 continued

Temperature (K)	144.5	127	109	88	77.5	66	50.7	40.5
$\chi_m' \times 10^3$	30.28	34.79	41.42	52.27	59.84	72.00	97.19	135.12
μ_{eff}	5.92	5.94	6.01	6.07	6.09	6.16	6.28	6.62

Temperature (K)	†30.1	24.95	20.3	18.45	13.75	10.0	7.2
$\chi_m' \times 10^3$	222.3	318.6	480.5	587.9	998.4	1917.0	2085.2
μ_{eff}	7.31	7.97	8.83	9.31	10.48	12.38	10.96

Temperature (K)	5.64	4.24	2.99	1.66
$\chi_m' \times 10^3$	2143.5	2168.6	2193.1	2224.8
μ_{eff}	9.83	8.58	7.24	5.43

† Values for highest field used.

$Fe(4\text{-CN-py})_2Br_2$ (θ = +4K)

Temperature (K)	298.5	277.5	243.0	206.5	178.0	144.5	107.0
$\chi_m' \times 10^3$	13.31	14.42	16.62	19.58	22.55	27.58	36.40
μ_{eff}	5.64	5.66	5.68	5.68	5.67	5.65	5.58

	Temperature (K)	$\chi_m' \times 10^3$	μ_{eff}
$Fe(3\text{-Br-py})_2Cl_2$	300	13.92	5.78
$Fe(3\text{ I-py})_2Cl_2$	299	13.16	5.61
$Fe(3,5\text{-}Cl_2\text{-py})_2Br_2$	298	13.25	5.62
$Fe(4\text{ CN py})_4I_2$	296	12.73	5.49
$Fe(3,5\text{-}Cl_2\text{-py})_4I_2$	296	12.27	5.39

CHAPTER 5 EXPERIMENTAL RESULTS AND DISCUSSION ON THE Fe^{II} COMPLEXES WITH DIAZINE LIGANDS

In this study, complexes of Fe^{II} chloride have been prepared with the ligands: pz, Mepz, pd, pm, 5-Mepm, 4-Mepm, 2-NH_2 pm. Attempts were made to prepare complexes of both $FeLCl_2$ and FeL_2Cl_2 stoichiometry. Using a preparative procedure analogous to that described in Chapter 4 for the pyridine complexes, but with an exact 1:1 ratio of ligand to metal, complexes of the $FeLCl_2$ type were obtained with all the ligands (except for 2-NH_2 pm, discussed later). The complexes precipitated immediately on mixing the ligand and ferrous chloride solutions, and in several cases the solids were so finely divided that separation could only be achieved by centrifugation.

Using an exact 2:1 ligand to metal ratio, only two pure FeL_2Cl_2 complexes (L = pz, 4-Mepm) could be isolated (again precipitation of the solids was immediate). With the remaining ligands, the $FeLCl_2$ complexes were again obtained, although the compound with Mepz appeared to contain a small excess (~ 5%) of ligand. It was found that great care was required to obtain pure samples of both $FeLCl_2$ and FeL_2Cl_2 compounds with pz and 4-Mepm, since a small deviation from the stoichiometric amount of ligand resulted in contamination with the other species.

Increasing the ligand to metal ratios to 4:1 and 6:1 produced no new FeL_2Cl_2 complexes, nor were any pure compounds isolated with stoichiometry higher than FeL_2Cl_2. A variety of solvent systems were tried, in an attempt to prevent the preferential precipitation of the $FeLCl_2$ species, but without success.

It is interesting to compare the stoichiometries of six-coordinate complexes formed by these ligands with Co^{II} and Ni^{II} chlorides.[117-119,129,135] With pm, pd and 5-Mepm, only $MLCl_2$ complexes have been obtained,[129,135] although ML_2X_2 compounds have been prepared for 5-Mepm with salts other than the chlorides. With 4-Mepm and 2-NH_2 pm, both $MLCl_2$ and ML_2Cl_2 compounds have been obtained, but $Co(2\text{-}NH_2\,pm)_2Cl_2$ has been found to be basically tetrahedral, and the corresponding Ni^{II} compound is believed

to contain bonded water.[135] A wider range of ML_2X_2 complexes have been obtained for the substituted pyrimidines with other Co^{II} and Ni^{II} salts, but not all possess a six-coordinate environment.[135] With Mepz, $MLCl_2$ compounds and, for Ni^{II}, the complex ML_5Cl_2, mentioned in Chapter 2, can be formed, and for pz, $MLCl_2$ and ML_2Cl_2 compounds have been prepared.[117-119] Therefore, there appears to be a predominance of $MLCl_2$ species, as found here for Fe^{II} chloride.

Some additional pyrazine complexes have been prepared for this study, with Fe^{II} bromide, thiocyanate and perchlorate. With the first two salts, $Fepz_2X_2$ complexes precipitated immediately from solutions containing 2:1 ligand to metal ratios, using a preparative method analogous to that for the chloride. However, for the bromide, the analyses, Mössbauer and reflectance spectra indicate the presence of a significant amount of presumably an $FepzBr_2$ species as impurity, although no pure $FepzX_2$ compounds could be obtained with either the bromide or thiocyanate. The complex $Fepz_2(ClO_4)_2 nH_2O$ was obtained only on reducing the solutions (containing 1:1, 2:1 or 3:1 ligand to metal ratios) to small volume. The water in this complex is presumably derived from the water of crystallisation of the perchlorate salt, even though the ethanolic solutions were dehydrated before mixing. The analysis suggests then n = 4, but the Mössbauer spectrum indicates a small amount of impurity in the compound.

It was not possible to recrystallise the compounds without decomposing them. They appear to be somewhat more stable than the substituted pyridine complexes, although the compounds with pm, 4-Mepm and pd tend to lose ligand after a few days, and are more moisture sensitive than the other complexes. The analyses of the compounds are collected in Table 5.1.

The $FeLCl_2$ Complexes

The spectral and magnetic measurements confirm that these compounds have six-coordinate structures, consistent with those represented in Figs. 2.2(a), (b). The Fe^{II} environment appears to be essentially similar to that found in the substituted pyridine complexes, i.e. a basically tetragonal geometry, but with the probability of additional

rhombic distortions, depending on the orientation of the rings and the arrangement of the bridging chlorides. These two factors should again be to some extent interdependent, especially in the compounds containing diazines with substituents adjacent to one or both of the coordinating nitrogen atoms, i.e. Mepz, 4-Mepm, 2-NH_2pm.

The methyl- and amino-groups have electron-donating inductive effects and the substituted diazines are stronger bases than the corresponding parent compounds (Table 2.1). They may therefore be expected to be stronger σ-donors, but weaker π-acceptors than the unsubstituted diazines. In the parent compounds themselves and in the derivatives which are symmetrically-substituted with respect to the coordinating nitrogen atoms, i.e. 5-Mepm, 2-NH_2pm, the σ-donor ability of both nitrogen atoms should be equivalent. However, in the asymmetrically-substituted ligands, i.e. Mepz, 4-Mepm, the nitrogen atom adjacent to the methyl group should have its σ-donor ability enhanced relative to the other atom, but, at the same time, greater steric interference with the chloride bridges may be experienced when bonding occurs through this hindered atom. If, with these ligands, the rings are arranged regularly so that each Fe^{II} ion is bonded to one hindered and one unhindered nitrogen atom, then only one Fe^{II} environment should exist. If, however, alternate Fe^{II} ions are bonded to two hindered and two unhindered atoms, respectively, two potentially inequivalent sites would be produced. If the arrangement is completely random, then three potentially different environments could arise.

Some structural differences are also expected between the complexes with pz, pd and pm, owing to the relative orientations of the nitrogen lone pairs on the individual diazines. Thus for pd, and possibly also pm, the N-Fe-N bond directions for adjacent Fe^{II} sites will not all lie parallel, and, if the Cl-Fe-N bond angles for each repeat unit approximate to 90°, the bridging chlorides will be non-planar (as is found, for example, in Cu(1,2,4-triazole)Cl_2,[199] where the heterocyclic ligand also bridges intrachain through adjacent nitrogen atoms). This may have some effect on the relative extent of covalent overlap with the metal orbitals, possible for the three diazines.

It may be mentioned here that the complex formed with 2-NH_2 pm (from $\frac{1}{2}$:1, 1:1, and 2:1 ligand to metal ratios) has a reproducible analysis (Table 5.1) but does not correspond exactly to an $FeLCl_2$ stoichiometry. The analysis indicates a slight excess of ligand, corresponding quite closely to a formulation $Fe(2\text{-}NH_2\,pm)_{1.1}Cl_2$. Analysis and melting point determination for the ligand indicate that it is free from contamination, and attempts to remove the excess ligand in the complex by controlled heating under vacuum resulted in the decomposition of the compound. The possible explanations for the anomalous analysis are

(a) the formation of a small but reproducible amount of, for example, an FeL_2Cl_2 species as impurity,

(b) occlusion of a reproducible quantity of free ligand, possibly due to a hydrogen-bonding effect of the $-NH_2$ group,

(c) the formation of very short diazine-bridged chains, such that the proportion of terminal units (of formal stoichiometry $Fe(2\text{-}NH_2\,pm)_{1.5}Cl_2$) is significantly large. The analytical figures would suggest an average chain-length of ten units in the direction of diazine-bridging.

The reproducibility of the analysis for different preparations suggests that (c) is the most reasonable explanation, especially since both bonded nitrogen atoms are sterically hindered in this ligand.

Electronic Spectra

The reflectance spectra of all the $FeLCl_2$ complexes contain a relatively weak resolved doublet in the 6000 - 10,000 cm^{-1} region (Table 5.2). In a previous report of the spectra of $FepmCl_2$ and $FepdCl_2$, only one broad band at ~ 10,000 cm^{-1} was observed, but the lower energy component is definitely present, although somewhat obscured by ligand modes. A strong band at ~ 21,000 - 25,000 cm^{-1} is also present in most of the compounds, due to charge transfer or ligand $\pi \leftrightarrow \pi^*$ transitions, and in the pyrimidine complexes a very weak band is observed in the 13,000 - 15,000 cm^{-1} region, which may be due to a formally spin-forbidden transition to a component of the higher-lying spin singlet or triplet levels.

The band positions are very similar to those found for the substituted-pyridine complexes, and the $d\sigma$ values are therefore assumed to be positive, corresponding to a stronger axial σ-antibonding strength of the diazine relative to that of the chlorides in the plane. There is again no obvious correlation between the $d\sigma$ and pK_a values of the ligands, which is not unexpected since the steric effects mentioned above may cause significant structural and bonding differences within the series.

For the parent diazines, $d\sigma$ decreases in the order pd > pz > pm, whereas the pK_a values decrease in the order pd > pm > pz. The reversal of the order of $d\sigma$ for pm and pz may indicate that the orientation of the nitrogen lone pairs for pm is less favourable than for pz for interchain σ-overlap with the metal d-orbitals.

For the complexes with Mepz, 4-Mepm and 2-NH_2pm, the $d\sigma$ values are lower than for those with the appropriate parent diazines. This suggests that the axial field is weakened by the steric effect of the substituents, even though the ligands are stronger bases. It is noted, however, that the more basic 2-NH_2pm gives a higher $d\sigma$ value than 4-Mepm, even though both bonded nitrogen atoms must be hindered in the former case. For the complex with 5-Mepm, the $d\sigma$ value is larger than that for the pm complex. There should be no significant steric hindrance with the methyl-substituent in this case, and the increase in $d\sigma$ therefore appears to reflect the higher basicity of this ligand.

The $d\sigma$ values for these complexes are slightly lower than those found for the substituted pyridine complexes, which may be partially due to a reduction in the σ-bonding ability of the diazine when both ring nitrogens must be simultaneously involved in donation. The 10 D_q values are, however, comparable to those in the pyridine complexes, and, for the pz, pm and pd complexes, are higher than that for $Fepy_2Cl_2$. This may indicate that the contribution to the ligand field strength from π-back bonding is considerably greater for the diazines than for pyridine, and compensates for the weaker σ-bonding. This would be consistent with the greater reduction in ring electron density, when two nitrogen atoms are involved in σ-bonding. It is noted that, although the $d\sigma$ value for $Fe(5\text{-Mepm})Cl_2$ is higher than that for $FepmCl_2$,

the 10 Dq value is lower. This would be consistent with a lesser degree of π-back bonding for the ligand substituted with an electron-donating group.

Mössbauer Spectra

The Mössbauer spectra of these complexes have been obtained at 300, 77, 4.2 and 1.4 K. The least-squares fittings of the data to Lorentzian line-shapes are shown in Figs. 5.1 to 5.7, and the parameters from the fittings are collected in Table 5.3.

All of the complexes, except $Fe(2\text{-}NH_2pm)Cl_2$ show one quadrupole doublet at 300 and 77 K. For $Fe(2\text{-}NH_2pm)Cl_2$, an additional very weak doublet is present outside the main bands, which indicates a second Fe^{II} site, and may correspond to the proportion of terminal units mentioned above.

The data for $Fe(Mepz)Cl_2$ and $Fe(4\text{-}Mepm)Cl_2$ cannot be fitted well to simple Lorentzian line-shapes and the half-widths are seen to be abnormally broad. This suggests that slightly inequivalent Fe^{II} sites are present, due to an irregular arrangement of the hindered and unhindered nitrogen donor atoms. The spectra may therefore correspond to near superpositions of quadrupole doublets from two or more sites, which differ slightly in their centre shifts and/or quadrupole splitting. The parameters given in Table 5.3 for these compounds are therefore averages for the various sites. It is unlikely that this very small variation in environment would be detected by any of the other techniques used.

There is also a marked asymmetry in the peak intensities and areas for $Fe(4\text{-}Mepm)Cl_2$, which may arise from the Goldanskii-Karyagin effect or from relaxation processes, as outlined in Chapter 4. Partial orientation of crystallites may again be discounted, since the solid is extremely finely divided.

The pz, Mepz and pd complexes show only one quadrupole doublet at 4.2 and 1.4 K, with again abnormally broad lines for the Mepz complex. All the pyrimidine complexes show additional peaks at low temperature due to magnetic ordering processes.

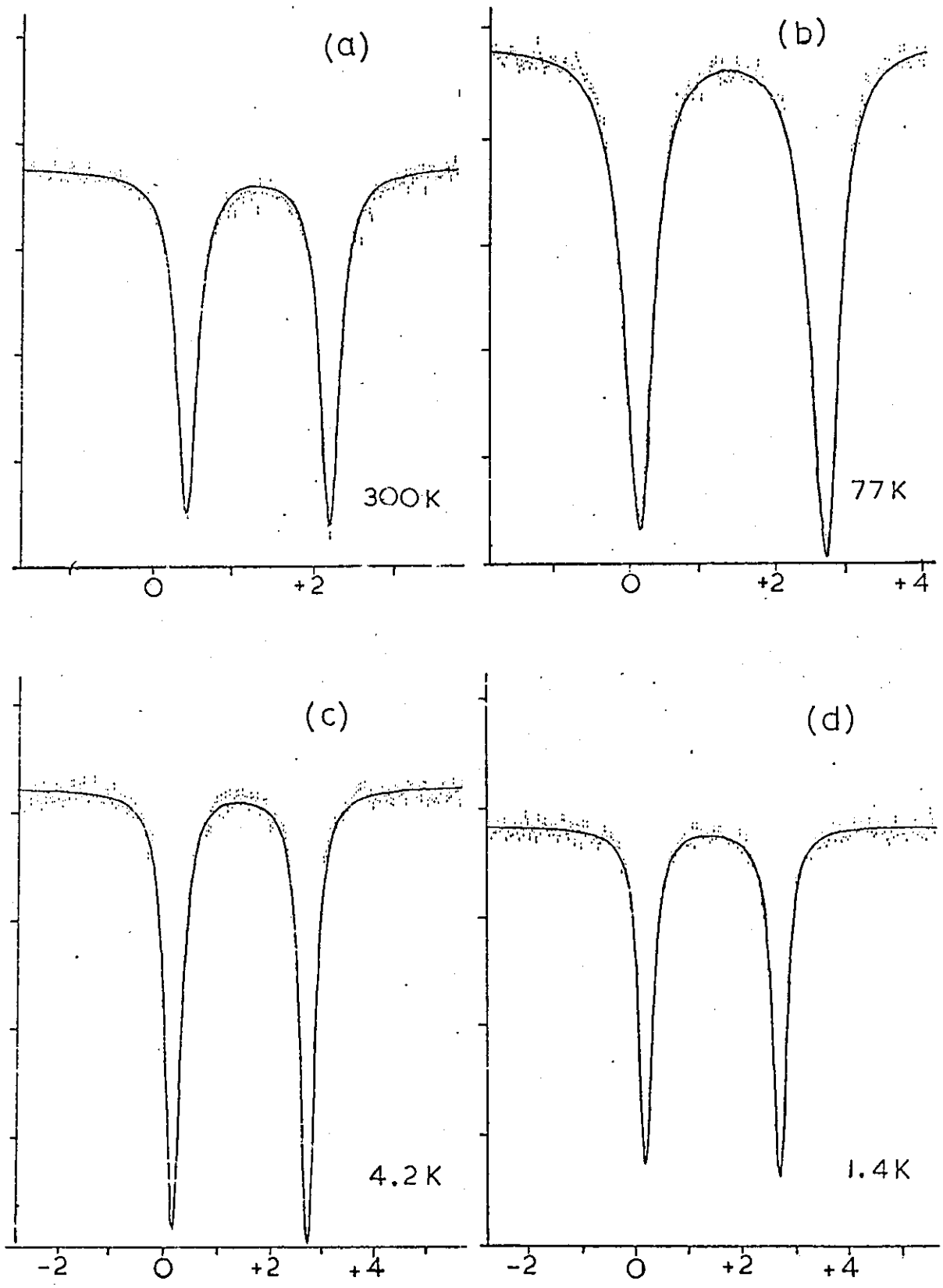

Fig. 5.1. Mössbauer spectra of $FepzCl_2$

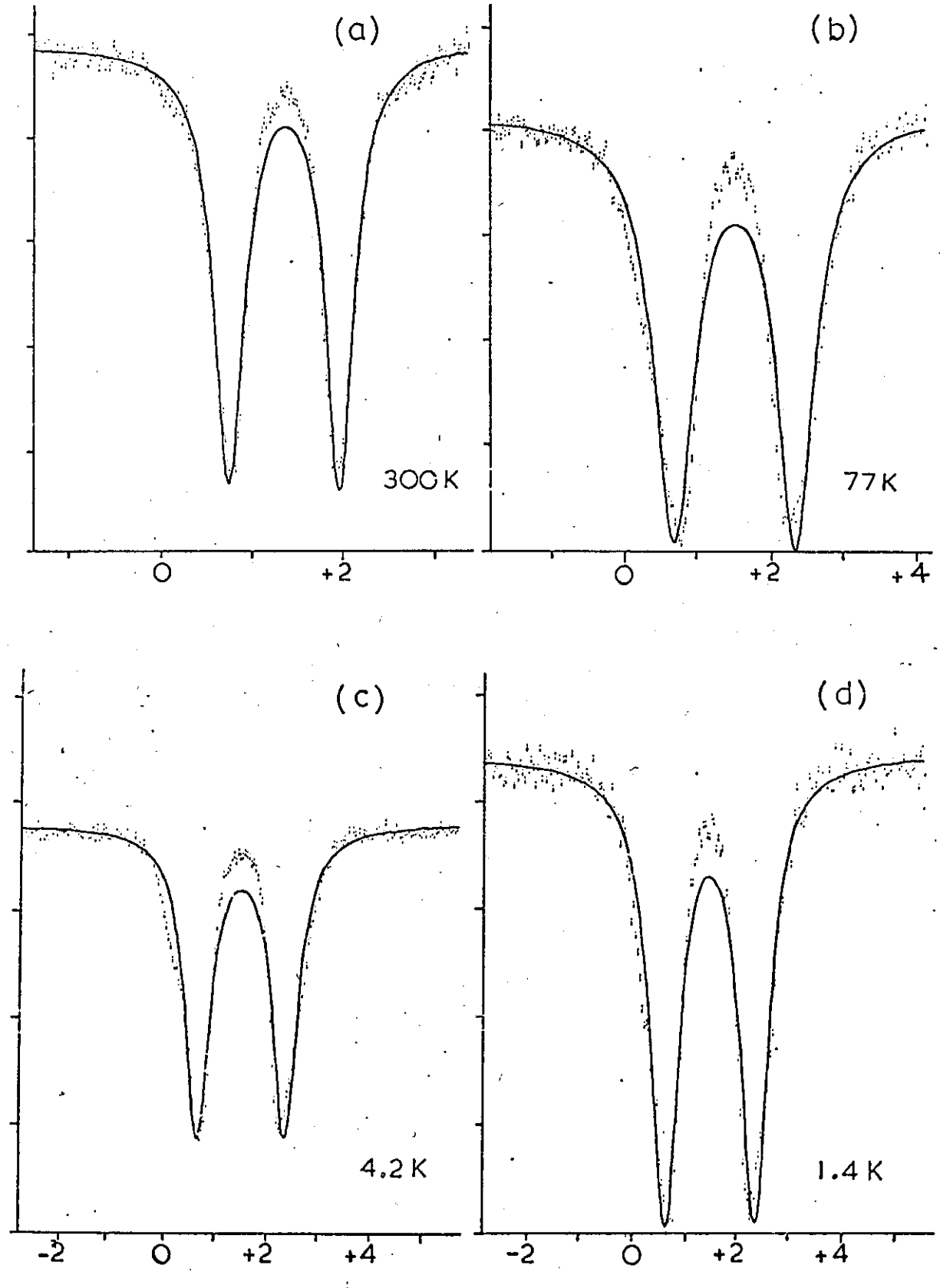

Fig. 5.2. Mössbauer spectra of $FeMepzCl_2$

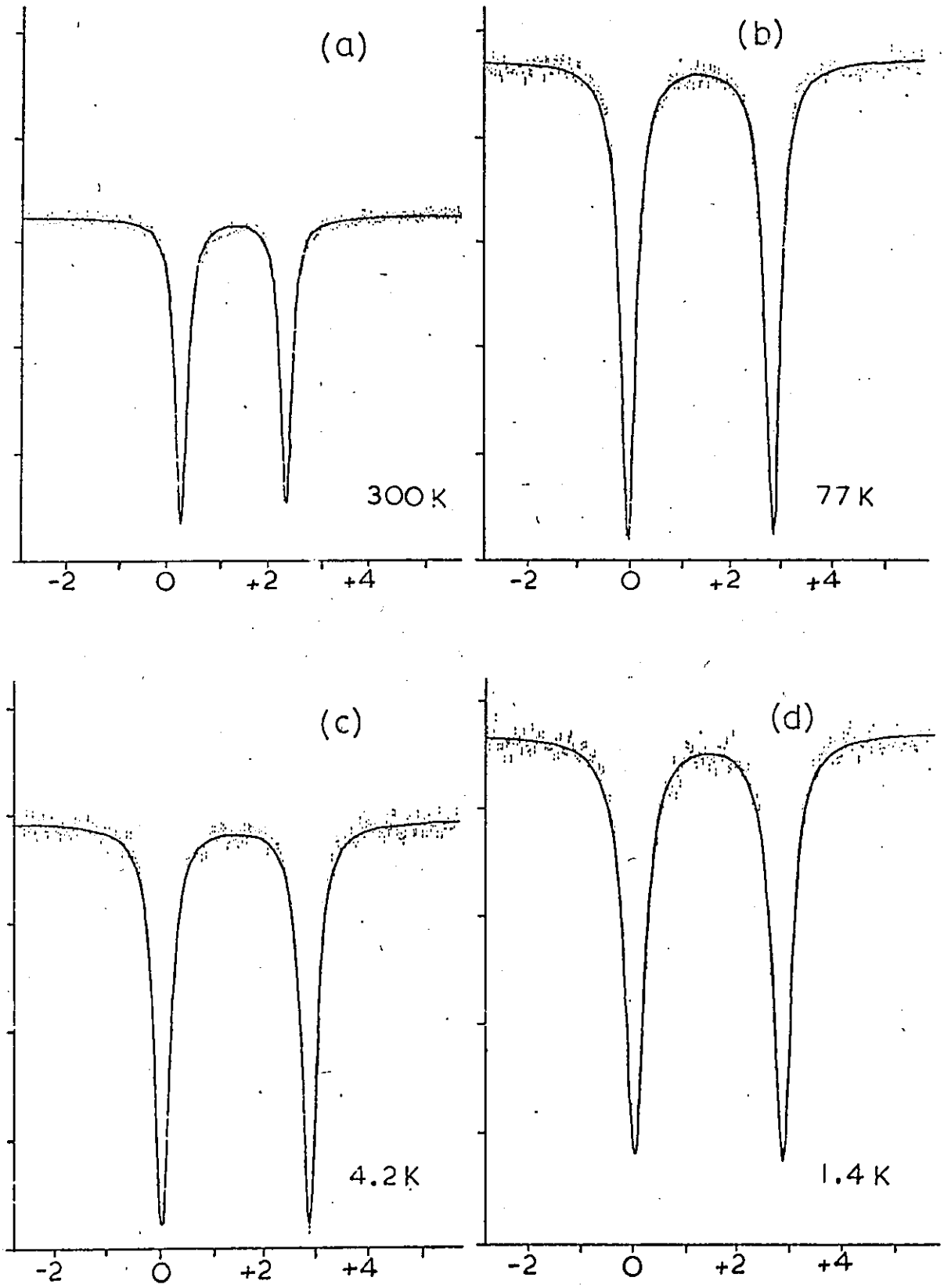

Fig. 5.3. Mössbauer spectra of $FepdCl_2$

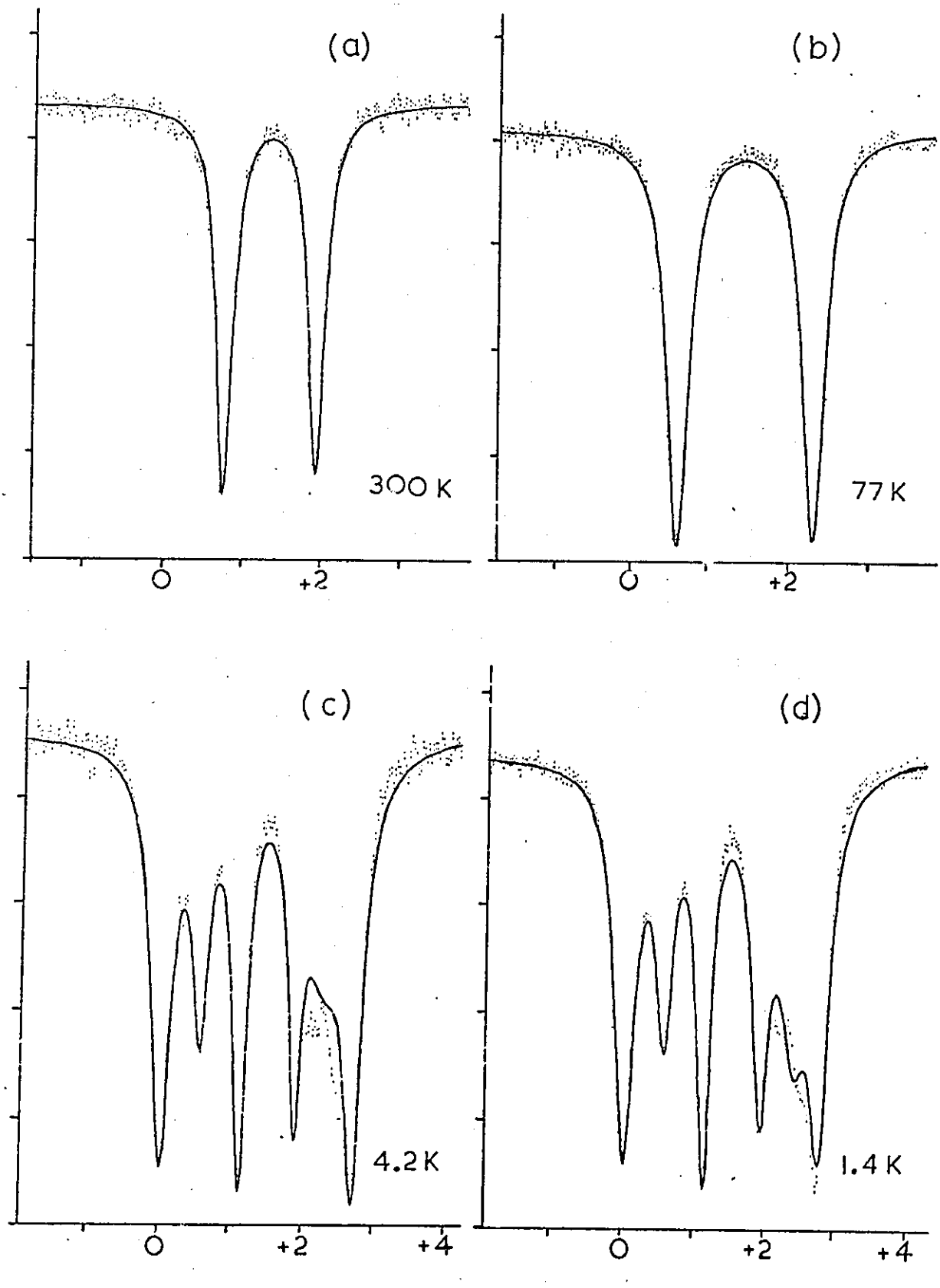

Fig. 5.4. Mössbauer spectra of $FepmCl_2$

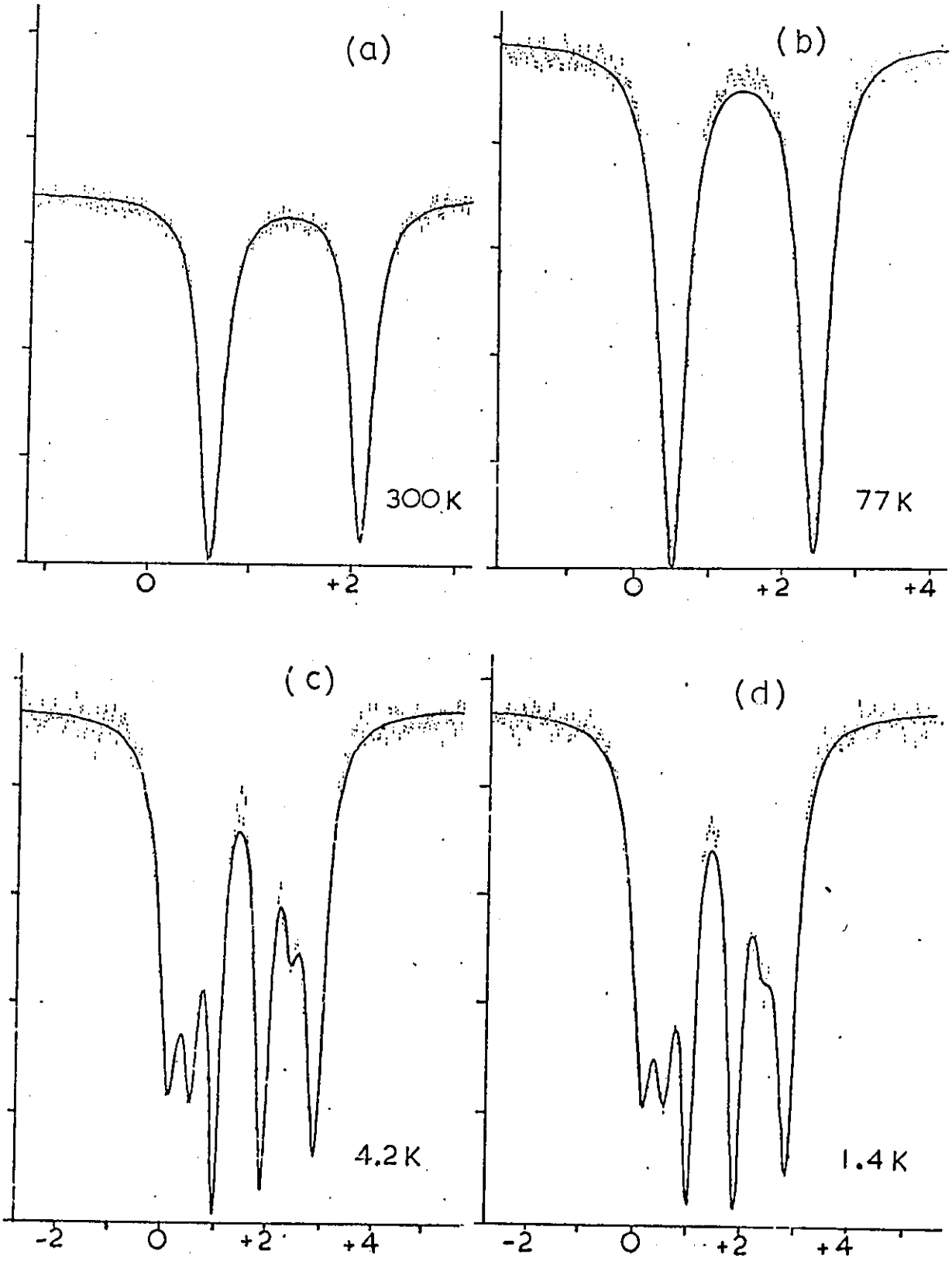

Fig. 5.5. Mössbauer spectra of $Fe(5\text{-Mepm})Cl_2$

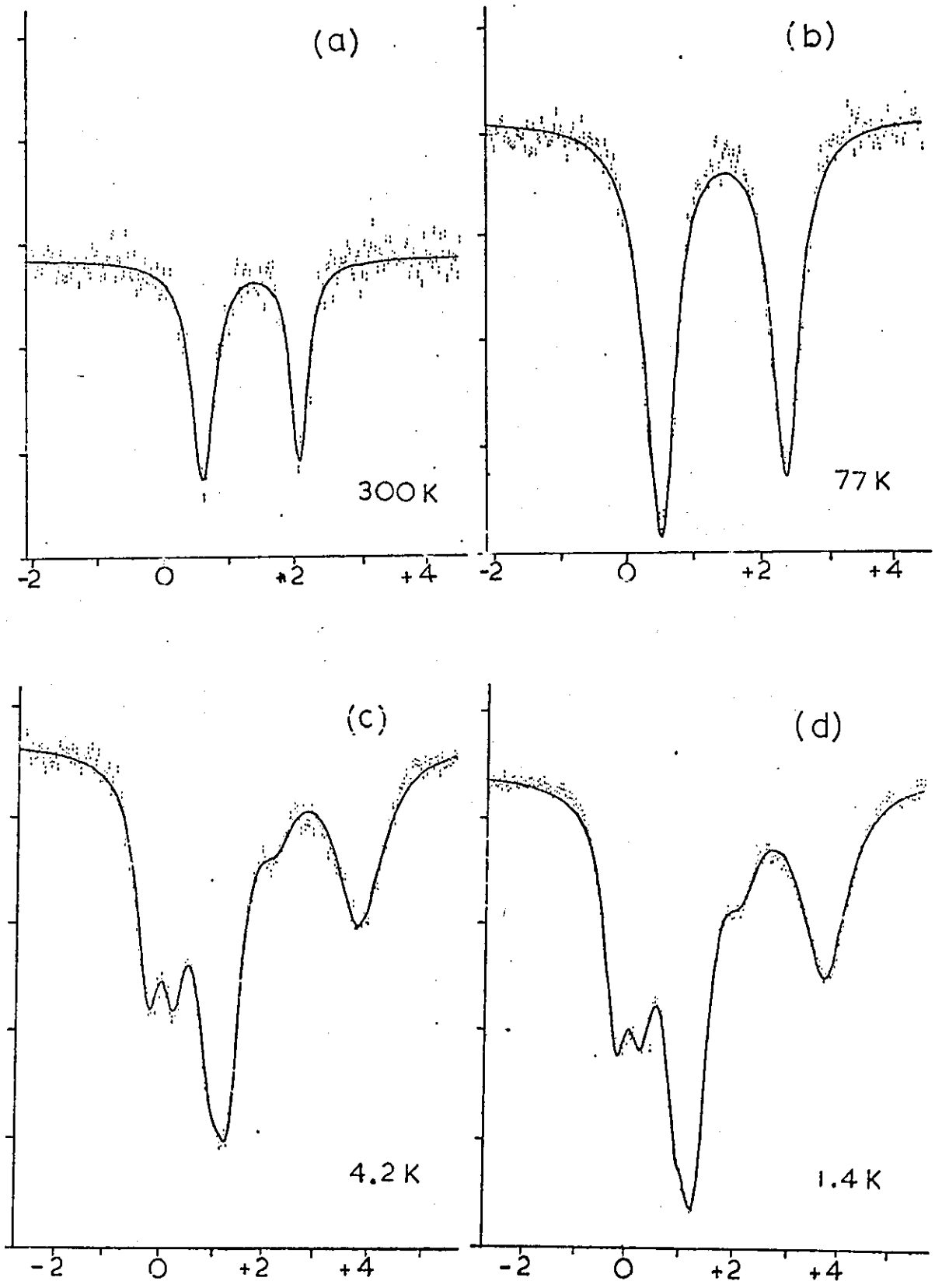

Fig. 5.6. Mössbauer spectra of $Fe(4\text{-Mepm})Cl_2$

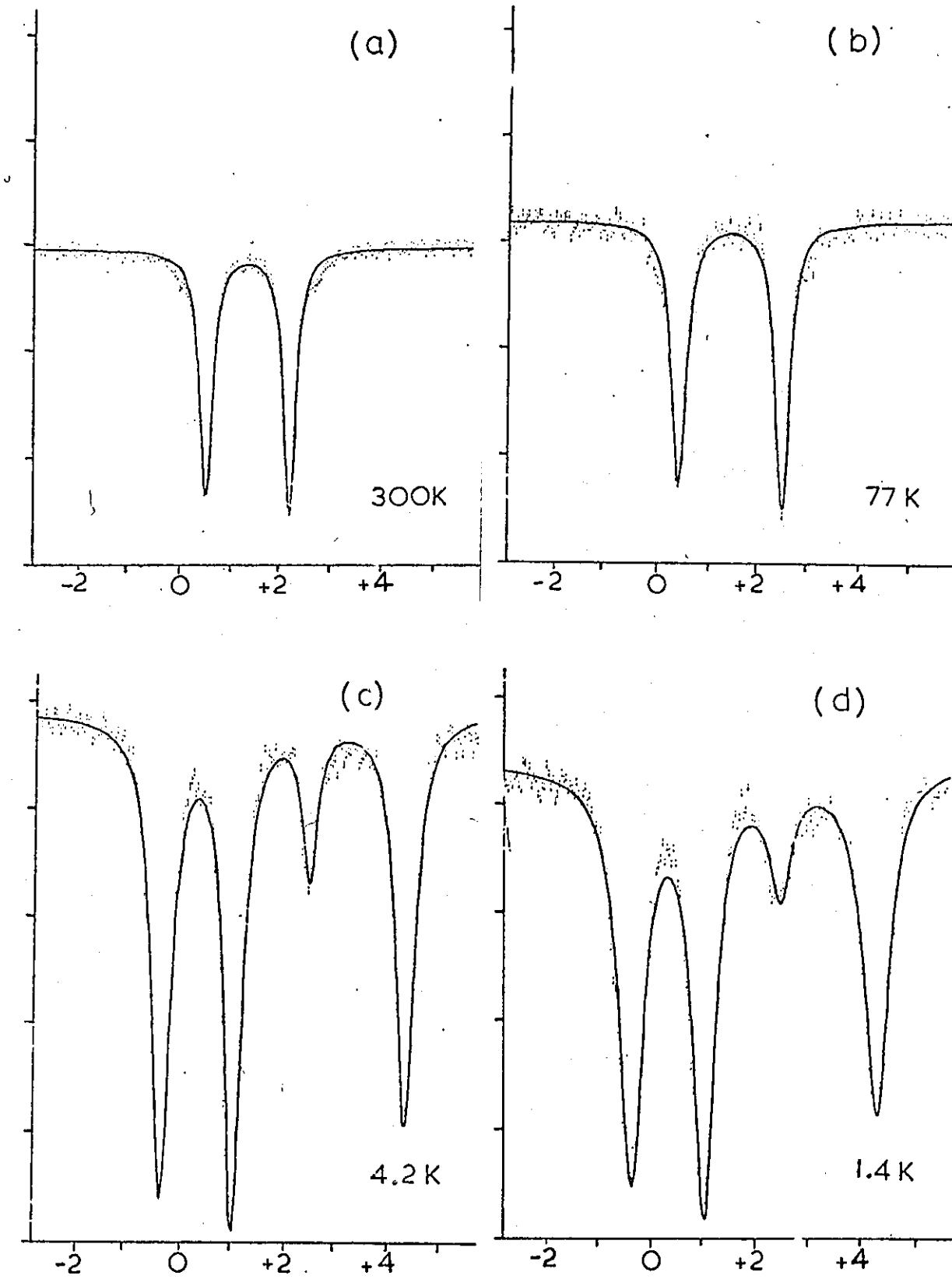

Fig. 5.7. Mössbauer spectra of $Fe(2\text{-}NH_2pm)Cl_2$

Centre Shifts

The values are comparable to, or slightly lower than those for the substituted-pyridine complexes.

Quadrupole Splittings

The values of ΔE_Q lie in the range 1.2 to 2.1 mm/sec. at 300 K, increasing to 1.7 to 2.8 mm/sec. at 77 K. For the complexes showing no magnetic splitting, there is little change in ΔE_Q between 77 and 1.4 K. The values are again very similar to those for the substituted-pyridine complexes, although $FepzCl_2$ and $FepdCl_2$ appear to give the largest low-temperature values of both series. The sign of ΔE_Q has not been determined for these compounds, but it seems reasonable to assume that it is positive (as found in the pyridine series) corresponding to an orbital singlet state lowest.

Magnetic Hyperfine Splittings

The magnetic ordering temperatures, determined from the temperature of collapse of the hyperfine splitting patterns are given in Table 5.4.

Table 5.4

Compound	Magnetic Ordering Temperature (K)
$FepmCl_2$	8.2 ± 1.5
$Fe(5\text{-Mepm})Cl_2$	9 ± 2
$Fe(4\text{-Mepm})Cl_2$	15 ± 2
$Fe(2\text{-}NH_2\text{pm})Cl_2$	26 ± 1

The splitting patterns are generally more complex than those observed in the substituted-pyridine complexes, and it has not been possible to analyse them in detail.

For $FepmCl_2$ (Fig. 5.4), seven peaks are present, although it has only been possible to fit six using the least-squares program. (The second peak at most positive velocity is an average of two). Six

peaks are present for both $Fe(5\text{-Mepm})Cl_2$ (Fig. 5.5) and $Fe(4\text{-Mepm})Cl_2$ (Fig. 5.6), but in the latter, the two strong central peaks are almost superimposed and the broadness of several of the peaks (especially that at most positive velocity) suggests that more than six transitions may be contained under the absorption envelope. This may be due to the proposed mixture of bonding sites, which may cause a slight variation in the internal field, or to a mixing of the nuclear spin state, so that the two formally forbidden transitions ($\mp \frac{1}{2} \leftrightarrow \pm \frac{3}{2}$) can occur. This latter case presumably applies to the $FepmCl_2$ complex. The compound $Fe(2\text{-}NH_2\,pm)Cl_2$ shows only four peaks at both 4.2 and 1.4 K. The observation of magnetic ordering from susceptibility measurements (presented below), eliminates the possibility that the extra peaks could be due to the impurity. Although the line widths do not appear to be greatly broadened compared with the other complexes, it seems likely that several of the six or eight possible transitions are virtually degenerate.

The complexity of these spectra suggest that there may be no simple relationship between the 'internal' field direction and the e.f.g. axes, and also that the asymmetry parameter may be quite significant in at least some of the compounds. However, it does appear that the 'internal' fields for all the complexes are less than ~ 150 kG.

Magnetic Measurements

The magnetic data for these complexes are presented in Table 5.5.

The room temperature values of μ_{eff} lie in the range 5.3 to 5.6 BM. For $FepzCl_2$ (300 - 100 K) and $FepdCl_2$ (300 - 50 K), μ_{eff} decreases gradually with decreasing temperature, yielding small positive θ values from the $1/\chi'_m$ v. T plots. For $FeMepzCl_2$, (300 - 100 K) there is a small increase in μ_{eff} on decreasing the temperature, with a resulting small negative θ value. For $FepmCl_2$ (300 - 100 K) and $Fe(5\text{-Mepm})Cl_2$ (300 - 50 K), μ_{eff} shows a slight maximum and then begins to decrease with decreasing temperature.

The complexes $Fe(4\text{-Mepm})Cl_2$ and $Fe(2\text{-}NH_2\,pm)Cl_2$ have been measured down to 1.6 K. The susceptibility and μ_{eff} v. temperature plots in

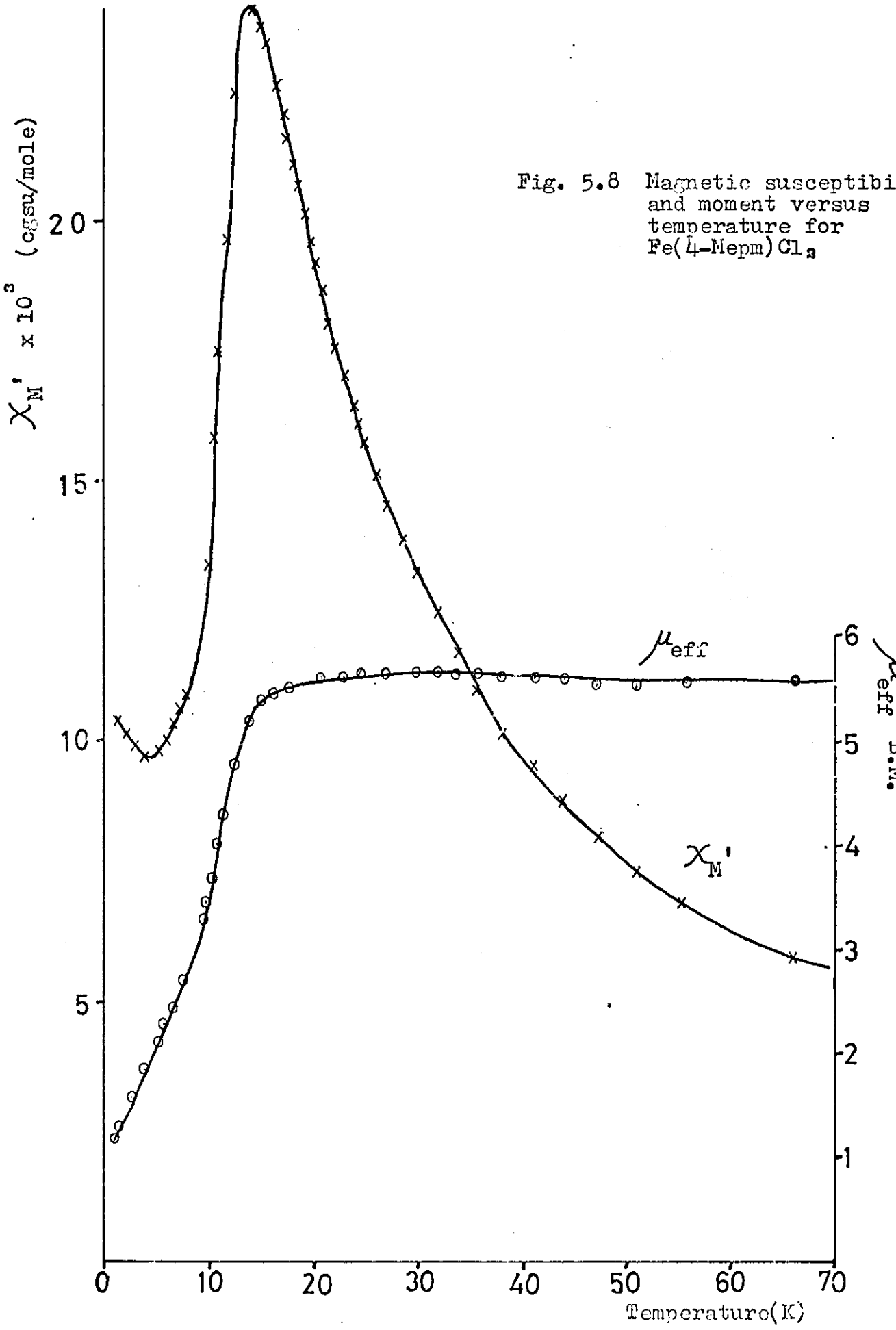

Fig. 5.8 Magnetic susceptibility and moment versus temperature for Fe(4-Mepm)Cl_2

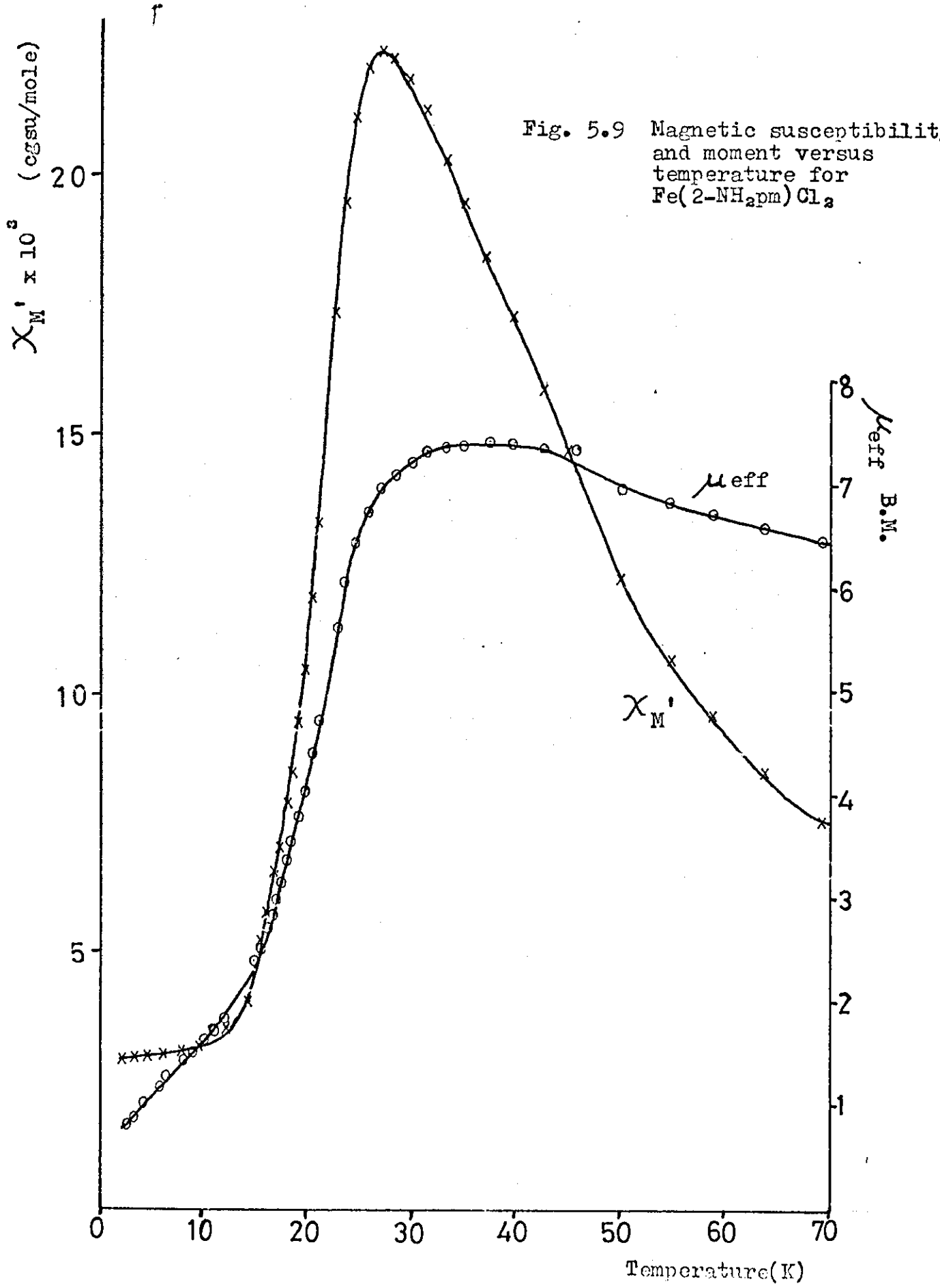

Fig. 5.9 Magnetic susceptibility and moment versus temperature for $Fe(2\text{-}NH_2pm)Cl_2$

the 70 to 1.6 K region are shown in Figs. 5.8 and 5.9, respectively, for the highest value of field used. The values for $Fe(2\text{-}NH_2pm)Cl_2$ have been calculated on the basis of a pure $FeLCl_2$ species, and may therefore be somewhat in error since the magnetic behaviour of the minor species present may differ from that of the major species. However, since the identity and magnetic properties of this minor species are not known, no attempt has been made to correct the values for its presence.

For both complexes, μ_{eff} increases steadily down to ~ 20 K ($Fe(4\text{-}Mepm)Cl_2$) and ~ 30 K ($Fe(2\text{-}NH_2pm)Cl_2$). On further cooling there is a sharp decrease in both susceptibility and moment, indicating the presence of antiferromagnetic ordering. The Néel temperatures, taken as the maxima in the χ'_m v. T plots are 13.5 K for $Fe(4\text{-}Mepm)Cl_2$ and 27.5 K for $Fe(2\text{-}NH_2pm)Cl_2$, which therefore agree quite well with the ordering temperatures determined from the Mössbauer measurements.

The residual susceptibility in both complexes at very low temperature is quite high. This may indicate a very small separation between the ground $S' = 0$ and an excited $S' = 1$ state, or it could be due to the presence of an impurity. For $Fe(2\text{-}NH_2pm)Cl_2$, a paramagnetic impurity with $\mu_{eff} = 4.90$ BM and constituting ~ 2% of the sample could account for the entire residual magnetism at 2 K. For $Fe(4\text{-}Mepm)Cl_2$, a small amount of paramagnetic impurity could also amount for the slight increase in susceptibility below 4 K.

It seems reasonable to assume, from the results on these complexes, that the ordering in all the pyrimidine complexes is antiferromagnetic.

The FeL_2X_2 Complexes

The measurements carried out on these compounds again indicate a six-coordinate environment, and they may therefore contain either bridging or terminal diazine (Chapter 2).

I.R. Spectra

The I.R. bands observed for $Fepz_2Cl_2$, $Fepz_2Br_2$, $Fepz_2(NCS)_2$ and $Fepz_2(ClO_4)_2 \cdot 4H_2O$ are listed in Table 5.6, together with those for the free ligand and for $FepzCl_2$, for comparison.

The shifts and splittings of the pyrazine modes are quite similar for all the complexes. Furthermore, it is noted that all the compounds show a band (with splitting in $Fepz_2Cl_2$ and $Fepz_2(NCS)_2$) in the 975 - 992 cm^{-1} region, with very weak intensity for $FepzCl_2$ and highest intensity in $Fepz_2(NCS)_2$. On the criterion of Lever et al. (Chapter 2), the observation of this band should indicate a terminal pz structure for all the complexes. However, its presence in $FepzCl_2$, which must contain bridging pz, casts doubt on the validity of this criterion, unless it is proposed that, in this compound, the weak band arises only from the small proportion of terminal units of the sheets, in which the pz molecules may be bonded through one nitrogen atom only.

The presence of water in the perchlorate complex is confirmed by the observation of the bands at 3,500 - 3,200 cm^{-1} (ν_1, ν_3) and at 1635 cm^{-1} (ν_2),[200] but no further bands could be detected which are definitely assignable to water coordinated to the metal. The ClO_4^- ν_3 absorption,[200] in the 1200 - 1000 cm^{-1} region, overlaps considerably with the strong hydrogen-bending modes of the pyrazine molecule, but does appear to be split into two components. The ν_1 symmetric stretching mode, which is I.R. inactive for the regular T_d symmetry of the ClO_4^- ion,[200] is also present, with weak to medium intensity, at 918 cm^{-1}. This indicates a lowering of the symmetry of the ClO_4 group to C_{3v}, which would be consistent with unidentate coordination to the metal. It is possible, however, that the symmetry may be lowered by crystal field effects or by hydrogen-bonding interaction with the water molecules.

The three fundamental modes of the NCS group, ν_1 (C-N), ν_2 (C-S) and δ (N-C-S), are all to some extent sensitive to the mode of coordination of the group, i.e. thiocyanato-, isothiocyanato-, or bridging form.[200] The characteristic regions for these modes are:

	ν_1 (cm^{-1})	ν_2 (cm^{-1})	δ (cm^{-1})
thiocyanato	2080-2120	690-720	400-440
isothiocyanato	2040-2080	780-860	450-490
bridging	2080-2130	780-790	~450-490

The δ mode is doubly degenerate and will generally split into two components as the M-S-C-N linkage departs from linearity, i.e. in the thiocyanato and bridging forms.

In $Fepz_2(NCS)_2$, the ν_4 band is at 2060 cm^{-1}, and the ν_2 band is at 790 cm^{-1} (there are, in fact, three bands in the 790 - 825 cm^{-1} region, but this assignment for ν_2 appears most likely, from comparison with the positions of the pyrazine γ(C-H) modes in the other $Fepz_2X_2$ complexes). The δ band is at 486 cm^{-1} and is essentially unsplit. It may therefore be concluded that the complex contains the N-bonded isothiocyanato group, with little departure of the Fe-N-C-S linkage from linearity. To achieve six-coordination in this complex, the pz molecules must therefore be bridging.

The shifts and splittings of the ligand bands in $Fe(4\text{-Mepm})_2Cl_2$ and $Fe(4\text{-Mepm})Cl_2$ are again quite similar, although there appears to be an additional weak band at 1210 cm^{-1} in the former.

Electronic Spectra

The positions of the bands assignable to metal d-d transitions in these complexes are contained in Table 5.2.

The band positions for $Fe(4\text{-Mepm})_2Cl_2$ are extremely similar to those observed in the $FeLCl_2$ complexes and in the substituted-pyridine complexes, which strongly suggests a chloride-bridged structure, with terminally-bonded pyrimidine molecules in axial positions. On this basis $d\sigma$ is positive, corresponding to a stronger axial field. It is noted that the analogous Ni^{II} and Co^{II} complexes have also been proposed to have this structure.[135] As mentioned earlier, the N(3) and N(1) atoms of this ligand have potentially inequivalent σ-bonding capability. Comparing the Δ_2, $d\sigma$ and $10Dq$ values with those of $Fe(4\text{-Mepm})Cl_2$ (which from the Mössbauer evidence are presumably averages of the various combinations of N(3) and N(1) bonding by the bridging ligand), it is seen that all the parameters are larger for $Fe(4\text{-Mepm})_2Cl_2$, but the difference in 10 Dq is quite small. σ_z would be expected to be greater when the ligand is terminal rather than bridging, but the similarity in 10 Dq values may suggest that the increase in σ_z is partially compensated by a decrease in σ_{xy} and/or the π-back bonding contribution to the ligand field. This would appear to be more consistent with bonding through N(3) in $Fe(4\text{-Mepm})_2Cl_2$, since weakening of the in-plane field may then arise from steric interaction between the chlorides and the 4-methyl groups, and the degree of π-back bonding should be lessened by the electron-donating effect of the methyl group, which may be more important at this end of the ring.

The spectra of the $Fepz_2X_2$ complexes are quite different from those of the chloride-bridged polymers. For the chloride, bromide and perchlorate compounds only one broad band, in the 11,000 - 12,500 cm^{-1} region, can definitely be assigned to a metal d-d transition, while for the thiocyanate, a small splitting of the band centred in this region is observed. (In the bromide samples and in some preparations of the chloride, a shoulder was observed at ~ 10,000 cm^{-1} and an additional weak band was present at ~ 6000 cm^{-1}. However, the analyses of these samples indicate the presence of an $FeLX_2$ impurity and it can be seen that these extra bands correspond closely to those observed for $FepzCl_2$. These bands are absent in $Fepz_2Cl_2$ samples with good analyses).

The band positions in these compounds are thus of the order of 3000 cm^{-1} higher in energy than those of the chloride-bridged polymers, and in fact approximate more closely to the higher energy component of the doublet observed for the FeL_4X_2 complexes with py, γ-pic, iso-quin[89] (the lower component in these latter compounds is at ~ 7000 - 10,000 cm^{-1}). From the I.R. evidence on the mode of bonding in $Fepz_2(NCS)_2$ and the observation made earlier that the ligand field strength of bridging pyrazine appears to be comparable to or slightly higher than that of pyridine, it therefore seems probable that all these complexes have FeN_4X_2 environments with bridging pyrazine (Fig. 2.2(d)). The axial ligand in $Fepz_2(ClO_4)_2 \cdot 4H_2O$ may be either unidentate ClO_4 or a water molecule.

On this basis, the in-plane field would be expected to be stronger than the axial field, so that the antibonding orbital of predominantly $d_{x^2-y^2}$ ($^5B_{1g}$) character should lie highest i.e. Δ_2 and $d\sigma$ negative. A small splitting in $Fepz_2(NCS)_2$ is consistent with an FeN_6 environment. However, from the positions of the axial ligands in the spectrochemical series, it might be expected that Δ_2 and $d\sigma$ should increase in the order $NCS < H_2O$ or ClO_4 (?) $< Cl < Br$, with the total ligand field strength decreasing in the reverse order. Therefore if the single band observed for the chloride, bromide and perchlorate complexes corresponds to the transition to the $^5B_{1g}$ state, a second component at lower energy would be expected, corresponding to the transition to the $^5A_{1g}$ (d_{z^2}) state. It is possible that a second weak band may be present in the 5000 - 4000 cm^{-1} region, where it may be obscured by the relatively

strong ligand modes. It is noted that only one band was observed in a previous report of the reflectance spectra of $Fepz_2Cl_2$ and $Fepz_2Br_2$,[129] and also that in the spectra of the analogous Ni^{II} complexes[118,119] no band splittings were observed, and the spectra were interpreted on an O_h model.

The single bands for the chloride, bromide and perchlorate are extremely broad and it therefore seems likely that both components of the $^5T_{2g} \leftrightarrow {}^5E_g$ transition are contained under the band envelope. The band positions given in Table 5.2 would therefore correspond to a measure of 10 Dq. The order of decreasing 10 Dq appears to be H_2O or ClO_4 (?) > NCS ≥ Br ≥ Cl. This order and the apparently larger axial fields in these compounds compared with the $Fepy_4X_2$ compounds, could be rationalised on the basis of more extensive π-back bonding with the pyrazine molecule. The ability of the Fe^{II} ion to delocalise its electrons into the empty π*-orbitals of the pyrazine ring would be expected to increase as the electronegativity of the axial group decreases, i.e. as the degree of charge transfer along the Fe-X bond increases. This order would be Br > Cl > H_2O or ClO_4 (?) > NCS, and thus the combination of σ- and π-bonding effects may produce the order of 10 Dq observed for these compounds. The enhancement of the axial σ-donation by the in-plane π-back bonding may then produce a higher total ligand field and a more uniform perturbation of the metal eg orbitals than is found in the pyridine compounds.

It is noted that for the pyrazine-bridged structure shown in Fig. 2.2 (d), it is probable that the planes of the rings will be tilted at an angle to the $Fe\text{-}N_1\text{-}N_4$ axis (as found for example in $Copy_4Cl_2$ [182]), to minimise steric interaction between the ring hydrogen atoms, and with the axial ligand. For such an orientation, overlap with the π*-orbitals of the ring should be possible for all three metal t_{2g} orbitals, the overlap increasing for the d_{xy}, and decreasing for the d_{xz}, d_{yz}, as the angle between the planes of the rings and the X-Fe-X bond direction decreases.

Mössbauer Spectra (Table 5.3)

The spectra of $Fepz_2Cl_2$ (Fig. 5.10) and $Fe(4\text{-Mepm})_2Cl_2$ (Fig. 5.11) have been measured at 300, 77, 4.2 and 1.4 K. For $Fepz_2(NCS)_2$ and $Fepz_2(ClO_4)_2.4H_2O$, room temperature spectra have been obtained (in the latter compound, two weak peaks due to an impurity were observed), but for $Fepz_2Br_2$ the resolution was very poor and it appeared that more than one species was present.

For $Fe(4\text{-Mepm})_2Cl_2$, the centre shifts and small ΔE_Q values at 300 and 77 K are again very similar to those found for the other chloride-bridged complexes. The small temperature dependence of ΔE_Q is reminiscent of that observed for $Fe(3,5\text{-}Cl_2\text{-py})_2Cl_2$ and $Fe(3\text{-Cl-py})_2Cl_2$ (A). There is again a marked peak asymmetry, as was found for $Fe(4\text{-Mepm})Cl_2$. The half-widths of the lines are considerably broadened at 77 K, which may suggest that a mixture of N(3) and N(1) bonding sites is, in fact, present, but this effect could also be due to relaxation processes since the compound exhibits magnetic ordering at 4.2 and 1.4 K.

The magnetic splitting pattern consists of only three very broad lines at both temperatures, with very little alteration in line positions or relative intensities. Several of the six or eight possible transitions must be virtually degenerate, and it has not been possible to analyse the spectrum in any detail. The 'internal' field appears to be less than ~ 80 kG, but does not coincide with the major e.f.g. axis. The ordering temperature was found to be 7 ± 2 K.

The $Fepz_2X_2$ complexes have significantly lower centre shifts than the chloride-bridged complexes with both the diazines and the substituted pyridines, which is consistent with stronger σ-bonding for the FeN_4X_2 environment. The values are also slightly lower than many of the FeL_4X_2 complexes with py, γ-pic and iso-quin,[89] which may suggest a greater degree of 3d-electron delocalisation. The ΔE_Q values are much larger than those for the chloride-bridged polymers, and for $Fepz_2Cl_2$, the value is similar to those found for FeL_4Cl_2 (L = py, γ-pic, iso-quin).[89] This compound shows no magnetic hyperfine splitting at low temperature, although the lines are somewhat broadened.

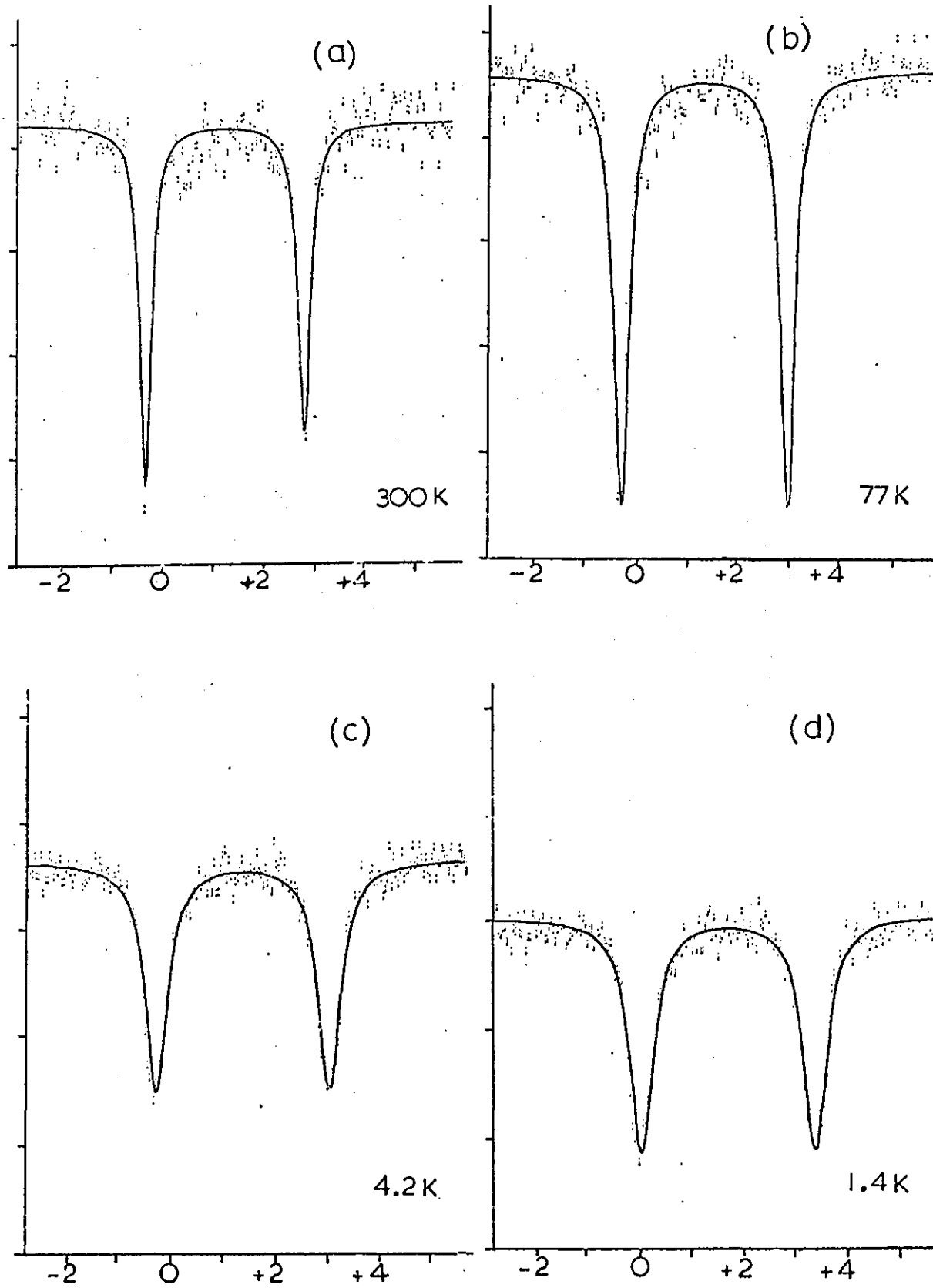

Fig. 5.10. Mössbauer spectra of $Fepz_2Cl_2$

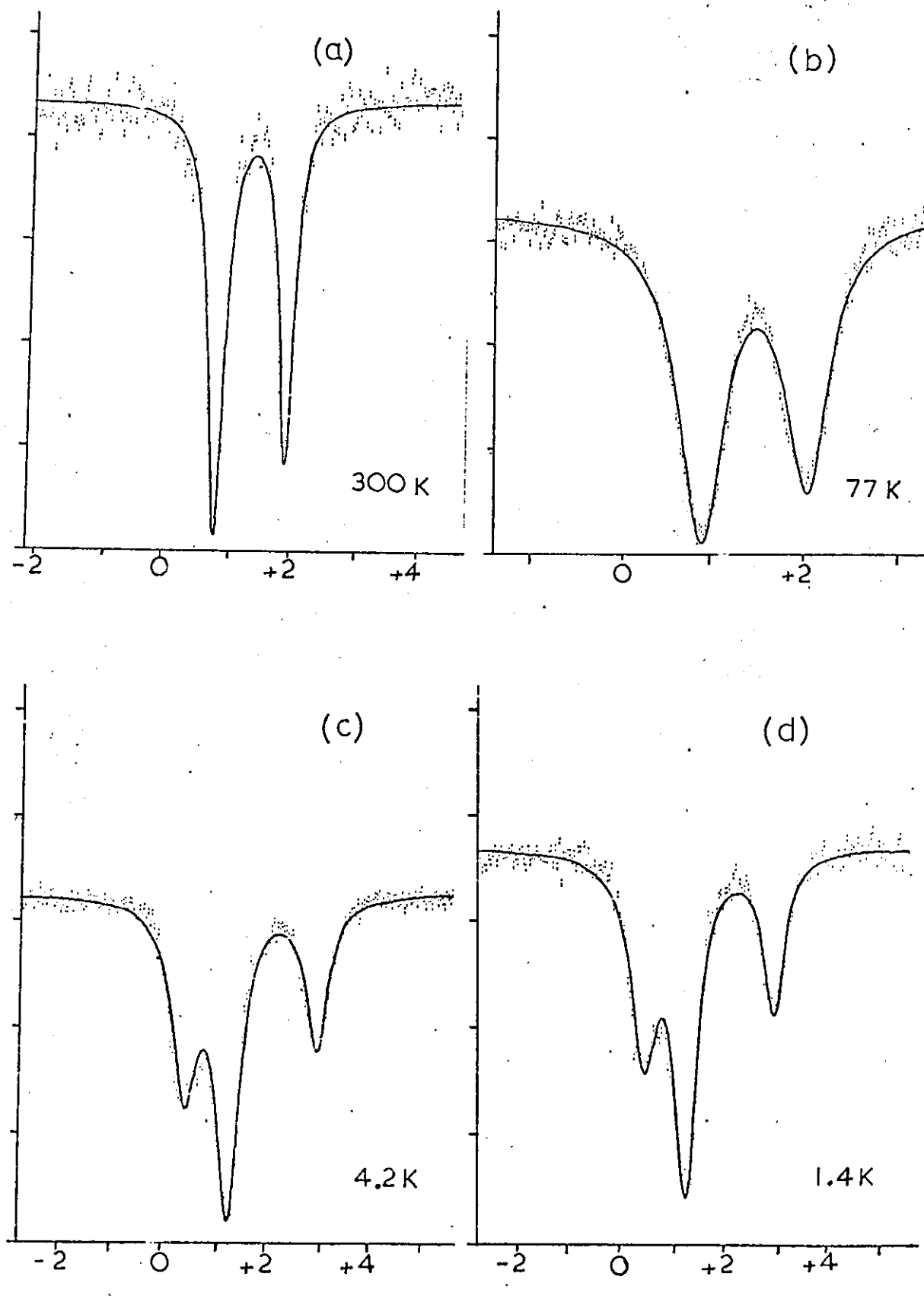

Fig. 5.11. Mössbauer spectra of $Fe(4\text{-Mepm})_2Cl_2$

Magnetic Measurements

The magnetic data obtained for $Fepz_2Cl_2$, $Fepz_2(NCS)_2$ and $Fe(4\text{-Mepm})_2Cl_2$ are listed in Table 5.5. For the remaining two compounds, the magnetic susceptibility was not measured over a temperature range since the samples contained some impurity.

For $Fe(4\text{-Mepm})_2Cl_2$, the high value of μ_{eff} at room temperature and the marked increase on decreasing the temperature, is very similar to the behaviour observed for the substituted-pyridine compounds, and suggests that the ordering at low temperature is ferromagnetic in sign. For $Fepz_2Cl_2$, the small decrease in μ_{eff} to the spin-only value at 50 K appears to be more consistent with an orbitally non-degenerate ground state, with little contribution from thermally accessible excited levels, rather than to the presence of an antiferromagnetic exchange interaction. For $Fepz_2(NCS)_2$, the μ_{eff} values obtained here agree quite well with a previous report,[26] and show a slight maximum at ~ 200 K.

Discussion of the Results

As in the case of the substituted-pyridine complexes, it has not been possible to obtain conclusive information on the exact nature and magnitude of the distortions in the $FeLCl_2$ complexes with the diazines. The electronic spectra are consistent with a tetragonal compression along the z axis (N-Fe-N bond direction), but the relatively low ΔE_Q values and the presence of considerable orbital contribution to the magnetic moments again suggest that the overall ground state splittings are not very large.

If the ΔE_Q values are assumed to be mainly due to q_{val}, and to reflect the overall splitting of the $^5T_{2g}$ level, then some correlation can be made between these values and the Δ_2 values from the electronic spectra. For the parent diazines, the decreasing order of ΔE_Q, and thus approximately of the ground state splitting, parallels that of Δ_2. Similarly, $Fe(Mepz)Cl_2$ has a smaller ΔE_Q value, and $Fe(5\text{-Mepm})Cl_2$ a larger ΔE_Q value than the appropriate parent compounds, which reflects the same trend as Δ_2. However, $Fe(4\text{-Mepm})Cl_2$ has a ΔE_Q value virtually identical to that of $Fe(5\text{-Mepm})Cl_2$ at both 300 and 77 K, and $Fe(2\text{-NH}_2\text{pm})Cl_2$

has the highest value of all the pyrimidine complexes, and the correlation with Δ_2 no longer appears to hold. The complexity of the magnetic splitting patterns in the low temperature Mössbauer spectra of the pyrimidine complexes may suggest that significant rhombic distortions are present in these compounds. The larger ΔE_Q values for the complexes with substituted pyrimidines compared with that with the parent ligand may also be partially due to a lesser degree of t_{2g} delocalisation through π-back bonding in the former compounds.

The lower values of μ_{eff} in the diazine compounds compared with the substituted-pyridine complexes may also reflect a greater degree of covalency in the former compounds. However, the opposite signs of the magnetic ordering in the pyrimidine and pyridine complexes may invalidate this proposal. There is no apparent correlation between the room temperature values of μ_{eff} and ΔE_Q for these compounds, as has been proposed for systems with D_{4h} symmetry,[53,54] which tends to confirm that the microsymmetry of the Fe^{II} environment in the diazine complexes is lower than axial. The magnitude of the temperature variation of μ_{eff} for the complexes in the high temperature region is insufficiently large to obtain any meaningful information from attempted fitting of the values to the variable parameter model.

For the $Fepz_2X_2$ complexes, the higher ΔE_Q values suggest larger ground state splittings, increasing in the order $ClO_4 > Cl > NCS$, with an orbital singlet state lowest. For an axial system with a stronger in-plane field, either the doublet (d_{xz}, d_{yz}) or the singlet (d_{xy}) level may lie lowest, the latter being stabilised as the ratio of the axial field parameters, $^{Dt}/_{Ds}$, increases. This ratio tends to increase as the degree of covalency in the compound increases and, since the assumption of a large covalent contribution was required to rationalise the electronic spectra of the $Fepz_2X_2$ complexes, it seems reasonable to propose that the singlet (d_{xy}) state lies lowest. A greater degree of π-back bonding for the d_{xy} orbital relative to that for the d_{xz}, d_{yz} orbitalscould contribute to the stabilisation of the former orbital. If it is proposed that the doublet state lies lowest, then a very large rhombic distortion, splitting the two components, would have to be postulated to explain the large ΔE_Q values. There does not appear to

be any compelling reason why a large rhombic distortion should be present in these complexes, and it is noted that a d_{xy} ground state has been found to be consistent with the results on the FeL_4X_2 complexes (L = py, γ-pic, iso-quin; X = Cl, Br, I).[89] It is noted, however, that the very small ΔE_Q values, and the correlation between ΔE_Q and μ_{eff}, for the complexes $FeL_4(NCS)_2$, indicates a doublet ground state for these compounds.[89] Although this possibility cannot entirely be discounted for $Fepz_2(NCS)_2$, the much larger ΔE_Q value does appear to be more consistent with a singlet ground state and thus tends to confirm this proposal of more extensive covalency in the pyrazine complexes.

The temperature variation of μ_{eff} for $Fepz_2Cl_2$ can be fitted quite well to an axial model, with a singlet d_{xy} ground state, for the ground state splitting, spin-orbit coupling and covalency parameters in the ranges: $\Delta_1 = +700 - 800\ cm^{-1}$, $\lambda = 70 - 80\ cm^{-1}$ and $K = 0.5 - 0.6$. The temperature dependence and low temperature limit of ΔE_Q are also reasonably compatible with these values. It is noted that, in a previous attempt[26] to fit the magnetic data for $Fepz_2(NCS)_2$ to the axial model, a considerable degree of covalency was indicated ($\lambda = 70 - 80\ cm^{-1}$, $K = 0.7\ cm^{-1}$), although the very small temperature variation of μ_{eff} prevented unambiguous determination of the sign and magnitude of Δ_1.

The experimental data on the complex $Fe(4\text{-Mepm})_2Cl_2$ suggest a very similar environment to that found in the substituted-pyridine complexes. The failure of the compound to adopt a pyrimidine-bridged structure, analogous to that in the $Fepz_2X_2$ complexes, may be partly due to the greater difficulty in accommodating the methyl substituents. Tilting of the planes of the rings should relieve steric hindrance between these substituents themselves, but may introduce steric interaction with the axial ligands. It is noted that an FeL_4Cl_2 complex has not been prepared with α-picoline.

The nature of the magnetic ordering found in the complexes with pyrimidine ligands can be rationalised in terms of the proposed structures. The susceptibility measurements on $Fe(4\text{-Mepm})_2Cl_2$ suggest a ferromagnetic interaction. On the proposed terminal pyrimidine structure, the only pathway for exchange is the $\sim 90^\circ$ Fe-Cl-Fe bridges,

which should result in a parallel coupling of the net spins of the metal ions, as found in some of the substituted pyridine complexes.

In the $FeLCl_2$ complexes (L = pm, 5-Mepm; 4-Mepm, 2-NH_2 pm), any exchange process through the chloride bridges should again be ferromagnetic, and it is possible that such an intrachain interaction is present in these compounds. (The increase in μ_{eff} for both $Fe(4\text{-Mepm})Cl_2$ and $Fe(2\text{-}NH_2\,pm)Cl_2$ before the long range ordering sets in, may provide some evidence for this). However, the overall coupling at low temperatures in these compounds is antiferromagnetic, which indicates that an additional interchain mechanism must operate to couple the spins on adjacent chains antiparallel. The obvious pathway is via the π-orbitals of the intervening diazine molecule. Overlap of the empty π*-orbitals of the ring with the d_{xz}, d_{yz} orbitals of the two Fe^{II} ions across which it bridges, enables delocalisation of the unpaired spins of each metal ion into the same ligand orbital. This must produce antiparallel alignment of the net spins by the Pauli principle. Although exchange involving π-overlap is generally weaker than that involving σ-overlap, it does appear that the former effect can become quite large when the π-system is highly delocalised.[62] It is also possible that some contribution to the antiferromagnetic exchange may arise from an Fe-Cl-Cl-Fe pathway since the chain separation, determined by the Fe-N---N-Fe distance, must be significantly less than in the substituted-pyridine complexes. This observation that 4-Mepm can transmit antiferromagnetic interaction between the two Fe^{II} ions across which it bridges tends to confirm the assignment of a chloride-bridged structure for $Fe(4\text{-Mepm})_2Cl_2$. It is also noted that antiferromagnetic interaction has been proposed, on the basis of magnetic measurements in the 300 - 80 K region, for the complexes $Co(5\text{-Mepm})_2Br_2.2H_2O$ and $Ni(5\text{-Mepm})Br_2.2H_2O$, which are believed to contain bridging pyrimidine only.[135]

It might be expected that the complexes $FepzCl_2$, $FeMepzCl_2$ and $FepdCl_2$ should also exhibit antiferromagnetic coupling, since the ligands also provide delocalised π-systems between metal ions. Small positive Weiss-constants were observed for the pz and pd complexes, but the Mössbauer spectra at low temperature provide no evidence for magnetic coupling. For $FepdCl_2$, the non-planarity of the chloride bridges,

mentioned earlier, may decrease the possibility of intrachain ferromagnetic exchange. Also, any antiferromagnetic coupling through the pyridazine molecule would also be intrachain, and would thus compete with any ferromagnetic interaction through the chloride bridges, which may result in no net magnetic ordering. The apparent lack of ordering in the pz and Mepz complexes could be due to the fact that the distance between Fe^{II} ions on adjacent chains is significantly larger than in the pyrimidine complexes.

The apparent absence of exchange in $Fepz_2Cl_2$ tends to confirm a pyrazine-bridged structure. For such an arrangement, the only plausible exchange pathway is through overlap of the metal t_{2g} orbitals with the ligand π^*-system, so that any coupling should be antiferromagnetic. However, if the degree of this π-overlap is greatest for the metal d_{xy} orbitals, then exchange may not occur, since these orbitals are completely filled.

It must be noted that the absence of magnetic hyperfine splitting in the Mössbauer spectra of these pyrazine and pyrimidine complexes is not necessarily conclusive evidence for no magnetic ordering, since the internal fields resulting from very weak coupling may be insufficiently large for splitting to be resolved. Although the susceptibility data obtained so far do not indicate the presence of ordering in these compounds, measurement down to 1.6 K is required before the possibility of exchange via these bases can be definitely ruled out.

From the observations made on these diazine complexes, the following conclusions may be drawn. Firstly, it appears that the mid-I.R. criterion of Lever et al. is not generally valid, since the pz complexes prepared here contain the critical band, but have been shown to possess bridging rather than terminally-bonded ligand. Secondly, by comparison of the 10 Dq values of the $FeLCl_2$ complexes with that of $Fepy_2Cl_2$, and of $Fepz_2Cl_2$ with $Fepy_4Cl$, it appears that the bridging diazines are comparable in total ligand field strength to pyridine, but that this is partially due to a greater degree of π-back bonding with the diazines. However, if, as in the case of the analogous Ni^{II} complexes,[118,119] comparison is made between $Fepz_2Cl_2$ and $Fepy_2Cl_2$, the ligand field strength of pyrazine appears misleadingly high. It may therefore be proposed that the Mpz_2X_2 complexes of Ni^{II} and Co^{II} also contain bridging rather than terminal pyrazine. This would then be compatible with the much greater 10 Dq value observed for $Nipz_2Cl_2$ compared with $NiMepzCl_2$, which, as mentioned in Chapter 2, was rationalised entirely in terms of the steric effect of the methyl group. It is noted that, by comparison of the 10 Dq values for $FepzCl_2$ and $FeMepzCl_2$, the effect of the methyl group appears to reduce the ligand field strength only by the order of 500 cm^{-1}.

During the course of this work, several recent papers have been published by Goldstein et al., which support the conclusions obtained here. From the study of some pyrazine complexes of stannic halides,[128] these workers have also refuted the general validity of the mid-I.R. criterion for the mode of bonding of pyrazine. They have concluded that a more valid means of distinguishing unidentate and bidentate pyrazine is by comparison of the I.R. and Raman spectra of the complex. For the former mode of bonding, the lack of a centre of symmetry for the molecule produces numerous coincidences of I.R. and Raman bands.

This treatment has been applied[196] to the $MpzX_2$ and Mpz_2X_2 complexes of Co^{II} and Ni^{II} halides, and, in conjunction with extensive far I.R. measurements, the bridging nature of the pyrazine molecule has been demonstrated for all the complexes. The assignment of a bridging-pyrazine structure for $Copz_2Cl_2$ has also been recently confirmed by crystal structure determination,[201] and the structure is essentially that shown in Fig. 2.2(d). The Co-Cl and Co-N distances are 2.415 and 2.18 Å, respectively, and there is no evidence for a significant rhombic distortion. The four pyrazine rings around each Co^{II} ion are arranged in a propellor-like manner, the plane of each ring being tilted at an angle of 44.4° about the Co-N-N axis.

Magnetic susceptibility measurement on the $Nipz_2X_2$ complexes, in the range 300 - 90 K, have also been interpreted[196] as showing negligible exchange interaction.

Although no definite evidence for exchange interactions via pyrazine or pyridazine bridges has been obtained in this work, it must be mentioned that antiferromagnetic coupling via these ligands has been proposed[131] from magnetic studies on some six-coordinate polymeric complexes of the $CuLCl_2$ type (L = pz, Mepz, pd, pm). The positive θ values, from susceptibility measurements in the 300 - 110 K region, increase in the order Mepz $\approx$ pz $\ll$ pm $<$ pd. It is noted, however, that exchange coupling via the chloride bridges has been postulated[198] as being antiferromagnetic in these compounds (see also Chapter 4), and thus the evidence for additional exchange via the Mepz and pz bridges is very tenuous. The relatively high degree of exchange in $CupdCl_2$ is not inconsistent with the observations made here, since, in the Cu^{II} case, antiferromagnetic

exchange through the diazine would augment the interaction through the chloride bridges, rather than opposing it as in the Fe^{II} case.

The only established example of antiferromagnetic exchange through a pyrazine bridge is in the complex $Cupz(NO_3)_2$,[202] which has a polymeric six coordinate structure, with each pair of Cu^{II} ions in the linear chain being linked by single pyrazine bridge.[203] Although the Cu^{II} ions are separated by 6.712 Å, a J value of $-6cm^{-1}$ has been obtained from fitting of the susceptibility data in the range 65 - 2.9 K. The mechanism for the interaction has been proposed as involving interaction between the single unpaired electron in the σ-antibonding level of the Cu^{II} ion with the π-electrons on the pyrazine molecule.

Table 5.1 Elemental Analyses for the Diazine Complexes

Compound	Colour	C % Required	N % Required	H % Required	C % Found	N % Found	H % Found	
$Fepz Cl_2$	Deep Orange-Red	23.23	13.54	1.95	23.18	13.56	2.05	
$FeMepz Cl_2$	Orange	27.19	12.68	2.74	28.03	12.63	3.29	
$Fepd Cl_2$	Orange-Brown	23.23	13.54	1.95	23.24	13.64	2.04	
$Fepm Cl_2$	Yellow	23.23	13.54	1.95	23.49	13.47	2.28	
$Fe(5\text{-}Mepm) Cl_2$	Orange-Yellow	27.19	12.68	2.74	27.35	13.12	2.82	
$Fe(4\text{-}Mepm) Cl_2$	Mustard-Yellow	27.19	12.68	2.74	27.44	12.76	3.00	
$Fe(2\text{-}NH_2 pm) Cl_2$	Pale Yellow	21.66	18.94	2.27	22.70	19.42	2.63	*
$Fepz_2 Cl_2$	Deep Orange-Red	33.49	19.53	2.81	33.28	19.43	2.60	
$Fepz_2 Br_2$	Orange-Brown	25.56	14.90	2.15	24.61	14.03	2.62	*
$Fepz_2 (NCS)_2$	Tan Brown	36.15	25.30	2.41	36.18	25.42	2.82	
$Fepz_2 (ClO_4)_2 . 4H_2O$	Yellow	19.70	11.50	3.29	18.60	11.46	3.17	*
$Fe(4\text{-}Mepm)_2 Cl_2$	Yellow	38.13	17.79	3.84	38.29	17.94	3.85	

* See text

Table 5.2 Reflectance Spectra

Compound	Band Positions (d-d transitions) cm^{-1}	Δ_2 cm^{-1}	$d\sigma$ cm^{-1}	10 Dq cm^{-1}
$FepzCl_2$	9780, 6600	+3180	+1190	8190
$FeMepzCl_2$	8970, 6460	+2510	+ 940	7720
$FepdCl_2$	9910, 6640	+3270	+1230	8280
$FepmCl_2$	9500, 6470	+3040	+1140	7980
$Fe(5\text{-}Mepm)Cl_2$	13720*			
	9550, 6350	+3210	+1200	7950
$Fe(4\text{-}Mepm)Cl_2$	14650*			
	8450, 6230	+2220	+ 830	7340
$Fe(2\text{-}NH_2pm)Cl_2$	14290*			
	8670, 6280	+2390	+ 900	7480
$Fepz_2Cl_2$	11360			
$Fepz_2Br_2$	11490			
$Fepz_2(NCS)_2$	13100, 10150	-2850	-1070	11580
$Fepz_2(ClO_4)_2 \cdot 4H_2O$	12350			
$Fe(4\text{-}Mepm)_2Cl_2$	13950*			
	9420, 5900	+3520	+1320	7660

* Very weak

Table 5.3 Mössbauer Data

$FeLCl_2$ Complexes

Compound	Temperature (K) (Figure)	Centre Shift (mm/sec)	ΔE_Q (mm/sec)	Half Widths (mm/sec)	Intensity Ratio†	Area Ratio†
$FepzCl_2$	300 (5.1(a))	1.32	1.78	0.30,0.29	0.97	1.00
	77 (5.1(b))	1.43	2.53	0.47,0.44	0.95	1.00
	4.2 (5.1(c))	1.43	2.56	0.35,0.33	0.97	1.03
	1.4 (5.1(d))	1.43	2.53	0.32,0.32	0.97	0.96
$FeMepzCl_2$	300 (5.2(a))	1.34	1.22	0.41,0.38	0.99	1.06
	77 (5.2(b))	1.49	1.67	0.68,0.63	0.99	1.06
	4.2 (5.2(c))	1.48	1.69	0.58,0.59	1.00	0.99
	1.4 (5.2(d))	1.48	1.72	0.68,0.66	1.00	1.04
$FepdCl_2$	300 (5.3(a))	1.30	2.09	0.29,0.27	1.06	1.12
	77 (5.3(b))	1.43	2.89	0.37,0.36	1.01	1.04
	4.2 (5.3(c))	1.44	2.83	0.36,0.35	1.01	1.03
	1.4 (5.3(d))	1.44	2.83	0.47,0.43	0.99	1.08
$FepmCl_2$	300 (5.4(a))	1.33	1.18	0.27,0.26	1.05	1.09
	77 (5.4(b))	1.46	1.72	0.35,0.33	1.01	1.05
$Fe(5\text{-}Mepm)Cl_2$	300 (5.5(a))	1.33	1.48	0.27,0.27	1.05	1.08
	77 (5.5(b))	1.45	1.92	0.45,0.44	1.02	1.05
$Fe(4\text{-}Mepm)Cl_2$	300 (5.6(a))	1.33	1.48	0.42,0.32	1.14	1.46
	77 (5.6(b))	1.47	1.91	0.56,0.51	1.15	1.29
$Fe(2\text{-}NH_2pm)Cl_2$	300 (5.7(a))	1.35	1.66	0.31,0.30	0.94	0.98
	77 (5.7(b))	1.48	2.06	0.36,0.34	0.91	0.97

† Lower velocity peak/higher velocity peak

Continued

Table 5.3 (continued)

Compound	Temperature (K) (Figure)	Peak Positions (mm/sec)	Half Widths (mm/sec)	Fractional Dips	Relative Peak Areas
$FepmCl_2$	4.2 (5.4(c))	0.14	0.35	0.045	84.2
		0.57	0.28	0.030	40.8
		1.13	0.25	0.046	60.2
		1.91	0.22	0.033	37.5
		2.31	0.70	0.021	76.6
		2.73	0.33	0.043	74.4
	1.4 (5.4(d))	0.01	0.36	0.049	89.8
		0.57	0.29	0.030	45.5
		1.37	0.25	0.049	64.4
		1.93	0.30	0.037	58.1
		2.40	0.48	0.029	72.0
		2.76	0.35	0.041	75.4
$Fe(5\text{-}Mepm)Cl_2$	4.2 (5.5(c))	0.11	0.51	0.035	68.7
		0.54	0.37	0.028	39.5
		0.98	0.27	0.045	46.9
		1.88	0.33	0.046	58.7
		2.41	0.38	0.015	21.8
		2.87	0.41	0.044	69.2
	1.4 (5.5(d))	0.14	0.50	0.043	80.9
		0.57	0.46	0.035	62.6
		1.01	0.30	0.053	61.1
		1.89	0.34	0.058	74.6
		2.42	0.46	0.020	34.4
		2.87	0.43	0.055	90.2
$Fe(4\text{-}Mepm)Cl_2$	4.2 (5.6(c))	-0.28	0.58	0.019	41.9
		0.22	0.53	0.014	28.0
		0.94	0.72	0.021	58.8
		1.29	0.55	0.022	46.5
		2.19	0.74	0.005	14.2
		3.79	1.016	0.016	62.3

Table 5.3 (continued 2)

Compound	Temperature (K) (Figure)	Peak Positions (mm/sec)	Half Width (mm/sec)	Fractional Dips	Relative Peak Areas
$Fe(4\text{-Mepm})Cl_2$	1.4 (5.6(d))	-0.26	0.55	0.028	58.9
		0.22	0.59	0.022	51.2
		0.88	0.55	0.025	52.7
		1.25	0.64	0.044	107.3
		2.14	0.68	0.009	22.7
		3.77	1.01	0.026	101.5
$Fe(2\text{-}NH_2\text{ pm})Cl_2$	4.2 (5.7(c))	-0.38	0.44	.077	129.8
		1.02	0.41	.082	128.9
		2.48	0.36	.025	33.7
		4.32	0.43	.067	108.8
	1.4 (5.7(d))	-0.38	0.57	.037	80.9
		1.02	0.52	.040	78.9
		2.50	0.51	.011	20.71
		4.32	0.59	.032	71.2

FeL_2X_2 Complexes

Compound	Temperature (K) (Figure)	Centre Shift (mm/sec)	ΔE_Q (mm/sec)	Half Width (mm/sec)	Intensity Ratio	Area Ratio
$Fepz_2Cl_2$	300(5.10(a))	1.25	3.16	0.28,0.30	1.18	1.10
	77(5.10(b))	1.37	3.30	0.36,0.34	1.00	1.07
	4.2(5.10(c))	1.37	3.35	0.53,0.53	1.02	1.03
	1.4(5.10(d))	1.37	3.35	0.54,0.54	1.01	1.03
$Fepz_2(NCS)_2$	294	1.27	2.46	0.27,0.30	1.01	1.00
$Fepz_2(ClO_4)_2 4H_2O$	294	1.30	3.35	0.26,0.30	1.07	1.05
		*1.38	1.41			

* very weak peaks due to an impurity

Table 5.3 (continued 3)

Compound	Temperature (K) (Figure)	Centre Shift (mm/sec)	ΔE_Q (mm/sec)	Half Width (mm/sec)	Intensity Ratio	Area Ratio
$Fe(4Mepm)_2^{\cdot}Cl_2$	300(5.11(a))	1.35	1.10	0.32,0.28	1.20	1.36
	77(5.11(b))	1.46	1.17	0.62,0.58	1.22	1.32

	Peak Positions (mm/sec)	Half Width (mm/sec)	Fractional Dips	Relative Peak Areas
4.2(5.11(c))	0.42	0.63	0.027	64.56
	1.27	0.56	0.044	93.23
	3.01	0.53	0.022	44.73
1.4(5.11(d))	0.46	0.63	0.031	74.9
	1.27	0.55	0.052	110.7
	2.98	0.50	0.030	49.4

Table 5.5 Magnetic Data

χ_m' , μ_{eff} - As in Table 4.5

$FeLCl_2$ Complexes

$FepzCl_2$ (θ = +23 K)

Temperature (K)	292.5	263	236.5	209.5	183	156.25	123.25	103.5
$\chi_m' \times 10^3$	13.31	14.70	16.21	18.11	20.48	23.44	28.79	33.18
μ_{eff}	5.58	5.56	5.54	5.51	5.47	5.41	5.33	5.24

$FeMepzCl_2$ (θ = -7 K)

Temperature (K)	294	263.5	223	182	140	122.5	100
$\chi_m' \times 10^3$	12.34	13.99	16.59	20.85	27.10	30.97	38.90
μ_{eff}	5.39	5.43	5.44	5.51	5.51	5.51	5.58

$FepdCl_2$ (θ = +8 K)

Temperature (K)	283	253	219.5	195	174	152	136	109
$\chi_m' \times 10^3$	12.69	14.29	16.51	18.51	20.56	23.35	25.93	31.69
μ_{eff}	5.36	5.38	5.38	5.37	5.35	5.33	5.31	5.26

Temperature (K)	77.4	68.9	57.9	48.2
$\chi_m' \times 10^3$	44.02	48.93	55.46	65.67
μ_{eff}	5.22	5.19	5.07	5.03

$FepmCl_2$ (θ = -3 K)

Temperature (K)	294	264.5	225.2	184	143.5	121	104
$\chi_m' \times 10^3$	12.54	14.13	16.69	20.60	26.45	31.26	35.97
μ_{eff}	5.43	5.47	5.48	5.51	5.51	5.50	5.47

Table 5.5 (continued)

$Fe(5\text{-Mepm})Cl_2$ (θ = 0 K)

Temperature (K)	292.5	264	237	219.5	193.5	165.7	135.8	109.7
$\chi'_m \times 10^3$	12.82	14.40	16.20	17.41	19.77	22.96	27.95	34.61
μ_{eff}	5.48	5.51	5.54	5.53	5.53	5.52	5.51	5.51
Temperature (K)	78.4	70.6	59.8	49.5				
$\chi'_m \times 10^3$	48.31	53.46	62.26	74.18				
μ_{eff}	5.50	5.49	5.46	5.42				

$Fe(4\text{-Mepm})Cl_2$ (θ = -4 K in the 300 - 90 K region)

Temperature (K)	*292	263	242	219.5	195	174	152	136
$\chi'_m \times 10^3$	12.31	14.04	15.38	17.07	19.44	21.73	25.00	28.00
μ_{eff}	5.36	5.44	5.46	5.48	5.50	5.50	5.51	5.52
Temperature (K)	109	88	77.5	66.3	51.5	41.2	30.5	20.45
$\chi'_m \times 10^3$	35.22	43.43	50.08	58.46	74.79	95.07	131.76	191.06
μ_{eff}	5.54	5.52	5.57	5.57	5.53	5.60	5.67	5.59
Temperature (K)	17.05	14.1	11.8	10.1	8.08	5.30	2.52	1.67
$\chi'_m \times 10^3$	219.77	238.85	195.50	132.75	106.67	95.49	99.92	102.99
μ_{eff}	5.47	5.20	4.29	3.27	2.63	1.81	1.42	1.17

$Fe(2\text{-}NH_2\text{pm})Cl_2$ (θ = -16 K in the 300 - 90 K region)

Temperature (K)	*294	264	222	182	140	121.5	100	78.3
$\chi'_m \times 10^3$	12.14	13.82	16.61	20.95	27.66	32.39	40.27	63.16
μ_{eff}	5.34	5.40	5.43	5.52	5.57	5.61	5.68	6.29
Temperature (K)	58.9	45.8	37.1	31.4	27.0	24.5	20.95	18.00
$\chi'_m \times 10^3$	94.75	146.21	183.81	220.34	223.0	210.17	132.50	78.11
μ_{eff}	6.68	7.32	7.38	7.30	6.94	6.41	4.71	3.35
Temperature (K)	16.98	15.30	11.75	10.04	6.58	4.25	3.19	2.33
$\chi'_m \times 10^3$	64.76	50.76	35.61	32.48	29.75	29.14	29.03	29.26
μ_{eff}	2.97	2.49	1.83	1.62	1.25	1.00	0.86	0.74

* Values given for highest field used.

Table 5.5 (continued 2)

$Fepz_2Cl_2$ (θ = +6 K)

Temperature (K)	283.8	253	236.8	201	174	144.5	118	98
$\chi'_m \times 10^3$	11.44	12.90	13.78	16.09	18.41	22.13	26.63	31.58
μ_{eff}	5.09	5.11	5.11	5.09	5.06	5.06	5.01	4.98

Temperature (K)	77.5	67.2	58.6	49.1
$\chi'_m \times 10^3$	39.69	45.84	51.21	60.48
μ_{eff}	4.96	4.96	4.90	4.87

$Fepz_2(NCS)_2$ (θ = +1 K)

Temperature (K)	296	264	234	205	186.5	159	121	102.5
$\chi'_m \times 10^3$	12.36	13.91	15.58	17.98	19.84	22.85	30.02	34.92
μ_{eff}	5.41	5.42	5.40	5.43	5.44	5.39	5.39	5.35

$Fe(4\text{-Mepm})_2Cl_2$ (θ = -18 K)

Temperature (K)	295	257.5	219	175	138.5	119.5	100
$\chi'_m \times 10^3$	13.52	15.53	18.91	24.13	31.54	36.92	44.40
μ_{eff}	5.65	5.66	5.76	5.81	5.91	5.94	5.96

Table 5.6 IR Spectra of Pyrazine Complexes (band positions in cm^{-1})

Pyrazine	$Fe(pz)Cl_2$	$Fepz_2Cl_2$	$Fepz_2Br_2$	$Fepz_2(NCS)_2$	$Fepz_2(ClO)_2 \cdot 4H_2O$
					3500-3200(s.br)‡
3066	3119 3110 (m) 3052	3103 3098 (m)	3099 (m)	3119 3099 (m) 3050	3101 (w)
				2060 (s)*	
					1640 (m)‡
1490	1488 (s)	1482 (s)	1488 (s)	1492 (m)	1480 (s)
1418	1425 1421 (s)	1418 1410 (s)	1415 1410 (s)	1420 1416 (s)	1425 (s)
1342	1310 (w)	1308 (w)	1302 (w)	1306 (w)	
1148	1168 (s)	1165 1155 (s)	1160 1155 (s)	1163 (s)	1165 (m) 1155 (s)
					1140 (s)†
1110	1120 (s)	1120 1115 (s)	1120 (s)	1128 1112 (s)	1115 (s)
1067	1090 (w)	1088 (w)	1080 (w)	1087 (w)	1090 (m)
1022	1058 (s)	1053 (s)	1055 (s)	1052 (s)	1060 (s)
					1032 (s)†
950 (i a)	975 (w)	992 988 (w)	990 (w)	983 973 (m)	992 (w)
					918 (m)†
804	795 (s)	820 815 (s) 810	825 (s)	826 (m) 800 (s)	820 (w)
				790 (s)*	
				486 (s)*	
417	466 (s)	457 (s)		457 (s)	469 (s)

* NCS bands)
† ClO_4 bands) see text
‡ water bands)

i a = I.R. inactive
s = strong
m = medium
w = weak
br = broad

CHAPTER 6 STUDIES ON SOME Cu^{II} COMPLEXES WITH 6-HYDROXYPURINE, 6-MERCAPTOPURINE AND 4-AZABENZIMIDAZOLE

There has been considerable interest in the interactions of metal ions with polynucleotides and related compounds,[204-206] and it has been shown that Cu^{II} ions reversibly denature DNA. The mechanism for this interaction has been postulated as involving coordination of the Cu^{II} ions with the constituent bases of DNA, namely adenine, guanine, thymine and cytosine, which would profoundly affect the hydrogen bonding that maintains the secondary helical structure.

A considerable amount of chemical study has been carried out to characterise the complexes which can be formed between the Cu^{II} ions and these and related bases.[137a-c,f,207] The bases generally possess several potential coordinating sites, and investigation has been carried out to determine the mode of bonding.

A crystal structure[208] of the inner complex $Cu(ad)_2 4H_2O$ has shown that four molecules of the base (Fig.6.1) (in the anionic form, through loss of the N(7) proton) bridge pairs of Cu^{II} ions, through coordination by atoms N(3) and N(9), to produce a centrosymmetric dimer. This observation is not biochemically important, since the N(9) site of adenine in DNA is the point of attachment of a ribose unit, and so is not available for coordination with metal ions. However, the structure of this compound is closely related to that of dimeric cupric acetate monohydrate,[209] and it has been shown[210-212] that antiferromagnetic exchange between the pairs of Cu^{II} ions occurs in the adenine complex, in a similar way to that found in the acetate and in many other dimeric Cu^{II} systems (refs. 56, 213, 214 contain extensive bibliographies of work on such systems). This interaction is effectively demonstrated by e.p.r. measurements (as mentioned in Chapter 1), which show the characteristic spectrum of a thermally-populated excited $S' = 1$ state, rather than that of an isolated $S = \frac{1}{2}$ state, as well as by magnetic susceptibility measurements.

It has also been shown by X-ray crystallography[215] that the dimeric structure is retained in the outer complex $[Cu(adH)_2Cl]_2Cl_2 . 6H_2O$, even in the presence of chloride ions which may themselves frequently function as bridges, and, on the basis of e.p.r. and magnetic data, it has been concluded[135,211,212] that the dimeric structure is common to a series of outer complexes, $Cu(adH)_2X_2 . nH_2O$, where X = Br, NO_3, ClO_4, $\frac{1}{2}SO_4$. The dimeric structure has also been shown[216] by e.p.r. measurements to persist in solution.

It is interesting to investigate whether this formation of dimeric species is limited to adenine or whether it is shown by other purines, or by related molecules which possess the same disposition of N(3) and N(9) atoms, (Fig.6.1). Other possible modes of bonding of the base that could be envisaged are coordination through one nitrogen atom only (on either the pyrimidine or imidazole ring), or chelation through N(7) and a substituent on C(6), which was initially proposed for the adenine inner complex.[217]

Complexes formed between Cu^{II} salts and various purine derivatives, unsubstituted at N(3) and N(9), have been isolated.[207b-d] Although several compounds with formally 2:1 base to metal stoichiometry have been obtained with guanine and xanthine, e.p.r. measurements have shown[135] that the purine-bridged dimeric unit is not present, and at the outset of this work, no other systems besides the adenine complexes had been shown unequivocally to possess this structure.

For the present study, complexes have been prepared of Cu^{II} salts with 6-hydroxypurine (hypoxanthine) and 6-mercaptopurine, and with the related compound 4-azabenzimidazole, which has the required disposition of N(3) and N(9) atoms (Fig.6.1). The compound 6-mercaptopurine has been shown[218] to exist in the solid state (as the monohydrate) in the thione rather than the thiol form, with the H atom bonded to N(1) (Fig.6.2), and it is probable that the 6-hydroxypurine molecule may also exist predominantly in the keto form.[219] In both cases, the aromaticity of the pyrimidine ring would be partially destroyed, although the electron density distribution in the imidazole ring appears to be virtually unaffected compared with purine itself.[220] In solution, tautomerism between the two forms probably occurs.

Attempts have been made to prepare inner complexes with these three ligands, using procedures analogous to that for the adenine complex.[207a] The pH of the solution was varied widely over the alkaline range and, although with 6-hydroxypurine and 4-azabenzimidazole, gelatinous precipitates containing the ligand were obtained at very high pH, no pure complexes containing the anionic forms of the bases could be isolated. The inability to form inner complexes with 6-hydroxypurine has been noted by Weiss and Venner.[207b]

Outer complexes with these bases have been prepared, and may be divided into two categories:

(i) complexes of the formula, $Cu(LH)_2X_2.nH_2O$,
LH = 6-hydroxypurine (hxH), X = Cl*, Br, ClO_4
LH = 4-azabenzimidazole (azbH), X = Cl, Br, ClO_4, NO_3, $\frac{1}{2}SO_4$.

(ii) Complexes of the formula, $Cu(LH)X_2.nH_2O$
LH = 6-hydroxypurine (hxH), X = Cl*, Br, $\frac{1}{2}SO_4$*
LH = 4-azabenzimidazole (azbH), X = Cl, Br
LH = 6-mercaptopurine (mpH), X = Cl*
* The preparation of these complexes has been reported by Weiss and Venner.[207b,c]

The preparative details are given at the end of this section, together with the analytical data. The degree of hydration of some of the complexes varied for different preparations.†

6-mercaptopurine was found to be extremely reducing, and several attempted preparations of Cu^{II} complexes were unsuccessful due to reduction to Cu^{I}. It was not known from Weiss' reported preparation,[207c] whether the compound $Cu(mpH)Cl_2$ does in fact contain Cu^{II} or whether, due to the reducing ability of the ligand and the highly acidic medium of the preparation, it is in fact a Cu^{I} species of the protonated purine base i.e. $Cu^{I}(mpH_2^{+})Cl_2$. Complexes of protonated purine bases are known, and crystal structures of the complexes Cu^{II}(guanine H^{+})Cl_3,[221]

† The complexes $Cu(hxH)_2X_2.nH_2O$ (X = Cl, Br) are referred to throughout the text as the monohydrates, although the analytical data given in the Preparative Section indicates that the number of water molecules appears to vary between one and two for different samples.

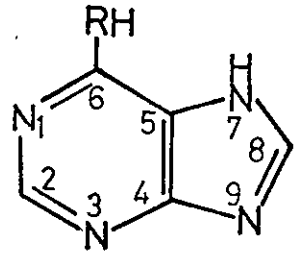

RH = OH 6-hydroxypurine
= SH 6-mercaptopurine
= NH_2 adenine

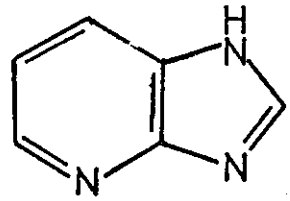

4-azabenzimidazole

Fig. 6.1

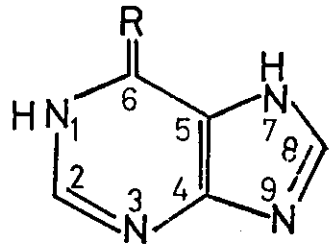

R = O 6-hydroxypurine
= S 6-mercaptopurine

Fig. 6.2

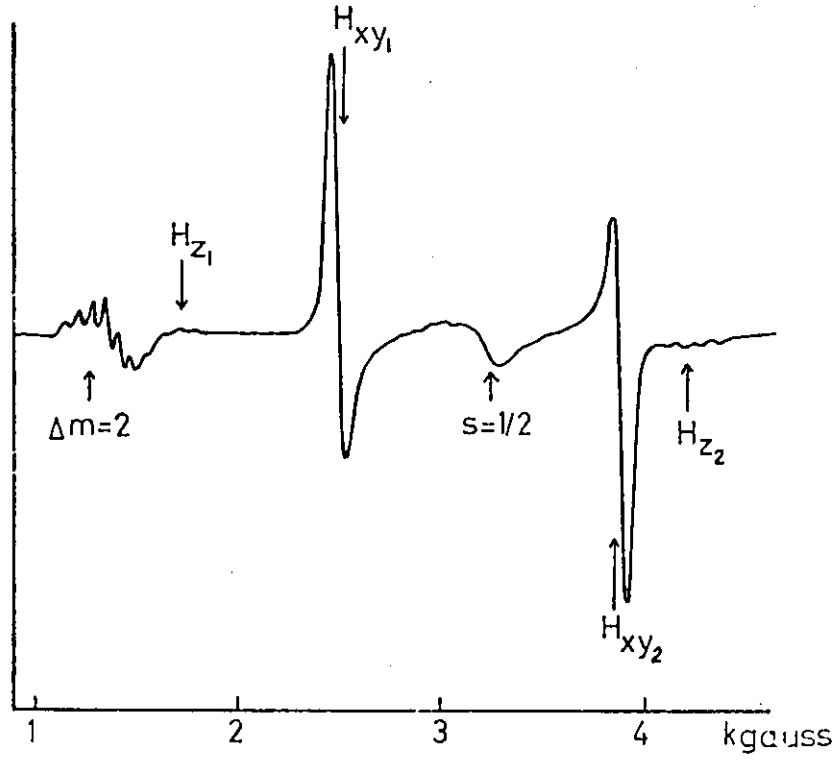

Fig. 6.3 X-band e.p.r. spectrum of polycrystalline $Cu(4\text{-azabenzimidazole})_2Br_2.2H_2O$ at 96K.

$Zn(guanineH^+)Cl_3$,[222] $Cu^{II}(adH_2^+)_2Br_4$[223] and $Zn(adH_2^+)Cl_3$[222] show that in the first three compounds the base is bonded through N(9) only, while in the last complex, bonding is through N(7) only.

The complexes have been studied by e.p.r. measurements, reflectance and I.R. spectroscopy, to assist in elucidating the structures. Unfortunately, owing to the small-scale of the preparations and the difficulties experienced with the Faraday Balance, it has not yet been possible to obtain magnetic susceptibility data, except for the complex $Cu(azbH)Cl_2$.

The Complexes $Cu(LH)_2X_2.nH_2O$

The powder e.p.r. spectra of these complexes at X-band have been investigated over a range of temperature from 293 to ~ 96 K. The spectra of all the complexes provide strong evidence that in each case, the 6-hydroxypurine and 4-azabenzimidazole molecules are bridging discrete pairs of Cu^{II} ions, as in the analogous adenine compounds.

The fine and hyperfine structure is well resolved at low temperatures and a typical spectrum is shown in Fig.6.3. The spectrum is characteristic of an S = 1 state,[55,64,65] and the decrease of the intensity of the triplet resonances with decreasing temperature indicates that this S = 1 state lies above an S = 0 ground state, such that thermal depopulation of the triplet occurs on cooling. There is thus an antiferromagnetic exchange interaction operating between the pairs of $S = \frac{1}{2}$ ions.

The analysis of the e.p.r. spectra of pairs of Cu^{II} ions coupled by exchange or dipolar interactions has received considerable attention.[55,64,65,216,224,225] Although single crystal studies are necessary for extraction of the maximum amount of information concerning the magnetic parameters and their relationship to the crystalline and molecular axes, it has been shown that much of the information can be obtained from the powder spectra. The treatment of Wasserman et al.[226] of randomly oriented organic triplets shows that the dominant features of the experimental powder resonance spectrum arise basically from transitions in the relatively few molecules which have one of the principal magnetic axes aligned with the external field, even though the spectrum is the sum over all possible orientations. Thus the observed resonance

fields are those required for calculation of the zero-field splitting and g parameters. This treatment has been used for analysis of powder spectra of the Cu^{II} adenine complexes,[210,211] and for some dimeric carboxylate complexes.[227-229]

In the dimer systems, the magnetic axes are defined as the coordinate system, x,y,z, referred to the Cu-Cu direction as principal symmetry axis (z). The spin-Hamiltonian for the triplet state of the coupled dimer in an external field is then:[226]

$$\mathcal{H} = \beta g H S + D S_z^2 + E(S_x^2 - S_y^2) - \tfrac{2}{3}D$$

where D, E are the axial and rhombic zero field splitting parameters. This form of the Hamiltonian assumes that the principal axes of the zero-field splitting and the g-tensor are coincident. Although this is not of general validity, it is found to obtain in the carboxylate dimers,[228] to which the present compounds are structurally related, and is therefore considered appropriate in these compounds. The nuclear interaction giving rise to hyperfine structure is neglected. In the spectra of all the complexes studied here, the features assignable to the xy transitions were observed to be unsplit at all temperatures. This indicates that the rhombic zero-field splitting parameter, E, is very small, and therefore the spin-Hamiltonian may be reduced to that appropriate to the axially symmetric case:

$$\mathcal{H} = g_z \beta H S_z + g_{xy} \beta H S_{xy} + D S_z^2 - \tfrac{2}{3}D$$

Solution of the Hamiltonian, for the cases in which the external field is aligned with the principal magnetic axes, gives the following expressions for the resonance fields corresponding to $\Delta m = 1$ transitions:[226]

$$H_{xy_1}^2 = (g_e/g_{xy})^2 H_o(H_o - D') \quad (1)$$

$$H_{xy_2}^2 = (g_e/g_{xy})^2 H_o(H_o + D') \quad (2)$$

$$H_{z_1} = (g_e/g_z)(H_o - D') \quad (3)$$

$$H_{z_2} = (g_e/g_z)(H_o + D') \quad (4)$$

where $g_e = 2.0023$, $D' = D/g_e\beta$ and $H_o = \frac{h\nu}{g_e\beta}$

From equations (1) and (2) and the measured values of H_{xy_1}, H_{xy_2} ($\sim$ 2,500 and 3,800 G, respectively), values of g_{xy} and D have been obtained. The fields were measured at a point on the side of the more intense peak closer to H_o (Fig.6.3), at a distance below the peak equal to the height of the less intense peak. No hyperfine splitting was observed on these resonance lines for any of the complexes.

The z transitions are very much weaker than the xy transitions and are more difficult to measure accurately. The low field H_{z_1} resonance at $\sim$ 1700 - 1900 G is somewhat obscured by the $\Delta m = 2$ feature (discussed below). Similarly, the high field H_{z_2} resonance generally coincides with the tail of the high field H_{xy_2} resonance. At low temperatures, hyperfine splitting is resolved on the z resonances for all the complexes, except $Cu(hxH)_2Cl_2 \cdot H_2O$ and $Cu(hxH)_2Br_2 \cdot H_2O$ which give only a broad absorption feature. For two equivalent exchange-coupled Cu^{II} ions of nuclear spin $I = 3/2$, seven equally spaces hyperfine lines of relative intensity 1:2:3:4:3:2:1 are predicted. The separation of the lines is $A/2$, where A is the hyperfine separation of the four equally intense lines predicted for a monomeric, magnetically-dilute $S = \frac{1}{2}$ Cu^{II} species. In most of the complexes, the maximum number of hyperfine lines resolved was six, and the H_z resonance fields were measured as the fourth resolved line.

The g_z values were determined from equations (3) and (4), and an additional estimate of D was obtained for comparison with that derived from the xy resonances. The calculated parameters are listed in Table 6.1. In general, the D values from the two calculations agree quite well, verifying that $E \approx 0$, and indicating that the positions of the z resonances have been estimated with reasonable accuracy.

In the compound $Cu(hxH)_2Br_2 \cdot H_2O$, an anomalous "step" was observed in the low-field tail of the H_{xy_1} resonance. Assignment of this feature as H_{z_1} results in a D value much lower than that calculated from H_{xy_1}, H_{xy_2}, and a g_z value inconsistent with those for the corresponding chloride and perchlorate complexes. This is not expected by comparison with the trends in the g_z values in the 4-aza-benzimidazole complexes. A similar feature is apparent in the reported spectrum of $Cu(adH)_2(ClO_4)_2 1.5H_2O$,[212] and has again not been assigned to H_{z_1}.

In all the complexes, a broad anisotropic derivative feature was observed in the 3100 - 3200 G region. This band increased in intensity on cooling and is presumably due to an $S = \frac{1}{2}$ impurity. The band was most intense in the compounds $Cu(azbH)_2X_2$ ($X = ClO_4$, NO_3, $\frac{1}{2}SO_4$), but no other species giving rise only to an $S = \frac{1}{2}$ signal could be isolated with these salts.

The spectra of all the complexes also contained a feature at $\sim$ 1350 - 1400 G, arising from the $\Delta m = 2$ or half-field transition, which is predicted[216] to occur in powdered samples when $D < h\nu$ (here $D \leq 0.13$ cm^{-1} and $h\nu \approx 0.3$ cm^{-1} at X-band). This feature has been observed in organic triplets,[230] and in some dimeric copper carboxylate complexes[225] at K-band (for these complexes D is of the order 0.3 to 0.4 cm^{-1}). The origin and nature of the feature has been discussed at length in several papers.[216,225,226,231]

The band appears to be of derivative shape (Fig.6.4) and shows resolved hyperfine splitting. In most of the complexes, all seven expected hyperfine components are resolved, although the three to higher field are somewhat obscured by the band shape and the coincidence with the low field side of the $\Delta m = 1$ H_{z_1} resonance. The hyperfine separation ($A/2 \approx 65$ - 70 gauss) is more characteristic of a z transition than an xy, although the values are lower than those observed on the $\Delta m = 1$ z transitions ($A/2 \approx 80$ - 90 gauss).

For systems with $D < \frac{1}{2} h\nu$, as in the present case, the transition moment, and therefore the intensity, of the $\Delta m = 2$ transition is zero along the principal magnetic axes, but can become quite large for species oriented such that the z-axis lies on a cone making an angle θ with the external field.[216] For a given value of D, the transition probability is a maximum for a certain value of θ which increases as D approaches $\frac{1}{2}h\nu$. Using the treatment of Kottis and Lefebvre,[231] for the case when $E = 0$, this angle θ may be related to the values of D and $h\nu$ by the expression

$$\cos^2\theta = \frac{18(h\nu)^2 - 16D^2}{27(h\nu)^2 - 36D^2}$$

Using the values of D from Table 6.1, the θ values for all these complexes lie in the range 31 - 33°. The $\Delta m = 2$ feature is therefore

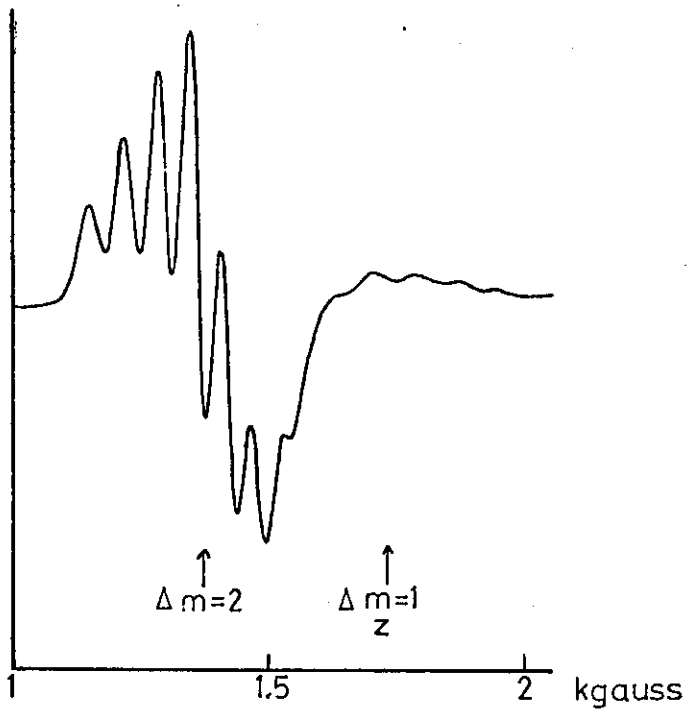

Fig. 6.4 The Δm=2 region of Fig. 6.3 at higher signal level.

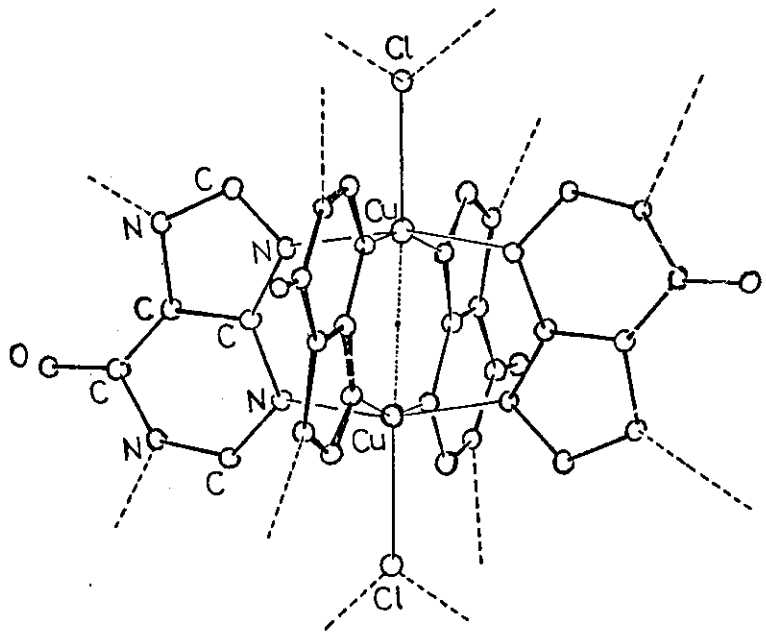

Fig. 6.5 The $(Cu(hxH)_2Cl)_2^{2+}$ cation (from reference 232)

assigned to transitions in species oriented with their z axes at $\sim 30^{\circ}$ to the external field. This is consistent with the reduced hyperfine splitting value, and the derivative shape of the feature.

Several of the complexes were studied by e.p.r. measurements in aqueous solution. The spectra obtained were generally pH dependent, and although the existence of dimeric species was still evident from the observation of weak triplet lines, it appeared that, on dilution, increasing amounts of species giving two g-value signals, characteristic of $s = \frac{1}{2}$ states, were produced.

The e.p.r. evidence for the existence of discrete dimeric units in the solid compounds indicates that 6-hydroxypurine and 4-azabenzimidazole are capable of bridging pairs of Cu^{II} ions, and of promoting antiferromagnetic exchange coupling between them, as in the analogous adenine complexes.

During the course of this work, a crystal structure has been published[232] of the compound $Cu(hxH)_2Cl_2 \cdot 3H_2O$, which confirms the presence of the complex dimeric cation $[Cu(hxH)_2Cl]_2^{2+}$ (Fig.6.5). The 6-hydroxypurine molecules are bonded through the N(3) and N(9) atoms, and a chloride ion completes the tetragonal pyramidal coordination about each Cu^{II} ion, as in the analogous adenine complex.[215] It is reported that this complex readily loses lattice water, to give eventually $Cu(hxH)_2Cl_2 \cdot H_2O$, which is the formulation given by Weiss.[207b] The samples prepared in this study appeared to contain between one and two water molecules per Cu^{II} ion, and are therefore probably a mixture of, or an intermediate between, the two hydrated forms. The e.p.r. parameters do not, however, appear to be sensitive to the degree of hydration.

The Cu-Cu separation in this complex is 3.024 Å, compared with 3.066 Å in the analogous adenine complex,[215] and both are significantly larger than that in the adenine inner complex (2.947 Å).[208] The Cu-Cl distances are almost identical in the 6-hydroxypurine and adenine complexes (2.431 and 2.429 Å, respectively), but the displacement of the Cu atom above the plane of the four nitrogen atoms is slightly less in the former complex (0.29 and 0.33 Å, respectively). The Cu-N bond lengths follow the same trend as in the adenine complex, the bond

with the imidazole N(9) atom (1.991 Å) being significantly shorter than that with the pyrimidine N(3) atom (2.005 Å), but both are smaller than in the adenine complex (2.008 and 2.041 Å, respectively). It is also interesting to note that the C(6) substituent is, in fact, a keto group, the H atom being transferred to N(1). It has been suggested[135] that tautomerism in the guanine molecule, which also produces a keto group at C(6), disturbs the resonance system sufficiently to prevent dimer formation. Since this does not appear to apply in the case of 6-hydroxypurine, it may be suggested that the inability of both guanine and xanthine to form dimeric bridged species is due to the steric effect of the C(2) substituent in these molecules (NH_2 and OH, respectively).

It might be expected that the electron-withdrawing effect of the keto group would reduce the σ-bonding ability of the N(3) atom in the pyrimidine ring. However, it can be seen that the Cu-N(3) bond in the 6-hydroxypurine complex shortens significantly more than the Cu-N(9) bond, compared with the analogous adenine complex.

$Cu(hxH)_2Br_2H_2O$ and the analogous chloride and bromide complexes with 4-azabenzimidazole may be assumed to possess a similar structure to $Cu(hxH)_2Cl_2 \cdot 3H_2O$, with the halide ions occupying the axial coordination positions. However, in the remaining complexes, a water molecule may replace the anion in the axial position. The I.R. spectra of the perchlorate and sulphate complexes suggest that the anions are non-bonding,[200] although a slight splitting of the ClO_4 ν_3 band was found in $Cu(azbH)_2(ClO_4)_2 \cdot H_2O$, which may be due to a lowering of the symmetry of the anion through lattice packing or hydrogen-bonding effects. The I.R. spectrum of $Cu(azbH)_2(NO_3)_2 \cdot H_2O$ did not however provide any conclusive evidence of whether the anion is bonded in this complex. It is noted that for $Cu(adH)_2(NO_3)_2$, it has been concluded[135] that the nitrate group is bonded to the Cu atom, since no water is present in the complex.

The reflectance spectra (Table 6.2) of the chloride and bromide complexes of 6-hydroxypurine and 4-azabenzimidazole consist of two broad bands at 15 - 16,000 cm^{-1} (I) and 25 - 26,000 cm^{-1} (II), respectively, the positions being very similar to those in the analogous adenine complexes.[135] In the remaining complexes, band (I) is shifted to higher energy (17 - 18,500 cm^{-1}) and in the broad tail of the lower

energy side of the band at least one shoulder is present at ~ 14-15,000 cm^{-1}. In $Cu(azbH)_2SO_4 . 5H_2O$, a second shoulder at ~ 11,700 cm^{-1} is also resolved in some preparations of the compound. The higher energy of band (I) in these complexes is consistent with that observed for $Cu(adH)_2SO_4 . 4H_2O$[135] and for $Cu(adH)_2(ClO_4)_2 . 1.5H_2O$.[212]

It has been concluded, from the study of Cu^{II} carboxylate dimers, that the splitting of the singly-excited ligand field states of each Cu^{II} ion is determined primarily by the local tetragonal field, and the band at 14,400 cm^{-1} (with lower energy shoulder) observed for cupric acetate monohydrate has been assigned to d-d transitions within the $3d^9$ configuration of each Cu^{II} ion.[214] The band at ~ 27,000 cm^{-1} observed in this and many other carboxylate complexes has been considered to be characteristic of the binuclear structure, and there has been much debate concerning its origin (Ref. 233 contains the most recent developments in this problem). It seems reasonable therefore to assign band (I) in the present complexes to d-d transitions within each tetragonally-distorted Cu^{II} ion, but the origin of band (II) (i.e. whether charge-transfer or a doubly excited transition) must remain speculative.

If it is assumed, from comparison with the carboxylate dimers, that the Cu-N bonds lie close to the x and y axes, then the environment of each Cu^{II} ion is approximately a tetragonally-elongated octahedron (or square pyramid). The splitting of the orbital states of the Cu^{II} ion as a function of increasing tetragonal distortion has been given,[234] and three spin-allowed transitions are predicted, between the half-filled $d_{x^2-y^2}$ orbital and the d_{z^2} (ν_1), the d_{xy} (ν_2) and the d_{xz}, d_{yz} pair (ν_3), respectively. If the tetragonal component is not very large compared with the overall ligand field strength, the order $\nu_1 <$ or $\simeq \nu_2 < \nu_3$ would be expected, but the order of ν_1 and ν_2 may be reversed as the distortion increases. It may also be noted that the order of the d_{xy} and d_{xz}, d_{yz} pair may be reversed, such that $\nu_2 > \nu_3$, and this situation has recently been proposed for cupric acetate monohydrate.[214]

In the chloride and bromide complexes of 6-hydroxypurine and 4-azabenzimidazole, the single broad band at 15 - 16,000 cm^{-1} appears to comprise all three transitions, as is often found in tetragonally distorted octahedral Cu^{II} complexes. The similarity of the band positions in these and the corresponding adenine complexes indicates

that the overall ligand field environment provided by each of the bases is quite comparable.

If, in the remaining complexes, the main band at 17 - 18500 cm^{-1} is assigned to a combination of ν_2 and ν_3 transitions, and the shoulder at 14 - 15,000 cm^{-1} to the ν_1 transition, then these compounds would appear to have a stronger overall ligand field and a smaller tetragonal component than the halide complexes. This would be consistent with a water molecule occupying the axial position. The band in $Cu(azbH)_2(NO_3)_2H_2O$ is $\sim$ 1500 cm^{-1} higher in energy than the single band at 15,870 cm^{-1} observed for $Cu(adH)_2(NO_3)_2$, which tends to confirm coordinated water rather than nitrate in the former compound. The band at $\sim$ 11,700 cm^{-1} in $Cu(azbH)_2SO_4 \cdot 5H_2O$ could be assigned to ν_1, indicating an even smaller axial distortion, and it is possible that similar bands may be present in the perchlorate and nitrate complexes, although unresolved in the low energy tail of band (I). The band positions in these complexes are sensitive to the identity of the anion, which must therefore exert some influence on the ligand field strength through either lattice packing or hydrogen bonding effects.

The g and D parameters from the e.p.r. measurements could potentially provide some information on the ligand field splitting, spin-orbit coupling and covalency effects in these complexes. It has been shown by e.p.r. measurements on Zn-doped samples of the dimeric Cu^{II} carboxylates,[225] that the presence of an exchange interaction has little effect on the g-values of the Cu^{II} ions, which are primarily determined by the local ligand field environment, and may be expressed as:[225]

$$g_z = 2.0023 - \frac{8\lambda}{\nu_2}\alpha^2\beta^2$$

$$g_{xy} = 2.0023 - \frac{2\lambda}{\nu_3}\alpha^2\beta_1^2$$

where ν_2 and ν_3 are as above, λ is the spin-orbit coupling constant of the Cu^{II} free ion (-830 cm^{-1}), and α^2, β^2 and β_1^2 are the covalency factors for mixing between the ligand orbitals and the metal $d_{x^2-y^2}$ (σ), d_{xy} (π) and d_{xz}, d_{yz} (π) orbitals, respectively.

The values of g_{xy} for all the 6-hydroxypurine, 4-azabenzimidazole and also the adenine dimers (Table 6.1) are virtually identical within

the accuracy of measurement, although those for the 4-azabenzimidazole complexes do appear to be consistently smaller (by ~ .01 to .02) than those for the other two bases. This may suggest a slightly higher degree of covalency in the bonding with this base, which has no electron-withdrawing substituents on the rings. The g_z values for the 6-hydroxypurine and 4-azabenzimidazole complexes appear to be slightly higher than those for the adenine compounds, but since the error in determination of these values is quite large, it is not possible to attach any great significance to the differences. There does not appear to be any correlation between the g values and the identity of the axial group.

The D values for exchange coupled Cu^{II} dimer systems may depend on several factors,[65] and have been expressed by:

$$D_{obs} = \frac{1}{32}[J_1(g_z - 2.0023)^2 - 4J_2(g_{xy} - 2.0023)^2] - [(g_z^2 + \tfrac{1}{2}g_{xy}^2)\beta^2/r^3]$$

The first term represents the 'pseudo-dipolar' term[55] which contains the contribution from the ligand field environment and the exchange interaction. J_1 and J_2 are the exchange coupling constants for the excited state, and are not necessarily equal to J, the ground state value relevant to susceptibility measurements, although they are generally of the same order of magnitude. The second term represents the direct dipole-dipole interaction,[216,235] which is dependent on the Cu-Cu separation, r, and has been found to be quite significant for the order of the internuclear distance found in these compounds.[216] Any contribution from antisymmetric spin-spin coupling should be zero for a centrosymmetric dimer system.

The D values within each series of complexes of 6-hydroxypurine, 4-azabenzimidazole and adenine are very similar, but decrease in the order azbH > adH > hxH (Table 6.1). The dipole-dipole terms for the chloride complexes of adH and hxH, calculated from the measured g values and the r values from the crystal structures are 0.105 cm^{-1} and 0.113 cm^{-1} respectively, which would partially account for the difference in D values. However, there is quite a significant error in the measured g_z values, and there may also be a contribution to the difference in D from the pseudo-dipole term.

Although it has not been possible in this work to determine the J values of the 6-hydroxypurine and 4-azabenzimidazole complexes by magnetic susceptibility measurements, a very recent report has been published[236] of magnetic studies on the chloride and bromide complexes of the former base. The J values for these and the analogous adenine complexes (reported previously[135]) have been determined by fitting the susceptibility data to the theoretical expression for pairs of exchange coupled S = $\frac{1}{2}$ ions,[55]

$$\chi = \frac{Ng^2\beta^2}{3kT}\left[1 + \frac{1}{3}\exp\left(\frac{-2J}{kT}\right)\right]^{-1} + N\alpha \qquad 6.1$$

Here, -2J is the separation between the ground singlet and excited triplet levels, and was found to be:

$Cu(adH)_2Cl_2 \cdot 1.5H_2O$	286 cm^{-1}
$Cu(adH)_2Br_2 \cdot 2H_2O$	289 cm^{-1}
$Cu(hxH)_2Cl_2 \cdot H_2O$	276 cm^{-1}
$Cu(hxH)_2Br_2 \cdot 2H_2O$	286 cm^{-1}

(Allowing for the difference in the number of water molecules in this preparation of the adenine chloride complex, the values for the adenine complexes are very similar to those previously reported).[135]

The similarity in J values for the adenine and 6-hydroxypurine complexes suggests that any variation in the pseudo-dipolar contribution to D may be due to differences in the ligand field environment, rather than to differences in the J_1, J_2 values. It is obviously desirable to obtain magnetic data on the 4-azabenzimidazole complexes to test this proposal.

It is very interesting that the magnitude of the exchange interactions is so similar in the adenine and 6-hydroxypurine complexes, in view of the mechanistic possibilities for the exchange coupling process. The possibility of direct metal-metal interaction, through δ-bond formation between the half-filled $d_{x^2-y^2}$ orbitals on each Cu^{II} atom, seems very unlikely in these complexes owing to the relatively large Cu-Cu separation. It may therefore be concluded that the coupling occurs predominantly via a superexchange mechanism involving the bridging bases.

The orientation of the heterocyclic molecules in these complexes are such that the filled d_{xy} orbitals on both Cu^{II} ions in a dimer are capable of π-overlap with the same empty π*-molecular orbital, extending over the N(9) - C(4) - N(3) moiety of the base. It has been proposed[135,210] for the adenine complexes, that a simultaneous one-electron transfer from each Cu^{II} d_{xy} orbital to this same ligand orbital (i.e. Goodenough's correlation mechanism[4]) must leave the net unpaired spins on the two Cu^{II} ions aligned antiparallel, and therefore to give rise to antiferromagnetic coupling. This proposal does not explain explicitly why unpaired spin density should be delocalised into the ligand π*-system from the formally filled d_{xy} orbitals. In the description of a similar π-mechanism for antiferromagnetic exchange in some Cu^{II} formate systems,[237,238] a 'promotion' of the positive hole in $d_{x^2-y^2}$ to the d_{xy} orbital has been invoked, to assist in delocalisation of unpaired spin from the latter orbital into the ligand π system. It has also been stated[214] that mixing of the singly-excited $^2B_2$ state (hole in d_{xy}) with the $^2B_1$ state (hole in $d_{x^2-y^2}$) via spin-orbit coupling would enable a π-system of the type present in these bases, to become available as a superexchange pathway for the antiferromagnetic interaction.

From this proposed π-mechanism, it may be expected that the magnitude of the exchange should be greatly dependent on the degree of covalent overlap of the ligand orbital with the Cu^{II} d_{xy} orbitals, and thus on the nature and energy of the delocalised π*-system over the N(9) - C(4) - N(3) section of these bases. As mentioned earlier, the presence of the keto-group in the 6-hydroxypurine molecule will disturb the π-system of the pyrimidine ring in this base, but, from the similarity in the J values for the complexes of adenine and 6-hydroxypurine, it must be concluded that this has little affect on the π*-orbitals over the N(9) - C(4) - N(3) region. Again, magnetic data for the complexes of 4-azabenzimidazole would be very useful for comparison purposes.

The Complexes $Cu(HH)X_2 . nH_2O$

The e.p.r. and reflectance spectra data for these compounds are presented in Tables 6.1 and 6.2, respectively.

The compounds $Cu(hxH)Cl_2 . H_2O$ and $Cu(azbH)X_2$ (X = Cl, Br) show one broad, almost symmetric derivative peak in the g = 2 region, with no

resolved structure, which appears to indicate a magnetically non-dilute system. $Cu(hxH)Br_2$ gives a very similar spectrum at room temperature, but the intensity is relatively much weaker than in the other complexes, and at ~ 90 K some very weak additional structure is present on each side of the main peak, which itself remains unsplit.

The reflectance spectra of these four complexes contain one very broad band in the visible region. In the 6-hydroxypurine complexes, the apex of the band extends from ~ 14,000 to 9,000 cm^{-1}, with a broad tail to lower energy, and appears to comprise more than one transition. (In the corresponding adenine complexes a resolved shoulder to lower energy on the main band has been observed[135]). In all four complexes, there is also an additional increase in intensity at higher energy, although the position of the peak could not be determined, and in the 4-azabenzimidazole compounds a shoulder appears to be present in the lower energy tail of this band.

The presence of an $S = \frac{1}{2}$-type e.p.r. signal in these compounds does not exclude the possibility that they contain bridging heterocyclic base, since the compound $Cu_3Cl_8(adH_2^+)_2.4H_2O$, which has a similar e.p.r. signal, has been shown[239] to contain both bridging adenine and bridging chloride. For the compounds $Cu(adH)X_2$ (X = Cl, Br), which have similar e.p.r. and reflectance spectra to the present compounds, a structure containing linear chains of Cu^{II} ions, bridged by both adenine and halide ions has been suggested.[135] Since the bridging tendencies of 6-hydroxypurine and 4-azabenzimidazole have been shown to be comparable to that of adenine, it does not seem unreasonable to suggest that a similar situation may occur in the complexes of these bases. Linear polymeric structures, similar to that shown in Fig. 2.2(b) have been found in Cu(1,2,4-triazole)Cl_2[199] and proposed in Cu pd Cl_2,[130] and the tetragonally-distorted, six-coordinate CuN_2X_4 environment is common to many Cu^{II} halide complexes with heterocyclic amines.[110] However, the d-d transitions in the adenine, 6-hydroxypurine and 4-azabenzimidazole complexes appear to be generally somewhat lower in energy than those found in other complexes with CuN_2X_4 environments, and the positions, but not the intensities, of the observed bands could be consistent with a pseudo-tetrahedral geometry.

Magnetic susceptibility data have also been recently presented[236] for the complexes $Cu(adH)Cl_2$, $Cu(hxH)Cl_2H_2O$ and $Cu(hxH)Br_2.0.5H_2O$, and

the compounds all exhibit antiferromagnetic exchange. The data in the 300 - 80 K temperature range have been fitted to equation 6.1, for pairwise interactions, and values of -2J of 61,145 and 186 cm^{-1}, respectively, have been obtained. This would tend to suggest the presence of discrete dimeric units rather than linear chains in these compounds, and the authors have suggested that some form of pairwise bridging of Cu^{II} ions by the bases is present, and presumably is involved in the exchange mechanism.

The magnetic susceptibility of $Cu(azbH)Cl_2$ has been measured here over the temperature range 300 - 50 K. The plots of χ'_m (the susceptibility per gm-ion of Cu^{II}, corrected for the diamagnetism of the ligands) and μ_{eff} versus temperature are shown in Fig.6.6. The compound also shows antiferromagnetic behaviour, the Néel temperature being ~ 110 K, although the maximum in the χ'_m v. T plot is quite broad. Attempts were made to fit the susceptibility data to equation 6.1, using the g value of 2.15, obtained from the e.p.r. measurement. However, a good fitting could not be achieved with a constant value of -2J e.g. for $N\alpha = 60 \times 10^{-6}$, -2J at 300 K = ~ 145 cm^{-1}, decreasing to ~ 110 cm^{-1} at 50 K. (These values are, however, of the same order of magnitude as that found for $Cu(nxH)Cl_2.H_2O$[236]).

A better fitting to the data above the Néel temperature can be achieved by use of the expression

$$\chi'_m = \frac{Ng^2\beta^2}{4kT} \exp(-2J/kT) + N\alpha \qquad 6.2$$

This is derived from the one-dimensional Ising model for exchange between nearest neighbours in an infinite chain of interacting ions, and is generally applicable in this form only above the Néel temperature. The solid curve in Fig. 6.6 is that calculated from equation 6.2 with g = 2.15, $N\alpha = 60 \times 10^{-6}$ and -2J = 47 cm^{-1}. (In the region of, and below, the Néel temperature, the full Ising expression,[79] allowing for anisotropy in the exchange interaction, should be used, but a successful fitting to this model has not yet been achieved, and it is not yet determined whether the alternative Heisenberg model may be more appropriate).

This result may suggest that this compound does possess a linear polymeric structure. It is interesting to note that the value of -2J

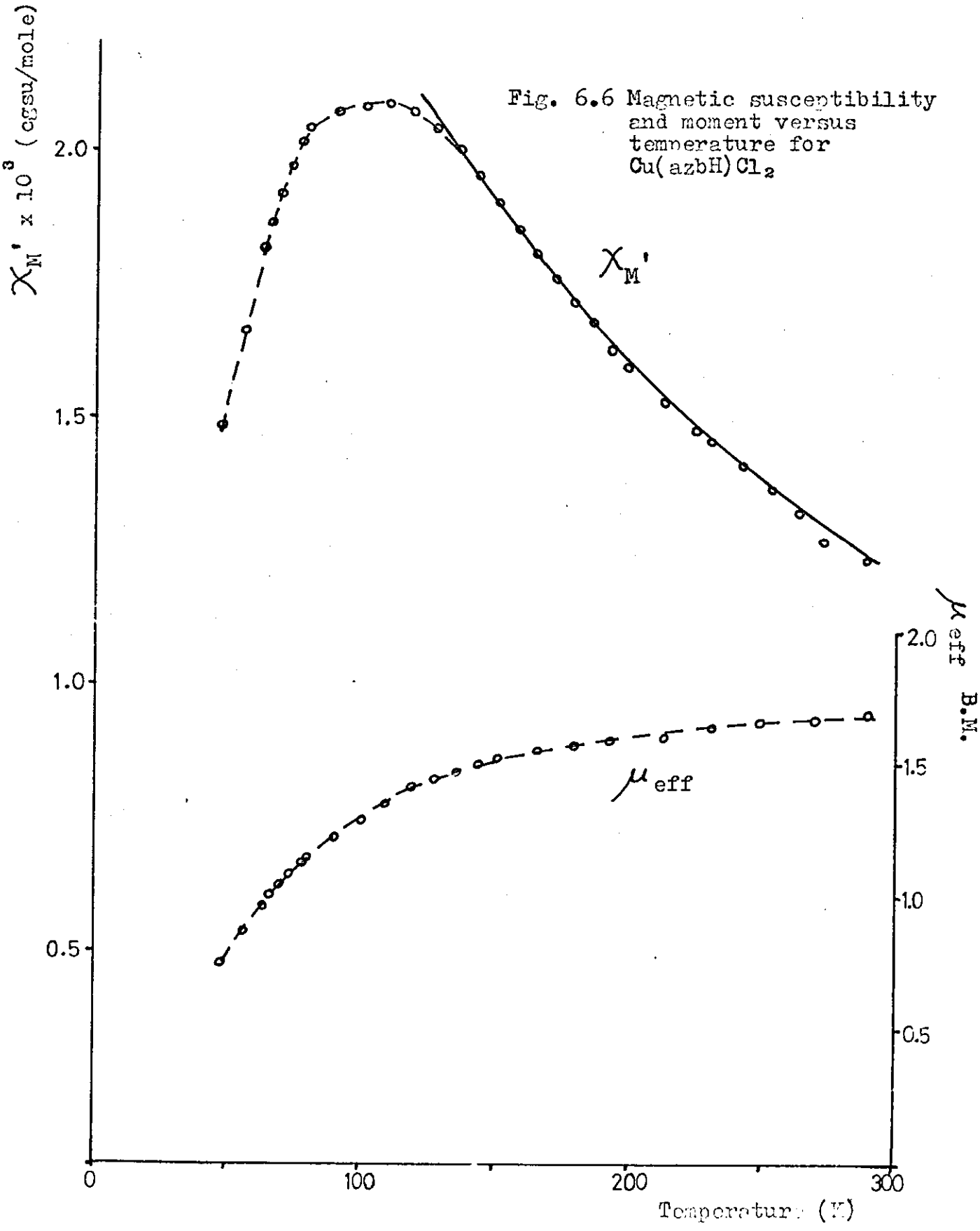

Fig. 6.6 Magnetic susceptibility and moment versus temperature for $Cu(azbH)Cl_2$

derived for this compound is very similar to that found[131] for Cu pd Cl_2, i.e. 48 ± 3 cm^{-1}, (also from fitting of the susceptibility data above the Néel temperature to equation 6.2). It has been mentioned in Chapter 5 that, in this latter compound, an antiferromagnetic superexchange process, involving the π-system of the heterocyclic base, appears to greatly augment that via the chloride bridges. If Cu(abzH)Cl_2 does possess a similar structure, with intrachain chloride and heterocycle bridges, then analogous pathways may be proposed for the exchange process in this compound, since 4-azabenzimidazole has been shown to be capable of promoting antiferromagnetic coupling in the Cu(azbH)$_2X_2$ complexes.

It must be mentioned, however, that a preliminary report[240] of magnetic studies on the complex Cu(guanineH^+)Cl_3, which has a dimeric structure with bridging chlorides and terminal purine molecules, bound through N(9) only, indicates that this compound also shows antiferromagnetic behaviour, but the mechanism cannot involve the purine π-system. The presence of bridging heterocyclic bases in the Cu(LH)X_2 complexes of adenine, 6-hydroxypurine and 4-azabenzimidazole cannot therefore be definitely inferred from the observation of antiferromagnetic exchange.

The compound Cu(hxH)SO_4.H_2O has a broad two g-value e.p.r. spectrum, with no hyperfine structure resolved. The I.R. spectrum of this compound suggests that the sulphate is coordinated, since the ν_3 band of the anion is markedly split.[200] The number of components is difficult to determine, since the base also absorbs in this region, but by comparison with the spectra of the other 6-hydroxypurine complexes, it appears that three bands are present, indicating a lowering of the symmetry from Td to C_{2v}. This could be caused by either bidentate bridging or chelating modes of coordination of the group, but it has not been possible to distinguish between the two in this case. The reflectance spectrum consists of a broad band at 14,290 cm^{-1} with a resolved shoulder at 10,560 cm^{-1}. The higher energy of the bands, compared with those in the halide complexes, suggests a stronger overall ligand field.

The compound Cu(mpH)Cl_2 gives a relatively strong e.p.r. signal in the g = 2 region, indicating the presence of Cu^{II} rather than Cu^{I}. The signal consists of a derivative feature, with a weaker absorption to lower field, and a series of very weak peaks between the two. The origin of these weak features is not known, and the g values in Table 6.1

have been calculated from the two main components of the signal. The bonding and coordination geometry in this complex have not yet been established. In the I.R. spectra of both the free ligand and the complex, no band assignable to ν(S-H) has been observed, which is not unexpected due to the tautomerism in this molecule. It has not, however, been possible to assign the expected ν(C=S) vibration and therefore no information has been obtained on the possibility of coordination to the metal through the sulphur atom in this complex, as has been suggested[241] for some Co^{II} inner complexes of this base. The unusual colour of this compound, compared with the other purine and 4-azabenzimidazole complexes, may suggest involvement of the sulphur atom in coordination, or a strong ligand to metal charge-transfer, owing to the highly reducing nature of the base. The reflectance spectrum of the compound consists or a relatively weak broad band centred at 13,490 cm^{-1}, with a resolved shoulder at 11,100 cm^{-1}, and an additional stronger band at 21,930 cm^{-1}.

Preparation of the Complexes

$Cu(hxH)_2Cl_2 \cdot nH_2O$ (n = 1,2)

This complex was prepared by the method of Weiss and Venner,[207b] using a 1:1 ligand to metal ratio.

6-hydroxypurine (0.345 gm, 2.5 mM) was dissolved in n HCl (7.5 ml.) and a solution of $CuCl_2 \cdot 2H_2O$ (0.425 gm, 2.5 mM) in water (1 ml.) was added. The solution became deep green-blue, and after ~ 1 hr, dark blue crystals began to form. After 24 hr, the crystals were filtered off washed with a small quantity of cold water and air dried.

$Cu(hxH)_2Cl_2 \cdot H_2O$ requires	C: 28.28%	N: 26.39%	H: 2.38%
$Cu(hxH)_2Cl_2 \cdot 2H_2O$ requires	C: 27.13%	N: 25.31%	H: 2.73%
Found (i)	C: 28.33%	N: 25.62%	H: 2.52%
(ii)	C: 27.64%	N: 25.23%	H: 2.59%

It was also found that the complex can be prepared in a similar manner to the analogous adenine complex,[207a] using a 2:1 ligand to metal ratio, with the ligand initially dissolved in one equivalent of 0.1 N HCl. The solution was boiled for ~ 15 min. and the crystals formed on cooling overnight.

$Cu(nxH)_2Br_2 . nH_2O$ (n = 1,2)

This compound could be prepared by either of the methods given above for the chloride complex, although in the second method the ligand was initially dissolved in one equivalent of NHBr. The compound was obtained as deep blue-green microcrystals.

$Cu(nxH)_2Br_2 . H_2O$ requires	C: 23.39%	N: 21.82%	H: 1.96%
$Cu(nxH)_2Br_2 . 2H_2O$ requires	C: 22.59%	N: 21.08%	H: 2.28%
Found (i)	C: 23.20%	N: 21.30%	H: 2.08%
(ii)	C: 22.92%	N: 22.03%	H: 2.35%

$Cu(nxH)Cl_2 . H_2O$

This complex was prepared by the method of Weiss and Venner.[207a] 6-hydroxypurine (0.345 gm, 2.5 mM) was dissolved in hot N HCl (5 ml.) and $CuCl_2 . 2H_2O$ (2 gm, ~ 12 mM) in water (4 ml.) was added to the boiling solution. The dark green-yellow solution was boiled for ~ 5 min. when green-yellow crystals began to form. After ~ 2 hr, the crystals were filtered off, washed with cold 1 N HCl and then a small amount of methanol and air dried.

$Cu(nxH)Cl_2 . H_2O$ requires	C: 20.81%	N: 19.42%	H: 2.10%
Found	C: 21.30%	N: 19.79%	H: 2.25%

$Cu(nxH)Br_2$

This compound was prepared as for the corresponding chloride. The dark green-brown solution yielded brown microcrystals, which were washed with cold NHBr, and then methanol, and air dried.

$Cu(nxH)Br_2$ requires	C: 16.44%	N: 15.31%	H: 1.53%
Found	C: 16.71%	N: 15.59%	H: 1.12%

$Cu(nxH)SO_4 . H_2O$

This compound was prepared by the method of Weiss and Venner.[207b] 6-hydroxypurine (0.345 gm, 2.5 mM) was dissolved in NH_2SO_4 (7.5 ml.) and $CuSO_4 . 5H_2O$ (3.75 gm, 15 mM) in water (10 ml.) and added to the boiling solution. After ~ 1 min. a bright blue microcrystalline solid separated, which was filtered off, washed with cold water and air-dried.

$Cu(nxH)SO_4 . H_2O$ requires	C: 19.15%	N: 17.85%	H: 1.92%
Found	C: 19.08%	N: 17.67%	H: 2.21%

$Cu(hxH)_2(ClO_4)_2.H_2O$

6-hydroxypurine (0.345 gm, 2.5 mM) was dissolved in N $HClO_4$ (7.5 ml.), and $Cu(ClO_4)_2.6H_2O$ (0.93 gm, 2.5 mM) in water (1 ml.) was added to the hot solution. The pH of the pale blue solution was raised by dropwise addition of N NaOH, until a slight purplish precipitate was formed in the now deep-blue solution. The solution was filtered, and left overnight, when deep purple-blue crystals were formed. These were filtered off, washed with cold water and air-dried.

$Cu(hxH)_2(ClO_4)_2.4H_2O$ requires	C: 19.80%	N: 18.47%	H: 2.66%
Found	C: 19.34%	N: 18.98%	H: 2.45%

$Cu(azbH)_2Cl_2.2H_2O$

Attempts to prepare this complex from acidic aqueous solutions, by the methods used for the corresponding 6-hydroxypurine or adenine complexes, resulted in deep blue solutions which on cooling, evaporation or raising the pH yielded mixtures of the required compound and the green $Cu(azbH)Cl_2$ complex as impurity. Similar mixtures were obtained from neutral aqueous solution. The uncontaminated compound was prepared from ethanolic solution.

4-azabenzimidazole (0.6 gm, 5 mM) was dissolved in ethanol (5 ml.) and $CuCl_2.2H_2O$ (0.425 gm, 2.5 mM) in ethanol (10 ml.) was added with rapid stirring. The deep blue solution deposited a blue microcrystalline solid after a few minutes. The solid was filtered off, washed with a small quantity of cold ethanol and air-dried.

$Cu(azbH)_2Cl_2.2H_2O$ requires	C: 36.26%	N: 20.56%	H: 3.45%
Found	C: 36.04%	N: 20.38%	H: 3.05%

$Cu(azbH)_2Br_2.2H_2O$

The complex was prepared, by an analogous method to the chloride, as a green-blue microcrystalline solid.

$Cu(azbH)_2Br_2.2H_2O$ requires	C: 28.95%	N: 16.89%	H: 2.81%
Found	C: 29.30%	N: 16.47%	H: 3.08%

$Cu(azbH)Cl_2$

This complex could be prepared, as a green microcrystalline solid, by an analogous method to that for $Cu(hxH)Cl_2.H_2O$, or by addition of $CuCl_2.2H_2O$ (0.425 gm, 2.5 mM) in ethanol (10 ml.) to a solution of 4-azabenzimidazole (0.3 gm, 2.5 mM) in ethanol (5 ml.). In the latter preparation, the solid precipitated immediately and was filtered off, washed with ethanol and air dried.

$Cu(azbH)Cl_2$	requires	C: 28.42%	N: 16.57%	H: 1.99%
	Found	C: 28.95%	N: 16.73%	H: 2.21%

$Cu(azbH)Br_2$

The complex was obtained as brown microcrystals from acidic aqueous solution, or as a brown amorphous solid from ethanolic solution, by analogous methods to those for the chloride.

$Cu(azbH)Br_2$	requires	C: 21.04%	N: 12.27%	H: 1.47%
	Found	C: 21.51%	N: 12.42%	H: 2.01%

$Cu(azbH)_2(ClO_4)_2.H_2O$

4-azabenzimidazole (0.3 gm, 2.5 mM) was dissolved in hot ethanol (15 ml.), and $Cu(ClO_4)_2.6H_2O$ (0.46 gm, 1.25 mM) in ethanol (4 ml.) was added to the rapidly-stirred solution. A deep purple solid precipitated almost immediately, and was filtered off, washed with ethanol and air-dried.

$Cu(azbH)_2(ClO_4).H_2O$	requires	C: 27.74%	N: 16.18%	H: 2.92%
	Found	C: 27.53%	N: 16.60%	H: 2.31%

$Cu(azbH)_2(NO_3)_2.H_2O$

This complex was prepared as a mauve solid by an analogous method to the perchlorate complex.

$Cu(azbH)_2(NO_3)_2.H_2O$	requires	C: 32.43%	N: 25.23%	H: 2.70%
	Found	C: 32.50%	N: 24.76%	H: 2.97%

$Cu(azbH)_2SO_4.5H_2O$

4-azabenzimidazole (0.3 gm, 2.5 mM) was dissolved in N H_2SO_4 (7.5 ml.) and $CuSO_4.5H_2O$ (3.75 gm, 15mM) in water (10 ml.) was added

to the boiling solution. The deep blue solution deposited royal blue crystals overnight, which were filtered off, washed with a little cold water, and air-dried.

$Cu(azbH)_2SO_4 \cdot 5H_2O$	requires	C: 29.54%	N: 17.22%	H: 4.13%
	Found	C: 29.60%	N: 17.12%	H: 3.05%

$\underline{Cu(mpH)Cl_2}$

This complex was prepared by the method of Weiss and Venner.[207c]

6-mercaptopurine (0.45 gm, 3 mM) was dissolved in conc. HCl (4 ml.) and water (6 ml.). A solution of $CuCl_2 \cdot 2H_2O$ (2.05 gm, 12 mM) in water (10 ml.) was added to the stirred solution. A brick-red crystalline solid precipitated after ~ 5 min. and was filtered off, washed with 1 N HCl, water and methanol and air-dried.

$Cu(mpH)Cl_2$	requires	C: 20.95%	N: 19.55%	H: 1.41%
	Found	C: 20.49%	N: 19.15%	H: 1.79%

Table 6.1 E.p.r. data

$Cu(LH)_2X_2 \cdot nH_2O$ Complexes

Compound	* D(cm^{-1}) ($\pm$ 0.003)	g_z ($\pm$0.03)	g_{xy} ($\pm$0.01)	$A/2$ ($\times 10^{-4} cm^{-1}$)
$Cu(nxH)_2Cl_2 \cdot H_2O$	0.097(0.103)	2.25	2.06	**
$Cu(nxH)_2Br_2 \cdot H_2O$	0.097(0.099)	2.27	2.06	**
$Cu(nxH)_2(ClO_4)_2 \cdot 4H_2O$	0.099(0.102)	2.27	2.07	89 $\pm$ 7
$Cu(azbH)_2Cl_2 \cdot 2H_2O$	0.134(0.124)	2.29	2.05	86 $\pm$ 3
$Cu(azbH)_2Br \cdot 2H_2O$	0.130(0.130)	2.26	2.05	84 $\pm$ 3
$Cu(azbH)_2(ClO_4)_2 \cdot H_2O$	0.126(0.127)	2.25	2.04	90 $\pm$ 2
$Cu(azbH)_2(NO_3)_2 \cdot H_2O$	0.132(0.133)	2.26	2.05	90 $\pm$ 2
$Cu(azbH)_2SO_4 \cdot 5H_2O$	0.129(0.129)	2.25	2.04	88 $\pm$ 4
†$Cu(adH)_2Cl_2 \cdot 3H_2O$	0.117	2.20	2.06	
†$Cu(adH)_2Br_2 \cdot 2H_2O$	0.118	2.21	2.07	
‡$Cu(adH)_2(ClO_4)_2 \cdot 1.5H_2O$	0.110	2.22	2.05	88 $\pm$ 3
†$Cu(adH)_2(NO_3)_2$	0.116	2.20	2.06	
†$Cu(adH)_2SO_4 \cdot 4H_2O$	0.117	2.23	2.07	

$Cu(LH)X_2 nH_2O$ Complexes

Compound	g ($\pm$ 0.01)	g_z ($\pm$0.01)	g_{xy} ($\pm$0.01)
$Cu(nxH)Cl_2 \cdot H_2O$	2.20		
$Cu(nxH)Br_2$	2.17		
$Cu(nxH)SO_4 \cdot H_2O$		2.34	2.09
$Cu(azbH)Cl_2$	2.15		
$Cu(azbH)Br_2$	2.11		
$Cu(mpH)Cl_2$		2.23	2.04

* Value in brackets calculated from z transitions † from Ref.135

** hyperfine not resolved ‡ from Ref.212

Table 6.2 Reflectance Spectra

Compound	Band Maxima (cm^{-1})
$Cu(nxH)_2Cl_2.H_2O$	26,210, 15,230
$Cu(nxH)_2Br_2.H_2O$	25,450, 16,130
$Cu(nxH)_2(ClO_4)_2.4H_2O$	18,280, 15,070 (sh)
$Cu(nxH)Cl_2.H_2O$	v.br. centred at ~ 10,900
$Cu(nxH)Br_2$	v.br. centred at ~ 11,000
$Cu(nxH)SO_4.H_2O$	14,290, 10,560 (sh)
$Cu(azbH)_2Cl_2.2H_2O$	26,010, 15,530
$Cu(azbH)_2Br_2.2H_2O$	25,840, 16,000
$Cu(azbH)_2(ClO_4)_2H_2O$	26,460, 18,420, ~ 14,300 (sh)
$Cu(azbH)_2(NO_3)_2.H_2O$	26,010, 17,450, ~ 14,000 (sh)
$Cu(azbH)_2SO_4.5H_2O$	16,920, ~ 14,500 (sh), ~ 11,700 (sh)
$Cu(azbH)Cl_2$	~ 22,400 (sh), 12,500
$Cu(azbH)Br_2$	~ 19,200 (sh), 12,200
$Cu(mpH)Cl_2$	21,930, 13,490, ~ 11,100 (sh)

CHAPTER 7 OTHER SYSTEMS INVESTIGATED

During the studies on Fe^{II} complexes with heterocyclic amines of the pyridine and diazine type, some investigations were also carried out on the complexes formed between Fe^{II} salts and the bases, pyrazole and imidazole, which contain two nitrogen atoms in a five-membered ring. Primarily, attempts were made to prepare polymeric six-coordinate complexes with these ligands, for comparison with the series described in Chapters 4 and 5, but no complexes of this type could be isolated. Reaction of Fe^{II} chloride, bromide, iodide or thiocyanate with 1:1, 2:1 or 4:1 ratios of pyrazole to metal, in deoxygenated ethanol or propan-2-ol, yielded complexes of stoichiometry $Fe(pyrazole)_4X_2$ only, while, with Fe^{II} perchlorate or fluoroborate and 7:1 ratios of pyrazole to metal, complexes of the stoichiometry $Fe(pyrazole)_6X_2$ were obtained.

The chloride, bromide and iodide were relatively unstable, turning from almost white to yellow or brown on exposure to moist air. The thiocyanate was obtained from the yellow ethanolic solution as a pale mauve solid, which appeared to be more stable than the other $Fe(pyrazole)_4X_2$ complexes. This colour modification may be due to the presence of traces of Fe^{III} impurity (c.f. the well-known yellow and purple forms of $Fepy_4(NCS)_2$ [89]) but the Mössbauer spectrum showed no evidence of an impurity, and the colour did not deepen on exposure to moist air.

With imidazole, attempted preparation of the analogous FeL_4X_2 complexes produced oily deposits, and although solids could sometimes be isolated by addition of anhydrous ether and cooling, the compounds tended to oxidise rapidly, and no pure samples of this stoichiometry could be obtained. The difficulty in preparation of these compounds may be due to the relatively high basicity of this ligand, (pK_a values of imidazole and pyrazole are 7.2 and 2.5, respectively). The complex, $Fe(imidazole)_6(ClO_4)_2$, which has been reported previously,[89] was obtained by a similar method to the analogous pyrazole complex.

The reflectance spectra, Mössbauer spectra at 294 and 80 K (except for $Fe(pyrazole)_4Br_2$, which gave very poorly resolved peaks) and, in some cases, magnetic susceptibility of these complexes have been measured.

The results obtained are in very good agreement with those recently reported by Reedijk et al.,[244,245] and so are not detailed here. The interpretation of the data made here is also consistent with the conclusions drawn by Reedijk on the symmetry of the complexes and the nature of the ligand field splittings, but this latter author has carried out more extensive investigation and obtained more detailed information than was possible in this work.

The results of the measurements made here indicate that the $Fe(pyrazole)_4X_2$ complexes possess monomeric trans octahedral structures, with approximately D_{4h} symmetry about the metal ion. The reflectance spectra indicate that the total ligand field strength increases in the order NCS > Cl > Br > I, with the axial splitting of the ^5Eg excited state decreasing in the reverse order, as expected from the relative positions of the axial ligands and pyrazole in the spectrochemical series. The low values and small temperature dependence of ΔE_Q for the chloride and iodide complexes are consistent with a doublet ^5Eg (d_{xz}, d_{yz}) ground state, but Reedijk has proposed[245] a singlet $^5B_{2g}$ (d_{xy}) ground state for the thiocyanate.

The data for the FeL_6X_2 complexes are consistent with the presence of FeL_6^{2+} complex cations, but the observation of a resolved shoulder on the $^5T_{2g} \leftrightarrow {}^5Eg$ transition in the reflectance spectra, and the magnitude of the ΔE_Q values (1.2 - 1.3 mm/sec at 284 K) for these compounds suggest that the symmetry of the N_6 environment is lower than regular octahedral.

Investigations have also been carried out on some vanadyl (VO^{2+}) complexes. Several series of vanadyl compounds, which have been proposed to possess dimeric or polymeric chain structures, are known to exhibit antiferromagnetic exchange. In some cases, this behaviour parallels that in analogous cupric complexes, the two cations being magnetically similar in having one unpaired 3d electron.

Complexes of the type $VO(TSB)H_2O$ and $Cu(TSB)$[246] (where TSB is the tridentate Schiff's base, N-(2-hydroxyphenyl)salicylideneimine or some 5-substituted derivatives) exhibit antiferromagnetic exchange, and

their susceptibility data can be fitted by the model for coupling between discrete pairs of metal ions (Equation 6.1). Dimeric structures, as shown in Fig. 7.1, have therefore been proposed. The exchange interaction in the cupric complexes (unpaired electron in $d_{x^2-y^2}$) has been considered to proceed via a superexchange pathway involving the oxygen bridges, while that in the vanadyl compounds (unpaired electron in d_{xy}) has been considered to be due to direct σ-overlap between the d_{xy} orbitals.

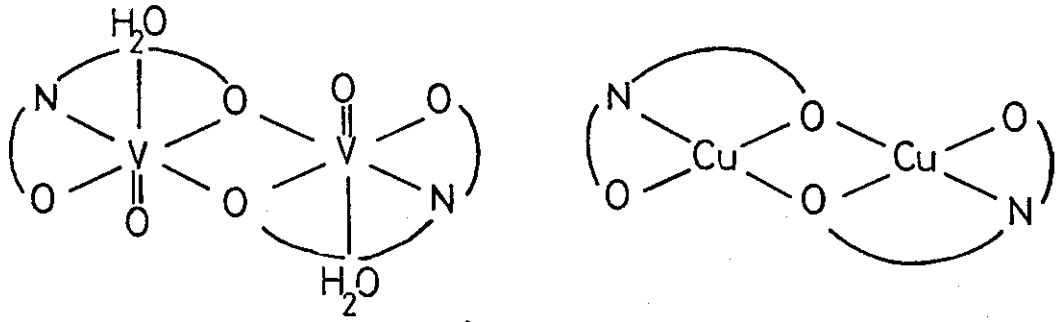

Fig. 7.1

Some preliminary measurements have been carried out in this work to investigate whether the existence of exchange in these dimeric vanadyl systems is manifested in their e.p.r. spectra by the presence of resonances attributable to transitions within an S' = 1 excited triplet state. The X-band spectrum of a powdered sample of VO(TSB)H_2O (TSB = the unsubstituted Schiff's base) contains a broad resonance feature in the g = 2 region (the absorption extending from ~ 2500 to 4500 gauss), with some poorly resolved structure at low temperature. The intensity of the signal decreases slightly with decreasing temperature, but it is not possible to distinguish resonances assignable to $\Delta m = 1$ transitions of an S = 1 state. However, an additional weaker feature is present at ~ 1500 gauss, similar in shape to the $\Delta m = 2$ transition observed in many copper dimers. At least nine or ten hyperfine components are resolved, and this feature may therefore be due to a similar half-field transition of an S' = 1 state of the vanadyl dimer (fifteen hyperfine components would be expected for an exchange-coupled pair of vanadium atoms, for which $I = \frac{7}{2}$). The observation of such a feature has been taken as evidence of dimer formation in vanadyl citrate,[247] and several very recent publications have appeared[248-250] on the e.p.r. study of dimerisation in vanadyl systems.

Vanadyl acetate has also been found[251] to exhibit pronounced antiferromagnetism, but unlike cupric acetate monohydrate, the susceptibility data cannot be fitted to the model for a dimeric system. The anisotropic Ising model for exchange in an infinite linear system has been found to provide the most adequate description of the observed behaviour, and this has led to the suggestion of a chain structure for the compound, involving both V = O --- V and carboxylate bridges (Fig.7.2). It has also been proposed that the exchange pathway involves the z-component of the spin, but not the x- and y-components, which raises the possibility of involvement of the V = O --- V bridges in the coupling mechanism.

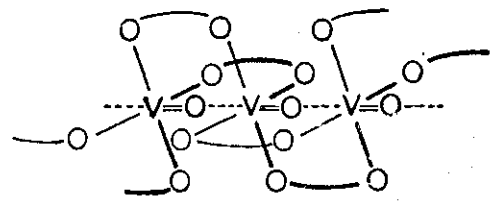

Fig. 7.2

A recent crystal structure of NN'-propylenebis(salicylaldiminato)oxovanadium(IV) has shown[252] that this compound contains V = O --- V bridges, but no other plausible pathway for exchange, and so provides a good system for checking the possibility of spin coupling via this vanadyl oxygen bridge. The details of the magnetic data obtained in this work have been presented in a publication.[253] The susceptibility obeys the Curie-Weiss law in the range 95 - 295 K, with only a small Weiss constant (7 K). The absence of significant exchange coupling in this compound therefore suggests that the unpaired electron is in the d_{xy} orbital and that the V = O --- V bridges do not provide an efficient exchange pathway, either via $\sigma(Op_z - Vd_{z^2})$ or $\pi(Op_x,p_y - Vd_{xz},d_{yz})$ overlap. This fact, and the observation that vanadyl sulphate, which also contains V = O --- V bridges, has a normal magnetic moment at room temperature,[254] implies that the vanadyl oxygen bridges do not contribute significantly to the antiferromagnetic coupling in vanadyl acetate. The bridging acetate groups could, however, provide a pathway for the exchange through π-overlap between the half-filled d_{xy} orbital on each vanadium atom and the π-symmetry orbitals of the acetate group. Intra-ionic exchange,

arising from acetate to vanadium π-bonding ($\pi \rightarrow d_{xy}$ and $\pi_{n.b.} \rightarrow d_{xy}$) and also from mutual overlap of the d_{xy} orbitals with the empty π^* orbitals on the acetate, would lead to antiferromagnetic coupling in each case.

Attempts have also been made to isolate complexes of adenine, 6-hydroxypurine and 4-azabenzimidazole with vanadyl and chromous salts, since it was hoped that these ligands might stabilise a dimeric system for these cations as they have been shown to do for cupric ions (Cr^{II} is known to form a dimeric acetate exhibiting antiferromagnetic coupling, similar to that for Cu^{II} [255]). Addition of vanadyl sulphate or chloride to neutral or alkaline aqueous solutions of these ligands (reaction in alcoholic solution was also investigated for 4-azabenzimidazole) produced dark green solutions, turning brown on standing. In some cases, the solutions deposited highly gelatinous dark green solids. Addition of aqueous solutions of adenine or 6-hydroxypurine to freshly prepared acidic solutions of chromous chloride, in a nitrogen atmosphere, produced no obvious colour change. However, on raising the pH by dropwise addition of NaOH, precipitates were obtained from the blue chromous solutions, the solids being pink-mauve(adenine) and pale lilac (6-hydroxypurine). No acceptable analyses have yet been obtained for any of these solids.

CHAPTER 8 CONCLUSION

The magnetic ordering found in the FeL_2Cl_2 complexes with the substituted pyridines and with 4-Mepm provides a good example of extended intrachain ferromagnetic superexchange between metal ions via $\sim 90^{\circ}$ chloride bridges. The direct observation of ferromagnetic interactions in coordination complexes is still relatively rare compared with the more commonly found antiferromagnetic behaviour, and the absence of a 'masking' interaction of the latter type (as is present, for example, in $FeCl_2 2H_2O$) in this series of compounds may be attributed to the bulk of the heterocyclic amine ligands, which effectively reduces the magnitude of additional interchain coupling.

On the other hand, for the $FeLCl_2$ complexes with pyrimidine and its substituted derivatives it has been shown that the delocalised π-system of the bridging diazine provides a pathway for interchain coupling of the spins of the metal ions, to produce overall antiferromagnetic behaviour. At present, it appears that the isomeric ligands, pyrazine and pyrimidine, may not possess the same ability for transmitting exchange coupling in these Fe^{II} complexes.

Mössbauer spectroscopy has proved extremely useful for detection of magnetic ordering and determination of the ordering temperature, where direct evidence from magnetic susceptibility measurements could not be obtained. Although the observation of magnetic hyperfine splitting at low temperature in the Mössbauer spectra of some paramagnetic Fe^{III} complexes with slow relaxation times is now quite well established, the number of coordination complexes in which resolved hyperfine splitting, attributable to magnetic ordering processes, has been found is still extremely small. It has been mentioned in Chapter 1 that Mössbauer spectroscopy has been of use to coordination chemists for detection of magnetic ordering in discrete cluster complexes, through the observations of quadrupole peak asymmetry and little enhancement of the effective field at the nucleus in applied field magnetically-perturbed spectra. However, direct evidence for magnetic coupling through observation of internal-field

hyperfine splitting has generally been confined to relatively strongly-ordered systems, such as the lattice oxide and halide compounds, studied mainly by physicists. The good agreement found for the complexes studied here between the magnetic ordering temperatures determined by Mössbauer spectroscopy and by direct magnetic susceptibility measurement indicates that the former technique could also be of great value in coordination chemistry for investigation of weak magnetic interactions, where the ordering is of the long-range intermolecular type.[242]

Although, owing to the very low site symmetry, no detailed information could be obtained on the exact nature and magnitude of the distortions present in these two series of Fe^{II} complexes, it does appear that the identity and position of the substituents on the heterocyclic bases can have a significant effect on the local environment, and thus on the electronic properties, of the central metal ion, both through their influence on the σ- and π-bonding abilities of the bases and also through their steric requirements in intra- and interchain packing considerations. Mössbauer spectroscopy has proved to be the most sensitive of the techniques used in this work to changes in the metal environment caused by small variations in the local symmetry and in the metal-ligand bonding. For one compound, $Fe(3\text{-}Cl\text{-}py)_2Cl_2$, two distinct structural modifications have been detected, the difference between them apparently involving a quite subtle variation in the metal-ligand bonding, but producing a quite marked effect on the electronic properties of the ground state of the metal ion. The possible occurrence of structural variations of this type within such a closely related series of compounds, emphasises the difficulties inherent in attempts to interpret meaningfully, and correlate, data from less sensitive techniques such as electronic spectroscopy and bulk susceptibility measurements, in terms of the ligand field distortion and bonding parameters.

The mid-I.R. criterion of Lever et al. for assignment of the mode of bonding of pyrazine has been shown to be invalid for the complexes studied here, and the conclusion that the $Fepz_2X_2$ complexes contain bridging pyrazine is consistent with the recent work of Goldstein et al. This structural assignment enables a more realistic comparison to be made between the relative ligand field strengths of pyridine and bridging

pyrazine, and indicates that the influence on the total ligand field strength of the steric effect of an α-methyl ring substituent in the diazine complexes is less important than previously considered.

The e.p.r. investigations on the Cu^{II} complexes with 6-hydroxypurine and 4-azabenzimidazole has shown that the ability of bases, containing the N(9) - C(4) - N(3) moiety of the purine ring system, to bridge discrete pairs of Cu^{II} ions and provide a superexchange pathway for antiferromagnetic interaction; is not limited to adenine. It has not yet been possible to determine definitely whether the bridging tendency of these two ligands is also manifested in the $CuLX_2$ complexes. The apparent inability of 6-mercaptopurine to stabilise the dimeric structure may be due to the involvement of the sulphur atom in bonding to the copper.

The studies on these systems are again of chemical rather than biochemical interest, since the N(9) atom in naturally-occurring nucleosides is blocked by a ribose unit. A recent crystal structure of the complex Cu(9-MeHxH)Cl_2 $5H_2O$,[243] which is biochemically more relevant, has shown that when the N(9) atom is unavailable for coordination, the purine is bonded through N(7) only.

Instrumental Section

Reflectance spectra were obtained using a Beckman DK2 instrument fitted with a Beckman 24500 reflectance unit, and also a Cary 14R instrument fitted with a Cary 1411 diffuse reflectance accessory.

Mössbauer spectra were measured at room and liquid nitrogen temperatures using a constant acceleration spectrometer with Laben 400 channel analyser at Queen Elizabeth College, London. The velocity scale was calibrated using sodium nitroprusside. The spectra at these temperatures were remeasured for some of the compounds, and all liquid helium and applied field measurements were made, by the P.C.M.U. Mössbauer Section at Harwell. Thanks are due to Dr B.W. Dale for his interest and helpful discussions. The data from Harwell were obtained with reference to an iron foil calibrant, and have been converted to sodium nitroprusside as reference for consistency with the data measured personally and with results reported for systems related to those studied here. The data, in the form of counts/channel, were processed by use of a least-squares fitting program, written by Dr P. Hannaford and modified by Dr I.A.G. Roos. I am indebted to the latter for making the program available to me.

E.p.r. measurements at X-band were made using Varian V-4502-15 and E9 spectrometers.

Magnetic susceptibility measurements were made as described in the Appendix.

REFERENCES

1. R.S. Tebble and D.J. Craik, 'Magnetic Materials', Wiley-Interscience, (1969).
2. Landolt-Bornstein, Zahlenwerte und Functionen, II 9, Magnetic Properties I. Chaps. 1, 2, 3, 5. Springer-Verlag (Berlin), (1962).
3. Bibliography of Magnetic Materials (compiled by T.F. Connolly and E.D. Copenhaver) Oak Ridge Nat. Labs. (1970).
4. J.B. Goodenough 'Magnetism and the Chemical Bond', Interscience N.Y. (1963).
5. B.N. Figgis and J. Lewis, 'Progress in Inorg. Chem.', 6, 37 (1964).
6. B.N. Figgis and J. Lewis, 'Technique in Inorg. Chem.', 4, 137 (1965).
7. B.N. Figgis and J. Lewis in 'Modern Coordination Chemistry' (Eds. J. Lewis and R.G. Wilkins) Interscience N.Y. p.406 (1960).
8. J. Owen and J.H.M. Thornley, Rept. Prog. Phys., 29.II 675 (1966).
9. P.W. Anderson in 'Magnetism' (Eds. G. Rado and H. Suhl) I, 25, (1963).
10. P. de Gennes in 'Magnetism' (Eds. G. Rado and H. Suhl) III, 115 (1963).
11. S. Foner in 'Magnetism' (Eds. G. Rado and H. Suhl) I, 384 (1963); C.W. Haas and H.B. Callen, ibid. 450; R.W. Damon, ibid. 552.
12. M.E. Fisher, Rept. Prog. Phys., 30, 615 (1967); P. Heller, ibid. 731.
13. J.H. Van Vleck 'The Theory of Electric and Paramagnetic Susceptibilities' Oxford Univ. Press, (1932).
14. J.S. Griffiths 'The Theory of Transition Metal Ions', Cambridge Univ. Press, (1961).
15. C.J. Ballhausen 'Introduction to Ligand Field Theory', McGraw-Hill, N.Y. (1962).
16. B.N. Figgis 'Introduction to Ligand Fields', Wiley Interscience, N.Y. (1966).
17. R.M. Golding 'Applied Wave Mechanics', Van Nostrand, London (1969).
18. A. Earnshaw 'Introduction to Magnetochemistry', Academic Press (1968).
19. B.N. Figgis, Nature, 182, 1568 (1958).
20. B.N. Figgis, Trans. Faraday Soc., 56, 1553 (1960).
21. B.N. Figgis, Trans. Faraday Soc., 57, 198, 204 (1961).
22. A. Bose, A.S. Chakravarty and R. Chatterjee, Proc. Roy. Soc. A261, 43 (1961).
23. B.N. Figgis, J. Lewes, F. Mabbs and G.A. Webb, Nature, 203, 1138 (1964).
24. idem, J. Chem. Soc. (A) 422 (1966).

25. idem, ibid. 1411 (1966).
26. idem, ibid. 442 (1967).
27. B.N. Figgis, J. Lewis, M. Gerloch, F. Mabbs, G.A. Webb, J. Chem. Soc. (A) 2086 (1968).
28. G.A. Webb, Coord. Chem. Rev. 4, 107 (1969).
29. E. König and A.S. Chakravarty, Theoret. Chim. Acta, 9, 151 (1967).
30. E. König and A.S. Chakravarty, Theoret. Chim. Acta, 9, 171 (1967).
31. M. Gerloch, J. Chem. Soc. (A) 2023 (1968).
32. M. Gerloch, J. Lewis, G.G. Phillips and P.N. Quested, J. Chem. Soc. (A) 1941 (1970).
33. B.N. Figgis, J. Chem. Soc. 4887 (1965).
34. K.W.H. Stevens, Proc. Roy. Soc. A219 542 (1953).
35. M. Gerloch and J.R. Miller, Prog. in Inorg. Chem. 10, 1 (1968).
36. C.J. Ballhausen and H.B. Gray 'Molecular Orbital Theory', Benjamin, N.Y. (1964).
37. C.K. Jorgensen 'Absorption Spectra and Chemical Bonding in Complexes', Pergamon Press, N.Y. (1964).
38. C.K. Jorgensen, Prog. in Inorg. Chem. 4, 73 (1962).
39. J. Hubbard, O.E. Rimmer and F.R.A. Hopgood, Proc. Phys. Soc., 88, 13 (1966).
40. G.J. Long and W.A. Baker, J. Chem. Soc. (A) 2956 (1971).
41. A.K. Gregson and S. Mitra, Chem. Phys. Letters 3, 392 (1969).
42. A.K. Gregson and S. Mitra, Chem. Phys. Letters 3, 528 (1969).
43. A.P.B. Lever, 'Inorganic Electronic Spectroscopy', Elsevier (1968).
44. A.P.B. Lever, Coord. Chem. Rev. 3, 119 (1968).
45. B. Bleaney and K.W.H. Stevens, Rept. Prog. Phys. 16, 108 (1953).
46. G.F. Kokoszka and G. Gordon, Tech. in Inorg. Chem. 7, 151 (1967).
47. A. Abragam and B. Bleaney, 'E.P.R. of Transition Ions', Oxford Univ. Press (1970).
48. B.R. McGarvey, Trans. Metal Chem. 3, 89 (1966).
49. N.N. Greenwood and T.C. Gibb 'Mössbauer Spectroscopy', Chapman and Hall (1971).
50. V.I. Goldanskii and R.M. Herber (Eds.) 'Chemical Applications of Mössbauer Spectroscopy', Academic Press, N.Y. (1968).
51. R. Ingalls, Phys. Rev., 133, A787, 1964.
52. T.C. Gibb, J. Chem. Soc. (A) 1439 (1968).
53. R.M. Golding, K.F. Mok and J.F. Duncan, Inorg. Chem., 5, 774 (1966).

54. C. Burbridge, D.M.L. Goodgame and M. Goodgame, J. Chem. Soc. (A), 349 (1967).

55. B. Bleaney and K. Bowers, Proc. Roy. Soc. (Lond.) A214, 451 (1952).

56. M. Kato, M.B. Jonassen and J.C. Fanning, Chem. Rev., 64, 99 (1964).

57. J. Lewis, Pure Appl. Chem., 10, 11 (1965).

58. F.A. Cotton, Quart. Rev., 20, 389 (1966).

59. F.A. Cotton, Rev. Pure Appl. Chem., 17, 25 (1967).

60. E. König, "Magnetic Properties of Coordination and Organometallic Transition Metal Compounds", Landolt Bornstein, II. Springer-Verlag, Berlin (1966).

61. R.L. Martin in 'New Pathways in Inorganic Chemistry' (Ed. E. Edsworth, A. Maddock, A. Sharp), Cambridge Univ. Press, p.175 (1968).

62. P. Ball, Coord. Chem. Rev., 4, 361 (1969).

63. E. Sinn, Coord. Chem. Rev., 5, 313 (1970).

64. G.F. Kokoszka and G. Gordon, Trans. Metal Chem., 5, 181 (1969).

65. G.F. Kokoszka and R.W. Duerst, Coord. Chem. Rev., 5, 209 (1970).

66. W. Heisenberg, Z. Phys., 38, 411 (1926).

67. W. Heisenberg, Z. Phys., 49, 619 (1928).

68. P.A.M. Dirac, Proc. Roy. Soc., A123, 714 (1929).

69. H.A. Kramers, Physica, 1, 182 (1934).

70. P.W. Anderson, Phys. Rev., 79, 350 (1950).

71. P.W. Anderson, Phys. Rev., 115, 2 (1959).

72. K.W.H. Stevens in 'Magnetism' (Ed. G. Rado and H. Suhl) I, 1 (1963).

73. K. Kambe, J. Phys. Soc. Jap. 5, 48 (1950).

74. J.S. Smart in 'Magnetism' (Ed. G. Rado and H. Suhl) III, 63 (1963).

75. A.N. Buckley, I.R. Herbert, B.D. Rumbold, G.V.H. Wilson and K.S. Murray, J. Phys. Chem. Solids, 31, 1423 (1970).

76. A.N. Buckley, B.D. Rumbold, G.V.H. Wilson and K.S. Murray, J. Chem. Soc. (A), 2298 (1970).

77. D. Cunningham, M.J. Frazer, A.H. Qureshi, F.B. Taylor and B.W. Dale, J. Chem. Soc. Dalton, 1090 (1972).

78. J.S. Smart, 'Effective Field Theories of Magnetism', W.B. Saunders, (1966).

79. M.E. Fisher, J. Math. Phys., 4, 124 (1963).

80. J.C. Bonner and M.E. Fisher, Phys. Rev., 135, A640 (1964); 140, A892 (1964).

81. J. Yamashita and J. Kondo, Phys. Rev., 109, 730 (1958).
82. F. Keffer and T. Oguchi, Phys. Rev., 115, 1428 (1959).
83. J. Kanamori, J. Phys. Chem. Solids, 10, 87 (1959).
84. J.C. Slater, Phys. Rev., 82, 538 (1951).
85. O. Baudisch and W.H. Hartnung, Inorg. Syn., 1, 184 (1939).
86. P. Pascal (Ed.) Nouveau Traite de Chimie Minerale, 18, Masson et Cie, (1959).
87. G. Spacu, Ann. Univers. Jassy, 8, 24, 162 (1964).
88. D.M.L. Goodgame, M. Goodgame, M.A. Hitchman and M.J. Weeks, Inorg. Chem., 5, 635 (1966).
89. C.D. Burbridge, Ph.D. Thesis, Imperial College (1968).
90. M.A. Porai-Koshits and A.S. Antishkena, Soviet Phys. Cryst., 3, 694, (1958).
91. J.A. Allan, D.H. Brown, R.H. Nuttall and D.W.A. Sharp, J. Chem. Soc., A1031, (1966).
92. G. Winter, Aust. J. Chem., 21, 2859 (1968).
93. P.B. Merrithew, P.G. Rasmussen and D.H. Vincent, Inorg. Chem. 10, 1401 (1971).
94. G. Beech, C.T. Mortimer and E.G. Tyler, J. Chem. Soc., A1111, (1967).
95. D. Forster and D.J. Dahm, Inorg. Chem., 11, 918 (1972).
96. C.D. Burbridge and D.M.L. Goodgame, Inorg. Chem. Acta, 4, 231 (1970).
97. D. Forster and D.M.L. Goodgame, J. Chem. Soc., 454 (1965).
98. C.D. Burbridge and D.M.L. Goodgame, J. Chem. Soc.,A1074 (1968).
99. G.J. Long and W.A. Baker, J. Inorg. Nucl. Chem., 33, 1196 (1971).
100. N. Saito, T. Tominaga, J. Morimoto and M. Takeda, Proc. Xth I.C.C.C., Tokyo (1967); Inorg. Nucl. Chem. Lett, 2, 193 (1966).
101. N.S. Gill, R.S. Nyholm, G.A. Barclay, T.I. Christie and P.J. Pauling, J. Inorg. Nucl. Chem. 18, 88 (1961).
102. G.J. Long, D.L. Whitney and J.E. Kennedy, Inorg. Chem., 10, 1406 (1971).
103. Gmelin, Handbuch der Anorganischen Chemie, 8, 59(B), 220, (1958).
104. R. Zanetti and R. Serra, Gazz. Chim. Ital. 90, 328 (1960).
105. J.D. Dunitz, Acta Cryst., 10, 307 (1957).
106. R.J.H. Clark and C.S. Williams, Inorg. Chem., 4, 350 (1965).
107. J.R. Allan, D.H. Brown, R.H. Nuttall and D.W.A. Sharp, J. Inorg. Nucl. Chem., 27, 1305 (1965).
108. M. Goldstein and W.D. Unsworth, Inorg. Chim. Acta, 4, 432 (1970).
109. M. Goldstein and W.D. Unsworth, Spectrochim. Acta, 28A, 1107 (1972).

110. R. Colton and J.H. Canterford, "Halides of the First Row Transition Metals", Wiley Interscience (1969).

111. H. Lux, L. Eberle and D. Sarre, Chem. Ber., 97, 503 (1964).

112. Reference 2, Chapter 3.

113. C. Stoehr, J. Prakt. Chem. 47, 439 (1893); 48, 18 (1893); 51, 449 (1895).

114. A.B.P. Lever, J. Lewis and R.S. Nyholm, J. Chem. Soc. 3156 (1963).

115. A.B.P. Lever, J. Lewis and R.S. Nyholm, Nature, 169, 58 (1961).

116. A.B.P. Lever, J. Lewis and R.S. Nyholm, in 'Advances in the Chemistry of Coordination Compounds', (Ed. S. Kirschner), Macmillan, N.Y. 419 (1961).

117. A.B.P. Lever, J. Lewis and R.S. Nyholm, J. Chem. Soc. 1235 (1962).

118. A.B.P. Lever, J. Lewis and R.S. Nyholm, J. Chem. Soc. 5042 (1963).

119. A.B.P. Lever, J. Lewis and R.S. Nyholm, J. Chem. Soc. 4761 (1964).

120. Lutteringhaus and Kullick, Tetrahedron Letters, 1, 48 (1959).

121. G.W.A. Fowles and R.A. Walton, J. Chem. Soc. (A) 4330 (1964).

122. B.E. Bridgeland, G.W.A. Fowles and R.A. Walton, J. Inorg. Nucl. Chem. 27, 383 (1965).

123. R.A. Walton, J. Chem. Soc. (A) 1485 (1967); J. Chem. Soc. (A) 61 (1969).

124. R.G. Vranka and E.L. Amma, Inorg. Chem., 5, 1020 (1966)

125. R.W. Matthews and R.A. Walton, Inorg. Chem. 10, 1433 (1971)

126. A.E. Allen, K. Feenan and G.W.A. Fowles, J. Chem. Soc. (A)1636 (1965)

127. S.A. Adeyeni, J. Amer. Chem. Soc., 94, 300 (1972).

128. M. Goldstein and W.D. Unsworth, Spectrochim. Acta, 27A, 1055 (1971).

129. J.R. Ferraro, J. Zipper and W. Wozniak, Appl. Spect. 23, 160 (1969).

130. C. Reimann and G. Gordon, Nature 205, 902 (1965).

131. K. Hyde, G.F. Kokoszka and G. Gordon, J. Inorg. Nucl. Chem., 31, 1993, (1969).

132. H.D. Stidham and J.A. Chandler, J. Inorg. Nucl. Chem., 27, 397 (1965).

133. J.R. Ferraro, C. Cristallini and G. Roch, Ric. Sci., 37, 435 (1967).

134. J.R. Ferraro, W. Wozniak and G. Roch, Ric. Sci., 38, 433 (1968).

135. K.A. Price, Ph.D. Thesis, Imperial College (1971).

136. A. Tennunen, Ann. Acad. Sci. Fenn. A2, 161 (1971).

137. R. Weiss and H. Venner (a) Z. Physiol. Chem. 317, 82 (1959);
(b) ibid. 317, 95 (1959);
(c) ibid. 341, 229 (1965);
(d) ibid. 350, 396 (1969);
(e) ibid. 350, 1189 (1969);
(f) ibid. 350, 1310 (1969).

138. J.R. Allen, G.A. Barnes and D.H. Brown, J. Inorg. Nucl. Chem., 33 3765 (1971).

139. M. Inoue, S. Emori and M. Kubo, Inorg. Chem. 7, 1427 (1968).

140. J.E. Andrew, P.W. Ball and A.B. Blake, Chem. Comm., 143 (1969).

141. J.E. Andrew and A.B. Blake, J. Chem. Soc. (A) 1415 (1969).

142. M.J. Campbell, R. Grzeskowiak and F.B. Taylor, J. Chem. Soc. (A) 19 (1970).

143. V. Schomaker and L. Pauling, J. Amer. Chem. Soc., 61, 1769 (1939).

144. R.C. Lord, A.L. Marston and F.A. Miller, Spectrochim. Acta, 9, 113, (1957).

145. S. Califano, G. Adembri and G. Sbrana, Spectrochim. Acta, 20, 385, (1964).

146. J.D. Simmons, K.K. Innes and G.M. Begum, J. Mol. Spect. 14, 190, (1964).

147. G. Beech and C.T. Mortimer, J. Chem. Soc. (A) 1115 (1967).

148. F.D. Ayres, G.B. Robertson and P. Pauling, Inorg. Chem., 3, 1303 (1964).

149. D.J. Cromer and A.C. Larson, Acta Cryst. B28, 1052 (1972).

150. M. Brierley and W.J. Geary, J. Chem. Soc. (A) 963 (1967).

151. R.W. Stotz, J.A. Walmsley and F. Walmsley, Inorg. Chem. 8, 807 (1968).

152. W.M. Reiff in "Mössbauer Effect Methodology" 7, 213 (1971).

153. D.S. McClure in 'Advances in the Chemistry of Coordination Compounds' (Ed. S. Kirschner), Macmillan, N.Y. (1961).

154. C.J. Ballhausen and A.D. Liehr, Ann. Phys, 3, 304 (1958).

155. B. Jezowska-Trzebiatowska and W. Wojciechowski in 'Transition Metal Chemistry' (Ed. R.L. Carlin) 6, 1 (1970).

156. A. Earnshaw, B.N. Figgis and J. Lewis, J. Chem. Soc. (A) 1656 (1966).

157. L.R. Walker, G.K. Wertheim and V. Jaccarino, Phys. Rev. Lett. 6, 98, (1961).

158. D.A. Shirley, Rev. Mod. Phys., 36, 339 (1964).

159. G.M. Bancroft, M.J. Mays and B.E. Prater, J. Chem. Soc. (A)956 (1970).

160. Y. Hazony, R.C. Axtmann and J.W. Hurley, Chem. Phys. Lett. 2, 440,673 (1968); J. Chem. Phys. 52, 3309 (1970).

161. Y. Hazony, Phys. Rev. B.3, 711 (1971).

162. Y. Hazony in 'Mössbauer Effect Methodology', 7, 147 (1971).

163. G.A. Sawatzky and F. Van der Wonde, Chem. Phys. Lett. 4, 335 (1969).

164. T. Birchall and M.F. Morris, Can. J. Chem. 50, 201 (1972).

165. B.D. Josephson, Phys. Rev. Lett. 4, 341 (1960).

166. Y. Hazony, J. Chem. Phys., 45, 2664 (1966).
167. E. Fluck in 'Advances in Inorganic Chemistry and Radiochemistry' (Ed. H.J. Emeléus and A.G. Sharpe) 6, 435 (1964).
168. Reference 17, Chapter 9.
169. R. Ingalls, Phys. Rev., 188, 1045 (1969).
170. K. Ito and A. Ho, J. Phys. Soc. Japan, 19, 899 (1968).
171. A.J. Nozik and M. Kaplan, Phys. Rev., 159, 273 (1967).
172. B.W. Dale, J. Phys. (C), 4, 2705 (1971).
173. C.E. Johnson in 'Symposia of the Faraday Society' 1, 7 (1967).
174. R.E. Watson and A.J. Freeman, Phys. Rev., 123, 2077 (1961).
175. H.H. Wickman and G.K. Wertheim, Reference 50, Chapter 11.
176. G.R. Hoy and S. Chandra, J. Chem. Phys., 47, 961 (1967).
177. P.G.L. Williams and G.M. Bancroft in 'Mössbauer Effect Methodology', 7, 39 (1971).
178. R.L. Collins, J. Chem. Phys., 42, 1072 (1965).
179. B. Morosin and E.J. Graeber, J. Chem. Phys., 42, 898 (1965).
180. M.S. Gill, R.H. Nuttall, D.E. Scaife and D.W.A. Sharpe, J. Inorg. Nucl. Chem., 18, 79 (1961).
181. D.G. Brewer and P.T.T. Wong, Can. J. Chem., 44, 1407 (1966) 46, 131 (1968).
182. M.A. Porai-Koshits, Tr. Int. Krist. Acad. Nauk. SSSR, 10, 117, (1954).
183. S.V. Karyagin, Doklady Akad. Nauk. SSSR, 148, 1102 (1963).
184. M. Blume, Phys. Rev. Lett., 18, 305 (1967); M. Blume and J.A. Tjon, Phys. Rev. 165, 446 (1968).
185. R.L. Collins and J.C. Travis, in 'Mössbauer Effect Methodology', 3, 123 (1967).
186. J.C. Travis in 'Introduction to Mössbauer Spectroscopy'.
187. S.M. Nelson and T.M. Shephard, J. Chem. Soc., 3276 (1965).
188. A.B.P. Lever, S.M. Nelson and T.M. Shephard, Inorg. Chem. 4, 810 (1965).
189. D.E. Billing and A.E. Undernill, J. Chem. Soc. (A) 29 (1968).
190. R.A. Walton, J. Inorg. Nucl. Chem., 28, 2229 (1966).
191. D.M.L. Goodgame, M. Goodgame and M.J. Weeks, J. Chem. Soc. 5194 (1964).
192. D.M.L. Goodgame, M. Goodgame, M.A. Hitchman and M.J. Weeks, J. Chem. Soc. (A) 1769 (1966).
193. R.A. Rowley and R.D. Drago, Inorg. Chem., 7, 795 (1968).
194. A. Narath, Phys. Rev., 139, A1221 (1965).
195. C.E. Johnson, Proc. Phys. Soc., 88, 943 (1966).

196. M. Goldstein, F.B. Taylor and W.D. Unsworth, J. Chem. Soc. (Dalton) 422 (1972).

197. M. Kobayisha and T. Haseda, J. Phys. Soc. Japan, 19, 765 (1964)

198. K.E. Hyde, B.C. Quinn and I.P. Yang, J. Inorg. Nucl. Chem., 33, 2377 (1971).

199. J.A.J. Jarvis, Acta Cryst., 15, 964 (1962).

200. K. Nakamoto, 'I.R. Spectra of Inorganic and Coordination Compounds' (Wiley-Interscience) 2nd Ed. (1970).

201. P.W. Carreck, M. Goldstein, E.M. McPartlin and W.D. Unsworth, Chem. Comm., 1634 (1971).

202. J.F. Villa and W.E. Hatfield, J. Amer. Chem. Soc., 93, 4081 (1971).

203. A. Santoro, A.D. Mighell and C.W. Reiman, Acta Cryst., B26, 979 (1970).

204. G.L. Eichhorn, Adv. in Chem. Series 62, 378 (1967).

205. U. Weser, 'Structure and Bonding' 5, 41 (1968).

206. R.E. Izatt, J.J. Christensen and J.H. Rytting, Chem. Rev., 71, 439 (1971)

207. R. Weiss and H. Venner (a) Z. Physiol. Chem. 333, 169 (1963)
(b) ibid. 340, 138 (1965)
(c) ibid. 345, 122 (1966)
(d) ibid. 350, 230 (1969)

208. E. Sletten, Chem. Comm., 1119 (1969); Acta Cryst., B25, 1480 (1969)

209. J.N. van Niekerk and F.R.L. Schoening, Acta Cryst., 6, 227 (1953).

210. D.M.L. Goodgame and K.A. Price, Nature, 220, 783 (1968).

211. D.M.L. Goodgame and K.A. Price, Proc. XIIth I.C.C.C. 131 (1969).

212. R.W. Duerst, S.J. Baum and G.F. Kokoszka, Nature, 222, 665 (1969).

213. R.W. Jotham and S.F.A. Kettle, J. Chem. Soc. (Dalton) 428 (1972).

214. A.K. Gregson, R.L. Martin and S. Mitra, Proc. Roy. Soc. (A), 320, 473 (1971).

215. P. de Meester, D.M.L. Goodgame, K.A. Price and A.C. Skapski, Nature, 229, 191 (1971).

216. J.M. Price, J.R. Pilbrow, K.S. Murray and T.D. Smith, J. Chem. Soc. (A) 968 (1970).

217. T.R. Harkins and H. Frieser, J. Amer. Chem. Soc., 80, 1132 (1958).

218. E. Sletten, J. Sletten and L.H. Jenson, Acta Cryst., B25, 1330 (1969).

219. A. Albert, 'Heterocyclic Chemistry', p.154 (1959).

220. D.G. Watson, R.M. Sweet and R.E. Marsh, Acta Cryst., 19, 573 (1965).

221. J.A. Carrabine and M. Sundaralingham, J. Amer. Chem. Soc., 92, 369, (1970).

222. L. Srinivasan and M.R. Taylor, Chem. Comm., 1668 (1970).

223. P. de Meester, D.M.L. Goodgame, K.A. Price and A.C. Skapski, Biochem. Biophys. Res. Comm., 44, 510 (1971).

224. J.F. Boas, R.H. Dunhill, J.R. Pilbrow, R.C. Srivastava and T.D. Smith, J. Chem. Soc. (A), 94 (1969).

225. G.F. Kokoszka, M. Linzer and G. Gordon, Inorg. Chem., 7, 1730 (1968).

226. E. Wasserman, L.C. Snyder and W.A. Yager, J. Chem. Phys., 41, 1763 (1964).

227. J.R. Wasson, C.S. Shyr and C. Trapp, Inorg. Chem., 7, 469 (1968).

228. J. Lewis, F.E. Mabbs, L.K. Royston and W.R. Smail, J. Chem. Soc. (A), 291 (1969).

229. F.G. Herring, R.C. Thompson and C.F. Schaerdtfager, Can. J. Chem., 47, 555 (1969).

230. J.H. van der Waals and M.S. de Groot, Mol. Phys., 2, 333 (1959); ibid. 3, 190 (1960).

231. P. Kottis and R. Lefebvre, J. Chem. Phys., 39, 393 (1963); ibid, 41, 397 (1964).

232. E. Sletten, Acta Cryst., B26, 1609 (1970).

233. L. Dubicki, Aust. J. Chem., 25, 1141 (1972).

234. D.E. Billing and A.E. Underhill, J. Inorg. Nucl. Chem., 30, 2147 (1968).

235. B. Bleaney, Rev. Mod. Phys., 25, 161 (1953).

236. T. Asakawa, M. Inoue, K. Hara and M. Kubo, Bull. Chem. Soc. Japan, 45, 1054 (1972).

237. R.L. Martin and H. Waterman, J. Chem. Soc., 1359 (1959).

238. M. Inoue and M. Kubo, Inorg. Chem., 9, 2310 (1970).

239. P. de Meester, D.M.L. Goodgame, K.A. Price and A.C. Skapski, Chem. Comm., 1573 (1970).

240. J.F. Villa, Inorg. Nucl. Chem. Lett. 8, 577 (1972).

241. J. Brigando and D. Colaitis, Bull. Chim. Soc., France, 10, 3440 (1969).

242. L.N. Mulay in 'Mössbauer Effect Methodology', 3, 79 (1967).

243. E. Sletten, Chem. Comm., 558 (1971).

244. J. Reedijk, Rec. Trav. Chim., 88, 1451 (1969).

245. J. Reedijk and D.W. Engelfriet, Rec. Trav. Chim., 91, 883 (1972).

246. A.P. Ginsberg, R.C. Sherwood and F. Koubek, Inorg. Chem., 5, 1656 (1966); J. Inorg. Nucl. Chem., 29, 353 (1967).

247. R.H. Dunhill and T.D. Smith, J. Chem. Soc. (A), 2189 (1968).

248. T.D. Smith, T. Lund, J.R. Pilbrow and J.H. Price, J. Chem. Soc. (A), 2936 (1971).

249. P.D.W. Boyd, T.D. Smith, J.H. Price and J.R. Pilbrow, J. Chem. Phys., 56, 1253 (1972).

250. S.G. Carr, P.D.W. Boyd and T.D. Smith, J. Chem. Soc. (Dalton), 1491 (1972).

251. A.T. Casey and J.R. Thackeray, Aust. J. Chem., 22, 2549 (1969).

252. M. Mathew, A.J. Carty and G.J. Palenik, J. Amer. Chem. Soc., 92, 3197 (1970).

253. D.M.L. Goodgame and S.V. Waggett, Inorg. Chim. Acta, 5, 155 (1971).

254. P. Kierkegaard and J.M. Longo, Acta Chem. Scand., 19, 1906 (1965).

255. L. Dubicki and R.L. Martin, Inorg. Chem., 5, 2203 (1966).

APPENDIX

MAGNETIC SUSCEPTIBILITY MEASUREMENTS

Since the classical work of Curie, Faraday and Gouy, a large number of instrumental methods have been devised for the measurement of magnetic susceptibility. These may be divided into two main categories depending on the basic principle utilised in the technique.

The first involves the measurement of the magnetic induction in the sample, when placed in a homogeneous magnetic field. Instruments based on this principle have been described in the literature.[1,2,3,4] More recently, the vibrating-sample and -coil magnetometers have been developed, which measure magnetisation by an a.c. technique.[3,5,6,7] These instruments can easily be adapted for determination of susceptibility as a function of temperature, field strength and crystallographic orientation, and are capable of high sensitivity. Their main disadvantage is that extraneous electrical "noise" interferes with the signal detection, and is often difficult to eliminate.

The second category involves the measurement of the force exerted on a material when it is placed in an inhomogeneous magnetic field, and many variations of the "force balance" have been designed.[3,4,8-11] They are generally either of the Gouy or the Faraday type, and are the most widely used by inorganic chemists for accurate susceptibility measurements over a wide temperature range on magnetically isotropic samples.

The Faraday method requires only a small quantity of sample, but necessitates special magnet design and very accurate positioning of the sample. The Gouy method requires larger samples, in the form of a long cylinder, and for powdered solids errors often result from non-uniform packing of the specimen tube. The Gouy method does however permit absolute susceptibility measurement with considerable accuracy. In the Faraday technique, knowledge is required of the precise value and variation of the non-uniform field, and although an absolute determination of susceptibility is possible,[12] it is more usual to make measurements relative to a known standard.

The force balance can be modified for magnetic anisotropy measurements, although objections have been raised[13] to the use of this method for highly anisotropic materials. Direct investigation of the magnetic field dependence of susceptibility involves some difficulty in interpretation, since the principle requires the presence of a magnetic field gradient to produce the force on the sample.

In this work, susceptibility measurements have been made using a variable-temperature Gouy balance ($\sim$ 80 - 300K) and a variable-temperature Faraday balance ($\sim$ 1.8 - 300K). The former was constructed by Dr D. Forster to the design of Figgis and Nyholm,[14] and is conventional in operation. The Faraday balance was constructed by Mr D.J. Lowe, in collaboration with Miss S.V. Waggett, and presented many problems, mainly concerning the cryogenic equipment for liquid helium work and the detection and elimination of errors during operation. An account will therefore be given of the construction and operation of the apparatus.

THE FARADAY BALANCE

Section I. Theory of the Method

Section II. Components and Construction

- (i) Magnet Assembly
- (ii) Microbalance
- (iii) Cryostat and Vacuum System
  Temperature control
- (iv) Temperature Measurement
- (v) Monitoring and Display of Readings
- (vi) Sample Container, Suspension and Sampling

Section III. Modes of Operation

- (i) Manual
- (ii) Automatic
- (iii) Calculation of Results

Section IV. Coordination and Protection of Components

Section V. Calibrations and Errors

- (i) Field Calibration
- (ii) Temperature Calibration
- (iii) Errors.

Section I. THEORY OF THE FARADAY BALANCE

The magnetic field axes are shown in Fig.1.

If a specimen, of mass m g. and of susceptibility χ emu. g^{-1}, is placed in an inhomogeneous horizontal magnetic field, H_x, a vertical force, F_z dynes, is exerted on it, where

$$F_z = m\chi \left(H_x \frac{dH_x}{dz} + H_y \frac{dH_y}{dz} + H_z \frac{dH_z}{dz}\right) \quad 8,15 .$$

With the arrangement in Fig.1,

$H_z = 0$, by symmetry on the z-axis,

and H_y is very small (considered negligible).

Hence,

$$F_z = m\chi H_x \frac{dH_x}{dz}$$

For susceptibility measurement by the Faraday method, all that is required is to suspend a sample, at constant temperature, in a region where the product of field by field gradient is constant over the entire sample, and measure the force developed. If measurements are required over a temperature range, then some means of varying the sample temperature and holding constant values must be incorporated.

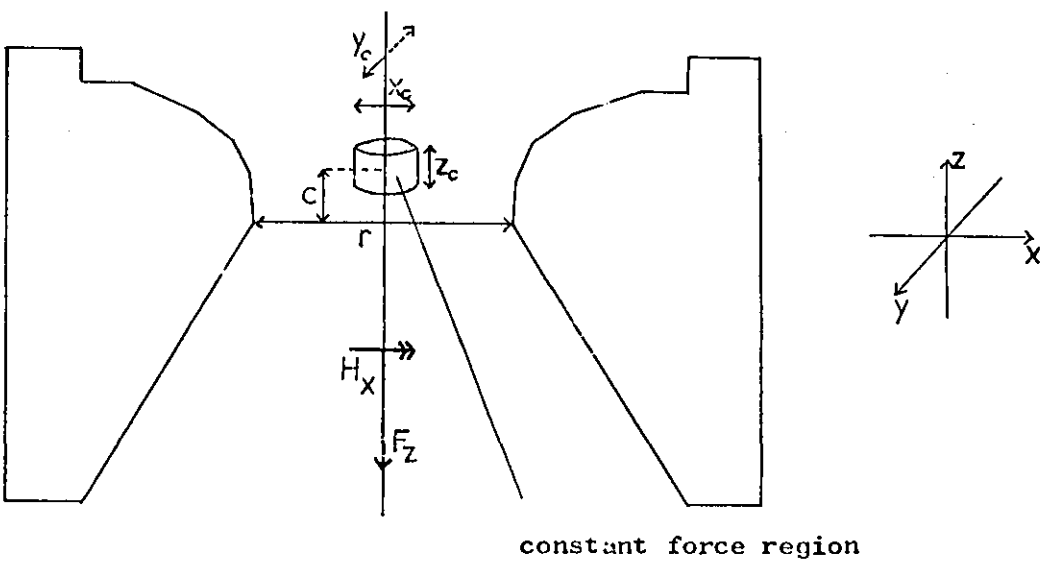

Fig. 1 Pole cap profile and axes of measurement, showing the dimensions of the constant force region.

Section II. COMPONENTS AND CONSTRUCTION

(i) MAGNET ASSEMBLY

For the Faraday method, the basic requirements of the magnet are that it produce relatively high values of $H_x \frac{dH_x}{dz}$ which are constant over an appreciable volume of the field, and that the fields in the z- and y-directions are negligibly small. It is also necessary that these specifications are fulfilled at an adequate pole gap for sample temperature control.

Parallel cylindrical pole pieces have been used, but these are very inefficient for the Faraday method. To increase the value, constancy and volume of the product $H_x \frac{dH_x}{dz}$, electromagnets with shaped pole pieces have been designed.[4,8] For the present apparatus, 7-inch diameter coned pole-pieces, the profile of which is shown in Fig.1, were chosen.

These pole caps were originally designed by Henry[15-17] (12-inch diameter), using an electrical analogy technique, and later modified by Heyding[18] for 4-inch diameter caps, the design criterion being the production of a constant force on a sample suspended in the pole gap. The profile should ideally be a smooth curved surface above, with tapering below to provide a stronger field, but the machining in straight-line segments has no significant influence on the field profile.

These pole pieces provide a small volume ($x_c \times y_c \times z_c$) of constant, maximum $H_x \frac{dH_x}{dz}$, centred in the z-direction at a distance, c, above the minimum pole gap, r. Investigations to determine these field characteristics have been carried out by the above authors and also by Hill,[19] and Martin and Hill,[20] and typical results are as follows:

	Henry[17]	Heyding[18]	Hill[19]
Diameter of pole tips (in)	12	4	4
r (cm)	3.6	2.6	2.6
c (cm)	2.3	1.3	1.3
x_c (cm)	not estimated	>0.8	1.5
y_c (cm)		4.0	>1.5
z_c (cm)	2.0	1.0-1.4 depending on field strength	1.6

These dimensions obviously impose stringent limitations on sample size and positioning, and these factors will be discussed in more detail with reference to possible sources of error in measurements.

(i) z-direction

Three experimental methods have been used for investigating the variation of $H_x \frac{dH_x}{dz}$ in the most critical z-direction. The first involves the measurement of the variation of H_x with z, and graphical differentiation. A graph of H_x^2 v. z has a slope of $2H_x \frac{dH_x}{dz}$, and, using this method, the above authors observed a linear relation for z_c extending over 1 to 2 cm. However, using the method of Thorpe and Senftle,[12] the actual value of $H_x \frac{dH_x}{dz}$ can be found at any point, and Hill showed that there is a significant variation of the field product within the so-called constant region. He verified this using a third method, namely measuring the force on a standard sample of known susceptibility as a function of z. It was concluded that in the region, z_c, found by the first method, the product $H_x \frac{dH_x}{dz}$ may be constant only to $\sim \pm 5\%$, and that to achieve an accuracy of better than $\pm$ 1% the sample should be limited in length to 2 or 3 mm.

In practice, the third method above may be used for calibration of a constant force region, which would take into account slight variations in the actual field value. Measurements on unknown samples can be made relative to a chosen standard, provided that the dimensions are similar, and the sample is always positioned vertically in exactly the same place in the field. To overcome this latter difficulty, the system[19] was adopted whereby the magnet can be moved vertically past the sample, so that the sample always traverses the constant force region and the maximum force can be measured.

(ii) x-direction and y-direction

Extensive investigation of the variation of $H_x \frac{dH_x}{dz}$ in these directions has not been carried out. Theoretical estimates of the effects of, and errors arising from, misplacement of the sample from the constant force region along these axes have been made, with some experimental verification.[15-17,19,21] Displacement along the y-direction generally gives rise to very much smaller errors than along the x-direction, and is usually ignored.

There are two principal effects of misplacement along the x-axis. (a) There is a variation in the measured vertical force due to the change of $H_x \frac{dH_x}{dz}$ with x (and possibly to a contribution from $H_z \frac{dH_x}{dz}$, since H_z is not necessarily zero off the z axis).

Expressions have been derived[17,19*] showing that a displacement, Δx cm, from the origin of the axes should decrease the measured vertical force by a fraction, $\frac{\Delta F_z}{F_z}$, where

$$\frac{\Delta F_z}{F_z} = \frac{f(z)\ (\Delta x)^2}{(dH_x{}^2/dz)_{x=0}}$$

and f(z) is a function involving powers of H and $\frac{dH^2}{dz}$.

The value of the right-hand side of the equations is of the order of $0.1\ (\Delta x)^2$, corresponding to a 0.1% error in the force for 1 mm displacement. Hill[19] has produced a plot of $\frac{\Delta F_z}{F_z}$ v. Δx which agrees well with this. Errors due to displacement along the y-axis should be expressible in a similar form, but Hill observed no significant variation in the force for displacements less than 1 cm.

If sample measurements are made relative to a standard calibrant, then variation in the x and y dimensions of sample and calibrant could be expressed as a diameter error. An expression has been given[17] for the fractional error in susceptibility introduced by a change, Δd, in a cylinder of diameter, d.

$$\frac{\Delta\chi}{\chi} = \frac{\Delta d.d}{8}\left[\frac{f(z)}{dH^2/dz}\right]$$

However, the form and value of f(z) are very difficult to assess, and the expression is of little practical importance.

(b) A horizontal force is introduced in the x-direction due to the term $H_x \frac{dH_x}{dx}$, which now becomes of increasing importance.

The usual suspension assembly for the Faraday method consists

---

* The expression quoted by Hill from the paper by Garber, Henry and Hoeve is in error, since his coordinate system differs from theirs. In his equation (2), f(x) should be replaced by f(z) to give the correct expression.

of the sample contained in a diamagnetic bucket (external radius r_B cm), attached to a long, light, freely-hung suspension (length ℓ cm), inside a narrow tube (internal radius R cm). A lateral force exerted on the sample will cause sideways movement of the bottom of the assembly, oscillation about the maximum force position, and, eventually, contact with the wall of the tube when the suspension has been deflected through an angle of $\sim \tan^{-1}\left(\frac{R-r_B}{\ell}\right)$. This obviously causes serious difficulties in the practical measurement of forces. A simple expression has been given,[19,20] based on the precept that the value of vertical force measurable is limited by the point at which the sample bucket touches the wall of the tube. Thus the maximum measurable value of the susceptibility of the sample is given by :

$$m_s\chi_s \approx \frac{(m_s + m_B)g}{\left[\left(\frac{\ell}{R-r_B}\right) H_x \frac{dH_x}{dx} - H_x \frac{dH_x}{dz}\right]} + m_B\chi_B$$

where m_s, m_B are the masses, and χ_s, χ_B the gram-susceptibilities of the sample and bucket, respectively. This indicates the advantage of using a diamagnetic bucket to contain paramagnetic samples. Hill has presented a graph showing that $H_x \frac{dH_x}{dx}$ increases with increasing x-displacement, and so the maximum force measurable decreases with increasing misalignment in this direction.

Stewart[21] has used a more rigorous approach to predict the conditions under which these instabilities occur, the type of motion induced in various situations, and to propose practical means of eliminating these difficulties. He has considered the total force due to field gradients acting on the suspension in the z- and x-directions, and has set up an equation of motion for the bottom of the sample, involving the vertical magnetic force, F_M, the sample and bucket weight, F_W, the suspension length, ℓ, an initial x-misalignment, h, and field gradient terms. The equation describes the motion in the x-direction following a small, initial x-deflection, such as is likely to occur when the magnet current is first switched on.

If there is no initial misplacement, i.e. h = 0, the system will only become unstable when

$$1 + \frac{F_W}{F_M} < \frac{\ell}{G}$$

where $G = \frac{dH_x}{dz} \Big/ \frac{d^2H_x}{dx^2}$

$\frac{\ell}{G}$ has been shown to remain approximately constant for any magnet current, and so instability will only occur when F_M increases to a certain critical value, say F_M^c. For values of $F_M < F_M^c$, the sample, given a small deflection, will execute S.H.M. about the mean position, and these oscillations should quickly die away due to the damping of the system. However, when $F_M \geq F_M^c$, any small deflection will produce a force acting in a direction so as to increase the deflection and the system becomes unstable.

If the sample is initially mispositioned by an amount h, the equation for the equilibrium value of the deflection x is

$$x \approx \frac{h}{1-F_M/F_M^c}$$

Thus, for small values of F_M, $x \approx h$, and the sample will come to equilibrium at approximately the initial position. However, as F_M increases, x, and hence the amplitude of the oscillation, becomes increasingly larger, and the sample moves further away from the region of maximum constant force. Eventually, at $F_M = F_M^c$, there is no equilibrium position and a violent instability is experienced.

It is therefore obvious that to reduce the practical difficulties caused by these instabilities, the sample must be accurately centred in the x-direction of the field. The problem remains of instability when $h = 0$, but if F_M^c is determined once experimentally, precautions can be taken to ensure that this value is never exceeded in subsequent measurements. The value of F_M^c for a particular system may be a function of magnet current, and will also be affected by misalignment of the magnet poles.

Stewart has suggested that the tendency for instabilities to occur may be reduced by:

(i) increasing the weight of the diamagnetic bucket, which will decrease F_M and increase F_W,

(ii) reducing the length of suspension, ℓ,

(iii) making the field gradient ratio, G, as large as possible. This could be achieved by increasing the pole gap, but this has the disadvantage of decreasing the maximum field product.

A similar treatment can be applied to misplacement and instability in the y-direction, but, in fact, paramagnetic samples are stable towards movement in this direction, as diamagnetic samples are stable towards movement in the x-direction.

The magnet assembly used in the present apparatus is a Newport Instruments 7-inch Type E water-cooled electromagnetic, with the shaped pole-pieces described above. It is mounted on a platform supported on a hand-driven hydraulic ram to allow the magnet position to be varied with respect to the sample. In making a force measurement, the magnet is initially raised so that the constant force region is above the sample. It is then allowed to fall slowly past the sample by opening a needle valve in the jack. The platform of the magnet moves on four vertical guide rods to ensure smooth travel.

The current for the magnet is supplied by a Newport Type C224B Power Supply, incorporating a console and motor-generator set. Reproducible, stable fields were obtained for values of current between 5 and 22 amps.

The original pole-gap used was 5 cm, giving values of $H_x \frac{dH_x}{dz}$ in the constant force region from (0.8 to 9.5) x 10^6 gauss^{2}cm^{-1}. The pole gap was subsequently increased to 6.5 cm to accommodate a larger cryostat tail, and this gave values of (0.5 to 6.5) x 10^6 gauss^{2}cm^{-1}. A value of z_c of $\sim$ 1.5 cm was specified by the makers.

Field calibration, investigation of the variation of force in the x-direction, and assessment of F_M^c, are presented in Section V.

(ii) MICROBALANCE

Most inorganic compounds have susceptibilities in the range 10^{-6} to 10^{-2} emu.g.$^{-1}$, and thus the range of force to be measured can be roughly estimated.

The product $H_x \frac{dH_x}{dz}$ for the magnet has values of $\sim$ 1 to 5 x 10^6 gauss^2 cm^{-1}, and using the equation

$$F = m\chi H_x \frac{dH_x}{dz}$$

it can be seen that for 2 mg of a sample with $\chi = 10^{-2}$ emu g^{-1}

$$F = 20 - 100 \text{ dynes}$$

and for 20 mg of a sample with $\chi = 10^{-6}$ emu g^{-1}

$$F = (2 - 10) \times 10^{-2} \text{ dynes.}$$

To obtain an accuracy of better than 1% in the smallest forces, a balance is required which is capable of detecting a change in force of 10^{-4} dyne; and this in the presence of a standing load of 1 to 2 g i.e. the weight of the suspension and sample container assembly.

Three types of balance are available which are capable of this sensitivity: quartz fibre torsion balances, Sucksmith ring balances and electronic microbalances. A Sartorius vacuum microbalance (model 4102) was chosen for this apparatus. It will support samples of up to 2.5 g and measure force changes up to 2, 20 or 200 mg wt, with a sensitivity of 0.1, 1 or 1_0 µg wt, in three basic ranges. It enables measurements to be made in vacuum or at controlled pressure, and, provided it is correctly mounted, it is stable towards vibration.

The measurement principle of this balance is based on self-compensation and gives, in effect, a null-system instrument. The weighing system consists of a metallized silica beam which supports the suspension wires for the sample and for the counter-weights. The beam is attached to a moving torque-coil, which is suspended by a fine torsion strip between the poles of a W-shaped permanent magnet. When the beam is displaced by a weight change in the sample, the position of the moving coil relative to a pair of fixed oscillator coils is measured by an H.F. a.c. signal. This signal is passed to the balance amplifier for rectification phase adjustment and amplification, and returned in the form of a compensating current (d.c.) to restore the beam to the horizontal equilibrium position. This current used in creating the counter-torque is directly proportional to the displacement force acting on the beam, and is measured and converted for reading in terms of weight change.

A constant voltage unit is incorporated to provide an alternative source of current to the torque-coil. Thus, part of the compensating current can be backed off with a manually-set decade series of electrical weight compensation, calibrated (0.00 to 1.99, 0.0 to 19.9, or 0 to 199 mg wt, depending on the basic range used) to provide a direct reading of the weight change, and with a variable tare potentiometer ($\pm$ 0.5, $\pm$ 5, or $\pm$ 50 mg wt). A portion of the current is also passed through a 100 µA meter (100 divisions f.s.d.), which has associated

factor settings such that a reading of from 1 to 100 scale divisions can be adjusted to correspond to the smallest decade change in each range. Thus by choice of the appropriate range, either the total weight change, or that part of it uncompensated by the decade settings, can be displayed on the meter. By adjustment of the decade settings to utilise the most sensitive factor setting, weight changes can be recorded with a maximum reading accuracy of 1 part in 20,000.

The control amplifier is also fitted with terminals for connection to a chart recorder for plotting weight changes (see Section II (vi)).

A discussion of the limitations and errors associated with this microbalance has been given.[9] It has been found that the restoring torque, provided by the permanent magnet and d.c. current, can be temperature dependent. To realise the maximum sensitivity of the balance, it has been suggested that the balance temperature should be stabilised to $\pm$ 0.1°C, and the power supply temperature to $\pm$ 1°C. A treatment has also been given of the tilt of the silica beam and vertical movement of the suspension wires under various conditions of adding weights to the balance.

The microbalance is supported on a heavy, wall-mounted bracket, to minimise instabilities due to mechanical vibrations set up by other components. It is encased in a μ-metal shield to protect it from stray fields. The sample side of the balance is connected to the sample tube of the cryostat by a vacuum-tight metal bellows arrangement. The balance can be moved clear of the cryostat to facilitate the loading of samples. The base-plate of the balance rests in guide grooves, to maintain the position of the balance with respect to the y-direction of the magnet poles during movement. The working position, in which the balance suspension is centred in the x-direction in the region of constant force, is defined by an end-stop on the travel. The initial determination of this position is discussed in Section V.

The microbalance calibration was checked regularly by the procedure stated in the Sartorius manual.

(iii) CRYOSTAT AND VACUUM SYSTEM. TEMPERATURE CONTROL

The temperature range over which susceptibility measurements were to be made was ~ 1.8 - 300 K. Cryogenic apparatus was required to

enable the temperature of the sample, suspended between the poles of the magnet, to be varied in a controlled manner and held constant, over the entire length of the sample, at desired values for force measurements.

Initially, it was decided to use a twin cryostat system to enable identical samples of the material under investigation to be suspended from the two arms of the microbalance. Comparative susceptibility measurements could then be made between the samples under identical cryogenic and pressure conditions, with the tail of one cryostat between the poles of the magnet while the other had no applied field. It was considered that this would reduce experimental errors due to buoyancy effects with changes of gas pressure in the sample tubes, weight changes due to condensation of gases on to the samples, etc. In practice, this arrangement introduced complications in tne experimental operation, and caused additional errors, since it was difficult to maintain both cryostats at exactly the same temperature over the whole range, and a correction had to be applied for the effects of a weak field experienced by the counter-balancing sample. It was therefore decided to use only one cryostat for control of sample temperature, and to enclose the counter-balancing weights in the standard glass tube supplied by Sartorius.

The original cryostats obtained for this apparatus were liquid helium modular dewars, with specially adapted tails, which were designed and constructed by the Oxford Instrument Co. They are of copper and stainless steel construction, and a simplified section is shown in Fig.2. However, it was discovered during use that this design was seriously faulty, and the cryostats could not be operated by the intended procedures. Means were adopted to overcome the defects, so that efficient temperature control could be achieved over the required range, but eventually serious leaks developed in the walls of the high vacuum chambers. Consequently, a new cryostat of improved design has been obtained, and is at present being incorporated into the system. This is an Oxford Instruments MD4A modular dewar, with a specially designed tail attachment and a variable temperature insert dewar. It is again constructed of stainless steel and copper, and a simplified section is shown in Fig.3. This new cryostat has the additional advantage that it is fully demountable.

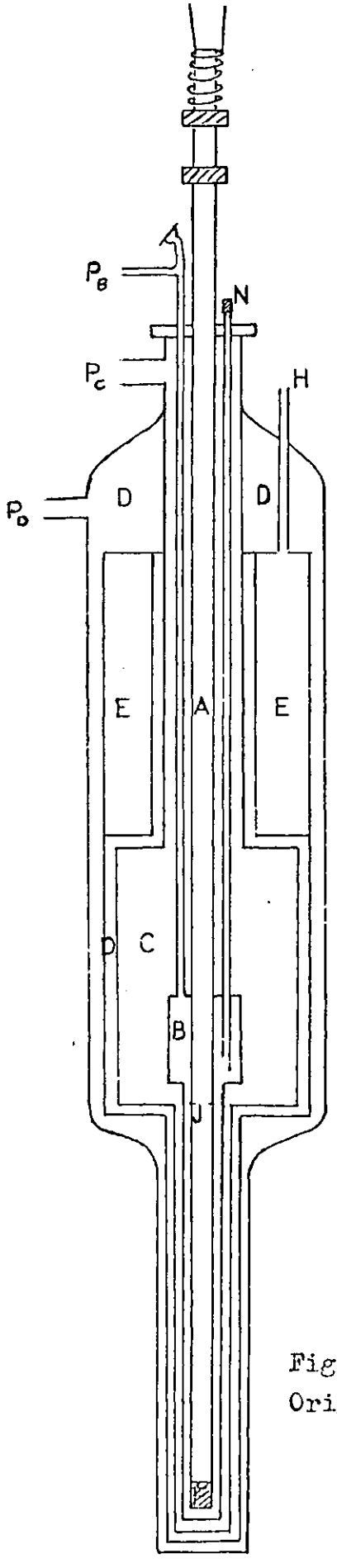

Fig. 2
Original cryostat

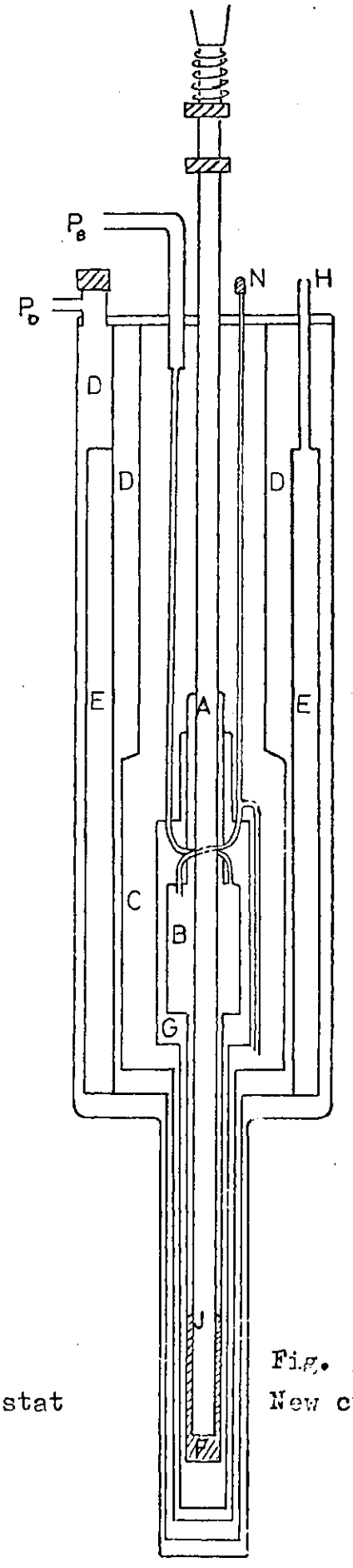

Fig. 3
New cryosiat

Both the original and new cryostats have a similar design of outer dewar, comprising a main tank, C, for the liquid refrigerant (helium or nitrogen), and an annular reservoir, E, for liquid nitrogen. An outer high vacuum space, D, separates the outer wall, the reservoir and the main tank. The reservoir is filled through three tubes situated on the shoulder of the cryostat. Access to the main tank is by a demountable liquid helium syphon through a guide tube, or by a vent tube, P_C, although the latter was adapted in both cryostats to enable the tank to be evacuated when required. The tank is vacuum-sealed to the top-plate by an O-ring.

The main tank surrounds the variable-temperature insert dewar. In the original cryostat, a chain of four carbon resistors was wound on the outside of the insert dewar, for use as a liquid helium level indicator and rough low-temperature thermometer for the main tank. In the new cryostat, this has been replaced by an electronic four-probe gallium arsenide liquid helium level indicator, supplied by Oxford Instruments.

The insert dewar of each cryostat comprises a sample tube, A, enclosed at the lower end in a low temperature pot, B. In the new cryostat the pot is further surrounded by a vacuum insulation space, G, separating it from the main tank. The top of the sample tube is attached by an O-ring seal to the base of a sliding metal bellows, completing the vacuum seal with the Sartorius balance. The balance and sample space can be evacuated, or exchange gas introduced, through the centre of the Sartorius balance. The base of the sample tube terminates in a copper block, on which are wound the heater elements and temperature sensing devices.

Access to the low temperature pot is via a needle valve, N, connecting it to the main tank, or via a pumping line, P_B. In the new cryostat, the pot insulation space can be evacuated, or exchange gas introduced, through a line, P_G.

The vacuum system for the new cryostat is shown schematically in Fig.4. It is constructed from Edwards "Speedivac" components and copper tubing.

The total temperature range of interest can be divided into four convenient ranges for practical operation.

Range 1. 4.2 to ~ 1.8 K, decreasing the temperature by pumping on liquid helium.

Range 2. 4.2 to ~ 60 or 80 K, increasing the temperature by balancing the cooling effect of liquid helium with electrical heat input.

Range 3. ~ 77 to ~ 63 K, decreasing the temperature by pumping on liquid nitrogen. This range can be extended down to ~ 50 K, by solidifying the nitrogen at ~ 63 K, and pumping on the solid.

Range 4. ~ 77 to 300 K, increasing the temperature by balancing the cooling effect of liquid nitrogen by electrical heat input.

It is, of course, possible to cover the entire range from 4.2 to 300 K in one run, but generally the decrease in susceptibility with increasing temperature makes it desirable to increase the sample weight during this range, to maintain the accuracy of force measurement.

The procedure for operation of the new cryostat over these ranges is as follows:

Ranges 1 and 3

The outer vacuum space, D, and the pot insulation space, G, are evacuated to $< 10^{-4}$ torr, and the balance and sample space is adjusted to the required exchange gas pressure or evacuated. The reservoir, E, is filled with liquid nitrogen. The main tank, C, is filled with the appropriate refrigerant liquid (the procedure is outlined at the end of this Section), and when the cryostat has cooled to the required temperature (4.2 or 77 K), the low temperature pot is filled from the main tank by cracking open the needle valve. The needle-valve is then closed, and the temperature is reduced stepwise by pumping on the liquid in the pot, through P_B, and holding required values of vapour pressure until the sample temperature has equilibrated.

Ranges 2 and 4

Range 2 follows immediately on Range 1 to conserve liquid helium. Range 4 is generally performed as a totally separate run.

The vacuum is maintained in D and G. For Range 2, any liquid helium remaining in the pot is boiled off using the heater, with the needle valve closed, so that liquid remains in the main tank. For Range 4, the main tank is filled with liquid nitrogen. The pot and sample space are adjusted to the required exchange gas pressure (Range 2) or evacuated (Range 4). Then, in each range, the temperature of the copper block, F, and the sample tube surrounding the sample, is raised stepwise by passing appropriate steady currents through the heater coils, and allowing equilibrium states to be reached.

In this new cryostat, the heater coils are controlled by an Oxford Instruments Mark 2 Harwell Temperature Controller. The temperature of the copper block is monitored by a gold-iron/chromel thermocouple (5 - 300 K), a copper/constantan thermocouple or a carbon resistor. The temperature required is dialled on a helipot and this voltage is automatically compared with the output voltage from the sensor. The error voltage then determines the amount of power given to the heaters to reach and maintain the required temperature. Susceptibility measurements may be made manually at each dialled temperature, but automatic temperature sweep facilities for these ranges are also being incorporated by using an Oxford Instruments Electro-mechanical Sweep Generator to drive the Temperature Controller helipot. The sensor reference voltage is thus altered in a continuous linear manner, at a rate slow enough for sample temperature equilibration at all points.

Automatic operation is discussed in Sections III and IV, and the selection of temperature sensor and mode of operation of the heater is outlined in the latter Section.

A similar method of operation over these temperature ranges was intended for the original cryostat, but could not be achieved owing to two major defects in the design. These are, firstly, the lack of thermal insulation of the low-temperature pot and sample tube from the refrigerant liquid in the main tank, and, secondly, the inadequate bore ($\frac{1}{4}$") of the pot pumping line, P_B. Since the magnetic results for this thesis were obtained using the original cryostat, the practical consequences of these defects and the procedure adopted to overcome them are discussed briefly below.

For ranges 1 and 3, the narrowness of P_B made pumping on the refrigerant liquid very inefficient. It was also difficult to reduce the temperature rapidly, since the wall of the low-temperature pot was in contact with the liquid at its boiling point in the main tank. This difficulty was overcome by pumping on both main tank and pot through the tank line, P_c, (1" bore), with the needle valve permanently open. The line P_B could then be used as a "no-flow" line for monitoring the vapour pressure of the liquid.

More serious difficulties were encountered in ranges 2 and 4, when attempting to raise the temperature of the sample in a controlled manner. To insulate the lower portion of the sample tube from the main tank, the pot had to be pumped continuously to reduce the "cold-leak" across this space by convection. Again, the narrow bore of P_B made it impossible to maintain a good vacuum in the pot, especially as leaks developed, at the base of P_B and at the needle valve siting, between the pot and the main tank. It was therefore very difficult to control and reproduce warming rates.

The lack of adequate insulation also resulted in prohibitively large and non-reproducible thermal gradients in the vicinity of the sample, when using the heater. The situation may have been improved if the heater could have been sited above the sample position, but this was impossible due to the lack of space between the walls of the sample tube and those of the pot. In the new cryostat, two heater coils with three terminal connections are wound along the sample position. The heater system may be energised in any combination of terminals (Section IV) and should eliminate thermal gradients.

Owing to these problems, a procedure was adopted for these ranges which did not require use of the heater, by simply relying on heat leaks to warm the sample. For both ranges, all liquid refrigerant was removed from the main tank and the low temperature pot, so that both spaces contained an atmosphere of helium or nitrogen gas, respectively. The inside of the cryostat then started to warm, mainly by conduction of heat from the outside down the various tubes and leads, and also by radiation and convection from the outside walls across the various chambers. The rate of warming was obviously dependent on the vacuum in the insulation space, D, and on mechanical leaks in the walls of the

of the cryostat, but it was found that a rate of warming slow enough for sample temperature equilibration at all points could be achieved by this method. Range 2 normally took ~ 4 hours, and Range 4 could take up to 36 hours. It was found that if the rate of warming exceeded ~ 25 K per hour, then sample equilibration was not assured and also small temperature gradients in the region of the sample could be present. The fastest warming rate was experienced over the range ~ 6 - 12 K.

Susceptibility measurements could be made manually at regular time intervals, but, owing to the long hours involved in Range 4 runs, the apparatus was automated to give a continuous record of magnetic force v. temperature. The automatic control is discussed in Sections III and IV. This procedure could also be used with the new cryostat in the event of breakdown of the Temperature Controller System.

The cryostat is supported on a horizontal table, clamped on to the magnetic platform guide rods. With the balance clamped in the working position with respect to the magnet poles, the position of the cryostat can be adjusted in both horizontal and vertical planes, so that the sample is centred at the base of the sample tube. These adjustments are necessary, since the sample tubes are not exactly parallel to the outside walls of the cryostats.

Transfer of Liquid Helium

It is essential to ensure that no mechanical leaks are present in the cryostat, especially in the wall separating the main tank from the outer vacuum. Unfortunately, it is not always possible to test this at higher temperature, since small leaks may open up due to unequal strains in the metal caused by cooling.

To conserve helium, the cryostat is pre-cooled to ~ 100 K by adding small quantities of liquid nitrogen to the main tank. It is important to ensure that no liquid collects, since this will freeze around the end of the syphon tube when helium transfer is begun, and either block the tube or cause the liquid helium to boil rapidly out of the cryostat without cooling it sufficiently for collection.

When the cryostat has been cooled to ~ 100 K, the main tank and pot are evacuated to remove all traces of nitrogen, and filled with

an atmosphere of helium gas. The needle valve is closed and the main tank connection, P_c, must be open to enable the exhaust helium gas to be vented to the atmosphere.

The transfer syphon is stainless steel, and is demountable in the centre of the horizontal portion. The cryostat-side of the tube has to be left permanently in the main tank, since the proximity of the balance support bracket makes it impossible to remove the syphon after the apparatus has been assembled for a run. The other half of the syphon tube is introduced into the helium storage can via a neck adaptor, with a football bladder and quick pressure-release tube attached. The tube is slowly lowered into the can until a white cloud of cold helium gas is issuing from the end of the tube, and the two halves of the syphon are then joined with an O-ring seal, and all leaks are sealed off.

An over pressure is immediately built up inside the can, inflating the bladder, and forces the liquid into the cryostat. The pressure is maintained by gently squeezing the bladder, and the rate of flow can be gauged by observing the stream of exhaust gas, and by monitoring the rate of fall of temperature. When the liquid helium begins to collect in the main tank, a drop in pressure usually occurs in the bladder. It must then be squeezed hard and held firmly to increase the rate of transfer. The needle valve may be cracked open at this stage and the pot pumped to cool it down. When the thermocouple indicates a temperature of less than $\sim$ 20 K in the pot, the needle valve should be closed. (It was possible with the original cryostat to transfer helium to both main tank and pot with the needle valve permanently open.) The pressure in the bladder is maintained until the main tank is full, as indicated by the level detector. The syphon tube is then uncoupled and the storage vessel removed. The syphon tube is closed with a rubber bung. The pot is filled from the tank, by opening the needle valve and pressurising the tank to a few p.s.i. of helium gas. A rapid increase in boil-off from the pot indicates when it is full, and the needle valve is then closed. The force on the sample at a chosen field is monitored until it reaches a constant value, showing that the sample temperature has equilibrated at 4.2 K. It was found difficult to transfer more helium into the cold cryostat, due to icing-up of the syphon tube.

Filling the tank with liquid nitrogen

Introduction of liquid nitrogen into the tank via the syphon tube is impractical owing to its narrow bore. It is therefore filled through the exhaust vent, P_c, using a polythene funnel and length of tubing.

(iv) TEMPERATURE MEASUREMENT

Since the temperature sensing device cannot be mounted directly on the freely-hung sample, it must be assumed that the sample is in thermal equilibrium with the surrounding copper tube and block, and the sensors are sited on the block.

In the original cryostat, a copper/constantan thermocouple (referenced externally to ice/water) was used for temperature measurement between ~ 50 and 300 K, and below this temperature, the voltage across a standard Allen Bradley 100 ohm (nominal) carbon resistor was used. For the latter a steady current supply of 6 μA was provided, for the range 1.8 to ~ 10 K, and above this the current was increased to 40 μA to increase the sensitivity of the voltage measurement. In the new cryostat, the same facilities are provided for use in ranges 1 and 3, although in this case the thermocouple is referenced to the main tank. For ranges 2 and 4, the Harwell Temperature Controller is used for temperature control and measurement, as outlined in Section II (iii). The selection of the appropriate sensor is shown in Section IV.

It was not possible to check whether the sample and tube temperature are identical over the whole range. It is theoretically possible to obtain an independent absolute temperature calibration of the sensing devices before mounting them in the cryostat, and then to compare the temperature recorded by these at the block with that of the sample, obtained by performing force measurements on a standard sample of known magnetic behaviour over the temperature range. However, since the calibration of the sensors may alter when they are wound and soldered on to the sample tube, the method could not be expected to provide a good comparison. The sensors are therefore calibrated in the cryostat against a standard magnetic sample (see Section V) and periodic checks are made on the reproducibility of the calibration.

Sensors can be obtained which are capable of a higher measurement accuracy than those used, e.g. calibrated germanium or gallium arsenide

thermometers. These were not chosen because temperature measurement in this system must be made in the presence of a large inhomogeneous magnetic field, and both these sensors show marked field dependence, for which an experimentally determined correction would have to be applied. The copper/constantan and gold-iron/chromel voltages are not field dependent after the field has stabilised, and the carbon resistors were found to show a small field dependence only after they had deteriorated structurally due to long usage.

It was considered that the vapour pressures of the liquid refrigerants, monitored during ranges 1 and 3, could be taken as no more than a rough guide to temperature, owing to the dependence of the boiling points of the liquids on impurities present.

(v) MONITORING AND DISPLAY OF READINGS

A Croyden Instruments Cropico Type 3DC Potentiometer (range 1.8 V to 10 μV) is used for adjustment of the magnet current and for measurement of the temperature sensor voltages.

A Hewlett-Packard 7005B XY-recorder is used for display of various outputs in both manual and automatic modes of operation (see Section III and IV). Both plotter axes have calibrated ranges from 0.4 mV/cm to 4 V/cm, with continuous vernier settings between ranges. The X-axis is connected to the high impedance output of the Sartorius amplifier. This output varies from 0 to 10 mV as the meter reading moves from zero to full-scale deflection. Using the highest sensitivity of the recorder (0.4 mV/cm), weight changes can be plotted with a sensitivity varying from 4 mg/cm to 0.4 μg/cm. By suitable choice of range and factor settings on the amplifier, and use of the vernier setting on the plotter, any weight change/cm calibration between these values can be obtained. The X-axis is calibrated against the decade series of the amplifier to allow for errors in the recorder range calibration and in the chart paper ruling.

The Y-axis of the recorder can be connected to either:

(a) a linear voltage transducer indicating the vertical position of the magnet, for use in manual operation,

or (b) the appropriate sensor voltage to provide a "temperature" calibration, linear in voltage, for use in automatic operation. The Y-axis is calibrated at two or more points by manual measurement of temperature on the potentiometer.

The selection facilities are outlined in Section IV.

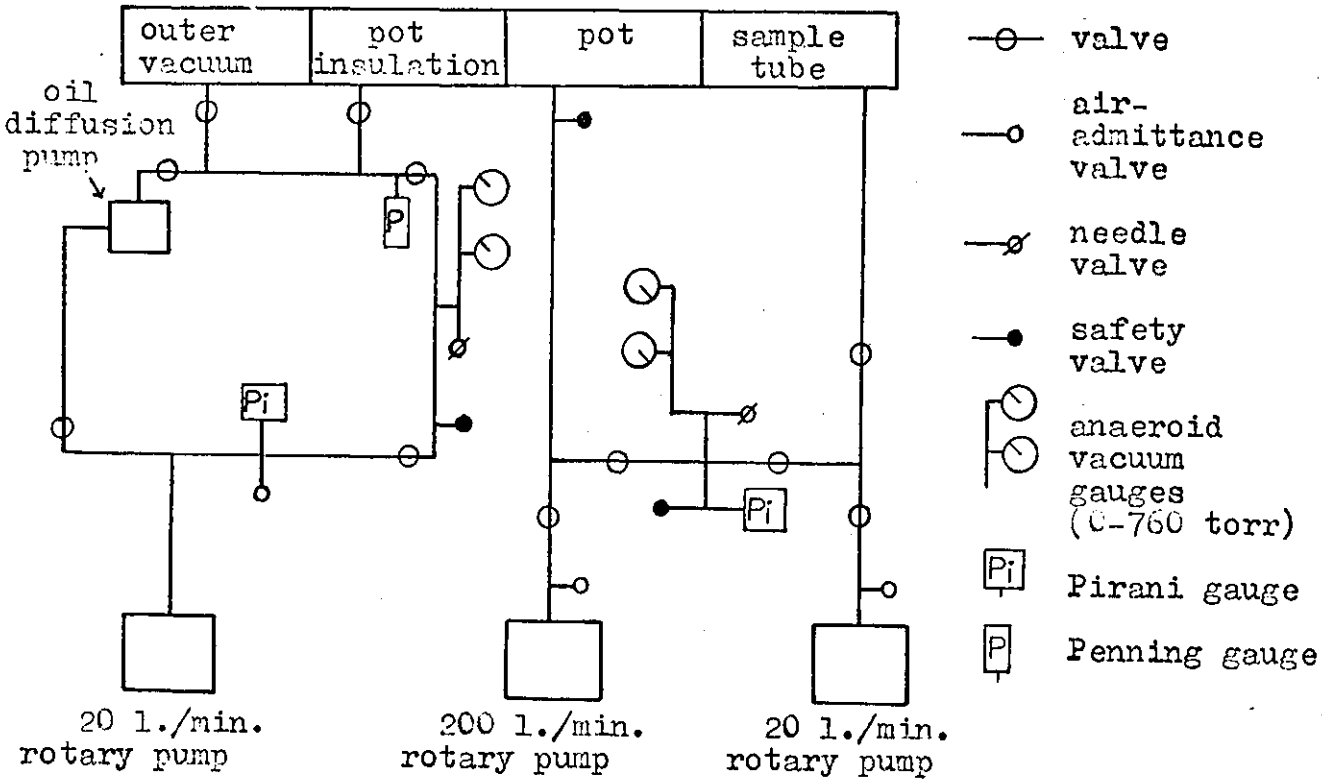

Fig. 4 Schematic representation of vacuum system.

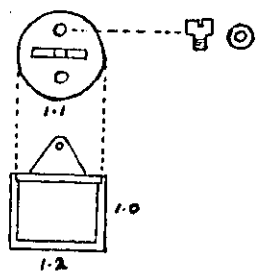

Fig. 5 Perspex sample container.

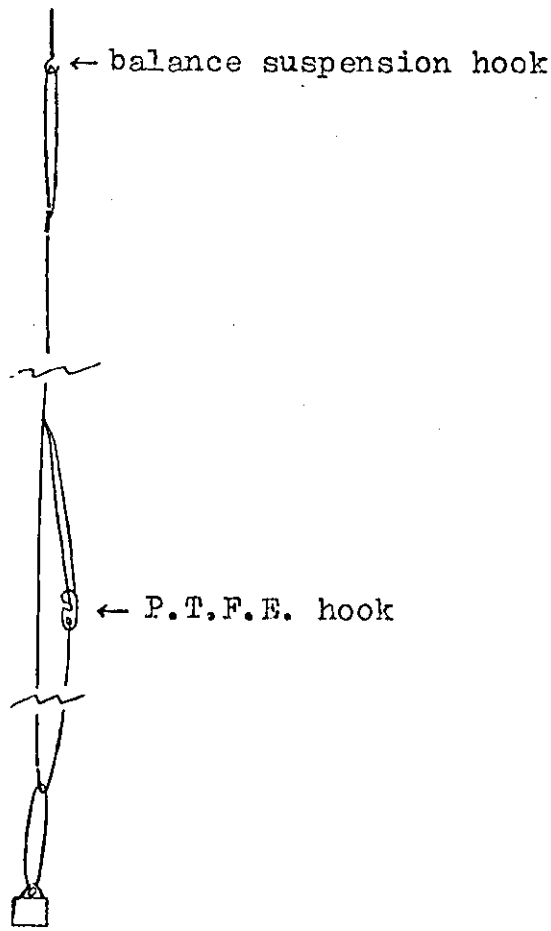

Fig. 6 Suspension arrangement.

(vi) SAMPLE CONTAINER, SUSPENSION AND SAMPLING

Most of the samples investigated are in the form of powdered solids and a container was required to hold them. The requirements of the container are as follows:

(1) the dimensions must be within the limits of the constant force region;

(2) it should be relatively heavy, within the load limit of the balance, to increase stability towards oscillation;

(3) it should preferably be of a diamagnetic material due to considerations of critical vertical magnetic force;

(4) it should be as free as possible from para- or ferromagnetic impurities, or, if present, the impurities should be distributed homogeneously;

(5) the material should be chemically inert, to allow easy cleaning without risk of dissolving either the surface of the container or paramagnetic impurities, and hence necessitating continual recalibration;

(6) it should have a lid, provided with openings to allow gas to be pumped out of the container without loss of powder, but which can be sealed to give an air-tight enclosure for unstable samples;

(7) it should have mechanical properties which enable it to be subjected to very low temperatures without fracturing;

(8) it should have thin walls to give poor thermal insulation to the material under study.

A very suitable material is high-purity silica, but this has the disadvantage of being brittle and difficult to work on a small scale. Several designs have been considered for a bucket with fitted lid, but no really suitable container has yet been constructed in this material.

The material chosen for use is high quality perspex. The container (Fig.5) consists of a cylindrical bucket (external diameter 1.2 cm, length 1 cm, wall thickness 1 mm), with a tight press-fit lid with a projection for suspension. The total weight is $\sim$ 600 mg. The lid has two 8BA tapped holes drilled in it for evacuation of gases, and these can be closed with P.T.F.E. screws and polythene washers to make the container air-tight.

Calibration runs were performed on the container, over the full temperature range and at the fields chosen for sample measurement, and the correction is applied directly in terms of the measured diamagnetic force. The gram susceptibility is $\sim -0.4 \times 10^{-6}$, but the batch used was found to contain some paramagnetic impurity, since the diamagnetism decreased on cooling.

The container was cleaned with water (or dilute acid) and ethanol and dried in vacuum. After repeated washings it was found to lose a very small amount of weight and also a little of the paramagnetic impurity (probably surface contamination from the initial machining). The container was recalibrated at regular intervals, but since, in general, the force on the sample was very large compared to the container correction, small changes in its calibration were not significant.

A smaller container (external diameter 6 mm, length 5 mm, wall thickness 1 mm, total weight $\sim$ 150 mg) was made to the same design, for use with small quantities of sample of the order of 1 to 2 mg, to reduce the container contribution to the total force and hence any error caused by changes in its calibration. However, the smaller weight was unfavourable with respect to oscillations.

The samples are finely powdered and weighed into the container on a chemical microbalance. Difficulty is experienced in weighing samples of the order of 1 to 2 mg to an accuracy of 1%, since the weight of the container can vary with atmospheric conditions by 10's of μg. For very small quantities of sample, the powder is distributed as evenly as possible on the bottom of the container. If the sample has a very low paramagnetic susceptibility, a calculated weight of a paramagnetic alloy (vanadium/10 atomic % chromium, kindly supplied by Dr W.E. Gardner, Harwell) can be added to counterbalance the diamagnetism of the container. This alloy has a very small temperature dependence of susceptibility over the full temperature range.

After washing and drying, the container often develops a static change on the walls, which can prevent it hanging freely in the sample tube. This can be removed before loading by very careful application of a flame.

The suspension material used is 15 denier untreated nylon fibre, kindly supplied by I.C.I. Fibres Ltd. The suspension arrangement is shown in Fig.6. The length could not be reduced below ~ 100 cm owing to the cryostat dimensions. The lengths of fibre were weighted and hung for some time before use to remove kinks and, it was hoped, to ensure that they did not subsequently change in length when used in the balance. In fact, small changes in length do occur over the full temperature range. It is intended for future work to use a fine quartz fibre suspension, which should eliminate this problem.

The sample is loaded into the balance by means of a ratchet and pulley system.

The choice of atmosphere in the sample tube and balance is governed by the stability of the compound and the temperature range to be covered. Below 4.2 K the system must be evacuated, and from 4.2 to 77 K it must contain a vacuum, or a small exchange gas pressure of helium (5 - 10 torr) to provide a better thermal link with the sample. Above 77 K, vacuum, helium or nitrogen may be used. It is essential to ensure that no oxygen is present, since this is strongly paramagnetic at low temperatures.

The sample tube must be opened to the atmosphere for changing samples, and in the old cryostat no means could be devised for flushing the sample tube during this process to prevent air entering. The procedure is improved by filling the sample tube with an atmosphere of argon before opening, since the higher density of this gas prevents rapid diffusion of air into the tube. After loading the sample tube can be evacuated and adjusted to the required atmosphere. If the sample is unstable in vacuum at room temperature, the argon in the sample tube is precooled (not lower than ~ 150 K) before loading. When the sample has cooled to a temperature where no components are volatile, the argon can be pumped out. In all cases, great care is needed in the initial pumping stages, as a sudden reduction of pressure can cause loss of sample through the holes in the container lid.

In the new cryostat, an inlet tube is provided on the neck of the sample tube, so that the mouth of the tube may be flushed with an inert gas during sample changing.

If force measurements on the sample are not made in vacuum, a correction should be applied for the magnetic force on the gas which the sample displaces. This is only necessary when the susceptibility of the sample is very small.

Section III. MODES OF OPERATION

Two basic methods of making measurements are employed in this apparatus; fully manual and automatic. The latter was introduced, as stated in Section II (iii), to allow the machine to be left unattended during long temperature runs.

(i) Manual Operation

In this mode, the recorder is used to give a plot of weight change of the sample against magnet position, at the desired field and at constant temperature. The X-axis of the recorder is connected to the balance amplifier output, and the Y-axis to the magnet position transducer.

First, it is ensured that the sample temperature has equilibrated at the desired value. The magnet is then raised above the constant force position and the magnet current is adjusted to zero. Using the decade series and tare control at the sensitivity required for the measurement, the weight change on the amplifier meter, and hence on the X-axis of the recorder, is set accurately to zero. The amplifier and recorder are desensitised, and the desired magnet current is set. The weight change is then compensated as far as possible by the decade series until the remaining portion is registered on the meter at the desired sensitivity. The recorder is sensitised and the magnet slowly lowered, so that a plot of weight change against magnet position is produced (Fig.7). As the curve passes through its maximum (or minimum, in the case of a diamagnet), corresponding to the constant force region, the temperature is measured. The balance and recorder are then desensitised, the magnet current returned to zero, and the "zero weight" of sample is checked, to ensure that no drift has occurred during the measurement. The procedure is then repeated at other magnet currents, checking the "zero weight" before and after each.

The amplifier sensitivity is chosen to give a well-rounded curve on the plotter. The shape of the curve is affected by the rate of fall of the magnet, and this is usually adjusted to give a Y-travel on the plotter of ~ 2 cm/min.

Manual operation must always be used if the centre of magnetisation of the sample and container assembly is changing with temperature,

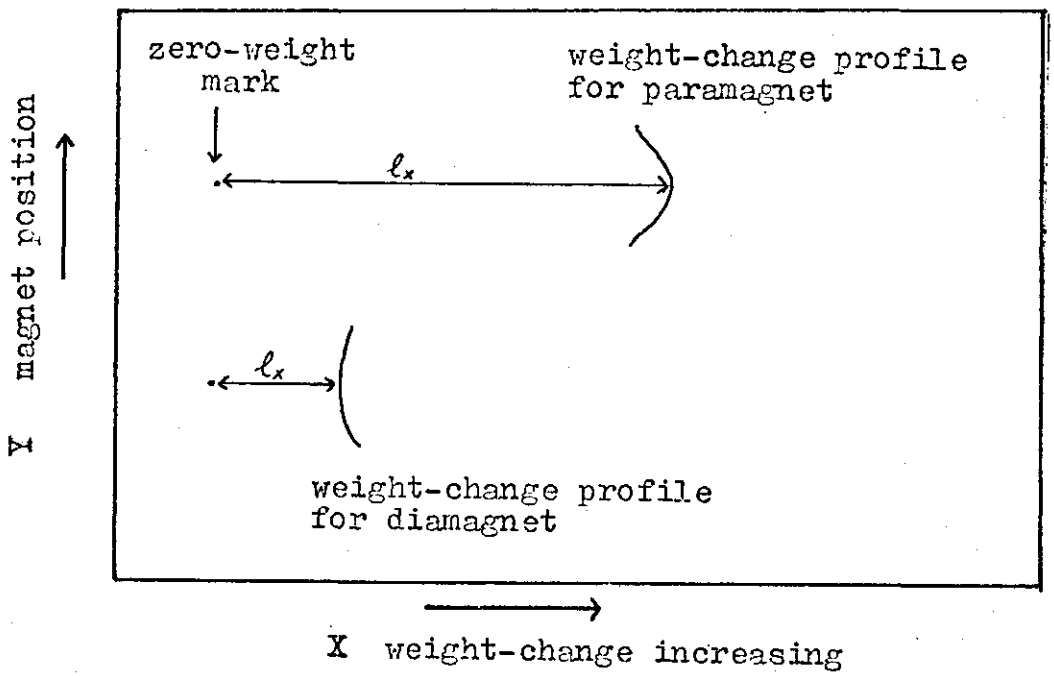

Fig. 7 Manual plot of weight change versus magnet position.

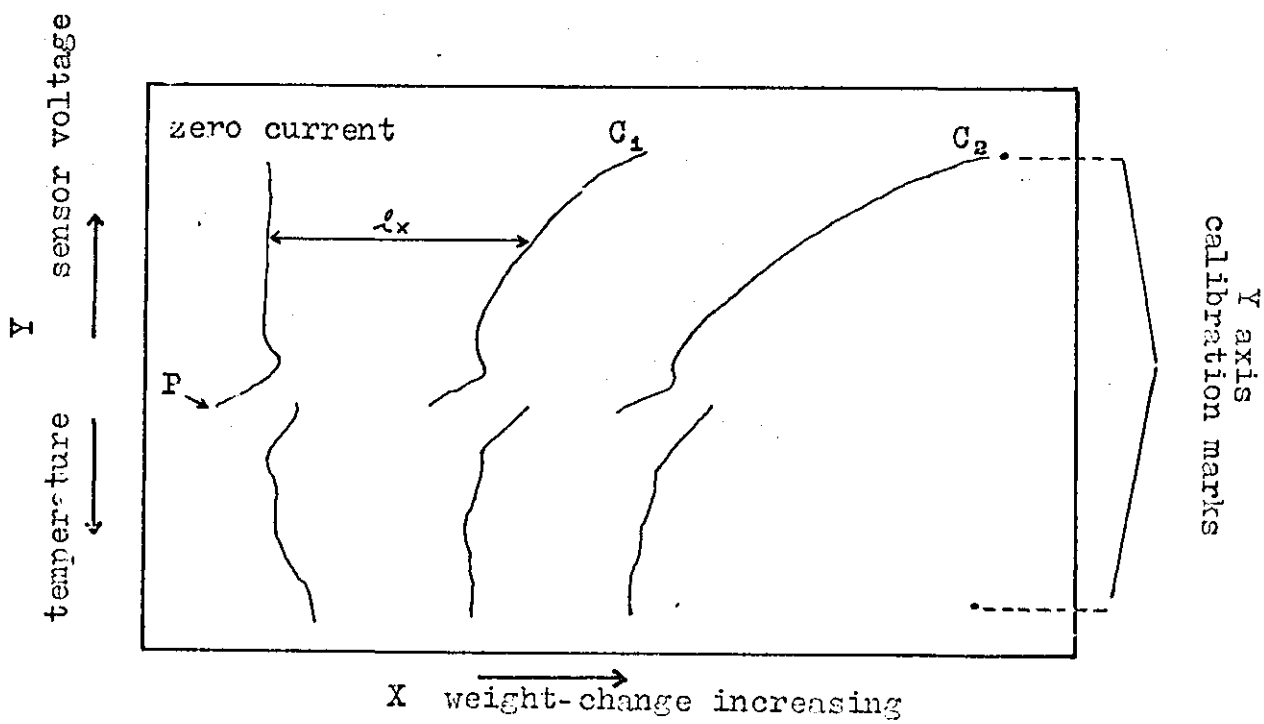

Fig. 8 Automatic plot of weight change versus temperature sensor voltage.

since the position of the maximum force on the Y-axis will then alter. The use of the recorder to plot weight changes also provides a sensitive means of checking that the sample temperature is constant, since, if not, the force will be changing with time and the plotter pen will be observed to move before the magnet is lowered.

(ii) Automatic Operation

In this mode, the recorder is used to produce a plot of weight change against "temperature", at one or two desired fields. It can only be used for ranges 2 and 4, where the temperature is rising slowly; for ranges 1 and 3, manual measurements must be made as the temperature is decreased. It is essential to adjust the magnet position initially so that the sample is exactly centred in the constant, maximum force region, i.e. at the maximum in the weight change v. magnet position profile.

The X-axis is connected to the amplifier output, and the Y-axis to the appropriate temperature sensing device for the range to be covered, to give a scale linear in thermocouple or carbon resistor voltage. For each temperature a record is required of the "zero-weight" of the sample, the total weight change when the field is applied, and a check that the "zero-weight" has not altered during the measurement. The procedure must be repeated if more than one field is desired. The magnet current must therefore be continually cycled between zero and the required values, and a point plotted at each steady field. This is accomplished through the control box as described in Section IV.

A typical plot is shown in Fig.8, which consists of the "zero-weight" line and two different field lines. The sensitivity of the amplifier and recorder are chosen initially so that the largest expected weight change occupies the maximum available X-distance on the recorder, and the sensitivity is increased as the force decreases, to maintain as high an accuracy of measurement as possible. X-axis calibrations are required for each sensitivity used.

An advantage of this mode is that, since the plot is virtually continuous, it shows clearly any sudden or gradual anomalies, which cannot be monitored so well by the manual mode. For example, the "kinks" in the "zero-weight" line indicate where gases have condensed

on to or evaporated from the sample. The gas can generally be identified from the temperature at which the "kink" occurs, and, if necessary, a correction can be made for its magnetic effect, since the weight is known from the X-axis calibration.

A possible source of error in automatic running is the departure of the sample from the constant force region in the z-direction. This may be caused by:

(a) changes in the suspension length with temperature and pressure conditions,

(b) changes in the buoyancy if working with an exchange gas pressure,

(c) changes in the centre of magnetisation of the sample assembly with temperature.

Periodic checks are made during the run to ensure that the sample has not moved out of the correct vertical position.

(iii) Calculation of Results

(a) Manual Mode

The total weight change, W_z mg, for each measurement is determined as follows:

$$W_z = W + (\ell_x \times C_x)$$

where W = change in decade series (field-zero) mg,

ℓ_x = distance (cm) from zero mark to maximum of curve,

C_x = appropriate X-axis calibration (mg/cm) for sensitivity used.

(b) Automatic Mode

The total weight change, W_z mg, for each temperature is obtained by:

$$W_z = (\ell_x \times C_x)$$

where ℓ_x = horizontal distance (cm) from "zero-weight" line to field line at appropriate Y value,

C_x = X-axis calibration (mg/cm).

Then, the total force, F_z dynes, is given by:

$$F_z = W_z g + D$$

where D = the force on the container (dynes) determined from previous calibration.

Assuming that distances can be measured to the nearest 0.5 mm, the measurement accuracy is 0.2% for a distance of 25 cm, and 0.5% for a distance of 10 cm. For manual measurements, only the remaining small percentage of the weight change is plotted and so a high accuracy is achieved. In the automatic mode, the sensitivity of amplifier and recorder are adjusted so that the plotted weight change is always $\geq$ 10 cm, to achieve an accuracy of 0.5%. The measurement accuracy in the Y-direction is of the same order of magnitude.

Errors may arise in measurement of automatic plots if (a) the recorder paper is misaligned, so that measured forces do not correspond to the correct temperature, (b) large drifts in the "zero-weight" occur, so that the gradient of the lines becomes very small.

Section IV. COORDINATION AND PROTECTION OF COMPONENTS

A control system was devised by Mr D.J. Lowe to coordinate the operation of the various components, especially for automatic operation, and to protect the components against damage which may be caused by, e.g. mains failure. This system has been slightly modified for use with the new cryostat, and a block diagram is shown in Fig.9.

The basic facilities provided are:

(1) the balance amplifier is supplied with power via an on/off switch;

(2) the X-axis of the recorder is connected to the balance amplifier output or to earth via an on/off switch, and level limits are applied to both X- and Y-axes;

(3) the recorder pen is raised and lowered (the pen control on the recorder overrides this);

(4) three magnet currents can be set and the desired one applied at any time to the magnet by the appropriate arrangement of switches. One current is set from the console (usually zero current), and the other two (denoted C_1 and C_2) by helipots on the control box.

An additional interconnection box has been designed by Mr S. Hardy for use with the new cryostat. The layout of the connections is shown in Fig.10, and by appropriate coupling of terminals, selection can be made of the required temperature sensor and the mode of operation of the heater. The heater drive and the backing e.m.f.'s for the sensors

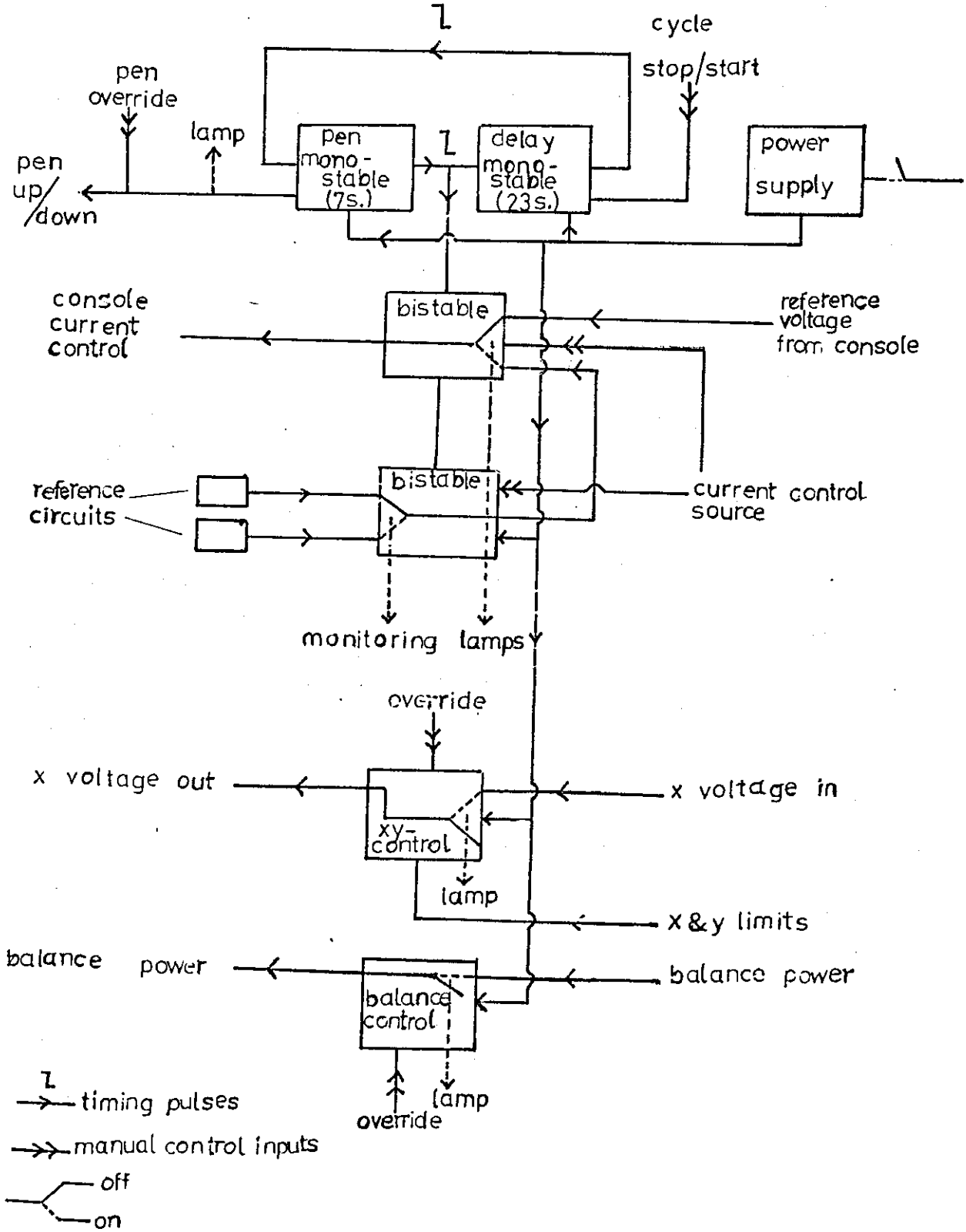

Fig.9 Block diagram of control system.

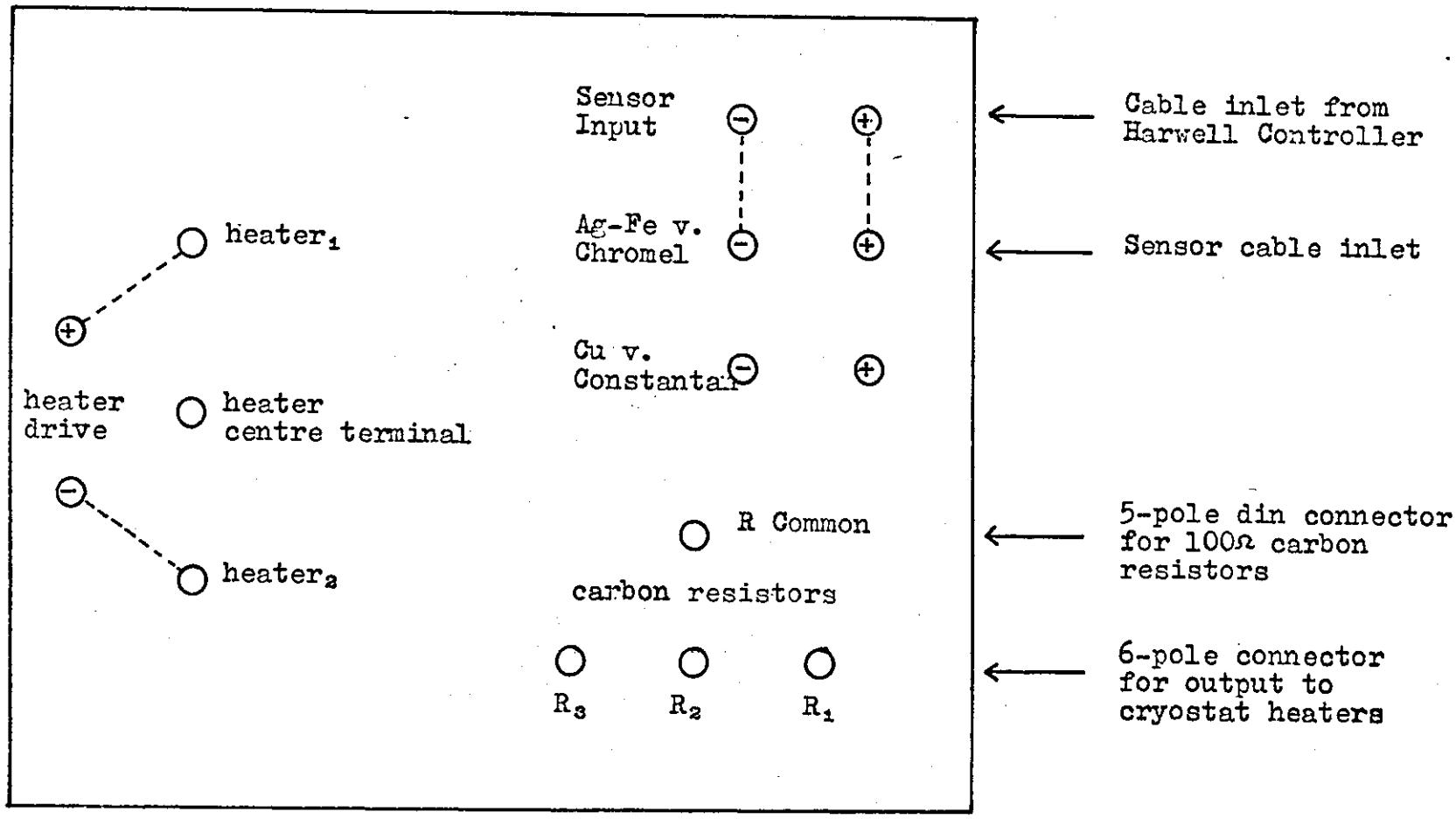

---- shows a mode of heater operation and choice of particular temperature sensor

Fig. 10 Layout of system interconnection box.

are provided internally in the Harwell Temperature Controller. The temperature sensor voltages may be measured manually on the potentiometer, or they may be applied to the Y-axis of the recorder, through a selection box, providing choice between the temperature sensor and the magnet position transducer.

The interconnection of all components is represented schematically in Fig.11.

Use of the Control Box

There are three basic modes for the control box: "off", "on" and "start".

"Off" configuration

The box has no power, with the following results:

(1) the balance amplifier has no power,

(2) the X-axis of the recorder is earthed,

(3) the recorder pen is raised,

(4) the magnet current control comes from the console.

"Stop" configuration

The box has power and the individual components can be operated independently for manual measurement. The prior setting of zero current and the two desired values C_1 and C_2, speeds up the making of manual measurements, where the same currents are used repetitively. The chosen current can be switched directly from the box, without requiring accurate setting each time from the console.

"Start" configuration

This mode is used for automatic recording. The balance has power and the X-axis is connected to the balance amplifier output. (The Y-axis is connected to the temperature sensor via the interconnection and selector boxes). The pen is raised and lowered at regular intervals (raised for ~ 23 secs. and lowered for ~ 7 secs.). Each time the pen is raised, the magnet current is changed, the sequence being:

$$C_1 \rightarrow \text{console(zero)} \rightarrow C_2 \rightarrow \text{console (zero)} \rightarrow C_1$$

or, if only one current is used, the current alternates between this value and the console zero.

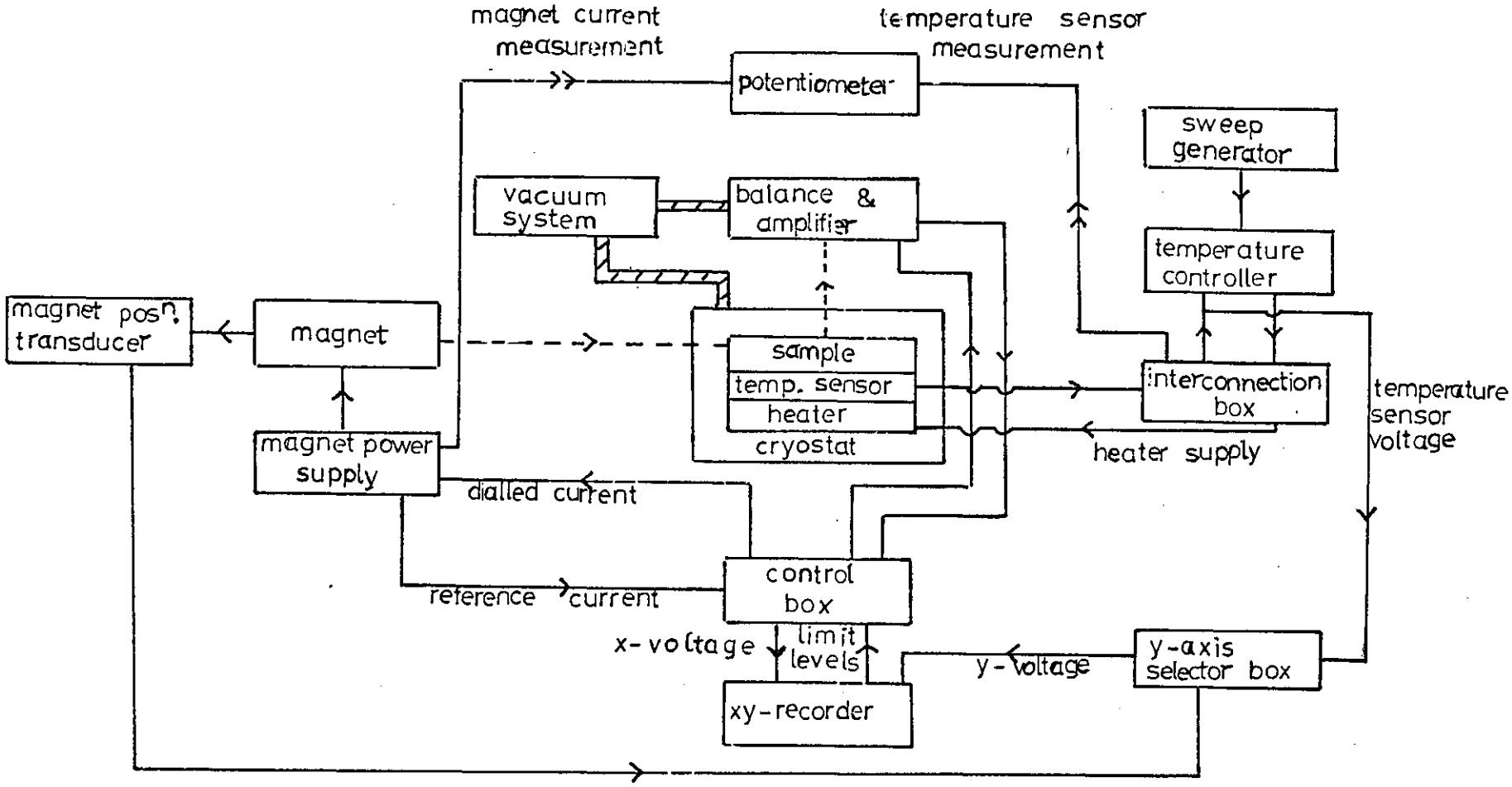

Fig. 11 Schematic representation of interconnection of all components.

Thus, with the correct sensitivity on the amplifier and recorder, a point, corresponding either to the "zero weight" or to the total weight change at each field, is plotted every 30 secs. against the temperature sensor output. The balance can therefore be left unattended for long periods of time, with occasional alteration of sensitivity.

The delay of 23 secs. between plotted points is sufficient to allow the magnet current to stabilise, small transient oscillations of the sample to die away, and the pen carriage arm of the recorder to respond and move to the correct position. The "pen-down" time of 7 secs. is long enough to indicate whether the sample temperature has equilibrated; if the temperature is not constant, a line rather than a point will be plotted.

It is also possible to change currents with the plotter pen permanently raised, to facilitate the initial setting of a suitable sensitivity without recording.

During the course of an automatic run, the pen-carriage travel may exceed the range capability of the recorder in the X-direction, due to an unexpected increase in the weight change, or to a large drift in the "zero weight". Roller switches are mounted at each end of the X-axis which operate a servo-motor driving the electrical weight compensation of the amplifier. When the carriage arm presses the microswitch closed, the decade series changes automatically in the appropriate direction to return the carriage arm on scale. This is illustrated in Fig.8, at point P, where all three curves have been moved by the same distance. An additional set of microswitches, activated by the carriage arm, are situated outside the roller switches, with a 7 sec. delay before operating. If the carriage arm deflection is not compensated by the decade series in the time interval (i.e. if the deflection is very large) these switches will shut down the control box, returning it to the "stop" configuration. The control box switches are arranged so that this "stop" configuration corresponds to the situation where the current is set to the console value, the pen is permanently raised, and the power to the amplifier and recorder inputs can be disconnected if desired. This serves as a protection for the balance and recorder

against prolonged deflections in excess of full-scale. Similar microswitches are positioned at the ends of the Y-axis to shut down the apparatus in case the level limit is exceeded in this direction. The circuits also assume the "stop" configuration if there is a mains failure of more than 1 second. A set of pilot lights, corresponding to each of the control switches, indicate the configuration and stage of operation at any time.

Section V. CALIBRATIONS AND ERRORS

Calibrations are required for:

(1) the product, $H_x \frac{dH_x}{dz}$, in the constant force region, at all magnet currents which may be used in measurement;

(2) the temperature of the sample with respect to the thermocouple e.m.f's and carbon resistor voltage, over the full temperature range. (The calibrations given below apply only to the original cryostat);

(3) the diamagnetic correction of the sample container (discussed in Section II (vi));

(4) the scale of the recorder chart, in both X- and Y-directions (discussed in Section II (v) and III (iii)).

As stated in Sections II (i) and (iv), the calibrations of field and temperature are most conveniently performed by force measurements on a standard sample of known magnetic behaviour, but it is a matter of some difficulty to find ideal standards. If the substance chosen for field calibration has a temperature dependent susceptibility, then the two calibrations are not necessarily independent, since the sample temperature must be known for calculation of $H_x \frac{dH_x}{dz}$, and similarly, this product must be known for calculation of temperature. If either calibrant has a field-dependent susceptibility (i.e. if it is ferro- or antiferromagnetic) additional difficulties arise since the field used in the Faraday method is inhomogeneous.

It is therefore desirable that the standard for field calibration should have a virtually temperature-independent susceptibility around room temperature, while that for temperature calibration should have a susceptibility which varies in a simple and accurately-known way over the full range, and that neither show field-dependence. Additional

requirements of the standards are that they should be obtainable in a state of high purity (especially, no ferromegnetic impurities should be present) and that they should be stable towards atmospheric conditions and vacuum, and chemically inert.

Some assessment of the advantages and disadvantages of some commonly-used calibrants has been given, together with the available magnetic data.[4,22,23] The reliability and accuracy of magnetic data reported in the literature depend essentially on the method and instrumentation used and the means of calibration adopted by the worker, and large discrepancies are often found between independent determinations on the same compound. As an example, the reported data on $HgCo(NCS)_4$, which has been widely used as both field and temperature calibrant, can be cited. Figgis and Nyholm originally reported[24] that the compound obeys the Curie-Weiss Law, $\chi_m^{corr} \alpha (T + \theta)^{-1}$, over the range 90 - 300 K, with θ = 10 K and $\chi_g = (16.44 \pm 0.08) \times 10^{-6}$ at 293 K. In a second paper,[25] they give values of μ_{eff} of 4.33 BM (300 K) and 4.18 BM (90 K), with the same Curie-Weiss behaviour. It has been pointed out[26] that the data in the two papers are not consistent; the values of χ_m^{corr}, calculated from the magnetic moments, agree with a θ value of 10 K, but correspond to a value of χ_g of 15.83×10^{-6} at 293 K, i.e. a discrepancy of ~4%. In a later investigation, Sullivan et al. report[27] that the compound obeys the Curie Law, $\chi_m^{corr} \alpha T^{-1}$, in the range 77 - 300 K, with μ_{eff} = 4.38 BM. This corresponds to a value of χ_g of 16.22×10^{-6} at 293 K, but introduces a discrepancy of ~10% into values at lower temperatures. It should however be pointed out that the experimental expression given for χ_g in this paper ($\chi_g = -1.32 \times 10^{6} + (48.39 \times 10^{-4})/T$) is not consistent with the other data, since it gives a value $\chi_g = 15.20 \times 10^{-6}$ at 293 K. It is also claimed that the Curie rather than Curie-Weiss Law behaviour is supported by the data of Candela and Mundy,[22] but in fact their reported values at 298.2 and 77.7 K do not appear to verify either of the previous results.

The reliability of the calibrant is often the major source of error in susceptibility balances, and there is an urgent need for extensive investigation of suitable standards. Further discussion on the requirements for a temperature calibrant is given in part (2) of this section.

(i) Field Calibration

A few metallic elements and alloys (mainly in the second and third transition series) fulfil most of the requirements for a field calibrant.[28] High purity platinum ($\chi_g = 0.971 \times 10^{-6}$ at 293 K, with a small temperature-dependence of χ_g around room temperature[29]) has often been used. For this apparatus, high purity tantalum was chosen, since its susceptibility is virtually constant around room temperature.

Some discrepancies occur in the reported values of its susceptibility. Kriessman[30] gives an experimental value of 0.827×10^{-6} at 298 K with no assessment of accuracy. Hoare et al.[31,32] have carried out over six hundred measurements of the susceptibility in the range 20 to 293 K, and give a value of $(0.8490 \pm 0.0006) \times 10^{-6}$ at 293 K, with a temperature dependence over the entire range of < 1%. In a later paper, Kriessman[33] quotes the best value of χ_g as 0.84×10^{-6}, and an independent determination by Asmussen and Soling,[34] in the temperature range 79 - 578 K, shows that χ_g decreases slowly and linearly with increasing temperature according to the empirical equation

$$\chi_g \times 10^6 = 0.860 - 0.000068\ T$$

This corresponds to a value of 0.840×10^{-6} in the range 288 - 298 K. Taking the mean of the results of Hoare and Asmussen, we have $\chi_g = (0.845 \pm .005) \times 10^{-6}$, giving an accuracy of $\sim \pm 0.5\%$. Since the error in temperature calibration is likely to be larger than this, the accuracy is acceptable.

The sample used was spectrographically Standardised Tantalum from Johnson-Matthey Chemicals Ltd. It was obtained in uniform rods of diameter 4.5 mm, and was cut into cylinders of length 5 mm (approximate weight 1.3 g). The relatively large weight is necessary to obtain a force of convenient magnitude for accurate measurement, since the susceptibility is small. For a material of $\chi_g \approx 10^{-6}$, the force on 1 g can be measured at a value of $H_x \frac{dH_x}{dz} \approx 10^6$ with a maximum accuracy of 0.1%.

The cylinders could be suspended without use of a container, so that possible errors in the container correction were removed. Several

cylinders of different weights were used initially to check the homogeneity of the specimen and were found to give field values consistent to 0.2%. One cylinder, of weight 1.3023 g, was then chosen as the standard field calibrant. Calibrations were performed in both vacuum and 760 torr of argon, and the field values agreed to 0.2% without applying a correction for the displaced gas.

Calibrations were performed for both methods of setting the magnet current, i.e. winding up slowly using the console controls, and presetting and switching via the control box. The values of field obtained from the latter were found to be slightly higher than those from the former (by $\sim$ 1% at low fields and 0.3% at high fields). This is presumably due to the fact that as the current is brought up faster in the latter method, a small amount of overshoot occurs before the current stabilises. The degree of overshoot is however constant for a given current, and the field values from this method are reproducible. Since this method is essential for automatic running and greatly simplifies manual measurement, it was adopted as standard procedure, and calibrations were made and checked with the currents switched from the control box. A check was made that the magnet currents set repetitively from the box remained constant, especially during long automatic runs. It was found that during a 36 hour period with the box functioning in the "start" mode, the drift in current was $\sim$ 0.1%.

The field calibration is shown in Fig.12. It was found that below 5 amp. the field was not reproducible, and all measurements were made with currents greater than this. The calibration was repeated at regular time intervals, and it was found that the fields were stable and reproducible over periods of many months.

It was hoped to verify the field calibration using a standard in the form of a powder contained in the perspex bucket i.e. under the conditions of a measurement on an unknown specimen. A determination using $HgCO(NCS)_4$ was carried out, but the calculated values of $H_x \frac{dH_x}{dz}$ depend on the value of χ_g for the compound used. Using a value based on $\chi_g^{293} = 16.44 \times 10^{-6}$, $H_x \frac{dH_x}{dz}$ was $\sim$ 1% lower than for tantalum, whereas using a value of $\chi_g^{293} = 15.83 \times 10^{-6}$, the product was $\sim$ 1 - 1.5% higher than for tantalum. The temperature of the sample for the measurement

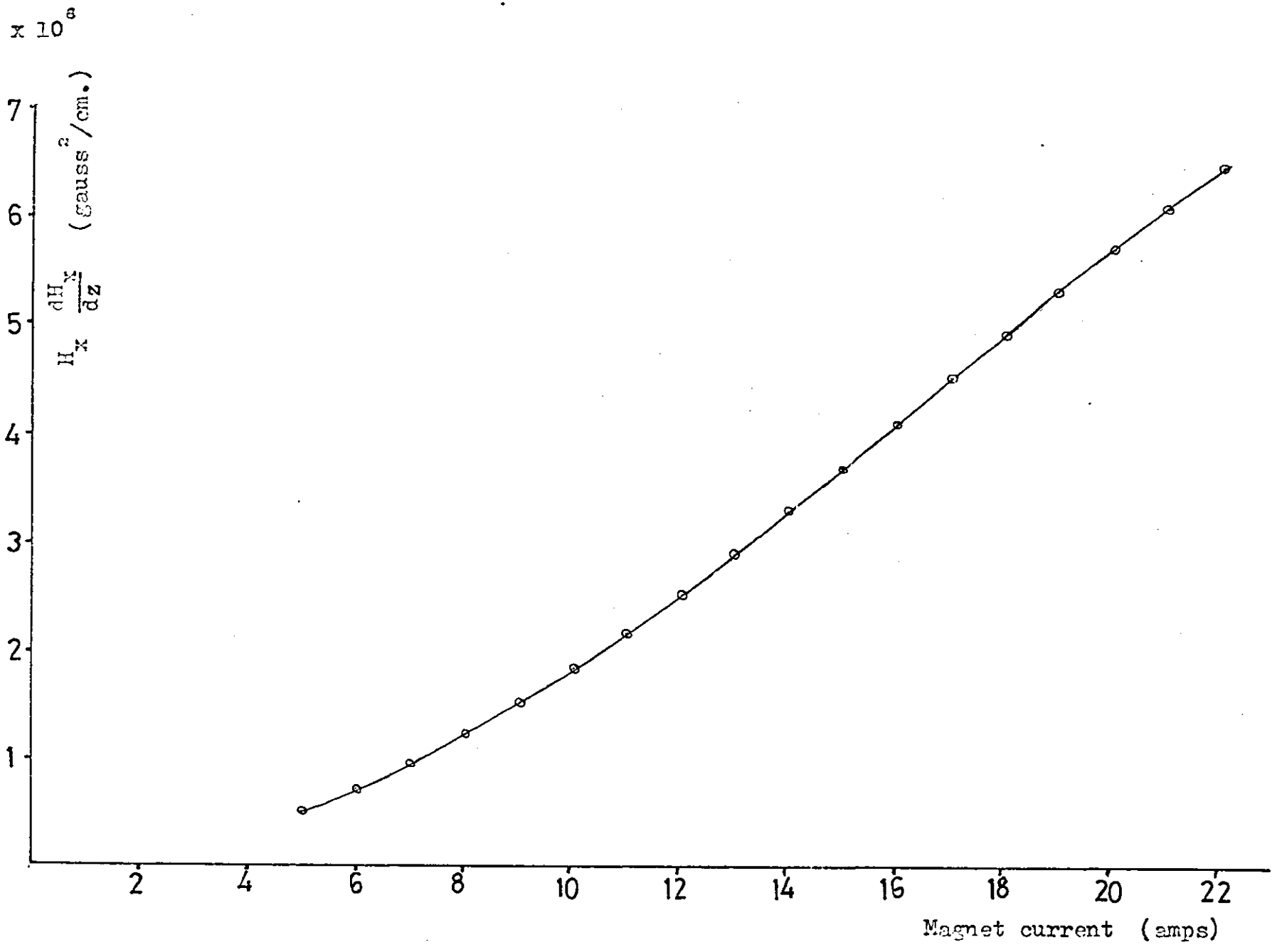

Fig. 12 Calibration for $H_x \frac{dH_x}{dz}$ in the contant force region.

was determined by destroying the outer vacuum jacket of the cryostat, leaving the sample to equilibrate with room temperature overnight, and measuring this temperature at several points around the cryostat.

Consideration was given to the possibility of introducing a dimension error (see Section II(i)), since the tantalum standard is smaller than the container used for measurement with powdered samples. The container is calibrated by experimental measurement of the force exerted on it in the field, and the correction to sample measurements is applied directly as this force. Since the container experiences identical field conditions during its calibration and during sample measurement, no error is introduced due to its longer length. Also, in practice, the length of paramagnetic sample rarely exceeded that of the tantalum cylinder. A small error may be introduced when very small volumes of powder are used, since, in this case, the centre of magnetisation in the z-direction of the container and sample may not coincide with that of the container alone. This error should be negligible unless very small forces are measured.

To investigate the possibility of error due to the greater diameter of the container, the extent of the constant force region in the x-direction was determined. This also provided a means of aligning the balance suspension in the correct position with respect to the magnet pole pieces. The force on the tantalum sample was recorded as the balance was moved across the x-direction of the pole gap in small regular stages. The force was found to be constant to 1% over a distance of ~ 1.4 cm, and the balance end-stop was adjusted so that the suspension could always be positioned in the centre of this region. The container is therefore always within the constant force region.

Experiments were also carried out to determine the value of F_M^c (see Section II(i)), at which lateral oscillation makes force measurement impossible. A powdered sample in the perspex container was used to reproduce the conditions of an actual measurement. As the magnetic force is increased, the transient oscillations, induced by the initial application of the magnet current, increase in amplitude and take longer to die away. It is very difficult to distinguish between very large transient oscillations and complete instability due to F_M^c being exceeded. However, since the former effect also makes it impossible to make rapid,

accurate force measurements, it was sufficient to set an upper force limit at the point where transient oscillations become inconveniently large. This limit was dependent to a certain extent on the magnet current value, but was generally in the range 40 - 50 dynes. The situation would be improved by bringing the magnet current more slowly, since the initial induced oscillation is then expected to be smaller.

(ii) Temperature Calibration

The variation of the susceptibility of the standard with temperature must be large enough to give an accurate calibration over the full range, with regard to the measurement sensitivity of the apparatus. The most commonly used temperature calibrants have been paramagnetic transition metal compounds.

Most of the compounds advocated as standards have only been investigated in a limited temperature range (generally 80 - 300 K).[4,22,23] Many show some temperature dependence of the magnetic moment, and their behaviour is often expressed by an experimental Curie-Weiss Law, $\chi_m^{corr} \propto (T + \theta)^{-1}$, at temperatures high relative to the Weiss constant, θ. It is extremely dangerous to extrapolate these reported values to lower temperatures when the origin of θ is unknown. It may be a manifestation of the existence of exchange interactions in the compound, in which case a Curie or Néel temperature will exist below which the magnetic behaviour becomes complex and often field-dependent. However, a Curie-Weiss Law dependence will also be shown if the magnetic ion has thermally-accessible levels above the ground level, due to the effects of spin-orbit coupling or low symmetry field components. In this case, θ has no real physical significance, but description of the magnetic behaviour by a Curie-Weiss Law will not be valid at temperatures comparable to θ. In either case, such compounds are not suitable for calibrants, unless reliable data are available over the full temperature range or the value of θ is very small compared with the lowest temperature to be measured.

Ideally, the magnetic behaviour of the standard should follow the Curie Law, $\chi_m^{corr} \propto T^{-1}$, where the effective magnetic moment is temperature independent, but very few systems have been found experimentally to exhibit this simple behaviour over the full temperature range. The basic requirement of the magnetic ion is that the ground state should be degenerate before application of the magnetic field, i.e. there should

be no higher-lying states separated from the ground state by the order of kT. Under these conditions the magnetic properties should be those of the ground state alone. A configuration giving rise to an A or E ground term in a cubic ligand field should theoretically fulfil this requirement, since lifting of degeneracy by spin-orbit coupling should not occur. However, spin-orbit interaction with higher-lying T terms of the same multiplicity may restore orbital contribution to the magnetic moment. For any configuration in which the "quenching" of the orbital angular momentum is not complete, the remaining orbital degeneracy can be lifted by both spin-orbit coupling and low-symmetry components of the ligand-field. The resultant ordering and separation of the levels, and hence the magnetic behaviour, will depend on the relative magnitude of λ, the spin-orbit coupling constant, Δ, the low-symmetry ligand field splitting, and kT. A temperature-independent contribution to the susceptibility, from the second-order Zeeman effect with higher-lying levels, may also be present, and introduce a temperature dependence in the magnetic moment.

In the transition series, one configuration is unaffected by these considerations; the ^6S free-ion ground term for high-spin d^5 systems. This term is unsplit by cubic ligand fields, corresponding to a $^6A_1$ representation. It is unaffected by spin-orbit coupling, since it has zero orbital angular momentum, and there are no higher-lying terms of the same multiplicity to mix in. There is also no second-order Zeeman effect for this term. The magnetic moment should therefore be very close to the spin-only value of 5.92 BM and independent of temperature. High-spin complexes of manganese(II) or iron(III), with ligands of a suitable size and nature to ensure complete magnetic dilution, should prove to be very good standards for temperature calibration, but as yet very little data on such compounds over the required temperature range have been reported. (The ligand arrangement must be regularly cubic, since lower symmetry elements will lift the 6-fold spin-degeneracy of the term to give 3 Kramers doublets. This zero-field splitting can produce a small temperature-dependence in the magnetic moment at low temperatures).

Complexes of the congeners of manganese(II) and iron(III) in the second and third transition series are almost invariably of the spin-paired

type and do not give rise to the ^6S state. The only other common case of an S-state ion is the f^7 ($^8S_{7/2}$) configuration for gadolinium(III) and europium(II) in the lanthanide series. Some Gd(III) compounds have been studied over the full temperature range,[35] but these are not magnetically dilute at low temperature.

No suitable compound of an S-state ion, with extensive reported magnetic data, could be found, and the calibrant chosen was chrome potassium alum, $K_2Cr_2(SO_4)_4\ 24H_2O$. This compound has a $^4A_{2g}$ ground term, and has been reported to follow the Curie Law down to 1.3 K.[1] However, later results show that it follows a Curie-Weiss Law, with θ = 0.2 K and μ_{eff} = 3.83 ($\pm$ 0.01) BM, down to very low temperatures (ref. 28, 3-117, and refs. therein). The magnetic behaviour has also been extensively studied below 1 K, and an antiferromagnetic Neel temperature of 0.004 K has been reported.[28] It has been stated[36] that the magnetic behaviour may become more complicated below 4 K, but there is little useful reported data on this. We have assumed the Curie-Weiss Law dependence for calculation of temperature over the full range, but it is possible that the error in calibrations may be higher below 4 K. The good agreement obtained for the calculated value at 4.2 K suggests that this treatment is valid at this temperature.

Chrome alum has some disadvantages as a calibrant. It can lose water of crystallization in vacuum above 0°C, and the procedure of precooling the balance before loading had to be adopted. The calibration was performed in vacuum below 0°C, but above this temperature the pressure in the sample tube was adjusted to 760 torr of helium gas. There is, in addition, the possibility of loss of water during grinding and weighing of the powdered sample. The compound was recrystallised from water (below ~ 50°C to prevent the transition of the violet form to the green form) and powdered immediately before use. The gram-susceptibility of the compound is relatively large at low temperature (~ 2000 x 10^{-6} at 2 K) and, to avoid oscillation problems, sample weights of less than 10 mg were used for calibration of the carbon resistor in the range 1.8 to ~ 60 K. The weight was increased to ~ 100 mg for calibration of the copper/constantan thermocouple between 60 and 300 K.

The calibrations are shown in Figs. 13 - 17. In the temperature ranges 2 and 4 (see Section II (iii)) the measurements were made by

Calibration of copper/constantan thermocouple

Fig. 13

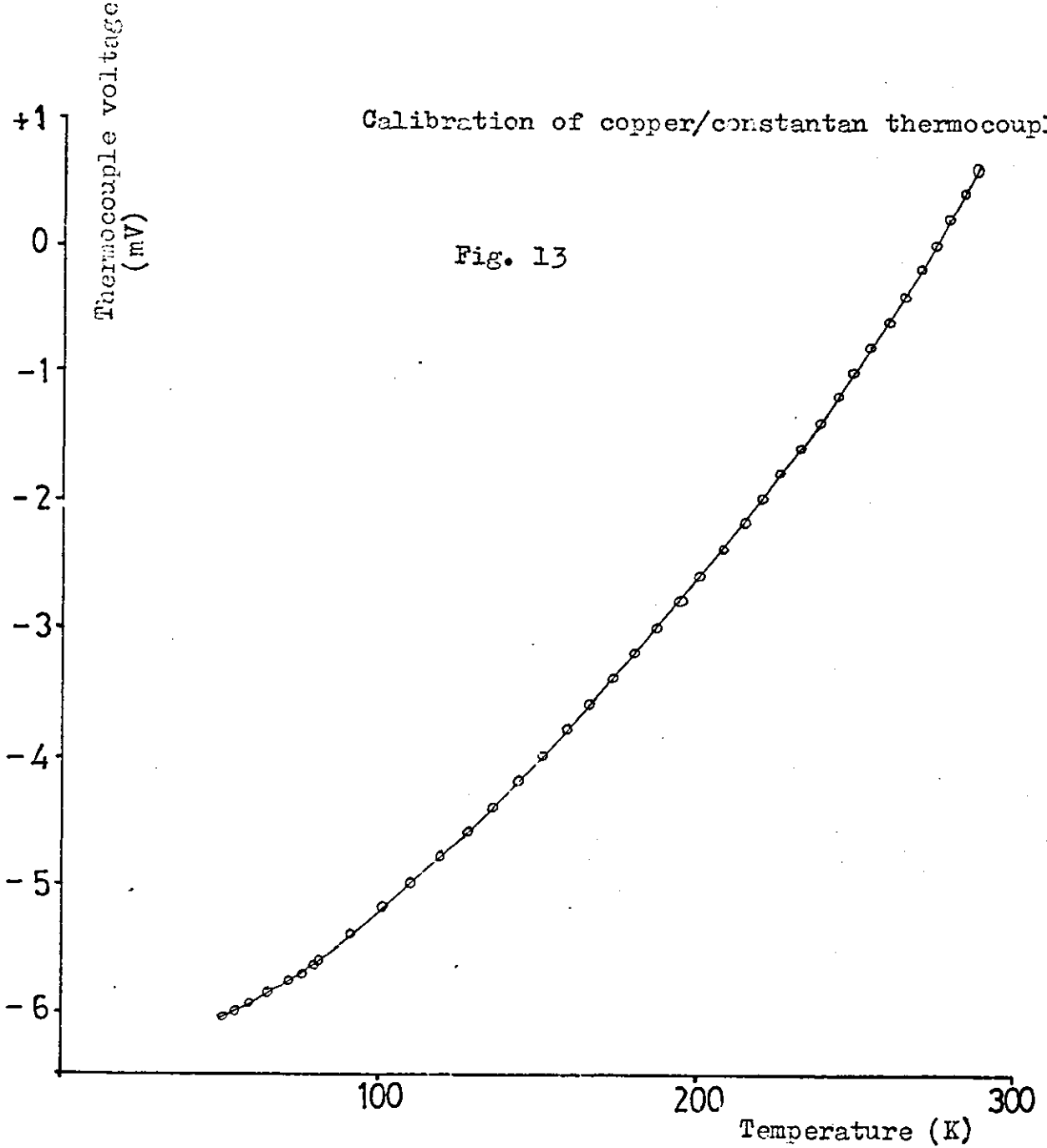

Fig. 14

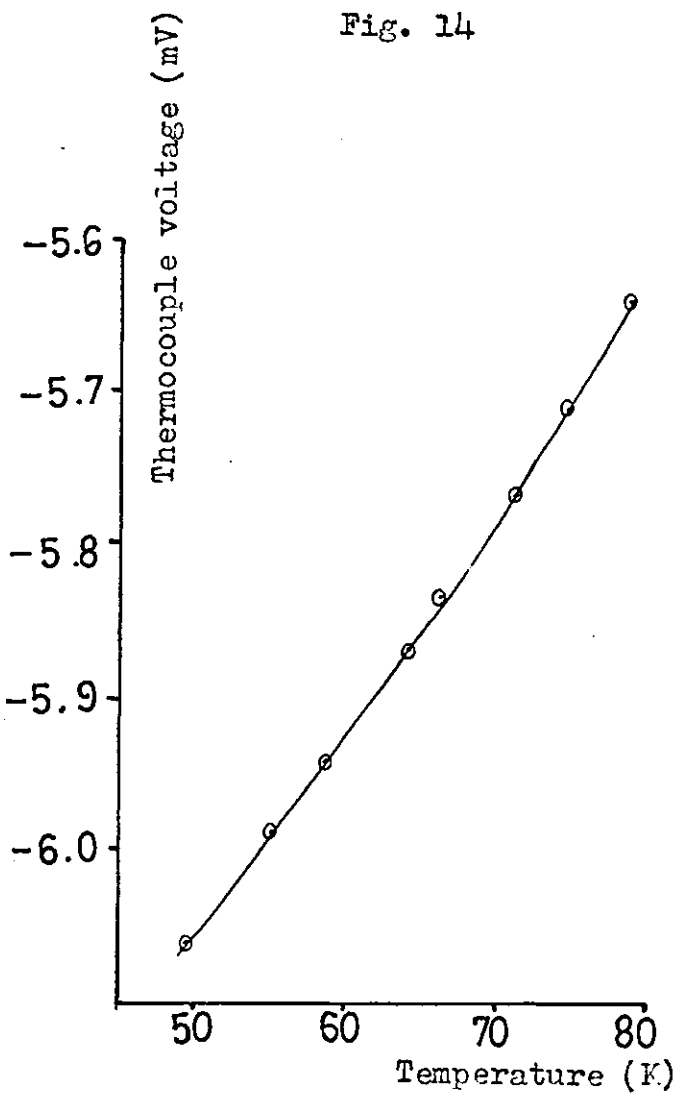

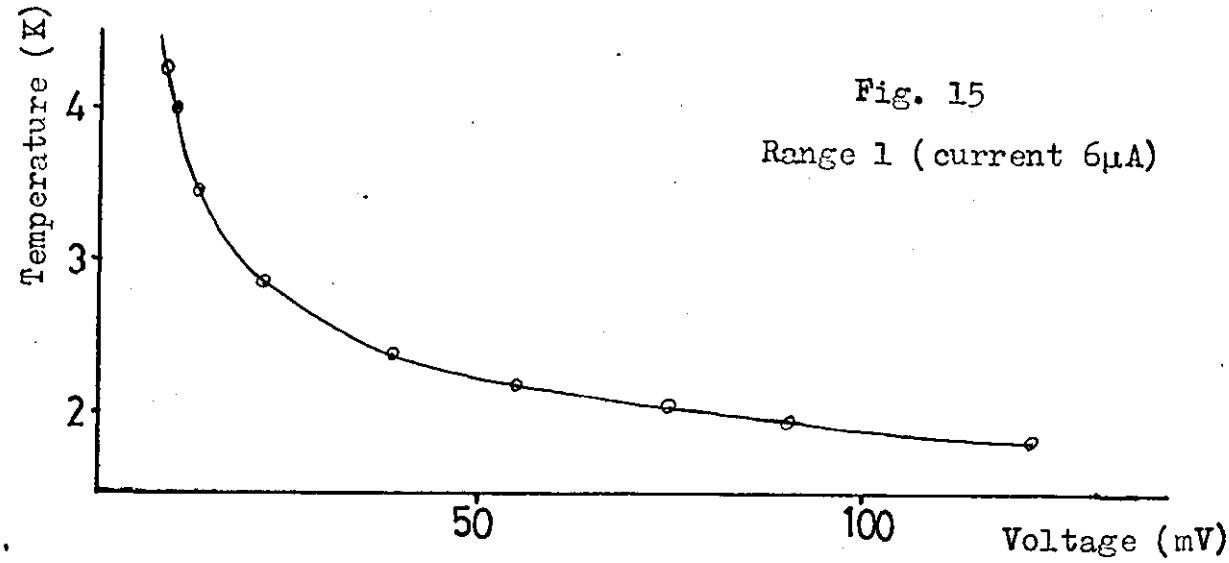

Fig. 15

Range 1 (current 6μA)

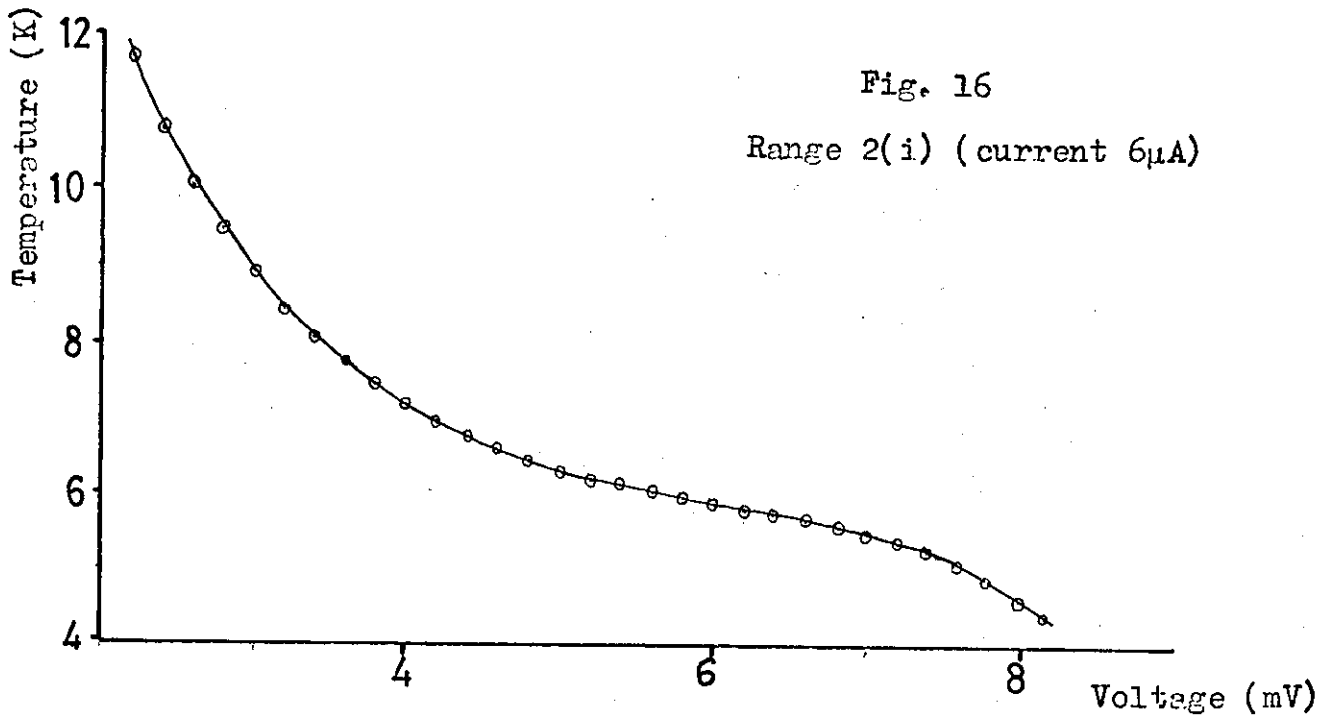

Fig. 16

Range 2(i) (current 6μA)

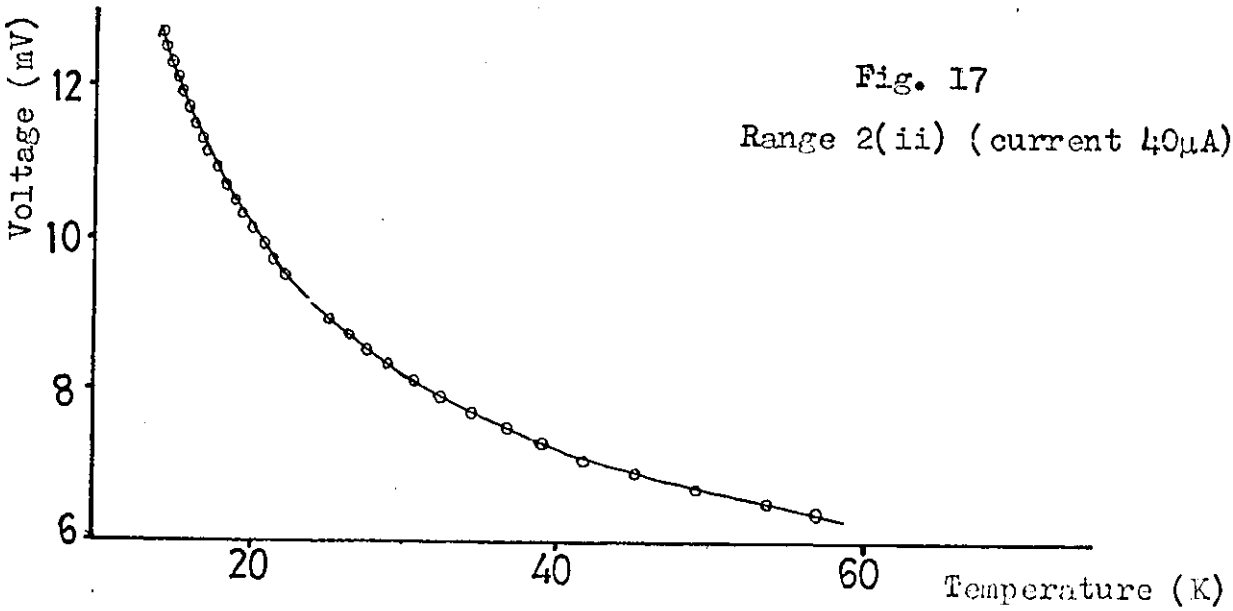

Fig. 17

Range 2(ii) (current 40μA)

Carbon resistor calibrations.

automatic operation to give a virtually continuous calibration. The shape of curve 2(i) (Fig.15) was found to be reproducible for two different carbon resistors. Taking into consideration the probable accuracy of the literature data for the susceptibility of the calibrant and any instrumental errors in performing the calibration, the overall error in the temperature calibration is expected to be of the order of 1%. The accuracy of subsequent temperature measurement using this calibration will be of the same order of magnitude, and this is the largest inherent source of error in susceptibility measurements over a temperature range in this apparatus.

(iii) Errors

The errors associated with the various components, the operating procedures, weighing of samples, calibrations etc, have been discussed in the appropriate sections.

Force measurements can be made with a maximum error of 0.5%, corresponding to the minimum accuracy of distance measurement on automatic plots. In general, the error will be much smaller than this, i.e. 0.01 to 0.2%. The accuracy of susceptibility measurement involves, in addition, errors in the field calibration, sample weighing and container correction. Comparative susceptibility measurements at the same temperature should be consistent to 0.5 - 1%, depending on the weighing accuracy of small samples. Susceptibility measurements over a temperature range, and calculated magnetic moments, also involve the error in temperature measurement. Assuming a 0.5% error in susceptibility and a 1% error in temperature, the error in the magnetic moment calculated from these would be 0.75%. The largest errors are likely to occur when very small quantities of samples of low susceptibility are measured at low temperature, and in this case, the error could be of the order 2 - 5%.

APPENDIX REFERENCES

1. E.C. Stonor, 'Magnetism and Matter', Methuen (1934).
2. R.L. Sanford and I.L. Cooter, 'Basic Magnetic Quantities and Measurement of Magnetic Properties of Materials'. N.B.S. Monograph No.47, Washington (1947).
3. H. Zijlstra, 'Experimental Methods in Magnetism, Part 2' Selected Topics in Solid State Physics, IX (1967).
4. B.N. Figgis and J. Lewis, 'Technique in Inorganic Chemistry IV' 137 (1965).
5. D.O. Smith, Rev. Sci. Instrum., 27, 261 (1956).
6. K. Dwight, N. Menyuk and D. Smith, J. Appl. Phys., 29, 491 (1958).
7. S. Foner, Rev. Sci. Instrum., 30, 548 (1959).
8. L.F. Bates, 'Modern Magnetism', Cambridge University Press (1961).
9. W.E. Gardner and T.F. Smith, 'The Proceedings of the 9th Conference on Vacuum Microbalance Technology', Plenum Press (1971).
10. B. Morris and A. Wold, Rev. Sci. Instrum., 39, 1937 (1968).
11. B. Dellby and M.E. Ekström, J. Phys. E., 4, 342 (1971).
12. A. Thorpe and F.E. Senftle, Rev. Sci. Instrum., 30, 1006 (1959).
13. W.P. Wolf, J. Appl. Phys., 28, 780 (1957).
14. B.N. Figgis and R.S. Nyholm, J. Chem. Soc., 331 (1959).
15. W.G. Henry and J.L. Rogers, Phil. Mag., 1, 223 (1956).
16. W.G. Henry and J.L. Rogers, Can. J. Phys., 38, 908 (1960).
17. M. Garber, W.G. Henry and H.G. Hoeve, Can. J. Phys., 38, 1595 (1960).
18. R.D. Heyding, J.B. Taylor and M.L. Hair, Rev. Sci. Instrum., 32, 161 (1961).
19. G.J. Hill, J. Sci. Instrum., (J. Phys. E.) 1, 52 (1968).
20. R.H. Martin and G.J. Hill, J. Sci. Instrum., (J. Phys. E.) 1, 1267 (1968).
21. A.M. Stewart, J. Sci. Instrum., (J. Phys. E.) 2, 851 (1969).
22. G.A. Candela and R.E. Mundy, I.R.E. Transactions on Instrumentation, 106, (1962).
23. B.N. Figgis and J. Lewis, 'Modern Coordination Chemistry', Interscience, 400, (1962).
24. B.N. Figgis and R.S. Nyholm, J. Chem. Soc., 4190 (1958).
25. B.N. Figgis and R.S. Nyholm, J. Chem. Soc., 338 (1959).
26. F.A. Cotton, D.M.L. Goodgame, M. Goodgame and A. Sacco, J. Amer. Chem. Soc., 83, 4157 (1961).

27. S. Sullivan, A.N. Thorpe and P. Hambright, J. Chem. Ed., 48, 345 (1971).

28. Landolt-Börnstein, Zahlenwerte und Functionen. II Band, 9 Teil, Magnetic Properties I, Chapters 1 and 2', Springer-Verlag, Berlin (1962).

29. F.E. Hoare and J.C. Matthews, Proc. Roy. Soc., A212, 137 (1951).

30. C.J. Kriessman, Rev. Mod. Phys., 25, 122 (1953).

31. F.E. Hoare and J.C. Walling, Proc. Phys. Soc. (London) B64, 337 (1951).

32. F.E. Hoare, J.S. Kouvelites, J.C. Matthews and J. Preston, Proc. Phys. Soc. (London) B67, 728 (1954).

33. C.J. Kriessman, Phys. Rev., 94, 837 (1954).

34. R.W. Asmussen and H. Soling, Acta Chem. Scand., 8, 563 (1954).

35. J.D. Cashion, A.H. Cooke, L.A. Hoel, D.M. Martin and M.R. Wells, Proc. Colloque International du C.N.R.S. sur les Elements de Terres Rares, 180, (II), 417 (1970).

36. B.N. Figgis and J. Lewis, Prog. in Inorg. Chem., 6, 37,(1964).